Regulation of DAG Lipase Activity – Implications for 'On-Demand' Endocannabinoid Signalling

Markwick, Rachel Loretta Lane

Awarding institution:
King's College London

KING'S College LONDON

Regulation of DAG Lipase Activity – Implications for 'On-Demand' Endocannabinoid Signalling

A thesis for the Degree of Doctor of Philosophy

Rachel Loretta Lane Markwick

Wolfson Centre for Age-Related Diseases,

King's College London

Acknowledgements

I would like to thank first and foremost my supervisor, Professor Patrick Doherty for his constant guidance and wisdom. Thank you also to the BBSRC and AstraZeneca for funding this project.

I'd like to thank Gareth Williams for his help with the bioinformatics and for his huge contribution towards elucidating the structure function relationship of the DAGLs. I'd also like to thank Dr. Mene Pangalos, Dr. Marcello Maresca, Dr. Mohammad Bohlooly and all at Astra Zeneca for assisting my PhD, especially with the CRISPR project, and for being a huge support.

A big thank you to all in the lab, both past and present, for their friendship throughout my four years at King's College London – especially Dr. Praveen Singh, Dr. Melina Reisenberg, Zhou Ya, Leanne Lu and Dr. Fiona Howell.

Thank you David Baker and Steve Alexander for examining this thesis.

Finally, a massive thank you to my family and close friends who have been a rock of sense, especially through the final stages of putting this thesis together. Thank you Maeve Lane, Dr. Cyril Lane, Jennifer Lane, Pat Dempsey, Julie Dempsey and Geraldine Kendall.

Of course, none of this would have been possible without my ever supportive husband, Dr. Lee Markwick.

Abstract

The diacylglycerol lipases (DAGL α and β) are key enzymes in the biosynthesis of 2-AG, the major endocannabinoid (eCB) in the brain. 2-AG acts on CB1 and/or CB2 receptors and DAGL-dependent eCB signalling regulates a large number of responses including axonal growth during development, as well as neurogenesis and retrograde synaptic plasticity in the adult. The enzymes also play a major role in driving pathogenic inflammatory responses via a DAGL/MAGL pathway that generates arachidonic acid as a precursor to prostaglandin synthesis. DAGL antagonists are being developed as novel therapeutics based on their ability to regulate eCB-mediated signalling and/or inflammatory responses, but the mechanisms underlying the regulation of these enzymes is poorly understood.

The DAGLs appear to display 'on-demand' synthesis, generating increasing amounts of 2-AG in response to cellular messengers. Using a bioinformatics approach, we have postulated that phosphorylation is key mechanism for regulation of DAGL function. We overexpressed each enzyme in U2OS cells that harbour the Tango assay system. We showed the transgenic DAGLs to be expressed at the membrane, and DAGLα to be active using surrogate substrates. We measured an eCB-dependent CB1 response in the Tango assay, with evidence for kinase activation-dependent eCB signalling, but only a portion of this response appeared to be DAGL-dependent. As a result, we are pursuing a genetic strategy to systematically 'switch off' endogenous eCB production. We first targeted the DAGLs using the CRISPR/Cas9 system, using both wild-type and nickase Cas9. Our next strategy will be to knock-out other eCB-producing enzymes in these cells to tease out which enzymes are resulting in the eCB-CB1 activation in the Tango assay. This will also provide us with a 'parent' cell line to support future mutagenesis studies to understand which (if any) phospho-sites are important for DAGL regulation.

Abbreviations

A	AA	Arachidonic Acid
	Abh-4	α/β-Hydrolase 4
	ABHD6	αβ-Hydrolase Domain-Containing Protein 6
	ABPP	Activity-Based Protein Profiling
	ACEA	Arachidonyl-2'-Chloroethylamide (CB1 Agonist)
	Ach	Acetylcholine
	AD	Alzheimer's Disease
	2-AG	2-Arachidonyl glycerol
	AM251	CB1 Antagonist
	Anadamide	*N*-arachidonoylethanolamine
	ANOVA	Analysis of Variance
	ATP	Adenosine Triphosphate
B	BDNF	Brain-Derived Neurotrophic Factor
	Bla	β-lactamase gene
	bp	Base Pair
C	CamKIIa	Calcium/Camodulin-dependent Protein Kinase IIa
	cAMP	Cyclic Adenosine Monophosphate
	CAMs	Cell Adhesion Molecules
	Cas	CRISPR associated proteins
	Cas9n	Cas9 nickase
	CB	Cannabinoid
	CB1	Cannabinoid Receptor 1
	CB2	Cannabinoid Receptor 2
	CBD	Cannabidiol
	CBN	Cannabinol
	cdDAGLα	Catalytically-dead DAGLα
	cDNA	Complementary DNA
	CIP	Calf Intestinal Phosphastase
	CNS	Central Nervous System
	CRISPR	Clustered Regularly Interspaced Short Pallindromic Repeats
	CST	Cell Signalling Technology
	C_t	Threshold Cycle (qPCR)
D	DAG	Diacylglycerol
	DAGL	Diacylglycerol Lipase
	DAGLα	Diacylglycerol Lipase α
	DAGLβ	Diacylglycerol Lipase β
	dCas9	Catalytially-dead Cas9
	DHEA	Docosahexaenoylethanolamide

	DiFMU	6,8-Difluoro-7-Hydroxy-4-Methylcoumarin
	DiFMUO	6,8-Difluoro-4-Methylumbelliferyl Octanoate
	DNA	Deoxyribonucleic acid
	DSB	Double-Strand Breaks
	DSE	Depolarisation Suppression of Inhibition
	DSI	Depolarisation Suppression of Excitation
E	eCB	Endocannabinoid
	ECL	Enhanced Chemiluminescence
	EPEA	Eicosapentaenoyl ethanolamide
	EPSCs	Excitatory Postsynaptic Currents
F	FABPs	Fatty Acid Binding Proteins
	FAC	Final Assay Concentration
	FACS	Fluorescence-Activated Cell Sorting
	FAAH	Fatty Acid Amide Hydrolase
	FCS	Foetal Calf Serum
	FGF	Fibroblast Growth Factor
	FLAT	FAAH-like Anandamide Transporter
	FRET	Fluorescence Resonance Energy Transfer
	FSK	Forskolin
G	GABA	Gamma-Aminobutyric Acid
	GAPDH	Glyceraldehyde 3-Phosphate Dehydrogenase
	GDE 1	Glycerophosphodiester Phosphodiesterase 1
	GFP	Green Fluorescent Protein
	GL	Gastric Lipase
	GPCR	G-Protein Coupled Receptors
	GP-NAE	Glycerophospho-*N*-Acyl Ethanolamine
	gRNA	guide RNA
H	HA	Homology Arm DNA
	HDR	Homology Directed Repair
	HEK	Human Embryonic Kidney
	HEPES	4-(2-Hydroxyethyl)-1-Piperazineethanesulfonic Acid
	HRP	Horseradish Peroxidase
	HSL	Hormone Sensitive Lipase
I	ICC	Imunnocytochemistry
	Indels	Insertions/Deletions
	IP_3	Inositol Triphosphate
	IPSCs	Inhibitory Post-Synaptic Currents
	iPSCs	Induced Pluripotent Stem Cells

K	KO	Knockout
L	LC/MS	Liquid Chromatogrpahy / Mass Spectrometry
	LPS	Lipopolysaccharide
	LTD	Long-term Depression
	LTP	Long-term Potentiation
M	MAFP	Methoxy Arachidonyl Fluorophosphonate
	MAGL	Monoacylglycerol Lipase
	mGluR	Metabotropic Glutamtae Receptor
	mRNA	messenger RNA
	MS	Multiple Scleorosis
	mw	Molecular Weight
N	NADA	*N*-arachidonoyl dopamine
	NAE	*N*-Acyl Ethanolamine
	NAPE	*N*-Arachidonyl Phosphatidylethanolamine
	NAPE PLD	NAPE Phospholipase
	NCAM	Neural Cell Adhesion Molecule
	NHEJ	Non-Homologous End Joining
	NT	Neurotransmitter
	$N_{18}TH_2$	Neuroblastoma Cell Line
O	OD	Optical Density
	OEA	Oleoylethanolamide
	ON	Overnight
P	PCR	Polymerase Chain Reaction
	PD	Parkinson's Disease
	PDE4	Phosphodiesterase 4
	PE	Phosphatidylethanolamine
	PEA	Palmitoylethanolamide
	PGD2	Prostaglandin D2
	PI	Phosphatidylinositol
	PIP_2	Phosphatidylinositol 4,5-Bisphosphate
	PKA	Protein Kinase A
	PKC	Protein Kinase C
	PL	Pancreactic Lipase
	PLA_2	Phospholipase 2
	PLC	Phospholipase C
	PLD	Phospholipase D
	PNPB	4-Nitrophenyl Butyrate
	PMA	Phorbol 12-Myristate 13-Acetate

	PPAR	Peroxisome Proliferators Activated Receptor
	PPIA	Peptidylprolyl Isomerase A
	PTM	Post-Translational Modification
Q	qPCR	Quantitative PCR
R	RFU	Relative Fluorescent Units
	RMS	Rostral Migratory Stream
	RNA	Ribonucleic Acid
	RNAi	RNA interference
	ROS	Reactive Oxygen Species
	rpm	Revolutions Per Minute
	RT	Room Temperature
	RT-PCR	Reverse Transcription Polymerase Chain Reaction
S	SAG	1-stearoyl-2-arachidonoyl-sn-glycerol
	SDS-PAGE	Sodium Dodecyl Sulfate - Polyacrylamide Gel Electrophoresis
	SEM	Standard Error of the Mean
	SpCas9	Streptococcus Pyogenes Cas9
	SVZ	Sub-Ventricular Zone
	STD	Short Term Depression
T	TALENs	Trancription Activator-Like Effector Nucleases
	Δ^9-THC	Δ^9-Tetrahydrocannabiniol
	THL	Tetrahydrolipstatin
	TLC	Thin Layer Chromatography
	TM	Transmembrane
	TRPV1	Transient Receptor Potential Vanilloid Type-1
U	U2OS	Human Osteosarcoma Cell Line
V	V5α11	Tango (U2OS) cells overexpressing DAGLα
	V5β4	Tango (U2OS) cells overexpressing DAGLβ
W	WB	Western Blot
	WT	Wild Type
	wtDAGLα	Wild-type DAGLα
Z	ZFNs	Zinc Finger Nucleases

Table of Contents

Table of Figures

CHAPTER 1. INTRODUCTION

1.1 History of Endocannabinoid Signalling

The Cannabis genus of flowering plants mainly comprises the *sativa* and *indica* species. Indigenous to Central and South Asia, cannabis has been widely used recreationally and therapeutically for millennia, with the earliest reference to its potential as a medicine being around 2700 BC, in the pharmacopoeia of the Chinese emperor, Shennong also known as the 'God of Chinese herbal medicine' (Russo *et al.*, 2008). Like very many other herbs, it has been used medically for a wide variety of diseases, especially throughout Asia and the Middle East, as well as a pleasure inducing drug. Cannabis can induce altered perception, euphoria, hallucination and enhanced appetite in humans, as well as reduced spontaneous motor activity, immobility, analgesia and impairment of short-term memory (Sugiura *et al.*, 2006). In Victorian times, it was used to promote uterine contractions in childbirth and as a sedative to induce sleep (Di Marzo, 2006). However, the first time the therapeutic effect of cannabis was assessed scientifically was by William O'Shaughnessy, an Irish physician who established his reputation while working in Calcutta by successfully treating tetanus and other convulsive disorders with a local preparation called 'Hemp Resin' and inevitably brought cannabis as a drug to the western world (O'Shaughnessy, 1843).

In the years that followed, the active ingredients of the cannabis plant were discovered, with pharmacological and pharmaceutical efforts beginning in the mid- to late-20th century (Di Marzo, 2006) and the potential therapeutic benefit of cannabis has received continued interest. Although efficacy varies substantially for different indications, the best evidence for the benefit of cannabis therapeutically is for use in painful HIV-associated sensory neuropathy (Phillips *et al.*, 2010), chronic pain (Martin-Sanchez *et al.*, 2009), chemotherapy-induced nausea and vomiting (Machado Rocha *et al.*, 2008; Flachenecker, 2013) and spasms in patients with multiple sclerosis (Flachenecker, 2013). Non-psychoactive substances of cannabis have also been examined for their therapeutic use. For example, cannabidiol (CBD)

is another constituent of cannabis plants may be a useful treatment of epilepsy and other neuropsychiatric disorders (Devinsky *et al.*, 2014). Today, cannabis is the most commonly used drug of abuse; over 2 million people in the UK smoke cannabis and half of all 16 to 29 year olds have tried it at least once (Global Drug Survey, 2015).

1.2 The Endocannabinoid System

Discovery of the Receptors

There was huge growth in the field of endocannabinoid (eCB) research that began with the identification of the receptors specific for the active component of cannabis. The mechanism of action of the plant *Cannabis sativa* was realised through the initial purification and characterisation of its active principles. The major psychoactive component of cannabis is Δ^9-tetrahydrocannabiniol (Δ^9-THC) (Matsuda *et al.*, 1990; Munro *et al.*, 1993). *C. sativa* contains much higher concentrations than *indica* and thus *sativa* strains often have more psychotropic effects (Watson *et al.*, 2000). While the discovery of other plant substances like morphine were already well established, the identification Δ^9-THC remained elusive until the 1960s, when the isolation and structure of this chemical compound was first reported (Gaoni & Mechoulam, 1964).

Initial binding experiments using Δ^9-THC or its natural analogues were unsuccessful due to the highly lipophillic properties of cannabinoids (CBs). New classes of potent and selective synthetic THC analogues were developed, such as HU-210 (Figure 1.1) (Mechoulam *et al.*, 1990). Labelling of HU-210 to generate [^{3}H] HU-245, alongside prior development of the highly potent bi-cyclic CP-55,940 (Pfizer in 1974), led to the pharmacological identification of CB-sensitive sites in the brain. These investigations were carried out in 1988 by Howlett's group using radio-labelled CP-55,940 which allowed the group to identify specific THC binding sites in cortical membrane preparations from rat brain (Figure 1.1) (Devane *et al.*, 1988). Subsequent qualitative and quantitative radioligand-binding studies revealed the distribution of

CB receptors in the brain, with dense binding of [^{3}H] CP 55,940 within the globus pallidus, substantia nigra and striatum of the basal ganglia, the cerebellum, the dentate gyrus of the hippocampus, as well as the cerebral cortex (Herkenham *et al.*, 1990).

These discoveries were quickly followed by the molecular identification of the CB receptors from orphan G protein-coupled receptors (GPCRs). These 7-transmembrane (TM) receptors were activated in response to Δ^9-THC and signalled through the *Bordetella pertussis* toxin-sensitive $G_{i/o}$ protein and subsequent inhibition of adenylate cyclase (Howlett *et al.*, 1986). Following a report on cDNA from a rat brain library encoding a CB receptor, the first human CB receptor was discovered in 1990, consisting of 472 amino acids (Matsuda *et al.*, 1990). The second was in 1993, when a second CB receptor of 360 amino acids was identified in human promyelocytic leukemia cell line, HL60. Rat or human CB receptor clones were able to hybridise with mRNA in undifferentiated HL60 cells and in those that had been differentiated into granulocytes and macrophages (Munro *et al.*, 1993). These receptors were subsequently termed cannabinoid receptor 1 (CB1) and cannabinoid receptor 2 (CB2) respectively, with 48% similarity between the two receptors (68% identity for the TM domains) (Howlett, 2002). Phylogenetic analysis of the relationship of vertebrate CB receptors with other GPRCRs revealed a close relationship between the two CB receptors, which originated from a gene duplication event from a common ancestor (Elphick & Egertova, 2001).

In 1999, the first CB1 knockout (KO) mouse was generated, where mutant mice were largely unresponsive to CB drugs. From this, the CB1 receptor was demonstrated to be the mediator of analgesia, hypotension and hypothermia as well as having an involvement in the motivational aspects of opiates (Ledent *et al.*, 1999); making it an attractive target for many disease implications. The CB1 receptor is highly expressed throughout the mammalian nervous system, but it is also found in some peripheral organs such as the lungs, small intestine and reproductive machinery (Galiegue *et al.*, 1995; Sugiura *et al.*, 2002). The generation of an antibody for the intracellular C-terminal tail of CB1 led to immunohistochemical validation of CB1 receptor localisation. This confirmed its expression in the olfactory system,

cerebellum, neocortex, hippocampus and basal ganglion and was mainly found to be localised in nerve fibre systems and axon terminals (Egertova & Elphick, 2000). CB1 is also expressed in a number of non-CNS neuronal tissues, including the dorsal root ganglion cells and the neuromuscular junction (Howlett *et al.*, 2002).

The creation of a CB2 receptor KO mouse followed shortly after the CB1 KO model (Buckley *et al.*, 2000) and CB2 was found to be mainly expressed in immune cells, such as in the spleen, tonsil and lymph nodes (Munro *et al.*, 1993; Galiegue *et al.*, 1995; Van Sickle *et al.*, 2005). The initial dogma that the CB2 receptor does not have a role in the brain has been revised based on more recent reports showing the CB2 receptor to be involved in neural stem proliferation in cell culture and in the adult mouse (Molina-Holgado *et al.*, 2007; Goncalves *et al.*, 2008; Gao *et al.*, 2010).

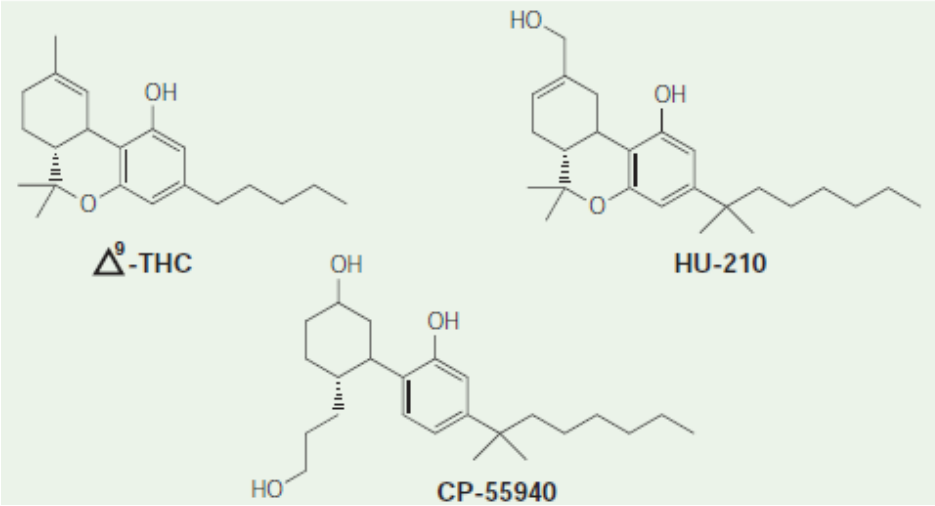

Figure 1.1 Chemical structure of plant-derived and synthetic cannabinoid receptor agonists which activate both CB1 and CB2 receptors

Even though cannabis had been used medically for 1000s of years, it wasn't until the 1960s that is major active component of cannabis, Δ^9-THC was purified and characterised. THC analogues were subsequently developed due to the hydrophobic nature of Δ^9-THC, such as HU-210. Labelling of HU-210 to generate [^{3}H]HU-245, and subsequent development of the bi-cyclic cannabinoid CP-55,940 (Pfizer) led to the pharmacological identification of the specific cannabinoid binding sites in the brain, CB1 and CB2. Neither of the synthetic compounds is more selective for one type of cannabinoid receptor over the other.

Adapted with permission from Piomelli, 2003.

Discovery of the Endocannabinoids

The discovery of the CB receptors in the 1990s implied the existence of natural ligands in the body, thereby initiating a quest to identify the 'endocannabinoids' (eCBs) (Figure 1.2). The first to be identified was the lipid *N*-arachidonyl ethanolamine, also known as anandamide based on the Sanskrit word *ananda* meaning 'bliss'. Because of the lipophillic nature of the chemical constituents of cannabis plants (phytocannabinoids), it was argued that lipid-soluble fractions of the brain should contain the eCB molecule, which led to the chemical identification of anandamide. Devane *et al.* (1992) tested the ability of fractionated organic solvent extracts from porcine brain to displace a radiolabelled probe (HU-243) from rat synaptosomal membranes. This enabled them to isolate and identify the first putative eCB. Anandamide also demonstrated cannabimimetic properties in isolated mouse vas deferens twitch assay in a dose-dependent manner (Devane *et al.*, 1992). This group also demonstrated that anandamide can elicit other properties associated with cannabis, such as spontaneous motor activities, immobility, hypothermia and analgesia when administered to mice.

However, the role of anandamide as an eCB had a few remaining issues. For example, anandamide is a partial agonist at the two CB receptors (unusual for an endogenous ligand) and is found at relatively low concentrations in the brain (Sugiura *et al.*, 2002; Pertwee *et al.*, 2010). Synthetic pathways (described below) were not able to generate sufficient amounts of anandamide, as precursor concentrations are also low (Sugiura *et al.*, 2002). Moreover, anandamide did not fully recapitulate the behavioural effects of Δ^9-THC (Smith *et al.*, 1994). Therefore, the existence of a second eCB was postulated.

Soon after the discovery of anandamide, another derivative of arachidonic acid (AA) was described as an eCB and this was 2-arachidonoylglycerol (2-AG) (Figure 1.2). 2-AG is generated by the rapid hydrolysis of inositol phospholipids by phospholipase C (PLC) and subsequent hydrolysis of the resultant diacylglycerol (DAG) by DAG lipase (DAGL) activity. This was first described by Prescott and Majerus as a degradation pathway for AA-containing DAGs in platelets (Prescott & Majerus, 1983). It was observed that 2-AG was released by simulated cells, such as

Swiss mouse 3T3 cells stimulated by platelet-derived growth factor (PDGF) (Hasegawa-Sasaki, 1985) or bradykinin-stimulated rat dorsal ganglion neurons (Gammon *et al.*, 1989). 2-AG was then shown to be released by other stimuli, for example the membrane depolarising agent, ionomycin. $N_{18}TH_2$ cells released 2-AG into the medium in a calcium-dependent fashion and in a concentration analogous to that released from 3T3 cells (Bisogno *et al.*, 1997b). Calcium-induced 2-AG generation was revealed in rat brain homogenate, with phosphatidylinositol (PI) being the most preferred substrate (Kondo *et al.*, 1998; Sugiura *et al.*, 2006). This group also pointed to the role for PLC, an enzyme regulated by G proteins, in 2-AG generation. This followed the observation that addition of GTPγS enhanced 2-AG generation in brain homogenate in the presence of a low concentration of calcium. It was not until 2003 that the focus shifted from PLC to DAGL, where the cloning and characterisation of the DAGLs was first reported (Bisogno, 2003).

2-AG as an eCB was first described by two separate groups. Mechoulam *et al.* isolated 2-AG from canine gut and then intravenously administered it to rats. This produced the tetrad of effects typically seen with Δ^9-THC; antinociception, immobility, reduction of spontaneous activity and lowering of body temperature. 2-AG also bound to both CB1 and CB2 in membranes from COS cells transiently expressing either one of the CB receptor types (Mechoulam *et al.*, 1995). The effects of anandamide, 2-AG and other related compounds were then compared in synaptosomal membranes. Only 2-AG showed similar displacement of a radiolabelled ligand [^{3}H] CP55940 in the presence of a monoacylglycerol (MAGL) inhibitor; that is it say, when the breakdown of 2-AG was prevented, the effects of 2-AG were revealed. Stella *et al.* (1997) confirmed 2-AG as a prominent constituent of brain tissue that acted as a full agonist at the CB1 receptor. It has the same effect as CB1 synthetic agonists in the hippocampus, whereby 2-AG inhibited long-term potentiation (LTP), an effect blocked by CB1 antagonists (Stella *et al.*, 1997). Furthermore, 2-AG can be released from cells following stimulation (Bisogno *et al.*, 1997b), an important function if 2-AG is to act as a retrograde signalling molecule at synapses.

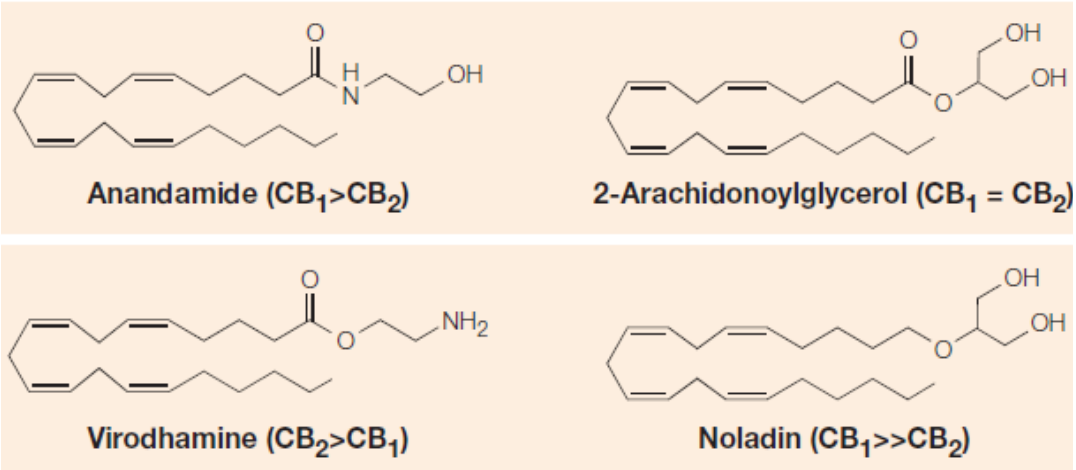

Figure 1.2 Structure of the Endocannabinoids

Structures of the two most well studied endocannabinoids (eCBs) – Anandamide and 2-Arachidonylglycerol (2-AG), and two compounds that may act as eCBs, Virodhamine and Noladin ether, are presented above. Anandamide and Noladin ether exhibit greater affinity towards CB1 when compared to CB2. 2-AG exhibits similar affinity towards both cannabinoid receptors. Virodhamine on the other hand exhibits greater affinity towards the CB2 receptor.

Adapted with permission from Di Marzo, 2004.

2-AG as the "true" endocannabinoid for CB1

Although it was initially viewed as an intermediate to AA synthesis, 2-AG subsequently became regarded as the major eCB in the brain and has been postulated to be the "true" endogenous ligand for the CB1 receptor (Sugiura *et al.*, 1999). There are many reasons for this belief. Anandamide is found in low amounts in mammalian tissues (Stella *et al.*, 1997) and the biosynthetic pathways discovered thus far for anandamide are not able to produce sufficient amounts of the eCB due to low substrate availability (discussed in more detail below). Importantly, there is 800-fold more 2-AG in the rat brain than anandamide (Sugiura *et al.*, 1999) and 2-AG is the most abundant eCB in the developing (Watson *et al.*, 2008), as well as the adult brain (Mechoulam *et al.*, 1995; Sugiura *et al.*, 1995; Stella *et al.*, 1997). This last study showed that the 2-AG isoform is strictly recognised by CB1 and was the most potent ligand, acting as a full agonist at both CB1 and CB2 receptors. Anandamide acted as a partial agonist at CB1 in NG108-15 neuroblastoma cells and a weak agonist for CB2 (Sugiura *et al.*, 1999; Piomelli, 2003; Ross, 2003; Sugiura *et al.*, 2006). Several investigators have also provided evidence that anandamide interacts with binding sites other than the CB receptors and there is evidence that a specific receptor may exist for anandamide. These points are discussed below.

Other eCBs and eCB receptors

Since the discovery of anandamide and 2-AG, a number of other potential ligands and receptors have been identified as eCBs and CB receptors, respectively. The occurrence of several novel structural analogues of anandamide *in vivo* has been reported. Porter *et al.* (2002) demonstrated that an ester-linked isomer of anandamide, *O*-arachidonoyl ethanolamine, is present in the rat brain and human hippocampus and named this compound 'Virodhamine'. Virodhamine acts as an agonist at CB2 and was found at substantial levels in rat striatum lysates, while anandamide was virtually undetectable (Porter *et al.*, 2002). It is not surprising that virodhamine can bind CB receptors in pharmacological assays due its structural similarity to 2-AG (Figure 1.2). However, virodhamine as a true eCB is still in

debate, as it does not contain essential structural groups at the correct location for CB activity. For example, the hydroxyl group adjacent to the ester linkage in the structure of 2-AG has been shown to be 'essential in exhibiting strong agonistic (CB) activity' (Sugiura *et al.*, 1999), which is absent in virodhamine.

N-arachidonoyl dopamine (NADA) has also been shown to act as an eCB. Huang *et al.* (2002) synthesised and purified NADA and showed it could bind to both the CB receptors and the vanilloid receptor, inducing analgesia upon systemic administration and hyperalgesia when intradermally injected (Huang *et al.*, 2002). NADA requires fatty amide amide hydrolase (FAAH) activity for its biosynthesis, which either liberates AA from anandamide or acts as a conjugation enzyme, or both (Bisogno *et al.*, 2000; Hu *et al.*, 2009). Therefore NADA's role in the eCB system is still unclear.

In terms of structural analogues of 2-AG, Hanus *et al.* (2001) reported that 2-AG ether (Noladin ether), an ether linked analog of 2-AG, is present in the pig brain and in small amounts in rat brain (Figure 1.2). Noladin ether could bind selectively to CB1 and CB2, producing behavioural effects in mouse tests (Hanus *et al.*, 2001; Fezza *et al.*, 2002). However, concentrations of noladin ether were not found in significant amounts in a variety of mammalian brains and doubt remains over whether it is a serious candidate as an eCB (Oka *et al.*, 2003; Alexander & Kendall, 2007).

The above related lipids clearly share an ability to bind to and activate CB1 and/or CB2 receptors but it remains to be determined to what extent they actually drive or modulate physiologically relevant eCB responses in the body. More recently, reports have suggested that the anti-proliferative/anti-cancer effects of the ethanolamide derivatives docosahexaenoylethanolamide (DHEA) and eicosapentaenoyl-ethanolamide (EPEA) may be due to their ability to bind, even with low affinity, to both CB1 and CB2 receptors, with DHEA thought to be produced by the same pathway as anandamide (De Petrocellis *et al.*, 2000; Brown *et al.*, 2010; Yang *et al.*, 2011). Therefore these lipids may also be candidate eCBs. On the other hand, these studies were carried out in recombinant or cancer cell lines and so their role as eCBs *in vivo* remains to be determined.

Two naturally occurring acylethanolamides: oleoylethanolamide (OEA) and palmitoylethanolamide (PEA), and two phytocannabinoids: cannabinol (CBN) and CBD, all lack affinity at CB1 / CB2 but still evoke pharmacological and / or cannabimmetic effects, suggesting other CB receptors may exist. Three orphan GPRCRs have been put forward as potential CB receptors and these are GPR119, GPR18 and GPR35. GPR119 is reportedly a receptor for OEA (Overton *et al.*, 2006). However, it is unclear whether the high concentrations of OEA required to activate recombinant GPR119 occur (patho-) physiologically, or whether another as-yet unidentified ligand with greater potency might be the endogenous ligand for GPR119 (Brown, 2007). GPR18, a receptor cloned in 1997, has also been linked to the eCB system when it was shown to be activated by anandamide (Gantz *et al.*, 1997; Kohno *et al.*, 2006; Pertwee, 2006b; a; Rajaraman *et al.*, 2015) and has been implicated in obesity (Rajaraman *et al.*, 2015).

A second orphan GPCR, GPR55 has been suggested as a third CB receptor (Baker *et al.*, 2006; Brown, 2007; Ryberg *et al.*, 2007). The effect of CBs on GPR55 was shown following an *in silico* search on public databases, where two patents described how some CB agonists and antagonists act on the GPR55 receptor. GPR55 is sensitive to certain eCBs and is expressed in the brain, including the hippocampus, where the CB system is thought to play a role in memory (Sylantyev *et al.*, 2013). However, [^{3}H] CP 55,940 (the compound that mimics the action of Δ^{9}-THC) was not shown to be bound in CB-receptor KO mice. There are also conflicting reports of this compound acting as an inverse agonist, rather than an agonist at this receptor (Baker *et al.*, 2006). These observations were based on pharmacological agents that act on CB1/CB2 acting on the GPR55 receptor. Therefore, more physiologically relevant evidence is needed before determining if GPR55 is indeed a CB receptor. In addition, GPR55 has low sequence identity with the CB1 or CB2 receptors. Therefore, the nature and scope of these effects are presently unclear and they may be influenced by the assay and cellular background used for their study.

Structural similarities between synthetic vanilloids and anandamide suggested possible interactions between CB and vanilloid signalling systems (Di Marzo *et al.*, 1998). The first revelations of the structural similarity of anandamide to capsaicin led to the discovery of anandamide's ability to bind the transient receptor potential vanilloid type-1 (TRPV1) (Zygmunt *et al.*, 1999; Smart *et al.*, 2000). The search for endogenous ligands for TRPV1 suggested that anandamide may be one such compound (Ross, 2003), as there is ample evidence that the interaction of anandamide with TRPV1 receptors is specific. For example, TRPV1 actions are blocked by receptor-specific antagonists and not antagonists of CB1 and CB2 receptors; desensitisation of TRPV1 via capsaicin pre-treatment blocks the effects of anandamide; neonatal capsaicin treatment prevents anandamide activation of TRPV1; anandamide-mediated TRPV1 effects are absent from untransfected cells that do not express TRPV1 receptors (Zygmunt *et al.*, 1999; Smart *et al.*, 2000; Ross *et al.*, 2001). Interestingly, both TRPV1 and CB1 are found in brain regions with high expression of the anandamide degrading enzyme, FAAH, pointing to a role for anandamide in acting on the TRPV1 receptor (Egertova *et al.*, 2003).

The peroxisome proliferators activated receptor (PPAR) may serve as a receptor for certain actions of some CB compounds (Burstein *et al.*, 2004; Burstein, 2005) and has been shown to be part of the eCB system through pharmacological methods. 2-AG was shown to activate PPARγ receptors, as evident by PPARγ-specific luciferase reporter in transiently transfected 3T3-L1 cells (Rockwell *et al.*, 2006). The putative role of PPARγ in IL-2 suppression could also be mediated by 2-AG and/or noladin ether in Jurkat T cells, the action of which was blocked by the PPARγ-specific antagonist, 2-chloro-5-nitro-N-(4-pyridyl)-benzamide (T0070907). Likewise, 2-AG suppressed the activity of two transcription factors crucial for IL-2 expression, nuclear factor of activated T cells and nuclear factor kappa B, in the absence but not in the presence of T0070907. 2-AG treatment also induced PPARγ binding to a PPAR response element in activated Jurkat T cells (Rockwell *et al.*, 2006). Furthermore, OEA, anandamide, noladin ether and virodhamine were also found to bind PPARα (Sun *et al.*, 2007). Together, these studies suggest TRPV1 receptors and PPARs as targets for eCBs, in a manner that is independent of CB1 and CB2. These

receptors systems may also exhibit a degree of cross-talk, as PPAR agonists can bind both CB1 and CB2 receptors (Priestley *et al.*, 2014).

In more recent studies, anandamide and 2-AG levels have been selectively elevated using drugs that inhibit FAAH and MAGL, respectively (Cravatt *et al.*, 2001; Schlosburg *et al.*, 2010), also showing that both anandamide and 2-AG can elicit cannabinoid-like effects. However these are again 'pharmacological' effects as the ligands are outside the range of their normal expression levels for considerable periods of time. Confounding factors include the facts that anandamide will also act on TRPV1 receptors (Zygmunt *et al.*, 1999) and high levels of 2-AG can readily desensitise, as well as activate CB1 (Chanda *et al.*, 2010). Due to the much greater pharmacological and physiological evidence available, the CB1 and CB2 receptors, together with anandamide and 2-AG as their endogenous ligands, remain the best characterised and most widely studied ligand/receptor components of the eCB system.

1.3 Synthesis & Degradation Pathways of the Endocannabinoids

In order to establish a more comprehensive understanding of eCB signalling, it is important to understand how and where the putative eCBs are synthesised and broken down. This dictates whether they have an opportunity to serve as ligands for the CB receptors. Unlike most other neurotransmitters (NTs), which are water soluble and stored in membrane-delineated vesicles before release, the eCBs are hydrophobic neutral lipids that appear to be biosynthesised and released at the moment of their intended action, using an 'on-demand' type of production (Marsicano *et al.*, 2003). The processes that underlie the biosynthesis of eCBs have been extensively studied for 2-AG and anandamide. It is believed that the diversity of the signalling pathways in which anandamide, 2-AG and other potential eCBs partake implies their significant roles in various physiological conditions and evidence suggests that these pathways are differentially regulated in the nervous system (Hoover *et al.*, 2008). These features indicate that the enzymes involved in eCB production and degradation are important regulators of signalling.

Anandamide: Synthesis and Degradation

Anandamide belongs to a class of signalling lipids called N-acyl ethanolamines (NAEs), which are ubiquitous trace constituents of animal and human tissues and cells (Schmid, 2000). Studies by Schmid and colleagues first identified NAEs as markers of ischemic shock in brain and heart tissues. They postulated that NAE-phospholipids are precursors of the biologically active NAEs (Natarajan *et al.*, 1982). NAEs have been implicated in diverse physiological processes, including nociception, cognition, anxiety, appetite and inflammation (Simon & Cravatt, 2006). In 1992, when anandamide was identified as an eCB, there was renewed interest in NAEs and interest into its biosynthesis began. However a detailed understanding of the biosynthetic pathway(s) for NAEs and anandamide has proven hard to pin down. Since anandamide is usually accompanied by much larger amounts of (CB receptor-

inactive) saturated and mono-unsaturated NAEs, it is of interest to determine to what extent anandamide is selectively synthesised, transported and degraded (Schmid, 2000).

Multiple synthetic pathways have been proposed for anandamide synthesis (Figure 1.3). Originally, two possible mechanisms of anandamide formation had been suggested: (1) energy-dependent condensation of free arachidonate with ethanolamine, or (2) release by phospholipase D (PLD)-mediated cleavage of the phospholipid precursor arachidonyl phosphatidylethanolamine (PE). Di Marzo *et al.*(1994) suggested that because levels of free arachidonate and ethanolamine are low in neurons, the first pathway was unlikely to be the primary pathway for anandamide biosynthesis, as it would require a plethora of enzymes to be co-activated in order to occur. For example, phospholipase 2 (PLA2) or PLC to generate arachidonate and PLD to generate ethanolamine and inhibitors of these enzymes had no effect on ionomycin-stimulated anandamide formation (Di Marzo *et al.*, 1994). By using [^{3}H] ethanolamine labelled cultured neurons, this group were able to demonstrate that ionomycin stimulated anandamide synthesis and that *N*-arachidonyl phosphatidylethanolamine (*N*-acyl PE, or NAPE) could act as an anandamide precursor. In one hydrolytic cleavage step, anandamide could be produced and this was presumably through the action of an endogenous phosphodiesterase (Di Marzo *et al.*, 1994). Indeed, stimuli that enhanced formation of anandamide increased NAPE turnover in cultured neurons. Certain physiological stimuli may cause anandamide formation specifically by activating distinct biochemical pathways, in analogy with platelet-activating factor (Yue & Feuerstein, 1994).

Calcium-stimulated anandamide synthesis was then described as a two-step process. First, calcium activates a (yet to be defined) transacylase which catalyses the formation of NAPE (Cadas *et al.*, 1997). This NAPE intermediate is then converted via a hydrolytic step by PLD into an NAE and phosphatidic acid (Figure 1.3 A) (Schmid, 2000; Leung *et al.*, 2006). The NAPE-specific PLD (NAPE-PLD) thought to be involved was then cloned (Okamoto *et al.*, 2004) and was shown to be expressed in various organs in mice, including the brain and is highly conserved in sequence from rodents to human. It belongs to the metallo-lactamase family of

enzymes and could catalyse the formation of anandamide from NAPE *in vitro* (Okamoto *et al.*, 2004). NAPE-PLD soon established itself as the likely synthetic enzyme for anandamide synthesis (Ligresti *et al.*, 2005). However none of these (or related studies) directly tested whether NAPE-PLD was required for anandamide biosynthesis *in vivo*.

Characterisation of this enzyme was next studied by way of a NAPE-PLD KO mouse and measured endogenous levels of NAPEs and NAEs by LC-MS (Leung *et al.*, 2006). While saturated and mono-unsaturated NAEs were decreased, surprisingly there were no differences in anandamide (i.e. polyunsaturated NAEs) levels observed in the brains of these KO mice. The fact that NAPE-PLD affected levels of certain NAEs while leaving others unaffected, suggested cells could exert significant control over NAE biosynthesis by expressing distinct NAPE-PLDs. The results suggested the existence of multiple biosynthetic pathways for NAEs *in vivo;* NAPE-PLD being principally responsible for generating very long chain saturated NAEs and other, as of yet, unidentified enzymes contributing to the production of long chain saturated and polyunsaturated NAEs, including anandamide. Consistent with this premise, brain homogenates from NAPE-PLD KO mice possessed a residual calcium-independent enzymatic activity equivalent to WT controls, converting NAPEs to NAEs, indicating that in the absence of millimolar calcium which is required for maximal activation of NAPE-PLD (Ueda *et al.*, 2001), a significant fraction of NAE biosynthesis proceeds through an alternative pathway.

At least two other pathways have since been suggested. Simon *et al.* (2006) reported that a significant amount of NAPE-PLD-independent anandamide synthesis could be blocked by methoxy arachidonyl fluorophosphonate (MAFP), a general inhibitor of the serine hydrolase class of enzymes in both NAPE-PLD (+/+) and (-/-) mice brains. They suggested that NAE synthesis from NAPE proceeds through a serine hydrolase-catalysed double deacylation of NAPE to generate glycerophospho-NAE (GP-NAE), followed by the phosphodiesterase-mediated cleavage of this intermediate to liberate NAE. This led to the cloning and identification of the serine hydrolase α/β-hydrolase 4 (Abh4), which can selectively deacylate both NAPEs and lysoNAPEs en route to generating GP-NAE (Simon & Cravatt, 2006). This was

subsequently demonstrated *ex vivo* (Simon & Cravatt, 2008). The EDTA-sensitive conversion of GP-NAE to anandamide was attributed to metal dependent glycerophosphodiester phosphodiesterase 1 (GDE1), whereby double *O*-deacylation by Abh4 to yield GP-NAE, followed by GDE1-mediated conversion of this lipid intermediate to anandamide (Figure 1.3 B). Both Abh4 and GDE1 are expressed in various tissues including the brain (Simon & Cravatt, 2008). However neither GDE1 KO mice nor GDE1/NAPE-PLD double KO mice showed significant decrease in anandamide levels in the brain compared to WT control. Treatment with FAAH inhibitors in the double KO also resulted in the accumulation previously seen (Johnson *et al.*, 2009), indicating GDE1 and NAPE-PLD together contribute towards NAE synthesis with potential cross-talk between the two pathways, as this was not seen in GDE1 KO alone (Simon & Cravatt, 2010a). Additionally, rat brain tissues have been shown to contain lyso-PLD activity that can generate anandamide from lyso-NAPE (Sun *et al.*, 2004).

A third pathway involved in the bacterial endotoxin, lipopolysaccharide (LPS)-stimulated synthesis of anandamide in macrophages has also been described. This pathway involves an unidentified PLC and dephosphorylated by phosphatase 22 (PTPN22), previously described as a tyrosine phosphatase (Figure 1.3 C). The LPS-induced synthesis of anandamide in macrophages is mediated exclusively by the PLC/phosphatase pathway, which is up-regulated by LPS. Conversely, NAPE-PLD is down-regulated by LPS and functions as a salvage pathway of anandamide synthesis when the PLC/phosphatase pathway is compromised (Liu *et al.*, 2006). Although it is generally accepted that NAPEs are the precursors for NAEs, the precise enzymatic steps leading to release of NAEs, anandamide in particular, from NAPEs are unclear.

Anandamide signalling is terminated through its cellular uptake and subsequent catabolism by the endoplasmic reticulum-localised enzyme, FAAH (Deutsch & Chin, 1993; Cravatt *et al.*, 2001). Due to the intracellular localisation of FAAH, an anandamide transporter has been postulated to mediate internalisation and diffusion across the hydrolytic cytosol. Identifying this transporter has generated interest as a therapeutic target and to date, several proteins capable of binding anandamide have been identified. For example, trafficking of anandamide from the plasma membrane via a non-vesicular mechanism can be mediated by cytosolic carriers, such as Hsp70 and serum albumin (Oddi *et al.*, 2009). Fatty acid binding proteins (FABPs) were also shown to mediate anandamide transport. Anandamide uptake and hydrolysis were significantly potentiated in N18TG2 neuroblastoma cells after overexpression of FABP5 or FABP7 (Kaczocha *et al.*, 2009). Similarly, a catalytically-silent, partly cytosolic variant of FAAH was shown to drive anandamide transport in Neuro-2A cells and was termed FAAH-like anandamide transporter (FLAT) (Fu *et al.*, 2012). FLAT bound anandamide with low micromolar affinity and facilitated its translocation into cells, an effect blocked by the known anandamide transport inhibitors, AM404 and OMDM-1 (Beltramo *et al.*, 1997; Ortar *et al.*, 2003). However, all of these studies used overexpressing recombinant systems and examined anandamide accumulation at long time points, leaving the results obtained open to debate. Furthermore, elevation of anandamide via AM404 can be assigned to inhibition of COX-1 and COX-2 activity (discussed in more detail below) (Hogestatt *et al.*, 2005). Anandamide transport has subsequently been described as a diffusion process. More recently, a study showed that fluorescently-labelled anandamide was transported into endothelial cells exclusively by TRPV1 in a calcium-dependent manner (Hofmann *et al.*, 2014). Therefore, anandamide transport into the cells is still in debate.

While synthetic pathways and cellular uptake mechanisms for anandamide are still uncertain, there is a clear consensus that anandamide degradation in the CNS and in peripheral tissues is mediated by the well characterised enzyme, FAAH (Figure 1.3 D) (Cravatt *et al.*, 1996). FAAH KO mice had barely detectable levels of anandamide hydrolytic activity and 15-fold higher brain anandamide levels compared to WT control. FAAH KO mice also displayed cannabimimetic

behavioural effects that ‘rivalled THC’ in terms of efficacy and duration (Cravatt *et al.*, 2001). Genetic (Cravatt *et al.*, 2001; Lichtman *et al.*, 2004b) and pharmacological (Lichtman *et al.*, 2004a; Jhaveri *et al.*, 2008; Ahn *et al.*, 2009) disruption of FAAH not only elevates brain levels of anandamide but also produces CB1-dependent analgesia in multiple pain assays. These findings clearly show that anandamide can act at CB1 receptors, but again this has to be viewed as “pharmacological” activity, as the anandamide levels are substantially higher than those normally seen in the body.

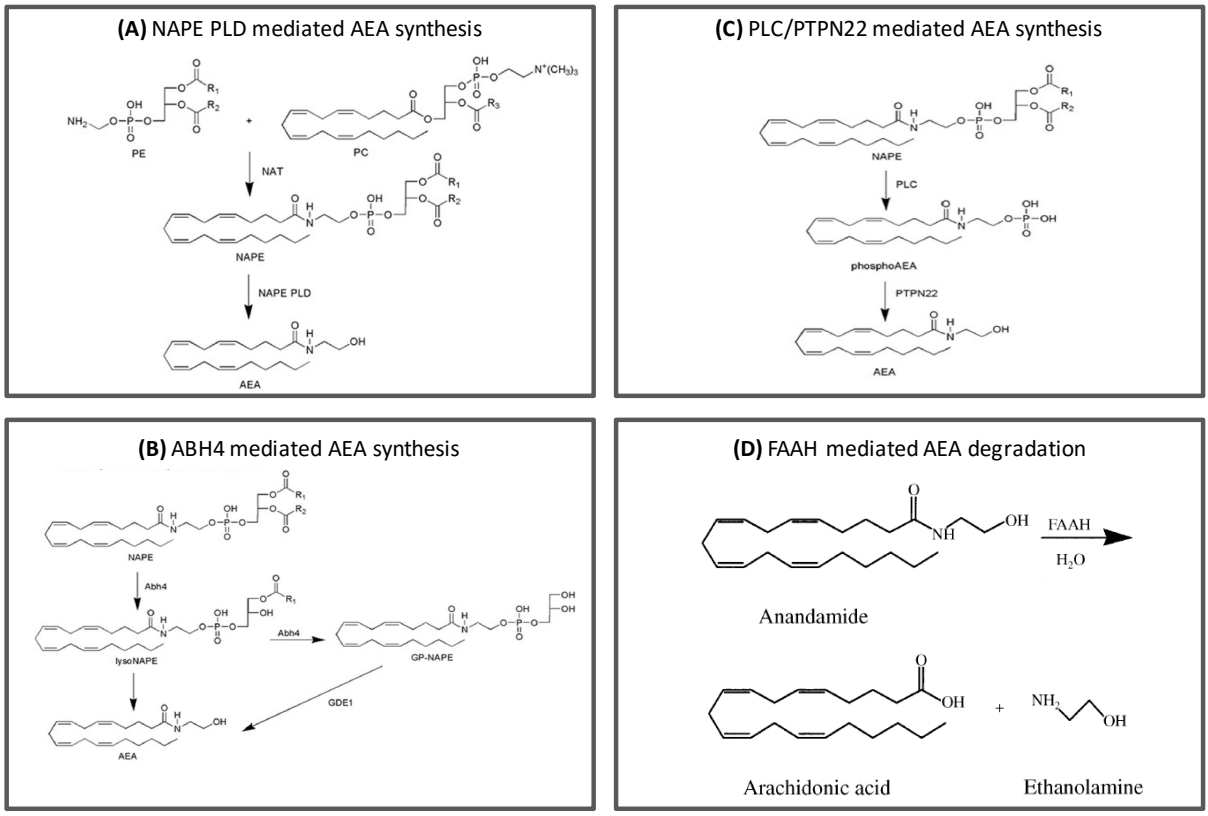

Figure 1.3 Putative pathways involved in AEA synthesis and the primary pathway involved in AEA degradation

A. N-acyl transacylase (NAT) is believed to catalyse the formation of N-acyl phosphatidylethanolamine (NAPE) using phosphatidylethanolamine (PE) and phosphatidylcholine (PC). NAPE can then be hydrolysed to Anandamide (AEA) by a NAPE-specific phospholipase D (NAPE-PLD).

B. The serine hydrolase α/β-hydrolase 4 (ABH4) can deacylate both NAPE to lyso-NAPE and then lyso-NAPE to glycero-NAPE. Glycerophosphodiesterase 1 (GDE 1) can then convert glycerol-NAPE to AEA. Rat tissues also contain lysoPLD activity that can convert lyso-NAPE to AEA.

C. A third pathway involved in lipopolysaccharide (LPS) stimulated synthesis of AEA in macrophages involves an unidentified phospholipase C (PLC) converting NAPE to phosphor-AEA and then phosphatases including protein tyrosine phosphatase 22 (PTPN22) that convert phosphor-AEA to AEA.

D. Fatty acid amide hydrolase (FAAH) hydrolyses AEA to arachidonic acid (AA) and ethanolamine.

Adapted with permission from Deutsch et al., 2002 and Placzek, 2008.

2-AG: Synthesis and Degradation

Even though 2-AG has been shown to be generated through combined actions of PLA1 and PLC (Sugiura *et al.*, 1995) and from AA-containing lysophosphatidic acid in the rat brain through the action of a phosphatase (Nakane *et al.*, 2002), the main synthetic pathway for formation of 2-AG is through combined actions of PLC and diacylglycerol lipase (DAGL). 2-AG is formed from AA-containing phospholipid bilayers in response to cellular stimuli. The steady-state levels as well as the 'on-demand' synthesis of 2-AG are regulated by two sn-1 specific DAGLs, DAGLα and DAGLβ (Bisogno, 2003). This pathway consists of hydrolysis by PLC of inositol phopholipids containing AA at sn-2 position and further hydrolysis by DAGL of the resultant AA-containing DAG. PI serves as the most preferred phospholipid substrate for 2-AG formation in the brain (Sugiura *et al.*, 2006). This is the beginning of 2-AG synthesis, consisting of hydrolysis of phosphatidylinositol 4,5-bisphosphate (PIP_2) by PLC into DAG and inositol triphosphate (IP_3), and further hydrolysis of DAG by DAGL to 2-AG (Figure 1.4).

DAG is an essential second messenger in mammalian cells and is synthesised in response to the activation of a number of cellular signalling cascades, including activation of GPCRs (Brose *et al.*, 2004). DAG is able to bind to C_1 domains of a large number of proteins with diverse functions. The most prominent DAG targets belong to the PKC family of serine/threonine kinases. Binding of DAG, often in synergy with IP_3 release of intracellular Ca^{2+} leads to the membrane translocation and activation of certain PKCs (Brose *et al.*, 2004). In a second pathway, as mentioned above, 2-AG may be produced by sequential hydrolyses of PI via lyso PI, which are catalysed by PLA1 and lyso PI-specific PLC (Ueda *et al.*, 1993). However since the identification and cloning of the two DAGLs, α and β, these enzymes are now accepted as the synthetic enzymes for 2-AG generation, and are discussed in more detail below.

Following synthesis and release, 2-AG can be taken up through the anandamide transporter and metabolised by FAAH. However FLAT expression in HEK-293 cells did not alter [^{3}H] 2-AG transport, nor did the FLAT inhibitor ARN272 increase

plasma 2-AG in mice (Fu *et al.*, 2012). Furthermore, inactivation of FAAH by pharmacological or genetic intervention does not result in elevation of 2-AG (Cravatt & Lichtman, 2002; Deutsch *et al.*, 2002; Di Marzo, 2008).

The main degradative enzyme for 2-AG *in vivo* is MAGL, which hydrolyses 2-AG to AA and glycerol (Figure 1.4) (Beltramo & Piomelli, 2000; Piomelli *et al.*, 2000; Dinh *et al.*, 2002; Muccioli *et al.*, 2007; Long *et al.*, 2009a; Schlosburg *et al.*, 2010). The selective MAGL inhibitor, JZL184 raises brain 2-AG concentrations by 8-10 fold (without altering anandamide) and JZL184-treated mice exhibit the tetrad of CB activity (analgesia, hypothermia, hypomobility and catalepsy) and mimic much of the pharmacological profiles typically seen with CB1 agonists (Cravatt *et al.*, 2001; Wiley & Martin, 2003). Therefore, MAGL is considered the 2-AG hydrolysing enzyme. However, two other serine hydrolases have also been to shown to hydrolyse 2-AG, namely ABHD6 and ABHD12 (Blankman *et al.*, 2007). This study showed that approximately 85% of brain 2-AG was hydrolysed by MAGL, while the remaining 15% was hydrolysed by either ABHD6 and/or ABHD12; JZL195 was also shown to be capable of inhibiting ABHD6, albeit at a lower potency than that seen for MAGL (Long *et al.*, 2009b). Interestingly, these three 2-AG hydrolysing enzymes have distinct subcellular distributions, suggesting that they may control different pools of 2-AG in the nervous system (Blankman *et al.*, 2007).

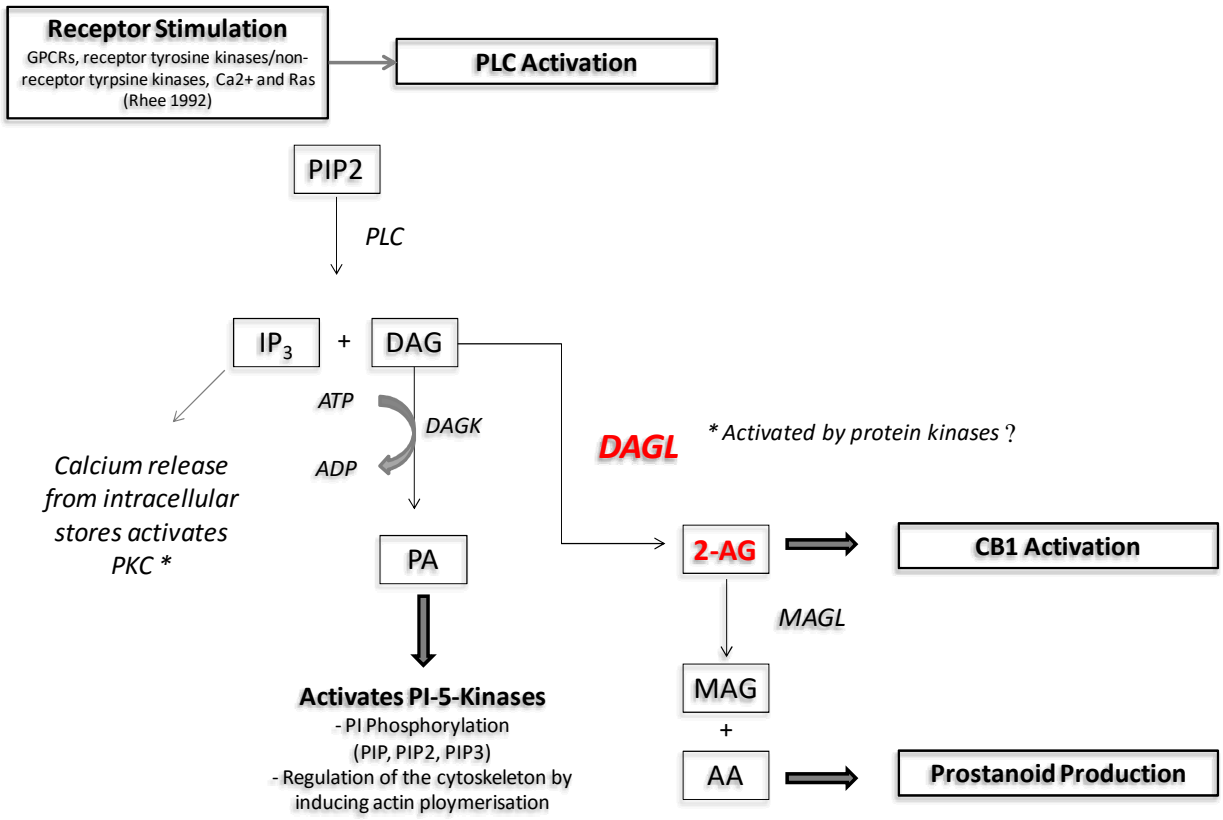

Figure 1.4 On-demand Synthesis of 2-AG is regulated by the DAGLs

2-arachidonylglycerol (2-AG) synthesis begins with activation of phospholipase C (PLC) following cell stimulation, which hydrolyses phosphatidylinositol 4,5-bisphosphate (PIP_2) into inositol triphosphate (IP_3) and diacylglycerol (DAG) (A). IP_3 initiates intracellular calcium release and PKC activation. DAG is further hydrolysed to 2-AG by DAG lipase (DAGL, both in red) which itself is activated by PKC. 2-AG is further hydrolysed by monoacylglycerol lipase (MAGL) to arachidonic acid (AA), the precursor to prostaglandin synthesis. However, it is believed that an increase in DAGL activity can lead to an increase in 'on-demand' 2-AG production, which is then available for signalling through the CB1 receptor.

2-AG and Anandamide as substrates for COX-2

Oxidation is another route for eCB metabolism. Both 2-AG and anandamide have been found to be substrates for cyclooxygenase (COX)-2, the key enzyme required for the conversion of AA to prostaglandins (Kozak *et al.*, 2004). Two COX isoforms have been identified, COX-1 and COX-2. In general, COX-1 is produced constitutively by gastric mucosa, whereas COX-2, discovered more recently, is inducible at sites of inflammation and also in the CNS. Several observations prompted investigations into the ability of COX-2 to utilise the eCBs as substrates, including co-localization of components of the eCB system. For example, the expression of COX-2 in the central nervous and immune systems parallels the distribution of the CB1 and CB2 receptors, respectively (Herschman, 1996; Felder & Glass, 1998). In addition, 2-AG is present at high levels in regions of the brain and in immune cells where COX-2 is expressed (Stella *et al.*, 1997; Bisogno *et al.*, 1999).

Evidence for anandamide and 2-AG as COX-2 substrates has mainly been provided through *in vitro* studies, such as oxygenation of anandamide by recombinant COX-2 (and not COX-1) to the prostaglandin E2 ethanolamide in cell lysates and human cell lines (Yu *et al.*, 1997). COX-2 mediated 2-AG oxygenation generated the 'novel lipid' prostaglandin H (2) glycerol ester (PGH_2-G) *in vitro* as well as in cultured macrophages, the production of which was prevented by inhibition of DAGL, PLC, as well as PGD synthase (Kozak *et al.*, 2000). Endogenous cellular stores of 2-AG have been shown to support PGH_2-G biosynthesis in a stimulus-induced manner (Kozak *et al.*, 2000). Additionally, PGH_2-G has been shown to be a substrate for PGD synthase, raising the possibility that the class of glyceryl PGs is as diverse as the well-known AA-derived metabolites, but again so far has only been shown *in vitro* (Kozak *et al.*, 2002). There is some evidence *ex vivo* from isolated rabbit lung, where anandamide increased pulmonary hypertension via COX-2 metabolites following enzymatic degradation by FAAH into AA products, an effect completely obliterated by the FAAH inhibitor methyl arachidonyl fluorophosphanate (MAFP) (Wahn *et al.*, 2005). However, this study showed anandamide as a precursor for COX-2 substrates, and not as a substrate itself. Finally, anti-nociceptive effects of eCBs were enhanced when FAAH was inhibited in a hind paw model of inflammatory hyperalgesia. COX-2 inhibition increased anti-nociception,

presumably by blocking action of COX-2 on eCBs (Jhaveri *et al.*, 2008). These findings are the result of how specific polyunsaturated fatty acids, the substrate for eCB biosynthesis, and the signalling of the eCB system may influence COX and its activity, with subsequent implications in neuroinflammatory diseases.

Identification and Characterisation of DAGL signalling

DAGL activity first came to the fore as a key enzymatic step for AA release from membrane phospholipids as an alternative to the established pathway involving PLA_2 activity. AA concentrations released from thrombin-stimulated platelets depended on both DAGL and PLC activity, and DAGL activity could be stimulated by calcium. DAGL had 'sufficient activity to provide for the burst of arachidonate released after platelet stimulation', and was not due to PLA_2, as previously thought (Bell *et al.*, 1979). The metabolism of DAG to AA was later identified as a two-step mechanism. This signalling pathway involves the generation of the substrate DAG by PLC and subsequent hydrolysis by DAGL at the sn-1 position, leading to release of 2-AG (Prescott & Majerus, 1983) which is subsequently hydrolysed by MAGL to AA and glycerol (Figure 1.4).

Isolation of purified DAGL was first attempted from bovine brain. Its activity was identified to be adenosine triphosphate (ATP)-dependent, displaying a more potent inhibitory activity from ATP compared to ADP, while cAMP marginally increased activity and AMP had no effect (Farooqui *et al.*, 1984). DAGL was subsequently purified from bovine brain microsomes. At low concentrations neither calcium nor magnesium had a direct effect on enzyme activity but a threefold increase was observed after phosphorylation by a cAMP-dependent protein kinase (Rosenberger *et al.*, 2007). This became relevant to neuroscience, when the DAGL-MAGL pathway was demonstrated to release AA from cultured dorsal root ganglion neurons (Allen *et al.*, 1992).

Early DAGL studies relied heavily on the semi-selective DAGL inhibitor RHC80267 (Sutherland & Amin, 1982), which also displays a considerable efficacy towards other serine lipases. Comparing another DAGL inhibitor tetrahydrolipstatin (THL) with RHC80267, a minimal overlap of target profiles was seen, indicating that an effect seen by both drugs has a high likelihood to be a DAGL-dependent event. Furthermore, in the case of a known CB1/CB2 receptor-dependent event, RHC80267 remains helpful regarding the differentiation between a 2-AG- and an anandamide- mediated event (Hoover *et al.*, 2008). THL, also known as orlistat, is

more prominently known for its inhibition of pancreatic lipase. This lipase is well studied in the context of weight loss (Hadvary *et al.*, 1991). OMDM-188 (an analogue of THL) is very specific and promised to be the leader for the next generation of DAGL inhibitors (Ortar *et al.*, 2008). More recently, relatively selective DAGLβ inhibitors have been developed which reduce 2-AG and AA synthesis in macrophages (Hsu *et al.*, 2012) and could help differentiate between DAGLα and DAGLβ activities. Cloning of the DAGLs and generation of KO mice has highlighted the importance of these enzymes for 2-AG synthesis and that regulatory mechanisms may exist for their function.

1.4 Identifying potential regulatory mechanisms for the DAGLs

In order to assess the regulatory mechanisms of the DAGLs, detailed analysis of the structure is essential to see if there is any potential for a role of post-translational modifications (PTMs). Characterisation of lipases was initially driven by the food industry, where the lipid composition of fungi was essential for oil and fat processing, as well as in medicine, food additives, diagnostic reagents and cleaners. For example, the gene encoding for a 39 kDa enzyme that can hydrolyse mono- and diacylglycerides was crystalised from *Penicillium camembertii*, a fungus used in the manufacture of Camembert and Brie cheeses (Yamaguchi *et al.*, 1991; Derewenda *et al.*, 1994). Although biochemical characterisation the DAGLs was first attempted over 30 years ago (Farooqui *et al.*, 1984; 1986), to date very little is known about how these enzymes are regulated. Due to the vast area of therapeutic implications associated with the DAGLs and the eCB system (discussed in more detail in section 1.5), there is an increasing interest into how these enzymes are regulated.

The DAGLs are membrane bound proteins which are notoriously difficult to crystallise, owing to their partially hydrophobic surfaces, flexibility and lack of stability (Carpenter *et al.*, 2008) and as such the crystal structures for the DAGLs are not yet available. Using homology and bioinformatics to build a working model of the DAGLs has provided a template for developing testable hypotheses on the mechanisms that regulate DAGL activity and has allowed our group to identify key sites on the enzymes that most probably regulate function (Reisenberg *et al.*, 2012).

Conservation and domain structure of the DAGLs

The DAGLs α and β were cloned in 2003, by first aligning the fungal DAGL crystal structure with drosophila genome, which identified a single related molecule. This sequence was compared to the human genome, which identified the two homologues designated α and β (Yamaguchi *et al.*, 1991; Bisogno, 2003; Reisenberg *et al.*,

2012). DAGLα gene product is 1, 042 amino acids in length, with a molecular weight of ~120 kDa. DAGLβ on the other hand is 672 amino acids long and is ~74 kDa (SDS-PAGE) (Bisogno, 2003). The two gene products show extensive homology throughout, with the major difference being that the α isoform has a 'tail' region extending from the catalytic domain, which is absent in DAGLβ (Figure 1.5). The alpha isoforms appears to be under more tight evolutionary constraint as it harbours sequence stretches almost identical to those found in the fly (Gareth Williams, unpublished data). The α and β sequences show a high degree of conservation between human and mouse DAGL – 97% for DAGLα and 79% for DAGLβ. Homology between the two DAGLs is about 35%, which is even higher in the catalytic domain (Figure 1.5 and Gareth Williams, unpublished data.)

The membrane topology consists of a short cytosolic N-terminus, followed by the transmembrane (TM) domain, consisting of 4 helices that span the cell membrane and are separated and linked by short loops; two extracellular and two intracellular. The leading N-terminus is highly conserved between drosophila and vertebrate DAGLα, pointing towards an important, but unknown function. However this is less conserved between DAGLα and DAGLβ (63% homology) (Reisenberg *et al.*, 2012). The TM domains may serve as docking sites for other proteins in a functional complex, or form part of a channel that regulate DAG access to the catalytic domain, or indeed 2-AG release from cells. However deletion of the region does not impact on catalytic activity or 2-AG availability to CB receptors. (Won *et al.*, 2009).

Using online web search tools our group identified the two extracellular loops as potential sites for glycosylation (Su *et al.*, 2014). Glycosylation is a form of PTM in which a glycan is attached to a hydroxyl (or other functional) group. Glycans serve a variety of structural and functional roles in membrane and secreted proteins and have an important role in protein folding. Recently, a 'DAG-like lipase' from *Malassezia globose* was cloned and recombinantly expressed, which was indeed shown to be glycosylated (Xu *et al.*, 2015).

Tetraspanins, a family of membrane-bound proteins found in all eukaryotic cells, are thought to act as scaffolds, anchoring multiple proteins to one area of the cell

membrane. In a likeness to the DAGLs, tetraspanins have 4 TMs forming a distinct class of membrane domains, the tetraspanin-enriched microdomains by associating with other transmembrane receptors and with themselves. The TM domains of the DAGLs might also facilitate packing of the enzymes at the membrane, in analogy with tetraspanins into microdomains (Yanez-Mo *et al.*, 2009).

Following from the TM domain, the second intracellular loop extends into the catalytic domain (followed by the carboxyl-terminal 'tail' domain in the case of DAGLα). The structure of the DAGLs' catalytic domain is a member of the α/β hydrolase fold family of enzymes. The α/β hydrolase fold is a common tertiary protein structure to a large number of enzymes with diverse functions, yet have virtually no sequence similarity, and is therefore a typical example of evolution from a common ancestor. The family includes lipases, peptidases and esterases (Nardini & Dijkstra, 1999; Holmquist, 2000). The fold consists of 8 mostly parallel β strands (the second is anti-parallel) constituting a β sheet (Figure 1.6 A). This is surrounded on both sides by α helices. The catalytic residues in the family always constitute a triad: a nucleophile (serine, cysteine or aspartic acid), an acidic residue and an absolutely conserved histidine. The DAGLs' catalytic triad consists of a serine, aspartic acid, and histidine (Figure 1.6 B) (Bisogno, 2003; Pedicord *et al.*, 2011). Among members of this enzyme family, there may be differences in the degree of twisting of the β-sheet and also spatial positioning of the α helices. However, αC is highly conserved and is probably necessary for the appropriate position of the nucleophilic acid at the active site (Figure 1.6) (Nardini & Dijkstra, 1999).

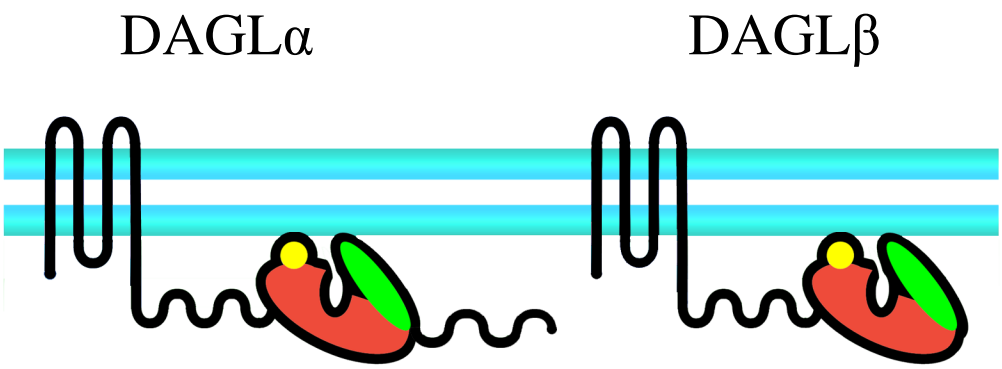

Figure 1.5 Structural features of the DAGLs

Diagram showing the overall domain structure of DAGLα and DAGLβ. The figure indicates the 4TM domains (black lines crossing the membrane), the intracellular catalytic domain (red), containing the cysteine rich insert and regulatory loop (yellow and green, respectively), with the extended tail domain in case of DAGLα.

Adapted from Reisenberg et al., 2012.

The nucleophile is always located in a sharp turn, the 'nucleophile elbow'. This structure plays an important role in presenting the substrate to the nucleophile and access of water molecule for hydrolysis (Nardini & Dijkstra, 1999). Within the α/β hydrolase fold family, it is located within a consensus Sm-X-Nu-X-Sm sequence (Sm=small residue, X=any residue and Nu=nucleophile); in the DAGLs this sequence is Gly-His-Ser-Leu-Gly (Figure 1.7, boxed). The catalytic residues and nucleophile elbow are absolutely conserved between human DAGLα and DAGLβ (and also in mouse), as highlighted in their primary sequence alignment in Figure 1.7. Therefore, the α/β hydrolase fold in the DAGLs' catalytic domain provides a stable scaffold for the active site.

Our group exploited sequence information from the fungal MAGL/DAGL from *Penicillium camembertii* in order to gain insights into the human DAGLα/β structural features (Derewenda *et al.*, 1994). In addition to the motifs conserved between fungus and man that we assume must define the catalytic activity of the enzyme, there are additional sequence stretches in the mammalian enzyme located within the catalytic domain. These are a cysteine-rich domain just before the catalytic serine residue and an intriguing domain between the catalytic aspartic acid and histidine residues. This latter domain is a common feature to lipase members of the α/β hydrolase fold family. This feature can move position and orientation depending on the conformational position of the enzyme, thereby regulating substrate access to the catalytic site (Nardini & Dijkstra, 1999; Karageorgos *et al.*, 2013; Xu *et al.*, 2015). This domain is intriguing as it harbours a highly conserved motif of ten residues completely conserved in the alpha, beta and fly versions of DAGL. Both inserts within DAGLs' catalytic domain are explored in more detail in the next section.

Figure 1.6 The core structure to the α/β hydrolase fold compared to that predicted for the DAGLs

(A) The structure of the 'canonical' α/β hydrolase fold consists of mostly parallel 8 β strands which make up the core β sheet, with only the second (β2) being anti-parallel (grey arrows). The β sheet is surrounded on both sides by α helices (white cylinders). The conserved nucleophile, acid and histidine constitute the catalytic triad (black dots). Insertions are tolerated amongst members of this enzyme family and can be found at certain locations, such as between the first two α helices and between the 7th and 8th β strands, as indicated by the dashed lines.

Figure A- Adapted (with permission) from Nardini & Dijkstra, 1999.

(B) The predicted structure of the DAGL catalytic domain with the canonical α/β hydrolase fold, consisting of a β-sheet linked by α helices, as seen in A. The DAGLs contain a 20-24 amino acid long cysteine-rich insert between the first two α helices, which may be a palmitoylation sites (as indicated). The catalytic triad (green circles) is harboured by a serine, aspartic acid and histidine. There is a second, 50-60 amino acid insert of unknown structure between the 7th and 8th β strands. Its proximity to the catalytic triad mean it may act as a lid to shield the catalytic site from substrate access. This has been termed the 'regulatory loop' (Reisenberg *et al.*, 2012).

A

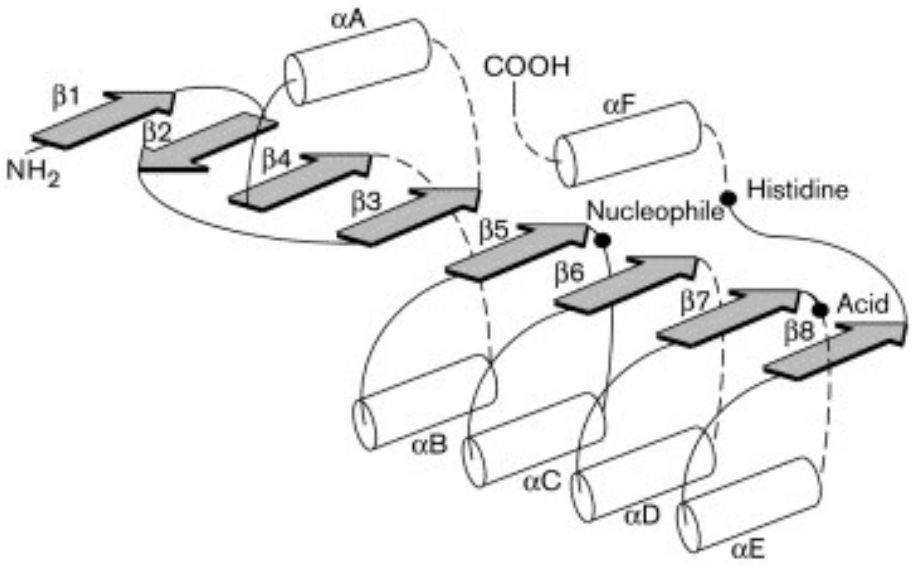
αA
COOH
β1
β2
NH2
β4
β3
αF
Histidine
Nucleophile
β5
β6
β7
Acid
β8
αB
αC
αD
αE

B

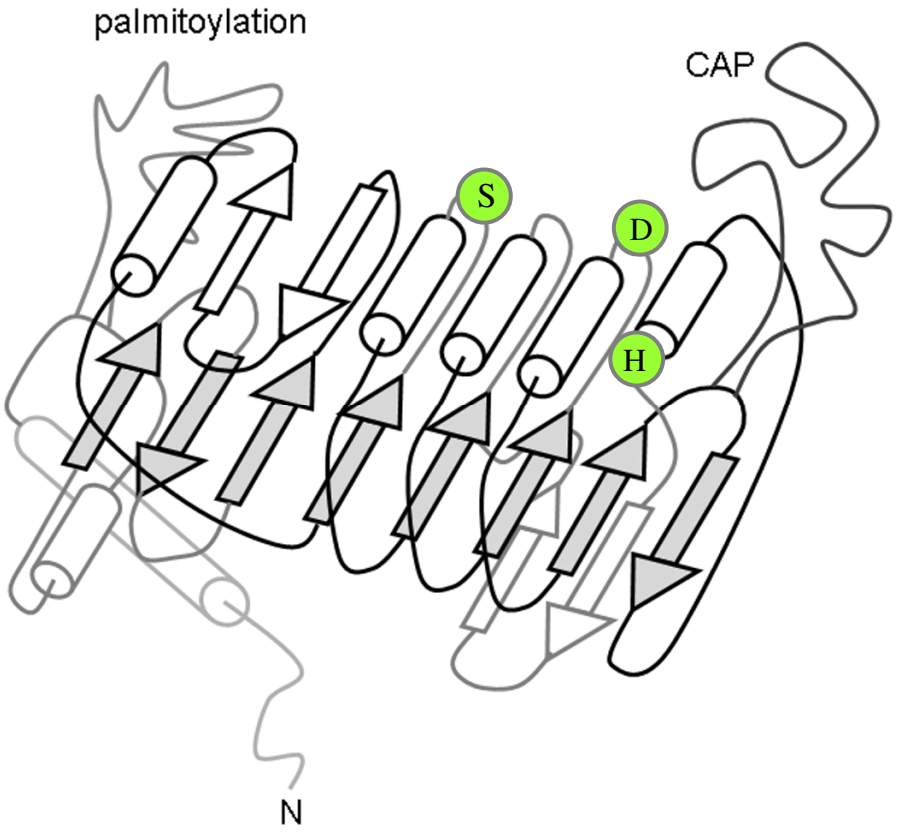
palmitoylation
CAP
S
D
H
N

The Cysteine Rich Insert

Aligning amino acid DAGL sequences from *P. camembertii* and human DAGLs revealed that DAGLα and DAGLβ sequences contain a 20-24 amino acid long cysteine rich insert within the catalytic domain (Figure 1.5, yellow; Figure 1.7, blue), between the first two alpha helices (Figure 1.6 B), which may contain a palmitoylation site (Reisenberg *et al.*, 2012). Protein palmitoylation refers to the PTM involving addition of a fatty acid to the side chain of a cysteine, forming a covalent thioester linkage. It is estimated that ~ 5% of the proteome comprises enzymes that perform more than 200 types of PTMs (Gonzalez-Montelongo *et al.*, 2013). Palmitoylation is reversible and is a potential regulatory mechanism for proteins, as well as their subcellular trafficking. It increases the hydrophobity of proteins, thereby enhancing membrane association (reviewed in (Mitchell *et al.*, 2006). This insert could therefore act to regulate DAGL activity by affecting its localization at the membrane.

Evidence for palmitoylation of both DAGLα and DAGLβ has been provided from three independent proteomic studies (Kang *et al.*, 2008; Martin & Cravatt, 2009; Yang *et al.*, 2010). One of these studies mapped this to cysteines 610/611 in the regulatory loop region within DAGLβ catalytic domain (Figure 1.7), although the authors did note the possibility of inaccurate localization of the palmitoylated site (Yang *et al.*, 2010). One lipase known to be palmitoylated is phospholipase D (PLD). Palmitoylation is essential for correct membrane localization and endocytosis of PLD (Du *et al.*, 2003). This process could also be important for DAGL location, as co-factors that collaborate with DAGL during development are also palmitoylated; for example the cell adhesion molecules L1 and NCAM. This might allow for coordinated function between these proteins and organization into signalling complexes in order to promote efficient signal transduction (Reisenberg *et al.*, 2012).

```
                                        TRANSMEMBRANE DOMAINS

            Intracelluar                      TM1
hDAGLα      MPGIVVFRRRWSVG                SDDLVLPAIFLFLLHTTWFVILS 37
hDAGLβ      MPGMVLFGRRWAIA                SDDLVFPGFFELVVRVLWWIGIL 37
            *** * * ***                   ***** *  *       *   *

            Extracelluar                      TM2
hDAGLα      VVLFGLVYNPHEACSLNLVD        HGRGYLGILLSCMIAEMAIIWL 79
hDAGLβ      TLYLMHRGKLDCAGGALLSS        YLIVLMILLAVVICTVSAIMCV 79
                        *                       *       **

            Intracelluar                      TM3
hDAGLα      SMRGGILYTEPRDSMQYVLY        VRLAILVIEFIYAIVGIVW 118
hDAGLβ      SMRGTICNPGPRKSMSKLLY        IRLALFFPEMVWASLGAAW 118
            **** *    ** **   **         ***    *   *  *  *

            Extracelluar                      TM4
hDAGLα      LTQYYTSCNDLTAKNV            TLGMVVCNWVVILSVCITVLCVF 157
hDAGLβ      VADGVQCDRTVVNG--            IIATVVVSWIIIAATVVSIIIVF 155
                                            **  *  *         **

            Intracelluar
hDAGLα      DPTGRTFVKLRATKRRQRNLR-TYNLRHRLEEGQATSWSRRLKVF  201
hDAGLβ      DPLGGKMAPYSSAGPSHLDSHDSSQLLNGLKTAATSVWETRIKLL  200
            ** *                        *   *       *

hDAGLα      LCCTRTKDSQSDAYSEIAYLFAEFFRDLDIVPSDIIAGLVLLRQR  246
hDAGLβ      CCCIGKDDHTRVAFSSTAELFSTYFSDTDLVPSDIAAGLALLHQQ  245
             *          * *  * **   * * * ***** *** ** *

hDAGLα      QRAKRNAVLDEANNDILAFLSGMPVTRNTKYLDLKNSQEMLRYKE  291
hDAGLβ      QDNIR------NNQEPAQVVCHAPGSSQEADLDAELEN-------  277
            *   *       *          *       **

hDAGLα      VCYYMLFALAAYGWPMYL  309
hDAGLβ      CHHYMQFAAAAYGWPLYI  295
                * ** ****** *

                          CATALYTIC DOMAIN

hDAGLα      MRKPACGLCQLARSCSCCLCPARPRFAPGVTIEEDNCCGCNAIAI  354
hDAGLβ      YRNPLTGLCRIGGDC----CRSRTTDYDLVGGDQLNCHF------  330
             * *  ***          *  *      *     **

hDAGLa      RRHFLDENMTAVDIVYTSCHDAVYETPFYVAVDHDKKKVVISIRG  399
hDAGLβ      GSILHTTGLQYRDFIHVSFHDKVYELPFLVALDHRKESVVVAVRG  375
                        *    * ** *** ** ** **    **   **

hDAGLα      TLSPKDALTDLTGDAERLPVEGHHGTWLGHKGMVLSAEYIKKKLE  444
hDAGLβ      TMSLQDVLTDLSAESEVLDVECEVQDRLAHKGISQAARYVYQRLI  420
            * *  * ****    * * **      * ***    * *

hDAGLα      QEMVLSQAFGRDLGRGTKHYGLIVVGHSLGAGTAAILSFLLRPQY  489
hDAGLβ      NDGILSQAFSIAP-----EYRLVIVGHSLGGAAALLATMLRAAY  460
                *****          *    ****** * ** *   **

hDAGLα      PTLKCFAYSPPGGLLSEDAMEYSKEFVTAVVLGKDLVPRIGLSQL  534
hDAGLβ      PQVRCYAFSPPRGLWSKALQEYSQSFIVSLVLGKDVIPRLSVTNL  505
            *   * * *** ** *    ***  *    *****  **     *
```

Figure 1.7 Multiple sequence alignment of human DAGL*α* and DAGLβ

Multiple sequence alignment was performed using the alignment program from EMBL, 'CLUSTALW'. Key structural features are segregated, including the transmembrane domains (TM 1–4) and their linking helices, the catalytic domain, including the cysteine rich insert (highlighted in blue), regulatory loop (orange text), catalytic triad (highlighted in green), nucleophile elbow (box) and the highly conserved signature motif (orange text, highlighted in purple). Key phospho-sites identified are notated in pink bold underlined text to highlight their position within the DAGLs' sequences.

The DAGLs contain a Regulatory Lid

Large insertions are tolerated amongst members of the α/β hydrolase fold family, while maintaining conserved catalytic activity (Nardini & Dijkstra, 1999) thereby accounting for the array of functional differences between members of this family (Suplatov *et al.*, 2012). Most lipases have their active site buried beneath a flap or lid-like domain that changes conformational shape to allow substrate access to the active site (Holmquist, 2000). Examples of this can be seen in gastric lipase (GL) and pancreatic lipase (PL) – when in the 'closed' state, this lid acts as a barrier to the substrate (van Tilbeurgh *et al.*, 1992; Canaan *et al.*, 1999). Lipases hydrolyze poorly soluble substrates (Rubin & Denis, 1997). The lid therefore is responsible for 'interfacial activation', a process consisting of the enzyme forming a complex with a protein, thus indirectly opening the lid to act on water-insoluble substrates at water-lipid interfaces (Winkler *et al.*, 1990; van Tilbeurgh *et al.*, 1992). While the size of the lid varies between lipases, it is always well positioned to act as a lid. For example, it consists of 24 amino acids in PL (Winkler *et al.*, 1990), 124 amino acids in GL (Miled *et al.*, 2003) and as an even larger 150 amino insert in hormone sensitive lipase (HSL) (Lampidonis *et al.*, 2011). In GL, the large 'surface loop' is described as two domains consisting of a 'cap' domain and a second 'lid' domain segment of 58 residues, where both are important for the activity of HSL (as evident from mutagenesis studies) (Miled *et al.*, 2003).

The lid-like structure in the DAGLs was first identified as a substantial 50-60 amino acid insert of unknown structure between the 7^{th} and 8^{th} β strands (Figure 1.6 B). This insert is coded by a single exon and has been referred to as the 'regulatory loop' (Reisenberg *et al.*, 2012). Homology with fungal DAGL confirms that this regulatory loop is well positioned to the catalytic triad to act as a lid shielding the catalytic site, as in the case of GL, PL and HSL. The DAGL lid is a considerably large, suggesting the potential for substantial conformational changes determining whether the lid is open or closed (Reisenberg *et al.*, 2012). The most remarkable feature of the regulatory loop is the presence of a highly conserved motif (PLYPPGRIIH) (highlighted in dark blue, Figure 1.7). This sequence is conserved in both human DAGLα and DAGLβ, as well as across mammalian, vertebrate and also found in plants, but less well conserved plant DAGLs (Reisenberg *et al.*, 2012).

Although this conservation indicates it as an important binding site, the interaction is probably intra-molecular rather than inter-molecular, as the latter would require conservation of a binding partner. Therefore this sequence is possibly involved in stabilisation of the 'open' or 'closed' conformation of the regulatory loop and has been termed the 'signature motif' (Reisenberg *et al.*, 2012).

Understanding how the activity of DAGL is regulated, or what causes the regulatory loop to shift from the 'closed' to the 'open' state, is essential in order to design small molecules that specifically target either one of the DAGLs for therapeutic use. The potential for this was highlighted in a study on phosphodiesterase 4 (PDE4). Inhibitors of this enzyme were shown to either stabilise the 'capped state' or occupy the uncapped catalytic packet. The discoveries helped to demystify complex inhibition kinetics associated with compounds that can inhibit certain enzymes, and highlighted the potential to develop inhibitors specific for PDE4 isoforms (Houslay & Adams, 2010). The ability to target the 'dual-gating' regulatory mechanism of PDE4 demonstrates that specific inhibitors could also be developed for the DAGLs, following a greater understanding of how they are regulated. Discovering key sites important for DAGL regulation would enable effective drug design for therapeutic intervention. However, in addition to generating the new hypothesis, there remains a requirement to develop new assays to directly measure DAGL activity in cells, and also DAGL-dependent eCB signalling in cells.

Creation of DAGL KO mice

Following cloning of the DAGLs, proof of their importance 2-AG synthesis was obtained in studies on DAGLα or DAGLβ KO mice which highlighted differential functions for the enzymes (Gao *et al.*, 2010; Tanimura *et al.*, 2010). In the brain and spinal cord (where DAGLα is enriched) of DAGLα -/- mice, there was an 80% reduction in 2-AG levels in these areas, whereas in DAGLβ -/- there was only a 50% reduction (Figure 1.8). In an independent study, DAGLα KO mice displayed an 80% reduction in 2-AG in the cerebellum, hippocampus and striatum, with little change to these brain regions in DAGLβ KO mice (Tanimura *et al.*, 2010). Importantly, this

study also showed that stimulus-induced increases in 2-AG are also lost in the brains of the DAGLα KO mice, such as depolarisation-suppression of inhibition (DSI) in cultured hippocampal neurons (2-AG's role in DSI is discussed in more detail later).

DAGLα is also expressed in adipose tissue and liver; in the KO animals these tissues had a 60% and 50% reduction in 2-AG, respectively (Gao *et al.*, 2010). DAGLβ KO had no impact on adipose tissue, but in the liver resulted in a 90% reduction in 2-AG. These studies show that the DAGLs are responsible for maintaining steady-state levels of 2-AG and their individual contribution depends on the tissue in which they are expressed. These results are highlighted in Figure 1.8.

Anandamide levels were also affected, with a 40% decrease in the brains of DAGLα -/- mice and 20% in DAGLβ -/- brains (Gao *et al.*, 2010). It has been suggested to be a result of phospholipid remodelling in KO mice, which affects the fatty acid composition of brain precursors for NAPE (Di Marzo, 2011), revealing a degree of crosstalk between these lipids. This was demonstrated when either MAGL or FAAH were inhibited individually, resulting in compensation activity of one enzyme when the other is inhibited (Long *et al.*, 2009b). The crosstalk between anandamide and 2-AG biosynthesis can make it difficult to dissect one from the other, and data needs to be interpreted with this in mind.

2-AG can act as a precursor to AA synthesis by way of MAGL hydrolysis. AA levels changed in parallel with 2-AG changes in the brain and spinal cord in DAGLα KO mice (~80% reduction) as well as 90% reduction in 2-AG in the liver of DAGLβ KO mice (Gao *et al.*, 2010), indicating 2-AG to be the main precursor and points to a role for DAGL activity in the regulation of AA synthesis. In combination with pharmacological studies, DAGLα and DAGLβ KO animals have unravelled crucial roles for these enzymes in development, synaptic plasticity, and adult neurogenesis and as mediators for prostaglandin synthesis; these functions are discussed below.

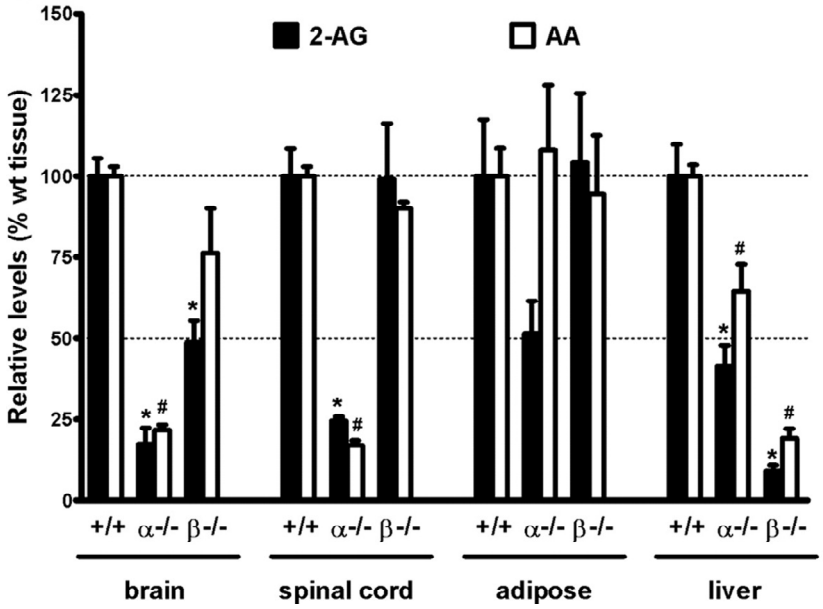

Figure 1.8 Comparison of 2-AG and AA levels in wild-type and DAGL KO mice

2-AG and AA levels were measured in tissues of mice lacking DAGLα (α -/-) and DAGLβ (β -/-) and compared to wild type mice control. Levels of 2-AG were markedly decreased in the brain and spinal cord in α-/- mice, resulting in a 80% decrease, whereas β-/- mice had no significant difference in the spinal cord and 50% reduction in the brain. There was a 50% reduction in 2-AG in the adipose tissue while no significant reduction was observed in β -/- mice. In the liver, there was a 50% reduction in 2-AG in α-/- mice, compared to a 90% reduction in the liver of β -/- mice. Reduction in AA levels changed in parallel with the reductions in 2-AG in the brain, spinal cord and liver, most notably was 80% reduction in AA levels in brain and spinal cord of α-/- mice and a 90% reduction in AA in the liver of β -/- mice.

Adapted with permission from Gao et al., 2010.

1.5 Functions of DAGL-dependent eCB Signalling

Axonal Growth and Guidance in Development

The growth cone is a dynamic, actin-supported extension of a developing axon that extends fine filopodia to explore the environment. The process of extending the axon is regulated in a highly specific manner by growth cone receptors, which can promote or inhibit directed growth in response to positive or negative cues, respectively (Tessier-Lavigne & Goodman, 1996). Fasciculated growth can be driven by cell adhesion molecules (CAMs) and involves axons extending together in an ordered manner. It was initially thought that CAMs role in promoting growth was to modulate adhesion of the growth cones to their substrates. It is now known that they can initiate a second-messenger signalling cascade, for example, activation of the fibroblast growth factor (FGF) receptor and that this signalling can drive the axonal growth response (Walsh & Doherty, 1997).

The eCB system plays a key role in development of the nervous system and its contribution to brain development is increasingly recognised (Bisogno, 2003; Begbie *et al.*, 2004; Keimpema *et al.*, 2010; Wu *et al.*, 2010; Keimpema *et al.*, 2013). There is considerable evidence to support this hypothesis, including the observation that the CB1 receptor is expressed by neurons during development (Buckley *et al.*, 2000; Begbie *et al.*, 2004), axonal growth stimulated by CAMs requires DAGL-dependent CB1 activation (Williams *et al.*, 2003), eCB signalling is both chemoattractive and chemorepulsive to cortical interneurons (Berghuis *et al.*, 2005; Berghuis *et al.*, 2007) and finally, eCBs are involved in proliferation of neural progenitor cells, as well as their differentiation into their glial and neuronal fates (Jin *et al.*, 2004; Aguado *et al.*, 2005; Jiang *et al.*, 2005; Aguado *et al.*, 2006). Much of the early work in cultured neurons, involving a morpholino-based strategy to knockdown CB1 in the developing zebrafish, showed that eCB signalling is essential for fasciculated axonal growth in the developing hindbrain (Watson *et al.*, 2008). The phenotype of these zebrafish was not dissimilar to that seen in the developing rat retina when DAGL activity is inhibited (Brittis *et al.*, 1996), whereby axons exhibited unusual behavior,

lacking fasciculated growth with some turning back on themselves. The signalling cascade within the growth cone, initiated by activation of the FGF receptor, involves stimulation of PLCγ to generate DAG, which in turn is hydrolysed by DAGL to generate 2-AG. This then acts on CB1 on the same growth cone to promote motility (Williams *et al.*, 2003).

Interestingly, a key role for DAGL activity in growth of the axon *in vivo* was proposed, before it was recognised that 2-AG was a CB1 receptor ligand (Brittis *et al.*, 1996; Lom *et al.*, 1998). In these early experiments, neurite outgrowth required a DAGL-dependent step in the FGF receptor pathway, downstream from PLCγ activation but upstream from calcium influx. Later experiments provided evidence that CB1 receptor activation was both required for and sufficient to account for the response (Williams *et al.*, 2003). Therefore, DAGL-dependent eCB signalling is required for axonal growth and guidance. Its importance was demonstrated in the growth promoting activity of FGF2 (FGF receptor agonist) and a number of CAMs by making 2-AG available for CB1 activation (Bisogno, 2003). In support of this is the fact that MAGL is excluded from the motile neurite tip of the growth cone, being confined further back along the axon, thereby allowing 2-AG to be available to activate CB1 in a highly restricted manner and this is required for axonal growth (Figure 1.9) (Keimpema *et al.*, 2010).

Understanding the role of the eCB system during development is also important in the context of human health, as cannabis is one of the most widely used drugs during pregnancy (Hall & van Teijlingen, 2006). In conjunction with the key role of the eCB system during development, the impact of THC exposure during pregnancy has gained considerable attention, given the long-lasting effects of prenatal cannabis use on emotional control, social behaviours and cognition in affected offspring (Huizink & Mulder, 2006).

Figure 1.9 DAGL-dependent eCB signalling is required for axon growth and guidance

(A) The signalling cascade within the growth cone is initiated by activation of the FGF receptor followed by stimulation of PLCγ to generate DAG, which in turn is hydrolysed by DAGL to generate 2-AG. In this version of eCB signalling, 2-AG does not need to leave the cell, whereby it acts on the CB1 receptor on the same growth cone to promote motility and fasciculated growth.

(B) Pyramidal cells emit the first axons in cerebral circuits. Their axons exhibit moderate CB1 expression (CB1R), being distributed along the axis of the elongating axon. The DAGLs are co-expressed in excitatory axons, allowing eCB signalling to drive elongation of the growing axon. 2-AG is in much greater abundance than anandamide (AEA) and is therefore the more likely eCB to be involved. However this does not eliminate the possible, but as yet unidentified, role of anandamide.

Adapted with permission from Harkany et al., 2008.

(C) Schematic of the the axonal growth cone. MAGL (green) expression is restricted further down along the axon. This allows 2-AG, synthesised by DAGLα (orange), to be available for CB1 (red) activation resulting in stimulatation of motility and direction of the growth cone.

Adapted with permission from Oudin et al., 2011.

A

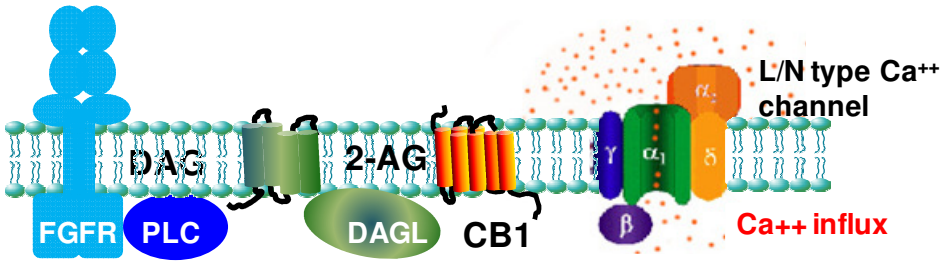
DAG
2-AG
FGFR
PLC
DAGL
CB1
L/N type Ca++ channel
Ca++ influx

B

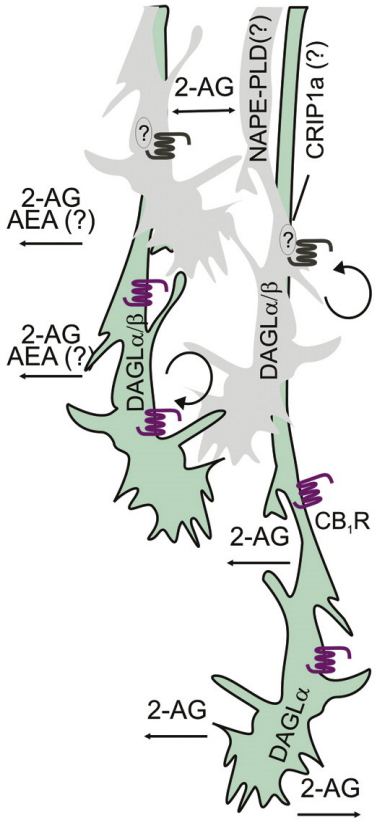
2-AG
NAPE-PLD(?)
CRIP1a (?)
2-AG
AEA (?)
2-AG
AEA (?)
DAGLα/β
DAGLα/β
CB1R
2-AG
2-AG
DAGLα
2-AG

C

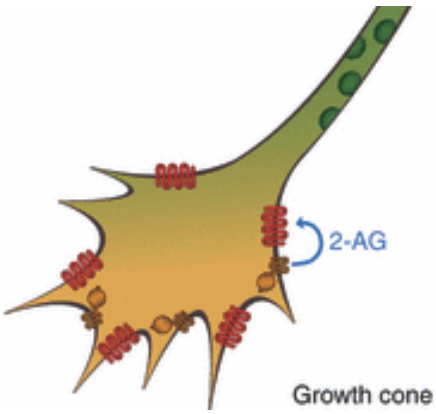
2-AG
Growth cone

Synaptic Plasticity – Investigating the role for DAGL in the Adult Brain

In the paper that reported the cloning of the DAGLs, a switch in DAGLα expression from the growing axon during development to dendritic fields in the adult was noted. It is now clear that DAGLα expression is lost from axons after synapses form, but retained at high levels in dendritic spines throughout the CNS (Bisogno, 2003; Yoshida *et al.*, 2006). This switch in expression explains the switch in function of DAGL-dependent eCB signalling from the role in axonal growth and guidance during development, to the role in retrograde synaptic signalling at functional synapses in the adult. Coupled with the fact that CB1 is restricted to the presynaptic terminal in the adult, the eCB system exhibits a molecular architecture that underpins its key role in synaptic plasticity. In this context, the role of the eCB system in retrograde synaptic signalling and synaptic plasticity was established in 2001, prior to the identification of the DAGLs (Kreitzer & Regehr, 2001; Maejima *et al.*, 2001; Ohno-Shosaku *et al.*, 2001; Wilson & Nicoll, 2001). It is now recognised that DAGL-dependent eCB signalling plays a role in both short- and long-term synaptic plasticity throughout the brain and spinal cord (Kano *et al.*, 2009).

Synaptic plasticity is the ability of both excitatory and inhibitory synapses to strengthen or weaken over time in response to increases or decreases in their activity. There are several underlying mechanisms that cooperate to achieve synaptic plasticity, including changes in the quantity of neurotransmitters (NTs) released into a synapse and changes in how effectively cells respond to those NTs. For most of the past century, communication between nerve cells was considered to be polarised and that it took place at synapses between a sending cell that was presynaptic and a receiving cell that was postsynaptic.

Retrograde signalling refers to the process by which a messenger is released by a postsynaptic dendrite and travels "backwards" across a chemical synapse to bind to the axon terminal of the presynaptic neuron (Regehr *et al.*, 2009). Retrograde signalling regulates release of a NT, thereby affecting synaptic strength. In this sense retrograde neurotransmission mainly serves to regulate typical, anterograde

neurotransmission. In the 1990s, retrograde signalling became an accepted phenomenon. During this decade there were many reports on retrograde inhibition of neurotransmission. For example, brief activation of Purkinje cells in cerebellar slices induced a retrograde inhibition of presynaptic terminals (Llano *et al.*, 1991). Using inhibitory post-synaptic currents (IPSCs), suppression of gamma-aminobutyric acid (GABA)-ergic signalling was shown in CA1 pyramidal cells of the hippocampus following post-synaptic modulations in calcium (Pitler & Alger, 1992). This phenomenon, whereby depolarisation of postsynaptic neurons induces a transient suppression of inhibitory synaptic transmission, was termed depolarisation suppression of inhibition (DSI) (Alger & Pitler, 1995). The fact that DSI is triggered by elevation in calcium concentration and is associated with a reduction of NT release from postsynaptic terminals (Pitler & Alger, 1992; Vincent & Marty, 1993) strongly suggested the involvement of retrograde signalling (Figure 1.10).

One of the first studies to describe inhibition of neurotransmission by CBs was in 1970, where acetylcholine (Ach) release in the guinea-pig ileum was inhibited by Δ^9-THC (Gill *et al.*, 1970). Following the generation of CB1 antibodies and subsequent immunohistochemical studies, together with KO studies, CB1 was identified as a predominantly presynaptic receptor throughout the adult brain and spinal cord (Katona *et al.*, 2006; Kawamura *et al.*, 2006) at both excitatory and inhibitory synapses (Egertova & Elphick, 2000), including at presynaptic terminals of glutaminergic synapses in the hippocampus and other areas of the brain (Ferraro *et al.*, 2001). The CB1 receptor therefore is well positioned to modulate NT release via a retrograde messenger and this has been backed up by extensive pharmacological studies - reviewed by Schlicker and Kathmann (Schlicker & Kathmann, 2001). For example, Cadogan *et al.* demonstrated that anandamide and the CB1 agonist CP-55,940 could inhibit dopamine release in electrically stimulated rat striatal and cortical slices, which was reversed by Rimonabant (SR141716), a selective CB1 antagonist (Cadogan *et al.*, 1997). The CB1 agonist WIN 55,212-2 inhibited release of noradrenaline in the hypothalamus and striatum, as well as GABA and ACh release from human hippocampal slices, an effect blocked by the CB1 antagonist, SR141716 (Gobel *et al.*, 2000; Katona *et al.*, 2000). CB agonists inhibited serotonin activity in the cerebral cortex (Nakazi *et al.*, 2000) and ACh release in the medial

prefrontal cortex, hippocampus, and striatum (Carta *et al.*, 1998; Gessa *et al.*, 1998) an effect again blocked by SR141716 (Gessa *et al.*, 1998; Tzavara *et al.*, 2003). CB1 activation inhibits glutamate release in the cerebellum, hippocampus, prefrontal cortex and substantia nigra (Sullivan, 1999; Auclair *et al.*, 2000; Hoffman & Lupica, 2000; Nakazi *et al.*, 2000). CB1 activation was also shown to modulate synaptic transmission itself. This was demonstrated in a study looking at Purkinje cells in rat cerebellar slices, where both excitatory postsynaptic currents (EPSCs) and sIPSCs were strongly inhibited by WIN 55212-2, an effect again blocked by SR141716 (Takahashi & Linden, 2000).

In 2001, two groups provided evidence that an eCB was serving as a retrograde messenger in DSI using cultured hippocampal neurons (Ohno-Shosaku *et al.*, 2001) and hippocampal slices (Wilson & Nicoll, 2001). At the same time, Kreitzer and Regehr discovered the counterpart for DSI, depolarisation suppression of excitation (DSE) is also mediated by eCBs in cerebellar Purkinje cells (Kreitzer & Regehr, 2001). (An overview of the role of the eCB system in DSI and DSE is highlighted in Figure 1.10) In the same year, two groups discovered another form of eCB-mediated short term depression (STD) in the cerebellum (Maejima *et al.*, 2001) and in the hippocampus (Varma *et al.*, 2001). Activation of group 1 metabotropic glutamate receptors (mGluR1s) on postsynaptic neurons induced a transient suppression of synaptic transmission at excitatory synapses on cerebellar Purkinje cells (Maejima *et al.*, 2001) and inhibitory synapses on CA1 pyramidal cells (Varma *et al.*, 2001), which was sensitive to CB1 antagonists and therefore used an eCB as a retrograde messenger.

A form of striatal synaptic plasticity, long-term depression (LTD) was also shown to be dependent on the eCB system. Striatal LTD induced by high frequency stimulation of corticostriatal afferents was prevented by pharmacological or genetic depletion of CB1, indicating the involvement of eCBs in a circuit necessary for habit formation and motor control (Gerdeman *et al.*, 2002). LTD was demonstrated at glutamatergic synapses of the nucleus accumbens, which was eCB-dependent and involved mGluRs and elevation in postsynaptic intracellular calcium stores,

revealing a role of the eCB system in the endogenous brain reward system (Robbe *et al.*, 2002).

The precise mechanisms of eCB production for retrograde signalling, initiated by physiologically relevant synaptic activity was next examined. eCB-mediated retrograde suppression can be triggered by membrane depolarisation that elevates intracellular calcium concentrations to a micromolar range (Brenowitz & Regehr, 2003). Activation of Gq-coupled receptors, including mGluR1, coupled with PLCβ pathway (leading to the production of DAG) also causes eCB-mediated suppression of synaptic transmission (Maejima *et al.*, 2001; Kim *et al.*, 2002; Ohno-Shosaku *et al.*, 2003) Muscarinic Ach receptor activation also stimulates eCB release, resulting in DSI in the hippocampus (Kim *et al.*, 2002). Finally, eCB-mediated retrograde suppression results from cooperative action of Gq-coupled receptor activation and elevated intracellular calcium concentration (Varma *et al.*, 2001; Hashimotodani *et al.*, 2005; Maejima *et al.*, 2005). Of these, the third mode appears physiologically most relevant as eCB-mediated retrograde suppression is induced by weak activation of Gq-coupled receptors and physiological increase in intracellular Ca^{2+} to a submicromolar range, neither of which by itself produces suppression (Hashimotodani *et al.*, 2005; Maejima *et al.*, 2005)

As the eCB system's role in regulating NT release at both excitatory and inhibitory synapses became clear, it was important to know which of the eCBs is involved. 2-AG proved to be the better candidate over anandamide, as it is the most abundant eCB in the brain and is strictly recognised as a retrograde messenger (Alger, 2002; Kano *et al.*, 2009) being synthesised 'on-demand' by DAGL (Stella *et al.*, 1997). Studies using inhibitors for 2-AG synthesis showed that 2-AG indeed mediates short-and long-term eCB-mediated retrograde suppression (Melis *et al.*, 2004; Safo & Regehr, 2005). As mentioned above, DAGLα was found to be located postsynaptically in the adult brain, being present in dendrites and absent from axons in the brain of the adult mouse (Bisogno, 2003). A number of more detailed studies have confirmed and extended this key finding. For example, immune-electron microscopy has shown DAGLα to be localised to postsynaptic dendritic spines in cerebellar neurons (Yoshida *et al.*, 2006) and concentrated in heads of dendritic

spines of glutamatergic synapses throughout the hippocampal formation (Katona *et al.*, 2006). DAGLα is therefore in the right place to synthesise 2-AG in response to depolarisation signals.

In support of this, 2-AG meets all of the criteria as a retrograde NT, as outlined by Regehr and colleagues (Regehr *et al.*, 2009): the appropriate machinery for synthesising and releasing the retrograde messenger must be located in the postsynaptic neuron (DAGL localised to the postsynaptic neuron), disrupting the synthesis and/or release of the messenger from the postsynaptic neuron must prevent retrograde signalling (DAGL blockade and KO studies, discussed below), the appropriate targets for the retrograde messenger must be located in the presynaptic bouton, disruption of which eliminates retrograde signalling (inhibition of the presynaptic CB1 receptor disrupts retrograde transmission) and exposing the presynaptic bouton to the messenger should mimic retrograde signalling, as seen when exogenous CBs suppress NT release (Cadogan *et al.*, 1997; Gobel *et al.*, 2000; Katona *et al.*, 2000). Therefore, DAGLα-synthesised 2-AG is the likely NT to signal in a retrograde fashion to activate the presynaptic CB1 receptor, thereby contributing to suppression of DSI and DSE.

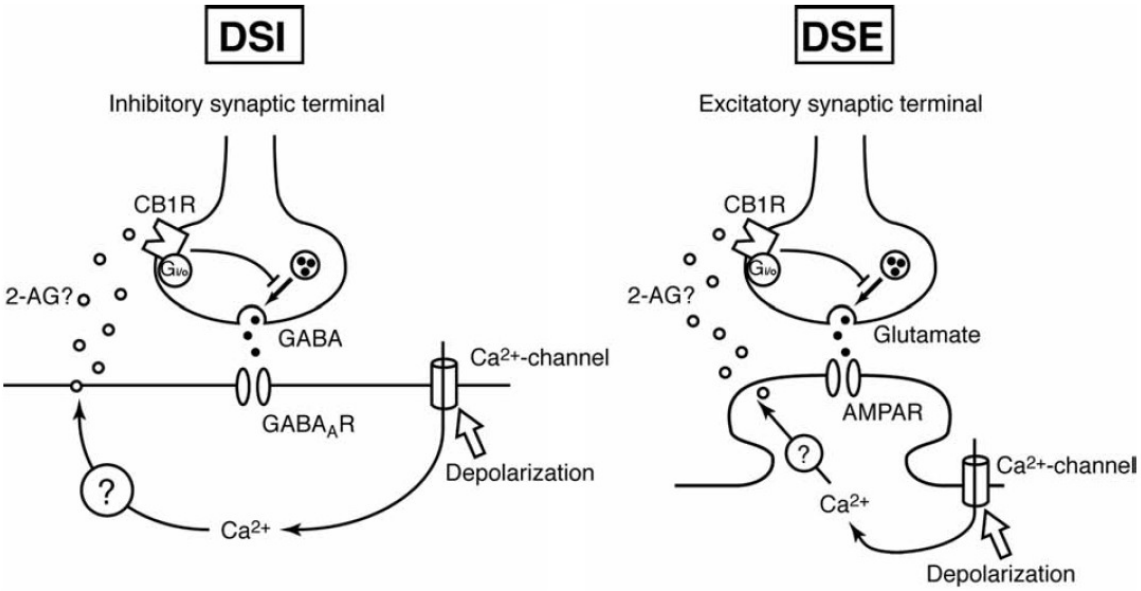

Figure 1.10 Depolarisation suppression of inhibition / excitation (DSI/DSE)

The role of the eCB system in the mechanisms of DSI and DSE. Postsynaptic depolarization induces Ca^{2+} influx through voltage-gated Ca^{2+} channels. Elevation of intracellular Ca^{2+} concentration triggers biosynthesis of eCBs, which are then released from postsynaptic neurons, activate presynaptic CB1 receptors, and suppress inhibitory GABA (DSI, *left*) or excitatory glutamate (DSE, *right*) release. The exact mechanism of how Ca^{2+} influx into the cell increases activity of DAGL, and 2-AG synthesis, has not yet been characterised.

Adapted with permission from Hashimotodani, et al., 2007

DAGL-dependent Retrograde Signalling

The exquisite nature of the relationship between the components of the eCB system is exemplified in pyramidal neurons of the basolateral amygdala, where the level of CB1 on the presynaptic terminal is matched to the amount of DAGLα at the postsynaptic site for three different types of synapse found on the same neuron (Yoshida *et al.*, 2011). Pharmacological blockade of DAGL also provided further evidence for DAGL's role in retrograde control of neurotransmission. THL blocked DSI and DSE in the cerebellum and hippocampus (Szabo *et al.*, 2006; Hashimotodani *et al.*, 2013). Subsequently OMDM-188, a relatively specific inhibitor for DAGL (Ortar *et al.*, 2008), effectively blocked DSI in slices from the hippocampus, striatum and cerebellum and mGluR-induced retrograde eCB signalling in cultured hippocampal neurons (Hashimotodani *et al.*, 2013).

Concrete evidence for the role of 2-AG and DAGL came from KO studies performed by two independent groups (Gao *et al.*, 2010; Tanimura *et al.*, 2010). eCB-mediated retrograde signalling was lost at synapses of DAGL-KO mice, with DSI being entirely absent in the hippocampus, striatum and cerebellum (Figure 1.11). In contrast, loss of DAGLβ resulted in only small and insignificant reduction in the DSI response (Gao *et al.*, 2010; Tanimura *et al.*, 2010). The general paradigm for 2-AG metabolism and signalling at adult synapses is that it results from DAGLα, rather than DAGLβ activity, as retrograde suppression is normal in DAGLβ KO mice (Gao *et al.*, 2010; Tanimura *et al.*, 2010). A third study also showed a dominant role for DAGLα in synaptic plasticity in the prefrontal cortex, where DSI was abolished in DAGLα KO mice and was unaffected in DAGLβ KO mice (Yoshino *et al.*, 2011). Together these studies pointed to DAGLα, rather than DAGLβ, as the postsynaptic 2-AG synthesising enzyme for eCB-mediated suppression of NT release.

A more recent study suggested the cooperative production of 2-AG by both the DAGLs, as seen using RNAi in autaptic hippocampal neurons (Jain *et al.*, 2013). However, these are tissue culture experiments and the authors did not comment on the known unreliability of off-targets commonly associated with the use of RNAi - the chance of which in some cases can be as high as 80% (Qiu *et al.*, 2005). DAGLβ may be capable of playing a role in modulation of neurotransmission, but to what

extent has yet to be elucidated. In this context there is as yet no evidence for DAGLβ being expressed in post-synaptic spines.

In summary of the findings discussed, the increase in 2-AG production is mediated by three different mechanisms; postsynaptic depolarisation-induced calcium influx (DSI/DSE), activation of $G_{q/11}$ protein-coupled receptors (including mGluR1) with less robust calcium signals, or mGluR activation alone in a calcium-independent manner (Maejima *et al.*, 2001; Ohno-Shosaku *et al.*, 2001; Hashimotodani *et al.*, 2005; Maejima *et al.*, 2005; Kano *et al.*, 2009) mGluR1 activation results in the formation of DAG via Gq protein and PLCβs (Masu *et al.*, 1991), followed by increases in DAGL activity and 2-AG levels.

How these processes influence the action of DAGL, and hence allow an increase in 2-AG production remains unclear and is the focus of this study. One report demonstrated a functional role for the interaction of calcium/camodulin-dependent protein kinase IIa (CamKIIa) with DAGLα (Shonesy *et al.*, 2013). DAGLα activity was increased by genetic deletion of CamKIIa, resulting in an increase in short-term retrograde eCB signalling at striatal glutamatergic synapses. Activated CamKIIa interacted with the C-terminal domain of DAGLα, phosphorylated two serine residues, resulting in inhibition of DAGLα activity *in vitro,* suggesting that calcium influx into the postsynaptic cell could activate CamKIIa, which in turn could inhibit the activity of DAGLα thereby modulating retrograde signalling (Shonesy *et al.*, 2013).

The precise mechanism of how CB1 itself acts to suppress Ca^{2+} influx into the cell is still controversial. The reduction in calcium entry into boutons following CB1 activation could be the consequence of either a direct decrease of voltage-gated calcium channel function or an indirect effect through the opening of presynaptic potassium channels (Daniel & Crepel, 2001). In contrast, the mechanism underlying the reduction of inhibitory synaptic transmission upon CB1 activation at single-bouton level is still unknown. However, recently it was found that in the CA3 region of the hippocampus, inhibition of N-type voltage-gated calcium channel function is the main mechanism underlying CB1-mediated suppression of synaptic inhibition

(Szabo *et al.*, 2014). This was in line with data obtained from an earlier study, where CB1 activation reduced the amplitude of voltage-gated calcium currents in a neuroblastoma-glioma cell line in a potent and reversible manner (Mackie & Hille, 1992). More details on how CB1 regulates NT release are yet to be studied in detail, but should open up new avenues for a better understanding of how eCBs (and Δ^9-THC) exert their influence on the CNS.

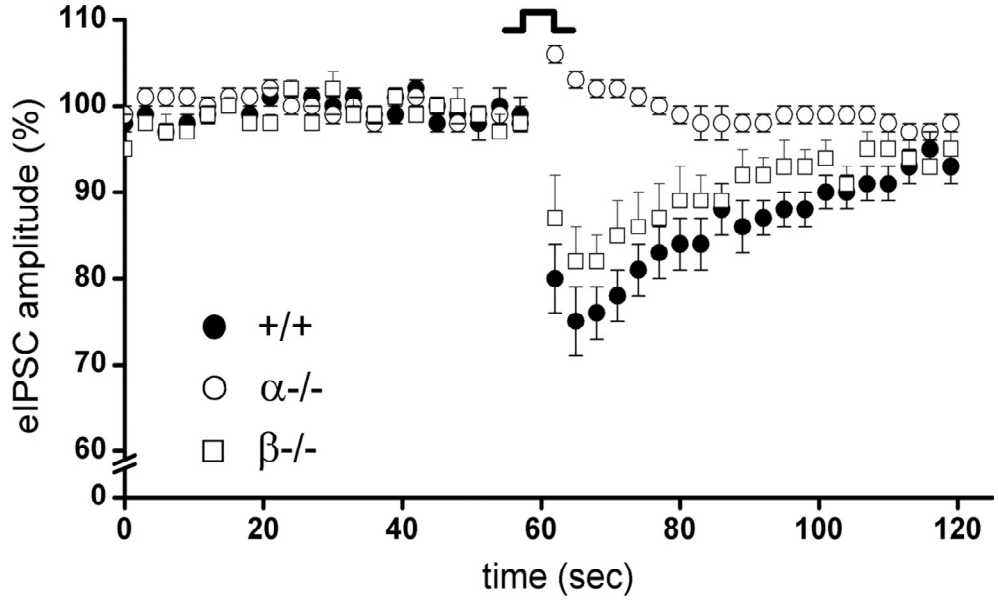

Figure 1.11 Inhibition of neurotransmitter release by retrograde signalling is lost in DAGLα KO mice

DSI in the hippocampus of DAGLα KO (α –/–) and DAGL β KO (β –/–) mice compared with wild-type (+/+) mice. The graph above shows a comparison of the average time course for eIPSC amplitudes after depolarization between wild-type, DAGLα KO and DAGLβ mice. No difference was observed between wild-type and DAGLβ mice. However DSI is absent in DAGLα KO mice highlighted a key role for DAGLα in retrograde suppression of neurotransmitter release. DSI for each genotype was averaged across all cells sampled, four to five DSI protocol repeats per sampled cell (+/+, n = 35; α−/−, n = 21; β–/–, n = 21).

Adapted with permission from Gao et al., 2010.

Adult Neurogenesis

Adult neurogenesis was first described in the adult brain by Joseph Altman in 1962 (Altman, 1962) and again in 1977, where Kaplan suggested the existence of dividing neurons in the hippocampus and olfactory bulb (Kaplan & Hinds, 1977). However, these remained contentious findings for many years and it was not until the 1990s that the study of adult neurogenesis became a mainstream pursuit. The potential of adult neurogenesis for the treatment of disease was soon realised when neuronal progenitors were isolated from the adult rat hippocampus, cultured *in vitro* and transplanted back into the hippocampus, where they differentiated into neurons. This suggested that these cells retained the capacity to generate mature neurons when grafted into the adult rat brain (Gage *et al.*, 1995). Adult neurogenesis is now known to constitute a form of cellular plasticity in the developed brain that impacts on memory, depression and neurodegenerative diseases (Zhao *et al.*, 2008).

Adult neurogenesis occurs in two areas of the mammalian brain; the sub-ventricular zone (SVZ) (Alvarez-Buylla & Garcia-Verdugo, 2002) and the hippocampus (van Praag *et al.*, 2002). In the SVZ, stem cells generate migratory neuroblasts that traverse the rostral migratory stream (RMS) to populate the olfactory bulb. In the case of the hippocampus, neurogenesis is localised to the granule cell layer in the dentate gyrus, an area associated with the formation of new memories.

The roles of DAGL in axonal growth and guidance during development and in retrograde regulation of synaptic plasticity in the adult could have been predicted based on the expression patterns of the DAGLs and CB1 receptors. Based on this approach, the expression of DAGLα in the lateral walls of the ventricle in the adult brain raised the possibility of a function in neurogenesis. In this context, DAGLα is present in all the proliferating cells in the SVZ (Goncalves *et al.*, 2008). Pharmacological evidence in young adult mice has shown a role for DAGLα/β in adult neurogenesis, where use of RHC80267 and THL resulted in a ~ 60% decrease in new neurons formed in the olfactory bulb two weeks after drug administration had ceased (Goncalves *et al.*, 2008), an effect which could be replicated by blocking CB2 but not CB1 receptors (Goncalves *et al.*, 2008). This was also seen in DAGLα KO

animals, with a 50% reduction in proliferation in the SVZ in DAGLα -/- (but not DAGLβ KO mice) and a 50% reduction in the hippocampus in both DAGLα -/- and DAGLβ -/- animals (Gao *et al.*, 2010). DAGL-dependent eCB tone is also important for the migration of the SVZ-derived neuroblasts to the olfactory bulb, where CB1 and CB2 antagonists dramatically changed the morphology of the migratory cells in the RMS to non-migratory phenotype (Oudin *et al.*, 2011a). Based on both pharmacological and KO studies, it has been shown that DAGL activity is required for adult neurogenesis in both the SVZ and hippocampus and that this directly impacts on the number of proliferating neuronal stem cells in the adult brain.

Adult neurogenesis in the SVZ declines with age in both the mouse (Goncalves *et al.*, 2008) and the adult brain (Knoth *et al.*, 2010) and may be due to an overall decline in eCB tone that might account for age-related deterioration in neurogenesis. The therapeutic implications for targeting the eCB system to treat neurodegeneration are vast. A greater understanding of how this process is regulated, as well as discovering targets for small molecule drugs, is therefore of huge importance.

1.6 Therapeutic implications of targeting the eCB system

Neuroprotection following brain injury

There is growing evidence that the eCBs can have neuroprotective and anti-inflammatory effects in response to harmful stimuli. Both 2-AG and anandamide have been shown to be elevated following brain injury and are believed to exert their neuroprotective effects by preventing neuronal damage and protecting against excitotoxicity (Hansen *et al.*, 2001; Panikashvili *et al.*, 2001; Marsicano *et al.*, 2003; Mechoulam & Lichtman, 2003). For example, 2-AG, anandamide and a non-hydrolysable analogue of anandamide all increased viability and cell survival in primary cultures of cerebral cortical neurons in an *in vitro* model for ischemia (Sinor *et al.*, 2000). 2-AG levels were elevated in the brains of mice following closed head injury and when synthetic 2-AG was administered, there were significant and concentration-dependent reductions in brain oedema and cell death, indicating a protective role of the eCB system in damage and repair (Panikashvili *et al.*, 2001). Furthermore, anandamide was shown to be neuroprotective following inflammation-induced neuronal damage (Eljaschewitsch *et al.*, 2006). The eCB system therefore can respond differently to various harmful stimuli. For example, hippocampal levels of 2-AG, but not anandamide, were elevated in response to Aβ42 infusion, a model of Alzheimer's disease (AD) (van der Stelt *et al.*, 2006). In contrast, anandamide (and not 2-AG) levels were raised following treatment with the excitotoxin, kainic acid (Marsicano *et al.*, 2003). These findings demonstrate the 'on-demand' synthesis of the 2-AG and anandamide in response to harmful stimuli and may play a role in brain function homeostasis.

The mechanism for eCB neuroprotection has been linked to an enhanced neuronal sensitivity to eCBs by brain-derived neurotrophic factor (BDNF), where BDNF increases the expression of CB1 receptor transcripts and decreases expression of MAGL transcripts (Maison *et al.*, 2009). Another potential mechanism may be that 2-AG has the ability to suppress the formation of reactive oxygen species (McCarron

et al., 2003), a key player in oxidative stress in a number of neurodegenerative diseases, including Parkinson's disease (PD), Huntington's disease, AD, Down's syndrome, ataxia, multiple sclerosis, amyotrophic lateral sclerosis, schizophrenia, and Tardive Dyskinesia (Kovacic & Somanathan, 2012). However, their neuroprotective effects may also be linked to their anti-inflammatory properties.

Anti-inflammatory properties of the eCBs

CBs, both endogenous and exogenous can suppress inflammation (Tanasescu & Constantinescu, 2010), while CB receptor expression can be upregulated in immune cells by pro-inflammatory cytokines (Jean-Gilles *et al.*, 2015), pointing to a role for the eCB system in regulation of neuroinflammation. Both 2-AG and anandamide levels have been found to be elevated in the basal ganglia of animal models of PD, a disease characterised by a loss of dopaminergic neurons in the basal ganglia. Full restoration of locomotion in PD animal models was observed in the presence of CB1 antagonists (Di Marzo *et al.*, 2000) and anandamide levels in the cerebrospinal fluid of PD patients were found to more than double that of controls, pointing to a compensatory / protective role of eCBs when dopaminergic neurons have been compromised (Pisani *et al.*, 2010). In a rat model of PD, levodopa treatment did not affect eCBs in the basal ganglia, while direct activation of CB1 alleviated abnormal involuntary movements (Ferrer *et al.*, 2003; Morgese *et al.*, 2007). Interestingly, anandamide elevations in these animals as a result of the FAAH inhibitor, URB597 were only seen when TRPV1 was inhibited (Morgese *et al.*, 2007). Raised eCB levels were also found in animal models of Alzheimer's disease (AD) (van der Stelt *et al.*, 2006). The raised eCB levels are likely to be linked with the inflammatory response associated with PD and AD, as increased 2-AG levels resulting from MAGL inhibition can suppress cytokines and microglial activation in response to a pro-inflammatory stimulus (Ramirez *et al.*, 2005; Nomura *et al.*, 2011).

Under normal physiological conditions, microglia, a type of glial cell / macrophage in the brain and spinal cord, exhibit a deactivated state associated with anti-inflammatory and neurotrophic factors (Streit, 2002). Microglia are then activated in

response to invading pathogens or tissue damage, resulting in an inflammatory response. In a normal state, this is self-limiting and resolves itself once the pathogen has been eradicated, or tissue has been repaired. However in some disease states, sustained inflammation implies persistence of the inflammatory stimulus, such as a protein aggregates seen in AD. Uncontrolled inflammation can result in production of neurotoxic factors that amplify underlying disease states. Neuroinflammation, a prominent feature in many neurodegenerative diseases, contributes to progressive cell damage and neuronal cell loss. Direct evidence for an innate inflammatory response in AD was described, with subsequent studies having been documented for inflammatory responses in PD and in multiple sclerosis (MS) (Glass *et al.*, 2010). MS is an inflammatory, autoimmune, demyelinating disease of the CNS (Compston & Coles, 2002) and eCBs are also raised in animal models of the disease (Pertwee, 2002). Administered CBs have some effect on spasticity and pain in MS, both experimentally and in clinical trials in humans (Baker *et al.*, 2000; Baker *et al.*, 2007; Zajicek *et al.*, 2012), possibly by reducing neuroinflammation. As a result Sativex®, has recently become the first botanical cannabis-based medicine to be licenced, in some European countries, for the treatment of spasticity (Kmietowicz, 2010), highlighting the benefit of therapeutically targeting the eCB system and the potential benefit for other disease states involving neuroinflammation.

The role of the eCB system in neuroinflammation appears to be two-fold; on the one hand eCBs can have anti-inflammatory effects, while on the other hydrolysis of 2-AG by MAGL results in AA production leading to prostaglandin synthesis. Prominent among the known pro-inflammatory stimuli in the nervous system are the prostaglandins, which are produced from AA by cyclooxygenase enzymes, COX-1 and COX-2; both of which are present in neurons and glial cells (Simmons *et al.*, 2004). Rodents treated with COX inhibitors or lacking COX enzymes show protection in models of neurodegenerative diseases that have an inflammatory component (Glass *et al.*, 2010). However, gastrointestinal and cardiovascular toxicities displayed by COX inhibitors have limited their translational potential for neuroinflammatory syndromes (Ng & Chan, 2010). Therefore, the eCB system may be a more attractive therapeutic target.

2-AG serves as the precursor for the primary AA pool of neuroinflammatory prostaglandins, by way of MAGL hydrolysis. Genetic or pharmacological blockade of MAGL results in elevated brain levels or 2-AG and corresponding reductions in AA (Cravatt *et al.*, 2001; Long *et al.*, 2009a; Zhong *et al.*, 2011). One study found that inactivation of MAGL also caused significant reductions in several prostaglandins and other eicosanoids in the brain and elevations in MAGs, including 2-AG (Nomura *et al.*, 2011). Mice treated with the pro-inflammatory agent, LPS resulted in an increase in brain eicosanoids, an effect inhibited by the specific MAGL inhibitor, JZL184 (Nomura *et al.*, 2011). MAGL inactivation robustly suppressed production and accumulation of β-amyloid, one of the hallmarks of the disease, in a mouse model of AD (Chen *et al.*, 2012). MAGL inactivation also prevented neuroinflammation, decreased neurodegeneration, maintained integrity of hippocampal synaptic structure and function, improved long-term synaptic plasticity, spatial learning and memory in animal models of AD (Chen *et al.*, 2012); this may be a result of a combination of reduced AA precursor and increased eCB levels.

It has also been shown that 2-AG can reduce COX-2 expression through signalling at the CB1 (but not CB2) receptor. Excessive expression of hippocampal COX-2 is reduced by 2-AG in response to proinflammatory and excitotoxic stimuli, thereby providing neurons with protection against harmful stimuli (Zhang, 2008). This could help explain the eCB system's role in pain, the activation of which being one component in pain alleviation (Pertwee, 2001). Suppression of COX-2 by 2-AG could also be of therapeutic benefit in age-associated muscle inflammation. This inflammation is a major factor in the degenerative decline in skeletal muscle (Schaap *et al.*, 2006), where COX-2 activity is a chief player in initiating and sustaining components in tissue inflammation.

Thus, taken together anti-inflammatory and antioxidant properties of eCBs may either add or synergise to enhance its activity as a neuroprotective agent (Panikashvili *et al.*, 2001), pointing to the role for the elevated eCB levels seen in PD, AD and MS. As a result, MAGL is attracting attention as a therapeutic target for treatment of AD (Aso & Ferrer, 2014).

Other therapeutic implications of targeting the eCB system

As discussed above, the DAGLs have a clear role in both inflammation and neuroprotection, implicating the enzymes in a number of diseases where these processes are compromised. The eCB system is now recognised as an important physiological modulator of other various CNS processes including pain (Butler *et al.*, 2008; Sagar *et al.*, 2009), appetite (Jesudason & Wittert, 2008; Stoving *et al.*, 2009), motor function (Fernandez-Ruiz *et al.*, 2002; Dowie *et al.*, 2009), neural cell fate (Guzman *et al.*, 2002) and as discussed in detail above, synaptic plasticity.

One recent study has linked the eCB system to fragile X syndrome, the most commonly known genetic cause of autism (Jung *et al.*, 2012). Fragile X mental retardation protein regulates signalling of mGluR5 receptors in the brain, deletion of which in mice causes enhancement of mGluR5-mediated LTD in both the hippocampus and cerebellum – a process regulated by the eCB system. The term 'eCB signalosome' was used to refer to a multiprotein complex of mGluR5 and DAGLα in the presynaptic neuron, which the authors hypothesised provides a structural scaffold to allow a 2-AG signalling pool to form, that is distinct from the intracellular pool of 2-AG involved in phospholipid remodelling and eicosanoid biosynthesis (Piomelli, 2003). This group showed that mGluR5-mediated LTD at excitatory synapses of the ventral striatum and prefrontal cortex is absent in fragile X KO mice, paired with inadequate 2-AG production and structural disorganisation of the eCB signalosome. Importantly, 2-AG enhancement, via JZL184 MAGL inhibition, normalised this synaptic defect and corrected the behavioural abnormalities in these KO mice (Jung *et al.*, 2012).

CBs, whether as endogenously released eCBs or administered drugs, have been shown to reduce symptoms of several disorders. Licensed medicines that exploit beneficial effects of direct CB receptor activation have already been developed (Pertwee, 2009). Three medicines that activate CB1/CB2 are currently in the clinic: Cesamet (nabilone), Marinol (dronabinol; Δ^9-THC) and Sativex (Δ^9-THC with cannabidiol). These medicines can be prescribed for nausea following chemotherapy (Cesamet and Marinol), appetite stimulation (Marinol), for pain relief in cancer, and

as mentioned above, neuropathic pain and for spasticity in adults with MS (Sativex) (Pertwee, 2009). The anti-obesity link with the eCB system led to the development of the CB1-specific compound SR141716A, known commercially as Rimonabant, which also had potential for treatment of metabolic syndrome and drug addiction (Pertwee, 2005; Le Foll *et al.*, 2009). However following the link of this drug with anxiety, depression, and suicide, the European Medicines Agency called for its withdrawal from the market in 2008 (Le Foll *et al.*, 2009). Since then, major pharmaceutical companies have stopped further clinical research on this class of drug and seem to have lost interest entirely in all drugs that block CB1 receptors. However the potential of targeting the eCB system is still generating a great deal of interest for areas such as neuropathic pain (Lau & Vaughan, 2014), liver disease (Basu *et al.*, 2014) and for eCB's anti-proliferative effects in cancer (Mimeault *et al.*, 2003), with the idea of designing more specific drugs to minimise off-target effects.

These points highlight the potential for therapeutically targeting the eCB system. Strategies for improving the efficacy and/or benefit-to-risk ratio of CB agonists in the clinic include targeting CB receptors outside the blood-brain barrier or targeting CB receptors expressed by a particular tissue. As the DAGLs produces 2-AG 'on-demand' in response to cellular queues, this enzyme could prove to be an attractive target, as the enzymes display different levels of activation and could result in an overall slower / lower increase in 2-AG across the CNS or elsewhere, thereby avoiding severe side effects.

DAGL as a more attractive target than MAGL

eCB signalling is terminated by hydrolysis of the eCBs by FAAH or MAGL. Specific tools to independently block anandamide and 2-AG metabolism have emerged from attempts to uncouple their signalling pathways and associated behavioural processes. JZL184 is a potent selective inhibitor of MAGL and was identified through activity-based protein profiling (ABPP) (Long *et al.*, 2009a). ABPP of serine hydrolases uses reported-tagged fluorophosphonates which serve as general activity-based probes for this large and diverse class of enzymes. Use of ABPP can evaluate the potency and selectivity of small-molecule enzyme inhibitors directly in complex proteomes (Liu *et al.*, 1999; Leung *et al.*, 2003). JZL184 raised brain 2-AG by 8-10 fold without altering anandamide and JZL184-treated mice exhibited a broad array of CB1-dependent behavioural effects, including analgesia, hypothermia, hypomobility and catalepsy (the tetrad test for CB activity) and mimicked much of the pharmacological profiles typically seen with CB1 agonists (Cravatt *et al.*, 2001; Wiley & Martin, 2003). These effects were mediated through the CB1 receptor, as in each case the effects of JZL184 were blocked by pre-treatment with the CB1 antagonist rimonabant.

Interestingly, FAAH inhibitors caused analgesia but no other CB behavioural phenotypes (Long *et al.*, 2009a). While it was thought that the CB phenotypes from this study could be pharmacologically uncoupled from more beneficial effects (e.g. analgesia) by titrating the magnitude of MAGL inhibition *in vivo*, 2-AG levels increased significantly across the entire dose-range tested, even though lower doses resulted in less blockage of MAGL activity; that is to say, even partial inhibition of MAGL was sufficient to augment 2-AG-mediated eCB signalling *in vivo*. In addition to this, prolonged MAGL inactivation causes profound alterations in the brain eCB system, while JZL184 lost its analgesic activity and produced cross-tolerance to CB1 agonists, an effect also seen in mice lacking MAGL. Chronic MAGL blockade also causes physical dependence, impaired eCB-dependent synaptic plasticity and desensitised brain CB1 receptors. In contrast, none of these effects were observed in mice with chronically disrupted FAAH, which instead maintained an analgesic phenotype and intact CB1 receptor system (Schlosburg *et al.*, 2010).

These findings suggest that therapeutically targeting DAGL, rather than MAGL, may have greater potential and benefit for enhancing eCB signalling or reducing the availability of AA for prostanoid synthesis. As discussed previously, establishment of the function of the DAGLs as central players in eCB signalling required gene knockout studies to complement the pharmacology experiments (Gao *et al.*, 2010; Tanimura *et al.*, 2010) and this was essential given the poor selectivity of the available drugs. The situation is perhaps even worse for anandamide given that there are no drugs that selectively block its synthesis and no genes that have been demonstrated to be essential for this pathway. At the outset of this thesis it was simply not practical to propose a genetic strategy as a timely and cost-effective means to dissect out the pathways that regulate eCB signalling in cells. However, this position has been radically transformed with the advent of CRISPR and the implications of this for a better understanding of eCB signalling are introduced next.

1.7 Precise Genome modification

Recent advances in the development of genome editing technologies have enabled cleavage of DNA in a site-specific manner, thereby substantially improving the ability to make precise changes in the genome of eukaryotic cells. This ability to engineer biological systems has enormous potential to interrogate genetic contribution to disease. There are currently three main technologies used; Zinc-Finger Nucleases (ZFNs), Transcriptor Activator-like Effector Nucleases (TALENs) and RNA-guided Clustered Regularly Interspaced Short Palindromic Repeats (CRISPR)-Cas nuclease system. ZFNs and TALENs use a strategy of a DNA-binding domain, to specifically recognise the gene of interest. This is combined with a DNA-cleavage (FokI) domain to induce a double-strand break (DSB). FokI cleavage domain must dimerise in order to cleave the target DNA, and so a pair of DNA-binding domains must be used (to target non-palindromic DNA). Although ZFNs and TALENs have proved effective for genetic manipulation, a new ZFN or TALEN protein must be generated for each DNA target site, which can have huge cost implications. In contrast, Cas9 endonuclease is guided by small RNAs to induce a DSB. It achieves this through its two active domains, RuvC (cleaves the complementary strand) and HNH (cleaves the non-complementary strand) (Gasiunas *et al.*, 2012; Jinek *et al.*, 2012; Nishimasu *et al.*, 2014). CRISPR/Cas9 system can facilitate gene editing by simply identifying a 20 nucleotide targeting sequence to guide Cas9 to a specific target locus. The CRISPR/Cas9 system is therefore markedly easier to design, highly specific, efficient and a much cheaper method for genome engineering.

What is the CRISPR/Cas System?

Bacteria and Archaea have evolved adaptive immune defences to cope with various environmental stresses, enabling them to defend themselves from invading viruses or plasmids. These are called CRISPR and CRISPR-associated (Cas) proteins (Horvath & Barrangou, 2010; Bhaya *et al.*, 2011). These defence systems rely on small RNAs for sequence-specific detection and silencing of foreign nucleic acids. CRISPR/Cas systems are composed of *cas* genes, organised in operons and CRISPR arrays consisting of genome targeting sequences, called spacers, interspersed with identical repeats (Bhaya *et al.*, 2011; Wiedenheft *et al.*, 2012).

Bacterial Immunity

CRISPR/Cas mediated immunity occurs in three broad steps. Firstly, in the adaptive phase (Garneau *et al.*, 2010; Marraffini & Sontheimer, 2010), bacteria respond to invasion of foreign nucleic acids by integrating short fragments of the foreign sequence, or spacers into the host genome. The sequence in the viral genome that corresponds to a spacer is known as the protospacer (Deveau *et al.*, 2008). The foreign sequences are incorporated at the proximal end of the CRISPR array, and so positional information represents a timeline of spacer acquisition events. Each of the CRISPR loci encode the acquired spacers and are separated by the repeat sequences of CRISPR. Transcription yields a pre-CRISPR RNA (pre-crRNA). This is followed by enzymatic cleavage to yield crRNAs, which consist of spacer-repeat fragments (Figure 1.12). crRNAs recognise complementary protospacer sequences, which directs Cas endonucleases to cleave foreign DNA. This interferes with viral replication (or plasmid activity) and imparts immunity to the host (Barrangou *et al.*, 2007; Bhaya *et al.*, 2011; Jinek *et al.*, 2012).

Figure 1.12 An overview of the endogenous Type II bacterial CRISPR/Cas9 system

Within the bacterial genome, a CRISPR array contains spacer sequences with homology to foreign DNA (for example from a viral genome) separated by short palindromic repeat sequences. The CRISPR array is transcribed to make pre-CRISPR RNA (pre-crRNA) (A), which is processed into individual crRNAs by trans-activating crRNA (tracrRNA), homologous to the short palindromic repeat which also enables recruitment of RNAse III and Cas9. Together these enzymes separate the individual crRNAs (B). The tracrRNA and Cas9 nuclease form a complex with each individual crRNA (C), and each crRNA:tracrRNA:Cas9 complex hunts down the target DNA sequence, complimentary to the crRNA. Type II CRISPR system requires a PAM (NGG) immediately downstream of the target DNA, and this is where the crRNA binds (D). After the complex binds the target DNA, Cas9 separates the double strands and cleaves both of them just after the PAM sequence (E). The crRNA:tracrRNA:Cas9 complex unbinds after the DSB (F).

From www.addgene.org/crispr/reference/history/ (with permission)

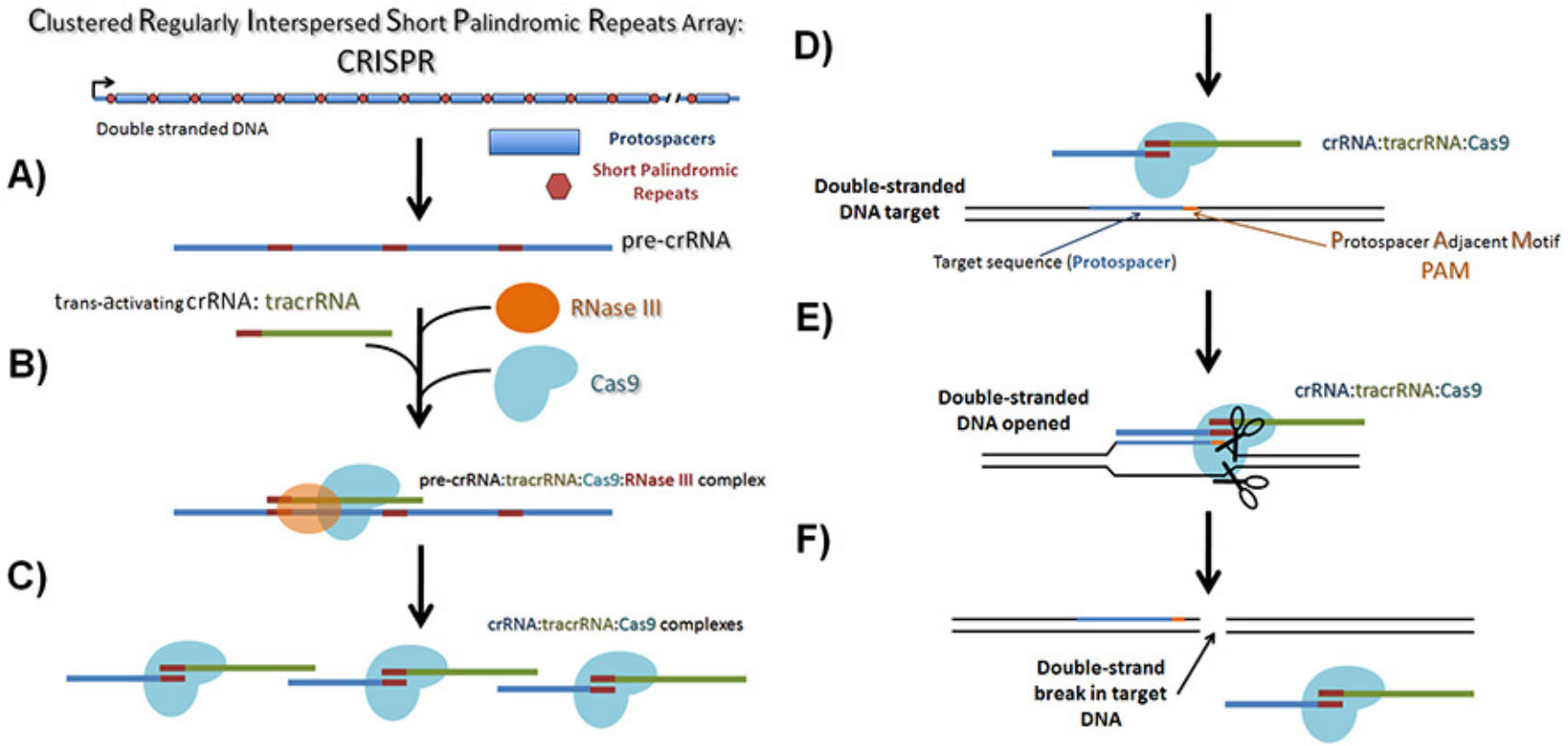
Clustered Regularly Interspersed Short Palindromic Repeats Array:
CRISPR
Double stranded DNA
A)
Protospacers
Short Palindromic Repeats
pre-crRNA
trans-activating crRNA: tracrRNA
B)
RNase III
Cas9
pre-crRNA:tracrRNA:Cas9:RNase III complex
C)
crRNA:tracrRNA:Cas9 complexes
D)
crRNA:tracrRNA:Cas9
Double-stranded DNA target
Target sequence (Protospacer)
Protospacer Adjacent Motif
PAM
E)
Double-stranded DNA opened
crRNA:tracrRNA:Cas9
F)
Double-strand break in target DNA

Types of CRISPR

The CRISPR/Cas system can be divided into 3 types, CRISPR I, II and III. These classes are based on phylogeny, sequence, locus organization, and content of the CRISPRs and associated *cas* genes (which encode various DNases, RNases, and other proteins). Type I and III systems share some overarching features; specialised Cas endonucleases that process the pre-crRNAs and once mature, each crRNA assembles into a large multi-Cas protein complex. In contrast, type II systems process pre-crRNAs by a different mechanism. Trans-activating crRNA (tracrRNA) triggers processing by the double-stranded RNA-specific ribonuclease, RNase III in the presence of Cas9 protein (Figure 1.12) (Deltcheva *et al.*, 2011; Gottesman, 2011). Cas9 is thought to be the sole protein responsible for crRNA-guided silencing of foreign DNA in this system (Barrangou *et al.*, 2007; Garneau *et al.*, 2010; Sapranauskas *et al.*, 2011). Type II CRISPR/Cas9 systems have been engineered to mediate robust RNA-guided genome modifications in multiple eukaryotic systems (Mali *et al.*, 2013b), substantially improving the ease of genome editing.

RNA-Guided Genome engineering via Cas9

Streptococcus pyogenes CRISPR II system can be heterologously reconstituted in mammalian cells, and this has been shown in human cell lines (Cong *et al.*, 2013; Mali *et al.*, 2013b). The type II CRISPR-Cas9 system requires crRNA and tracrRNA for Cas9 to cleave target DNA. One study has shown that crRNA fused to tracrRNA, mature crRNA, is fused to a partial tracrRNA via a synthetic stem loop to mimic the natural crRNA:tracrRNA duplex (Figure 1.12). This is sufficient to direct Cas9 to the target DNA matching the crRNA (Jinek *et al.*, 2012). Soon after this study, the Church lab at Harvard University demonstrated that expression of crRNA-tracrRNA fusion transcript, termed ‘guide RNAs’ (gRNAs) from human U6 polymerase III promoter, allowed Cas9 to cleave sequences of interest (Mali *et al.*, 2013b). In human cells, expression of a human codon-optimised Cas9 protein with an appropriate nuclear localisation signal is required, while U6 promoter naturally drives the transcription of small RNAs (Makinen *et al.*, 2006). RNase III recombinant expression is not required (Cong *et al.*, 2013). This system is

constrained only by U6 transcription requiring the gRNA to initiate with ‘G’ and the requirement for the sequence ‘NGG’ (where N is any nucleotide), known as the protospacer adjacent motif (PAM) (Figure 1.12). The PAM immediately follows the 20 bp target DNA sequence – $GN_{20}GG$ (Jinek *et al.*, 2012).

DNA repair following a double-strand break

Cas9 contains two active domains, RuvC and HNH domain. Together these cause a DSB in genomic DNA at a specific locus (Jinek *et al.*, 2012; Nishimasu *et al.*, 2014). The DSB can be repaired by one of two mechanisms; non-homologous end joining (NHEJ) or homology-directed repair (HDR). Either pathway can be leveraged depending on the desired outcome of gene modification (Figure 1.13).

In the absence of a repair template, DSBs are repaired by the error-prone NHEJ pathway. The term ‘NHEJ’ was first coined in 1996 and is referred to as "non-homologous" as it requires little or no DNA homology to join the ends of DNA. NHEJ can therefore result in the loss or gain of nucleotide number (Moore & Haber, 1996), with the end-joining product possibly having either nucleotide insertion mutations or deletions (indels) (Valerie & Povirk, 2003). As a result, NHEJ can be harnessed to cause maximum disruption and gene knockout via indel formation, leading to frameshift mutations and/or premature stop codons (Perez *et al.*, 2008). It is therefore desirable to target an exon closest to the N-terminus to cause maximum disruption to the gene of interest.

In contrast to NHEJ, HDR is a high fidelity pathway and requires a repair template. In general, HDR is considered to be error-free and most active in the S/G2 stage of the cell cycle, where the process of homologous recombination occurs (Valerie & Povirk, 2003). Although HDR occurs at lower rates than NHEJ, can be leveraged by introducing a repair template, either in the form of homology arms flanking the target sequence, or single-stranded DNA oligonucleotides, with the latter providing an effective method for making single nucleotide mutations (Ran *et al.*, 2013b).

Although CRISPR/Cas9 in its native form (with nuclear localisation signal) has been successfully used to disrupt a number of genes in different systems, there have been reports of its ineffectiveness. *Candida albicans,* a pathogenic yeast that causes mucosal and systematic infections, is known for being a challenge in terms of genome disruption. For example, chromosome number is not rigidly controlled resulting in numerous strains containing one (or more) additional copies. It also lacks a meiotic phase, meaning loss-of-function mutations can be maintained in a diploid (and identified after meiosis). However, one report has modified CRISPR/Cas9 (such as a codon-optimised Cas9) to successfully disrupt *C. albicans* genome, which could also be used in other fungi (Vyas *et al.*, 2015); this demonstrates how CRISPR/Cas9 can also be used in a modified form in more challenging systems.

The CRISPR/Cas9 system has been found to be an effective method for gene disruption in most mammalian systems, including U2OS cells (Feng *et al.*, 2015). Therefore, this method puts itself forward as effective method to specifically disrupt the DAGL genes, aiding us to study their function and ultimately the eCB system. Its use in a cell line to disrupt the DAGL genes is explored in detail in Chapter 6 (Results III).

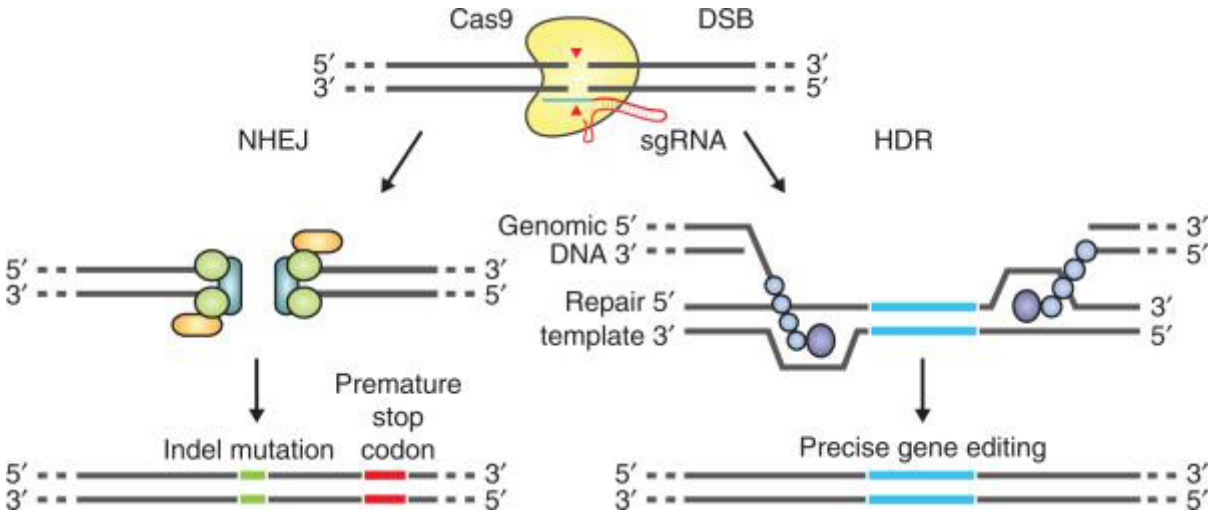

Figure 1.13 DNA Repair following a double-strand break (DSB)

The endonuclease Cas9 cleaves both strands of the target DNA, creating a DSB. A DSB can be repaired by one of two pathways; non-homologous end joining (NHEJ) or homology-directed repair (HDR). NHEJ occurs in the absence of a suitable repair template, during which a small number of nucleotides are either inserted or deleted (Indel, green) at the site of the DSB at random. Indel formations can cause major disruptions within the gene's open reading frame. This is due to a frameshift as a result of the indel. A frameshift can significantly alter the amino acid sequence or create a premature stop codon, either at the the site of the DSB or further downstream by shifting the reading frame. When a DNA repair template is available, the HDR pathway is activated. HDR is less error prone allowing more precise gene editing to occur (blue). Introducing a DNA repair template with homology to the sequence, both up- and down-stream of the DSB, allows for predictable, single nucleotide mutation.

Adapted with permission from Ran,et al., 2013

Off-Target effects of the CRISPR/Cas9 System

Although Cas9 is directed by a 20 nucleotide gRNA sequence, a certain number of mismatches are tolerated by the system, thereby promoting off-target mutagenesis. While each base within the 20 nucleotide sequence contribute to overall specificity, multiple mismatches between gRNA and its complementary target DNA sequence can be tolerated. Cas9 activity at the target DNA sequence is not altered by a one-base mismatch *in vitro* both in mammalian and bacterial cells (Jinek *et al.*, 2012; Cong *et al.*, 2013; Jiang *et al.*, 2013; Cho *et al.*, 2014). Single and double mismatches are tolerated to varying degrees depending on their position along the gRNA-DNA interface, the number of mismatches, and distribution. Perfect gRNA:DNA alignment is required in the 7-12 bp adjacent to the PAM end of the target site (3′ end of the gRNA), with mismatches tolerated at the 5′ end (Jinek *et al.*, 2012; Cong *et al.*, 2013; Pattanayak *et al.*, 2013). In fact, off-target mutations have been detected in human cells at sites that differed by up to 5 bp, a finding that may limit the use of the CRISPR/Cas9 system in research and therapeutic applications (Fu *et al.*, 2013; Hsu *et al.*, 2013; Pattanayak *et al.*, 2013).

Cas9 Nickase

Cas9 carries out strand-specific cleavage using the conserved HNH and RuvC nuclease domains, which can be mutated and exploited for additional function. An aspartate-to-alanine (D10A) mutation in the RuvC catalytic domain allows Cas9 nickase (Cas9n) mutant to nick, rather than cleave DNA yielding single-stranded breaks (Sapranauskas *et al.*, 2011; Gasiunas *et al.*, 2012; Jinek *et al.*, 2012). Individual nicks are efficiently repaired by the base-excision repair (BER) pathway (Dianov & Hubscher, 2013). However, when using paired Cas9 nickases to generate two single-stranded breaks / nicks on different DNA strands, high specificity and efficiency is retained, while avoiding off-target mutations by 50- to 1500-fold (Ran *et al.*, 2013a; Cho *et al.*, 2014).

Akin to ZFNs and TALENs, DNA cleavage relies on the synergistic action of two independent DNA-binding modules directing Cas9n. Appropriately offset gRNA pairs (- 4 to + 20 bp) can guide Cas9n to simultaneously nick both strands of the target locus, mediating DSBs and stimulating robust NHEJ. Following the DSB, the introduction of a repair template stimulates the HDR repair pathway (Figure 1.13) (Ran *et al.*, 2013a).

1.8 Aims

1. Utilise a bioinformatics approach to build testable models for DAGL activation.

2. Develop assays to directly measure the activity of our DAGL constructs in membranes and cells using the surrogate substrates, PNPB and DiFMUO.

3. Develop a cellular assay to measure a stimulus driven eCB-dependent CB1 activation to evaluate the contribution of endogenous DAGLs to the response and to use a gain of function approach to determine if the response is limited by enzyme level.

4. To determine the potential of the CRISPR/Cas9 system as a means of disrupting the function of DAGLα and DAGLβ in a model cell line.

CHAPTER 2. MATERIALS & METHODS

All reagents were purchased from Sigma (Poole, UK) unless otherwise stated

2.1 Materials

Cell Culture

Phosphate Buffered Saline (PBS)

One PBS tablet (Oxoid, Basingstoke, UK) containing KCl (0.20 g/L), KH_2PO_4 (0.2 g/L), NaCl (8 g/L) and Na_2HP0_4 (1.15 g/l) dissolved in 100 mL ddH_20 and autoclaved.

PBS-T

PBS + 0.1% Tween 20

Tris Buffered Saline (TBS)

0.5 M Tris, 1.5 M NaCl in ddH_20, pH 7.4

TBS-T

TBS + 0.1% Tween-20

PBS-EDTA

PBS + 0.05 M EDTA

Trypsin

0.5% Trypsin, from Life Technologies + 0.5 mM EDTA pH 8, in PBS

Cell Culture Dishes, Flasks & Trays; all from Thermo Scientific (Loughborough, UK)

Polystyrene Nunclon™ surface – 4-well dishes, 10 cm dishes, 15 cm dishes
Nunc Polystyrene T 75 cell culture flask
Nunc Bio-Assay Dishes (500 cm^2)

Transfection / 0% Serum Media

Opti-MEM® I Reduced Serum Medium, from Life Technologies

Transfection reagents

Fugene HD transfection reagent, from Promega
Lipofectamine 2000, from Life Technologies

Molecular Biology

DNA Ligation & Annealing Oligonucleotides

T4 DNA Ligase & Reaction Buffer (10 X Stock solution), from New England Biolabs (Hertfordshire, UK)
Quick Ligation™ Kit (Ligase & 2 X reaction buffer solution), from New England Biolabs

Temperature Control

Thermomixer, from Eppendorf

Restriction Digestion

All restriction enzymes purchased from New England Biolabs and used according to the manufacturer's instructions.

Agarose Gel Running Buffer

TAE (Tris, Acetic Acid and EDTA) Buffer – 40 mM Tris, 20 mM acetic acid, and 1 mM EDTA, pH 8.4

Agarose

SeaKem LE Agarose, from Lonza, dissolved in TAE Buffer

DNA Ladder

1 Kb Plus DNA ladder, from Invitrogen, Life Sciences

DNA Dye

2,7-Diamino-10-ethyl-9-phenylphenanthridium bromide (ethidium bromide), from Applichem

Gel Loading Buffer

Gel Loading Dye Orange, from New England Biolabs.

Gel Viewer

Molecular Imager® Gel Doc™ XR+ System and Quantitiy One software v4.6.5, from Bio-Rad

Spectrophotometer

Nanodrop 100, from Thermo Scientific

Plasmid DNA Purification (All from Qiagen, Manchester, UK)

Qiagen Spin Miniprep Kit (20 µg plasmid DNA purification from *E. coli* cells)
Endofree Plasmid Maxi Kit (500 µg plasmid DNA purification from *E. coli* cells)

QIAquick Gel Extraction Kit (purification of digested vectors from agarose gels)
Puregene Core Kit (DNA extraction from recombinant cells)

Transformation - Competent cells

C3019 NEB 10-beta chemically competent *E. coli* cells, from New England Biolabs
One Shot ® TOP10 Chemically Competent *E. Coli,* from Life Technologies (Paisley, UK)

TOPO Cloning

TOPO ® TA Cloning ® Kit for Sequencing, from Life Technologies

Agar

For blasticidin resistance - Fast-Media® Blas Agar, from Invivogen
For puromycin resistance **-** Fast-Media® Puro Agar, from Invivogen

Growth Liquid

For blasticidin resistance - Fast-Media® Blas TB, from Invivogen
For puromycin resistance- Fast-Media® Puro TB, from Invivogen

Selection Antibiotics

Kanomycin Sulphate (diluted in ddH_20)
Blasticidin, from Life Technologies

Polymerase Chain Reaction (PCR)

PCR Tubes

0.2 ml thin wall PCR tubes, from Axygen (distributed by Thermo Scientific)

PCR Plates

PCR microplates, from Axygen

PCR Polymerases / Master Mixes

Extensor Long PCR Master Mix, from Thermo Scientific (ab0792)
Phusion Flash High-Fidelity PCR Master Mix, from Thermo Scientific
Taq DNA Polymerase and dNTP Mix, from Thermo Scientific

Real-time Reverse Transcriptase PCR (RT-PCR)

Homogenisation

QIAshredder, from Qiagen

RNA Purification

RNeasy mini kit, from Qiagen

Genomic DNA Degradation

RNase free DNA set, from Qiagen - digestion of DNA during RNA purification using RNeasy mini kit.

Reverse Transcription

High Capacity cDNA Reverse Transcription Kit, from Applied Biosciences (Thermo Scientific)

Real Time RT-PCR (qPCR) Assay

Taqman Gene Expression Assay for human DAGLα (Hs00391374_m1), human DAGLβ (Hs00373700_m1) as well as endogenous control PPIA, from Life Technologies

Taqman Master Mix, from Life Technologies

RNAase Free Water, from Sigma

RT-PCR Tubes

MicroAmp® Reaction tube with cap, from Applied Biosystems

Cel I Assay

DNA Extraction

Puregene Core Kit, from Qiagen

Assay Kit

Surveyor Mutation Detection Kit, from Transgenomic (Glasgow, UK)

Cell Sorting

Large Dishes for Single Clone Selection

150 x 20 mm Nunclon™ Delta surface dishes, from Thermo Scientific

Cloning Disc

3 mm Scienceware® cloning discs, from Sigma

Fluorescent Cell Sorting

FACs Aria cell sorter, from BD Biosciences (Oxford, UK)

Incucyte live cell imager, from Essen Biosciences (Hertfordshire, UK)

Resistant Marker Cell Sorting

Blasticidin Solution from Invivogen, (California, USA)

Sequencing

DNA Amplification & Sanger Sequencing

BigDye® Terminator v3.1 Cycle Sequencing Kit, from Life Technologies

3730 DNa Analyzer, from Applied Biosystems Hitatchi (Thermo Scientific)

Sanger Sequencing, provided by Source Bioscience (Cambridge, UK) & GATC Biotech (Konstanz, Germany)

Cell Lysis & Membrane Preparation

Homogeniser

POLYTRON PT 1200 E handheld homogeniser, from Kinematica (Düsseldorf, Germany)

ODG Lysis Buffer

50 mM Tris pH 8.0, 150 mM NaCl, 10 mM $MgCl_2$, 2 mM $CaCl_2$, 5% glycerol, 1% Triton X-100, 1 mM Na_3VO_4, 10 mM NaFl, 1 mM PMSF, supplemented with Roche Complete Protease Inhibitors.

Lysis Buffer for Membrane Preparation

20 mM HEPES pH 7.0, 2 mM DTT, 0.25 M Sucrose, 10 mM NaF, 1 mM NA_3VO_4, supplemented with Roche Complete Protease Inhibitors. For final re-suspension, use buffer containing no sucrose.

Protein Quantitation Assays

Protein Assay Dye Reagent, from Bio-Rad
Pierce Coomassie® Plus Protein Assay, from Thermo Scientific

Western Blot

5 X Protein Loading Buffer

300 mM Tris pH 6.8, 10% SDS, 25% Glycerol, 0.015% Bromphenol Blue, 500 mM Dithiothreitol

1 X Running Buffer

25 mM Tris, 0.2 M Glycine, 0.1% SDS, in ddH_20

1 X Transfer Buffer

25 mM Tris, 0.2 M Glycine, 20% Methanol, in ddH_20

Table 2.1 SDS-Polyacrylamide Gel

REAGENT	7.5% Gel	5% Gel
30% Acrylamide, National Diagnostics	5 mL	1.67 mL
1 M Tris, pH 6.8		1.25 mL
1 M Tris, pH 8.8	7.4 mL	
10% SDS	200 µL	100 µL
ddH_20	7.25 µL	6.86 µL
TEMED, National Diagnostics	13.2 µL	20 µL
0% Ammonium Persulphate (APS)	132 µL	100 µL

Table 2.2 Primary Antibodies

ANTIBODY	ICC	WB	SPECIES	SUPPLIER
V5	1:500	1:5000	Mouse	Life Technologies
DAGLα		1:1000	Goat	AbCam (Cambridge, UK)
DAGLβ		1:1000	Rabbit	Cell Signalling (New England Biolabs)
Actin		1:10,000	Mouse	Cell Signalling
Hoechst	1:10,000			Sigma

Table 2.3 Secondary Antibodies

ANTIBODY	ICC	WB	SPECIES	SUPPLIER
Alexa Fluor 488 Anti-mouse	1:1000		Goat	Molecular Probes (Thermo Scientific)
Alexa Fluor 680 Anti-Rabbit		1:1000	Goat	Molecular Probes
Alexa Fluor 700 Anti-mouse		1:5000	Goat	Life Technologies
Alexa Fluor 680 Anti-Goat		1:1000	Rabbit	Life Technologies
Anti-Goat HRP		1:1000	Horse	Vector Labs (Peterborough, UK)
Anti-Rabbit HRP		1:1000	Goat	Vector Labs

Immunocytochemistry

Fixative

4% Paraformaldehyde (PFA) in PBS, pH 7.4

Permeabilising Blocking/Staining Solution for Cell Staining

0.2% Triton-X, 1% BSA, 0.1% Sodium Azide (NaN_3) in PBS

Mounting Solution

33% glycerine and 17% Mowiol 4-88, from Calbiochem (Nottingham, UK), in PBS

DAGL Activity Assays

Enzyme Assay Plates

96-well clear flat-bottom polypropylene plates, from Costar (Glasgow, UK)

Enzyme Assay Buffers

50 mM HEPES, made up in ddH_20 (for use with PNP-Butyrate / Absorbance)
50 mM MES, made up in ddH_20 (for use with DifMU-Octanoate / Fluorescence)

Readers

SpectraMax Plus 384 Absorbance Microplate Reader, from Molecular Devices (California, USA)
FlexStation® Fluorescent Microplate Reader, from Molecular Devices

Tango Assay

Parental Tango Cell Line (Tango)

Tango CNR1-bla U2OS cells, from Life Technologies

V5α11 Cells

Parental Tango cells stably over expressing DAGLα-V5

V5β4 Cells

Parental Tango cells stably over expressing DAGLβ-V5

Parental Tango Cell Line Media

McCoy's 5A Medium with 10% dialyzed FBS, 0.1 M NEAA, 25 mM HEPES (pH 7.3), 1 mM Sodium Pyruvate, 100 µg/mL Penicillin / Streptomycin, 200 µg/mL Zeocin™ all from Life Technologies

V5α11 / V5β4 Media

Parental Tango Cell Line Media supplemented with 10 µg/mL Blasticidin, from Life Technologies

Standard Plating Medium for Tango Assay

Freestyle™ F17 from Life Technologies

McCoy's 1% Plating Medium

McCoy's 5A Medium supplemented with 1% FBS, 0.1 M NEAA, 25 mM HEPES (pH 7.3), 1 mM Sodium Pyruvate, 100 µg/mL Penicillin / Streptomycin, all from Life Technologies

For 1% DMEM Plating Medium

DMEM / F-12, GlutaMAX^{TM} supplemented 1% FBS, 0.1 M NEAA, 25 mM HEPES (pH 7.3), 1 mM Sodium Pyruvate, 100 µg/mL Penicillin / Streptomycin, all from Life Technologies

Tango Assay Plates

Costar 96-well black clear bottom polystyrene plates, from VWR International (Leicestershire, UK)

Tango Detection Reagent

LiveBLAzer FRET B / G Loading Kit, from Life Technologies:
LiveBLAzer FRET B / G Substrate (CCF4-AM), Solution B, Solution C and Solution D, mixed together just prior to assay according to the manufacturer's instructions.

Fluorescent Reader

FlexStation® Microplate Reader, from Molecular Devices

Table 2.4 Compounds

COMPOUND	DESCRIPTION	SUPLPIER
4-Nitrophenyl Butyrate ***(PNP-Butyrate)***	Colorimetric surrogate DAGL substrate	Sigma
6,8-Difluoro-4-Methylumbelliferyl Octanoate ***(DiFMUO)***	Fluorescent surrogate DAGL substrate	Life Technologies
Tetrahydrolipstatin *(THL)*	Serine Lipase Inhibitor	Tocris (Bristol, UK)
OMDM-188	DAGL Inhibitor	Gift from Dr. Di Marzo
RHC 80267	DAGL Inhibitor	Tocris
Arachidonyl-2′-Chloroethylamide Hydrate ***(ACEA)***	CB1 Receptor Agonist	Sigma
AM251	CB1 Receptor Antagonist	Sigma
JZL184	MAGL Inhibitor	Sigma
JZL195	Dual MAGL / FAAH Inhibitor	Sigma
URB597	FAAH Inhibitor	Tocris
Forskolin	PKA Activator	Sigma
Phorbol 12-myristate 13-acetate ***(PMA)***	PKC Activator	Sigma
Ionomycin	Calcium Ionophore	Sigma

2.2 Methods

Cell Culture

All cell lines were incubated at 37°C in a humidified atmosphere with 5% CO_2. Once the cells were approximately 80% confluent, cells were plated for subsequent analysis (see below) or split for further culture and maintenance. Cells for maintenance were plated in 10 cm dishes or T75 flasks and cultured in full growth medium.

Passaging of Tango Cells

Using aseptic technique, growth medium was removed from the cell plate by aspiration. Cells were then washed once with an appropriate volume of PBS to remove residual serum. The PBS was then aspirated and replaced with an appropriate amount of trypsin e.g. 3 mL for a 10 cm dish. The plate was returned to the incubator for approximately 3 min. Trypsin was inactivated by addition of an equal volume of growth media (containing 10% serum) and centrifuged at 1200 rpm for 3 min. The cell pellet was re-suspended in 10 mL Tango media and either used for analysis or split as described above. Tango cells were incubated at 37°C, 5% CO_2. If used for analysis, the concentration of cells in the suspension was first determined using a haemocytometer and cells were plated in the appropriate plate type using a multi-channel pipette.

Transfection

Lipofectamine 2000

On the day before transfection, cells were plated either in a 6-well plate or a 10 cm dish without antibiotics such that they were 90-95% confluent at the time of transfection. The appropriate amount of Lipofectamine was mixed in Optimem and incubated for 5 min before combining with the individual DNA solutions by gentle mixing and the solutions were incubated at RT for 20-30 min. During the incubation, the media on the cells was replaced with Optimem (as per manufacturer's instructions). The DNA-Lipofectamine complexes were added to the cells and incubated for 4-6 h and the medium was replaced.

Fugene HD

Transfection carried using Fugene HD was according to the manufacturer's protocol. For example, 6 x 10^5 cells were plated in 8 ml of growth medium in a T25 flask. 8.8 µg of plasmid DNA was added to a total of 409 µL serum free medium. 31 µL of Fugene HD reagent was added mixed by pipetting and incubated at RT for 10 min. 400 µL of the complex was added to the flask and mixed thoroughly. The medium was changed either after 5 h or the following morning to growth medium without selection antibiotics. After 24 – 48 h selection antibiotics were introduced to the medium, if required.

Molecular Biology

DNA Ligation

Ligation reactions were performed on ice and in the following order: a solution of 2 µL T4 DNA ligase reaction buffer, an appropriate amount of digested vector backbone DNA and insert DNA were mixed together and made up to 20 µL with ddH_20. 0.1 µL of T4 DNA ligase was added to the mixture which was then incubated in a Thermomixer at 16 ºC for 2-4 h.

Annealing Oligonucleotides

Annealing was carried out using the quick ligation kit, without ligase. Reactions were set up using 10 µL of 2 X reaction buffer solution, equal concentrations of oligonucleotides and the volume was made up to 20 µL with ddH_20. The mixture was heated to 95 ºC in the Thermomixer, which was then switched off and allowed to cool slowly for 1-2 h.

Restriction Digest

Vector DNA was mixed with 1 unit of restriction enzyme per 1 µg DNA, the appropriate buffer for that enzyme (Buffer 1-4, New England Biolabs), and made up to an appropriate volume with ddH_20. The mixture was incubated at 37 ºC (or suitable temperature for restriction digest) in a humidified incubator for 1-2 h.

Agarose Gel

6 µL of gel loading dye was added to 20 µL restriction digest solutions and loaded into a well of 0.8% agarose gel. 20 µL of 1 Kb Plus DNA ladder was loaded to the farthest left well. The gel was run at 100 V for 30 min. Gels were viewed and analysed using Molecular Imager® Gel Doc™ XR+ System.

DNA Gel Extraction

DNA was separated on an agarose gel as described above. The desired band was cut out from the gel using a scalpel blade and placed in an eppendorf tube. QIAquick gel extraction kit was used according to the manufacturer's instructions. DNA concentration was then determined using the Nanodrop.

Plasmid DNA Purification

Following *E. coli* transformation, a single colony was selected from the agar plate and placed in 1 ml of LB-broth with the appropriate antibiotic(s). Plasmid DNA was purified using a Qiagen miniprep kit according to the manufacturer's instructions. DNA concentration was determined using the Nanodrop. This may be followed up with purifying larger quantities of plasmid DNA. This was done by retaining a sample of the cells grown and inoculating them with 100 ml media. DNA was then purified using a Qiagen maxiprep kit.

Transformation of Competent Escherichia Coli (E. coli) Cells

Competent *E. coli* cells were stored at -80 ºC until ready for use. A vial of the cells was removed from the freezer and thawed on ice. 4 µL of the DNA sample was placed into a clean eppendorf tube and also placed on ice. Once the cells began to thaw, 25 µL were added to the DNA sample and incubated for 30 min on ice. The cells were then heat shocked in a water bath at 42 ºC for 40 s – 1 min and then placed immediately on ice for a further 5 min. 200 µL of LB-broth was added to the mixture, which was then placed in a Thermomixer at 37 ºC for 1 h, shaking at 850 rpm. The transformed *E. coli* cells were plated out on agar and incubated at 37 ºC in a humidified incubator ON.

Polymerase Chain Reaction (PCR)

For PCR, each reaction was carried out according to the manufacturer's instructions for the master mix used. In brief, 1 µL DNA was combined with 0.1 µL of primer (each at 100 µM), 8.8 µL ddH_20 and 10 µL mastermix before the reaction was performed in a PCR machine (using the mastermix manufacturer's recommended settings).

RNA Purification and Reverse Transcription to cDNA

Tango cells for analysis were grown to confluency in a 6-well or 10 cm dish. The cells were washed once in PBS and using Qiagen's RNeasy kit, the cells were lysed with RLT buffer. Cells were homogenized by spinning through a QIAshredder column, before RNA was purified using RNeasy kit. RNA concentration and purity was determined using the Nanodrop. RNA was converted to cDNA using High Capacity cDNA Reverse Transcription Kit and a PCR step. In brief, 2 X reverse transcription master mix was made up on ice and mixed with the purified RNA in PCR tubes. The reaction tubes were loaded into the thermal cycler using the following protocol – 25 °C for 10 min, 37 °C for 120 min, 85 °C for 5 min and stored at 4 °C until ready for use.

Real Time RT-PCR

For real time RT-PCR, or qPCR, Taqman gene expression assay kits were used according to the manufacturer's instructions. Assays for both DAGLα and DAGLβ, as well as the endogenous control assays PPIA. GAPDH and 18S were used. RNA was extracted from Tango cells, including α11 and β4 cells for controls, and the RNA was reverse transcribed to cDNA, as described above. 1-100 ng of cDNA was used in 20 µL reactions in a 96-well PCR plate. The plate was sealed and loaded into the Lightcycler RT-PCR instrument using the following protocol – heat to 50 °C for 2 min, 95 °C for 10 min followed by 45 cycles of 95 °C for 15 s and 60 °C for 1 min. Analysis was performed using the LightCycler 480 Software.

Transformation for Sequencing

Genomic DNA (corresponding to the CRISPR cutting site) was amplified by PCR using Taq Polymerase, as described above. The PCR products were purified from agarose gels using QIAquick gel extraction kit and cloned into TOPO cloning vector by setting up the following 6 µL reaction; 1 µL salt solution (1.2 M NaCl, 0.06 M MgCl2), 4 µL PCR product, 1 µL TOPO vector. The reaction was incubated at RT for 5-10 min before 4 µL was transformed into chemically competent cells. Positive clones were selected and grown in LB broth. DNA from each clone was analysed by sequencing.

Sequencing

20 µL reactions with BigDye® Terminator enzyme were set up in PCR tubes according to the manufacturer's instructions. The tubes were placed in a PCR machine which was heated to 95 ºC for 2 min, before the following protocol was used; 95ºC for 10 min, 50 ºC for 20 min, 60 ºC for 4 min. This cycle was repeated 25 times in order to amplify the DNA and stored at 4 ºC until ready for use. Following PCR of one of the strands of DNA, it was then precipitated with ethanol/EDTA. 5 µL of 125 mM EDTA was added to each sample, followed by 60 µL of 99.5% ethanol and incubated at RT in the dark. The samples were then centrifuged for 15 min at 4000 g at 4 ºC and the supernatant was gently removed. 60 µL of 70% ethanol was added to each sample, which were centrifuged again at maximum speed (in a bench top centrifuge) for 5 min. The supernatant was removed, and while keeping the PCR tubes inverted, they were placed into a plate centrifuge and spun at lowest speed for 30 s to remove residual ethanol. Each DNA sample was then re-suspended in 10 µL ddH20 and placed in a v-shaped 96-well plate. The sequence for each sample was determined by 3730 DNA Analyzer from Applied Biosciences and comparing the results by 'blasting' it against the DAGL sequences. Sequencing was also analysed by Source BioScience, Cambridge.

Cel I Assay

Summarised in Figure 2.1

Genomic DNA from Tango cells was extracted using Puregene Core Kit (Qiagen) approximately 72 h after transfection as described above. The genomic regions flanking the gRNA site (for CRISPR/Cas9 genome editing) were PCR amplified using the technique above. The PCR products were purified using QiaQuick Spin Column (Qiagen) and subjected to re-annealing to generate heteroduplexes: 95°C for 10 min; 85°C for 1 min; 75°C for 1 s; 65°C for 1 s and ramping to 25°C at -0.3°C/s; and 25°C hold for 1 min and finally hold at 4°C. After re-annealing, 10 µL of PCR products were treated with 1 µL of Cel I Surveyor nuclease and 1 µL of enhancer (supplied with the kit). Cel I Surveyor nuclease cleaves mismatched DNA at the 3' side for each strand at the site of the mismatch. The samples were incubated at 40 ºC for 40 min and were then run on a 10% Acrylamide gel for 24 min at 240 V. The gel was washed twice in water and incubated on a roller with ethidium brominde solution for 1 h. The gel was visualized using UV light (Molecular imager from BioRad). Any smaller bands separate from the larger bands indicates cleavage by Cel I at a mismatched site on the DNA.

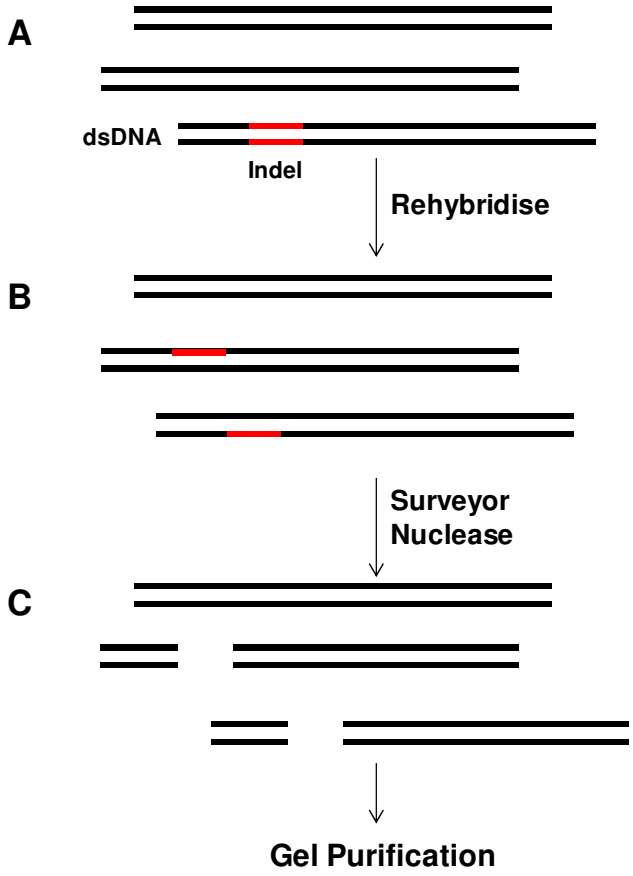

Figure 2.1 Schematic of the SURVEYOR Cel I assay for detection of double strand break-induced insertions and deletions (Indels)

(A) Genomic PCR is used to amplify the Cas9 target region from a heterogeneous population of modified and unmodified cells. Highlighted in red is an indel formation resulting from Cas9 endonuclease double-strand break. **(B)** The PCR products are boiled and then reannealed slowly to generate heteroduplexes. **(C)** The reannealed heteroduplexes are cleaved by SURVEYOR Cel I nuclease, which recognizes mismatched DNA, whereas homoduplexes are left intact. The SURVEYOR Cel I assay was used to determine Cas9-mediated cleavage efficiency with our selected gRNA sequences.

Cell Sorting

Fluorescent Cell Sorting with FACS

Cells were allowed to recover for 1-2 days following transfection. Cells were washed once, trypsinised and re-suspended in ice cold PBS containing 2% FCS. Cells were then sorted for GFP expression using the FACS aria. 100 - 200 cells were then plated into a large dish for colony selection. When single colonies were visible, they were removed using a cloning disc. The disc was carefully removed and placed into a well of a 24-well cell culture plate.

Resistance Marker Cell Sorting

Cells were co-transfected with CRISPR/Cas9 nickase construct for DAGLα and with a DNA repair homology arm containing a blasticidin resistance gene. Cells were allowed to recover for ~24 h post-transfection. 100 - 200 cells were then placed into a large dish for colony selection and again allowed to recover for 1-2 days, before being introduction of 4 μg / mL blasticidin to the medium. Clonal cells were selected as described above and expanded for analysis.

Cell Lysis

Cell Lysate Preparation

Cells were cultured in 6-well plates or in 10 cm dishes until reaching 70 – 80% confluence, washed in ice-cold PBS and lysed in 50-500 μL ODG lysis buffer. The lysate was collected in 1.5 mL eppendorf tubes and left to rotate for 30 min at 4°C to separate out cell debris. The lysate was centrifuged at 3,000 rpm for 5 min at 4°C. Protein concentration was determined using Protein Assay (Bradford) Dye Reagent, according to the manufacturer's instructions.

Membrane Preparations

Growth media on confluent Tango cells from either a dish or a tray was aspirated, the cell plate placed on ice and washed in ice-cold PBS three times. Cells were lysed by addition of lysis buffer (for membrane preparation) to the cell plate for 1-2 min, removed using a cell scraper and collected into a 1.5 mL eppendorf. Protein was homogenised on ice by Polytron homogeniser (3 cycles of 7 seconds, set to maximum speed). Following homogenisation, membrane protein was centrifuged using ultracentrifugation (Beckman Coulter Optima TLX-120 Ultracentrifuge; 54,000 rpm, 30 min at 4°C). The pellet was re-suspended in sucrose-free lysis buffer (2 ml / dish) using the Polytrone homogeniser, frozen into small aliquots and stored at -80°C. Protein concentration was determined using Coomassie (Bradford) Protein Assay Kit, according to the manufacturer's instructions.

Western Immunoblotting

SDS-PAGE

SDS-Polyacrylamide gels were pre-made and used on the same day or kept damp overnight at 4°C. When ready for use, the comb was removed to expose the wells, and the gel was immersed in 1 X running buffer. Equal amounts of protein lysate were made up in 5 X protein loading buffer, made up to a total volume of 50 µL and boiled for 5 min at 100°C. (These were either stored at -20°C or used immediately.) The samples were then separated on SDS-Polyacrylamide gels by running them at 100 V for 2 h and were then transferred to nitrocellulose hybond membranes (Amersham) for 1 h at 100V.

Western Blotting

The membrane was then blocked in 5% Milk at RT for 1 h and the primary antibody was applied overnight at 4°C, or for 1 h at RT. Next the membrane was washed 3 times in PBS-T for 10 min and then incubated with the secondary antibody solution at RT for 1 h. The secondary antibody was chosen according to development method (ECL or Odyssey) and suitable for the primary antibody used. This step was followed by another wash step - 3 times in PBS-T for 10 min.

For analysis using Li-Cor Odyssey, Alexa Fluor 700/800 fluorescently-labelled secondary antibody in 2% milk / PBS-T were used and incubated with the blot for 1 h at RT. The blots were analysed using the Li-Cor Odyssey infrared imaging and software.

Alternatively, blots were analysed using Amersham's enhance chemiluminescent (ECL) western blotting substrate i.e. chemiluminescent substrate for the detection of horseradish peroxidase (HRP) on immunoblots. Thus HRP-tagged secondary antibodies were used for this procedure and incubated with the blot for 1 h at RT in 2% Milk in the appropriate buffer. ECL substrate was made up according to the manufacturer's instructions. The solution was added directly to the blot and incubated for 1 min. The blot was then placed into a cassette and developed in a dark room.

If required, blots from either method were stripped using Re-Blot Plus (Chemicon International) according to the manufacturer's protocol and probed for Actin as a control using the same method.

Quantification

ECL/ECL plus visualised western blots were scanned in at 2400 dpi using a perfection V700 scanner (Epson) and quantified using Image J analysis software. Where possible, samples were loaded with an equal concentration of protein and were also normalised to the actin control. Western blots which were visualised by Odyssey infrared imaging were quantified using Odyssey software.

Immunocytochemistry

13 mm glass coverslips were individually coated in poly-lysine in a 4-well dish for 30 min. The poly-lysine was removed before addition of 5,000 - 20,000 cells/well in full growth medium and left to adhere overnight at 37°C 5% CO_2. The following day cells were fixed to the slide with 500 µL 4% PFA for 30 min followed by 3 x 5 min washes in PBS. Cells were blocked with 500 µL 0.2% Triton-X, 1% BSA, 0.1% sodium azide for 1 h, then incubated with the primary antibody overnight at 4°C. The primary antibody was removed, cells were washed 3 times in PBS for 5 min. Secondary antibody and the nuclear dye Hoecsht were added in the same solution and incubated for 1 at RT. The coverslips were then mounted with Miowol. Images were captured with an AxioCam using KS300 software (Carl Zeiss Microimaging, Inc)

Assays

A Surrogate Substrate DAGL Activity Assay

All DAGL activity assays were carried out at room temperature (RT) unless otherwise stated in accordance with the method previously described; DAGL activity assays were adapted from a protocol previously described (Pedicord *et al.*, 2011).

Membrane-based DAGL Activity Assay

200 µL reactions were set up in clear enzyme assay plates. For reactions with membrane protein (from membrane preparations, described above) and substrate only, 100 µL of 2 X final assay concentration (FAC) of membrane protein and 100µL of 2 X FAC of substrate were used. For reactions with inhibitors, 100 µL of 2 X FAC of membrane protein, 50 µL of 4 X FAC of inhibitor, and 100 µL of 2 X FAC of substrate were used.

For the colourimetric absorbent assay, 4-nitrophenol butyrate (PNP-Butyrate) was added directly from DMSO stocks to buffer containing 50 mM HEPES, pH 7.5 only i.e. 1:20 dilution. The final concentration typically used was 250 µM (5% DMSO). Reactions were monitored kinetically every 12 s, for a total of 30 min, by a Spectramax Plus (Molecular Devices) set at an OD of 400 nm. A linear regression of the first 10 min was used for calculation of the reaction rate.

For the fluorescent assay, DiFMU Octanoate was added directly from a DMSO stock to buffer containing 50 mM MES pH 6.0 only i.e. 1:20 dilution. The final concentration typically used was 10 µM. Reactions were monitored kinetically every 30 s by the Flexstation (Molecular Devices), set at an excitation wavelength of 360 nm and an emission wavelength of 450 nm. A linear regression of the first 10 min was used for calculation of the reaction rate.

Tango™ CNR1-bla U2OS Cell-Based Assay

Parental Tango cells (CNR1-bla U2OS Cells) were plated (20,000 cells/well) in Tango assay plates in 100 µL of plating medium and incubated at 37°C, 5% CO_2. Compounds were prepared in the same plating medium used and 50 µL total compound was added to each well i.e. for agonist assay, 50 µL of 3 X FAC of agonist compound; for antagonist assay, 25 µL 6 X FAC of antagonist followed by 25 µL of 6 X FAC of agonist (DMSO < 1%). After the incubation time with the compound, Tango substrate was made up according to the manufacturer's instructions (Life Technologies) and 30 µL of this substrate was added per well. Plates were incubated in the dark for 2 h at RT and read on the Flexstation, with the following filter selections:

	Scan 1	Scan 2
Excitation Filter	409 nm	409 nm
Emission Filter	460 nm	530 nm
Purpose	Measurement in the blue channel	Measurement in the green channel

Data Analysis

Data was analysed using Microsoft Excel or SigmaPlot. Student's 2-sided t-test was used for statistical analysis; * $p<0.05$, ** $p<0.01$, *** $p<0.001$.

CHAPTER 3. RESULTS I – Phosphorylation of the DAGLs; an updated perspective

3.1 Introduction

Biochemical characterisation of the DAGLs was first attempted approximately 30 years ago (Farooqui *et al.*, 1984; 1986), yet still very little is known about their regulatory mechanisms. Due to increasing interest in the therapeutic implications associated with the DAGLs and the eCB system, there is a growing need to understand how these enzymes are regulated. As discussed in the general introduction, we first identified the structural components of these enzymes to understand their regulatory mechanisms. In addition to identifying the regulatory loop, structural studies of the DAGLs identified a number of phospho-sites that may regulate activity.

Phosphorylation is the reversible PTM involving the addition of a phosphate group from ATP to the hydroxyl groups of serine, threonine and/or tyrosine residues. It is an ubiquitous regulatory mechanism in both eukaryotes and prokaryotes (Johnson & Lewis, 2001). Intracellular phosphorylation by protein kinases, triggered in response to extracellular signals, provides a mechanism for the cell to switch on or switch off many diverse processes. This includes enzyme activity, achieved mainly by introducing conformational changes to the protein. Several lipases are regulated by phosphorylation at specific sites; for example PLCγ (Gresset *et al.*, 2010), TGL4 (Kurat *et al.*, 2009) and hormone sensitive lipase (HSL) (Lampidonis *et al.*, 2011). HSL is the most studied in terms of phosphorylation controlling its activity. It is regulated by reversible phosphorylation on five critical residues. The closing and opening of the lid regulates access of the substrate to the catalytic site of the enzyme, and this is under control of phosphorylation (Holm, 2003). Phosphorylation alone is not enough to activate HSL and conformational alterations, resulting in a translocation from the cytoplasm to lipid droplets, may also be involved (Lampidonis *et al.*, 2011). However, phosphorylation stands as a likely mechanism

for regulating DAGL activity. For example, DAGL from brain microsomes was shown to be phosphorylated by PKA (Rosenberger *et al.*, 2007) and phosphorylation of bovine rod membranes by PKA resulted in a ~70% increase in DAGL activity (Perez Roque *et al.*, 1998). Similarly, PKA and PKC activation stimulated 2-AG synthesis (Vellani *et al.*, 2008).

As a result we have built a working model for each DAGL enzyme, allowing us to identify key phospho-sites based on the number of reports and location within their structure (Reisenberg *et al.*, 2012). Given that the publically available databases used to identify these sites are updated on a regular basis, the latest analysis on potential phosphorylation sites as a regulatory mechanism has been reported here.

3.2 Results

The DAGL Phospho-map

Using phospho-peptide databases, candidate regulatory phospho-sites within the DAGL sequence can be identified. This provides evidence that the DAGLs *can* be phosphorylated, indicating its role in regulation of activity. We first used the phosphorylation prediction tool, NetPhosK 1.0. This tool uses sequence and structural data of reported phosphorylation events to predict phospho-sites (~70% accuracy against known sites (Blom *et al.*, 1999; Iakoucheva *et al.*, 2004). We then cross examined identified sites with those identified experimentally, such as through mass spectrometry, on Cell Signalling Technology (CST) database (phosphosite.org). The software on this website identifies potential phospho-sites based on proteomic databases. I have compiled the results into a table, Table 3.1 for DAGLα, Table 3.2 for DAGLβ. A number of the CST studies have not yet been published; therefore we were mindful of the number of times a particular site has been identified. There were 30 sites identified from both CST and NetPhosK 1.0 for DAGLα, and 13 for DAGLβ (Tables 3.1 & 3.2). If one is to place a minimal requirement of 3 independent published studies to consider a phospho-site as genuine (as well as being identified by NetPhos K 1.0), then the total number identified for DAGLα is 10 and for DAGLβ is 1. These sites are highlighted in the 'phospho-map' in Figure 3.1 (4 other potential sites for DAGLβ that were not picked up by NetPhosK 1.0 have also been included because of the higher number of reports.) This a linearized diagram of each DAGL sequence, colour-coded to highlight the structural features. From this we can see where each of these phospho-sites is located on each DAGL. All 5 of the sites highlighted for DAGLβ are located within the regulatory loop (S570, S574, S576, S577, and S579). However, only one has been identified in this region for DAGLα (T560) with rest being located in the tail domain (S727, S732, S743, S782, S784, S806, S952, T1023, and T1030).

Table 3.1 Summary of DAGLα phospho-sites identified

DAGLα site	Location	CST	Net PhosK 1.0	Cell / Tissue Type	Predicted kinase	Published
T560	Regulatory Loop	9	Yes	K562 (Myelogenous leukemia); Jurkat (8)	PKC; cdc2	Hsu et al., 2011
S727	Tail	4	YES	Mouse & rat brain, HEK-293T (recombinant expression)	RSK, DNAPK	Schindler et al., 2013; Shonesy et al., 2013, Lundby et al., 2012, Munton, et al., 2007
S732	Tail	5	YES	Brown fat, kidney, synaptomsomes, PSD	CamKI	Schindler et al., 2013; Trinidad et al., 2012; Lundby et al., 2012; Huttlin, et al., 2010; Trinidad et al., 2006
S743	Tail	10	YES	HEK293T (recombinant expression), Brain (3), Synapse (2), PSD	RSK, p38MAPK	Trinidad et al., 2006; Trinidad, et al., 2008; Huttlin, et al., 2010; Wisniewski, et la., 2010; Goswami et al., 2012; Trinidad et al., 2012; Shiromizu et al., 2013; Shonesy et al., 2013
S782	Tail	3	YES	HEK293T (recombinant expression); Mouse cerebellum/brain	CamKI, CamKII	Shonesy, et la., 2013; Schindler et al., 2013; Lundby et al., 2012
S784	Tail	4	YES	Brain; Synapse	CamKII	Schindler et al., 2013; Trinidad et al., 2012; Lundby et al., 2012; Huttlin, et al., 2010
S806	Tail	5	YES	Brain, synapse, HeLa Cells	PKA	Lundby, et al. 2012; Huttlin, et al.,2010; Wiśniewski, et al. 2010; Chen, et al. 2009; Trinidad, et al., 2008
S952	Tail	4	YES	HeLa, Brain	GSK3	Sharma, et al., 2014; Lundby, et al., 2012; Huttlin, et al., 2010; Wiśniewski, et al., 2010
T1023	Tail	4	YES	HEK293T (recombinant expression); Brain	PKC, cdk5	Shonesy et al., 2013; Huttlin, et al., 2010
S1030	Tail	8	YES	HEK293T (recombinant expression); Brain	p38MAPK; GSK3; cdk5	Shonesy et al., 2013; Huttlin, et al., 2010; Trinidad, et al., 2012; Wiśniewski, et al., 2010

Table 3.2 Summary of phospho-sites identified for DAGLβ

DAGLβ site	Location	CST	Net PhosK 1.0	Cell / Tissue Type	Predicted kinase	Published
S570	Regulatory Loop	6	No	HeLa, mouse embryonic fibroblast, Purified protein, Jurkat T cell	CDK1, CDk2	Sharma, et al., 2014; Wu, et al., 2012; Kettenbach, et al., 2011; Olsen, et al., 2010; Mayya, et al., 2009; Daub, et al., 2008
S574	Regulatory Loop	23	No	HeLa, Purified protein, HeLa		Zhou, et al., 2013; Kettenbach, et al., 2011; Mayya, et al., 2009
S576	Regulatory Loop	4	Yes		CamKI, CamKII, PKC, PKG, cdc2, GSK3	CST Reports
S577	Regulatory Loop	4	No	Brain, Jurkat T cell, HeLa		Huttlin, et al., 2010; Tweedie-Cullen et al., 2009; Mayya, et al., 2009
S579	Regulatory Loop	9	No	HeLa,mouse embryonic fibroblast, myeloid leukemia cells, purified protein, Jurkat T Cell, brain		Sharma, et al., 2014; Zhou, et al., 2013; Wu, et al., 2012; Weber et al., 2012; Kettenbach et al., 2011; Huttlin, et al., 2010; Wiśniewski, et al., 2010; Raijmakers, et al., 2010; Olsen, et al., 2010

Figure 3.1 Phospho-map of human DAGLα and DAGLβ

Phospho-map highlighting predicated phosphorylation sites on DAGLα (top) and DAGLβ (bottom) in both A and B. The phosphorylation sites on the map were identified by mass-spectrometry analysis of various cells and tissues. Structural features are highlighted; TM domain in blue, catalytic domain in dark red, with regulatory loop in green and signature motif in red. The first report showing the potential of phosphorylation as a regulatory mechanism highlighted all sites reported for the DAGLs (A). We have updated this phospho-map to include only phospho-sites that have been reported 3 times or more, thereby gaining confidence that these sites are important for function. The number of times a potential phospho-site has been reported is indicated in brackets next to the site's name (B). The carboxyl-terminal tail region of DAGLα has been found to be especially heavily phosphorylated and may have a role in intra-molecular interactions with the catalytic domain (Shonesy *et al.*, 2013).

Figure A adapted from Reisenberg et al., 2012.

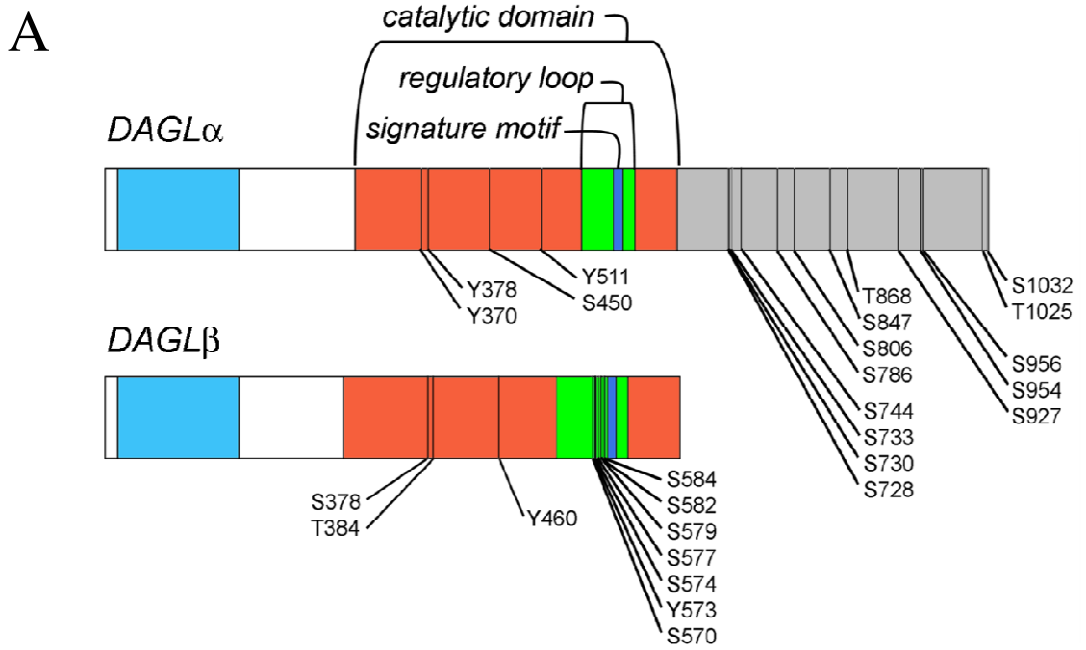
A
catalytic domain
regulatory loop
signature motif
DAGLα
Y378
Y370
Y511
S450
T868
S847
S806
S786
S744
S733
S730
S728
S1032
T1025
S956
S954
S927
DAGLβ
S378
T384
Y460
S584
S582
S579
S577
S574
Y573
S570

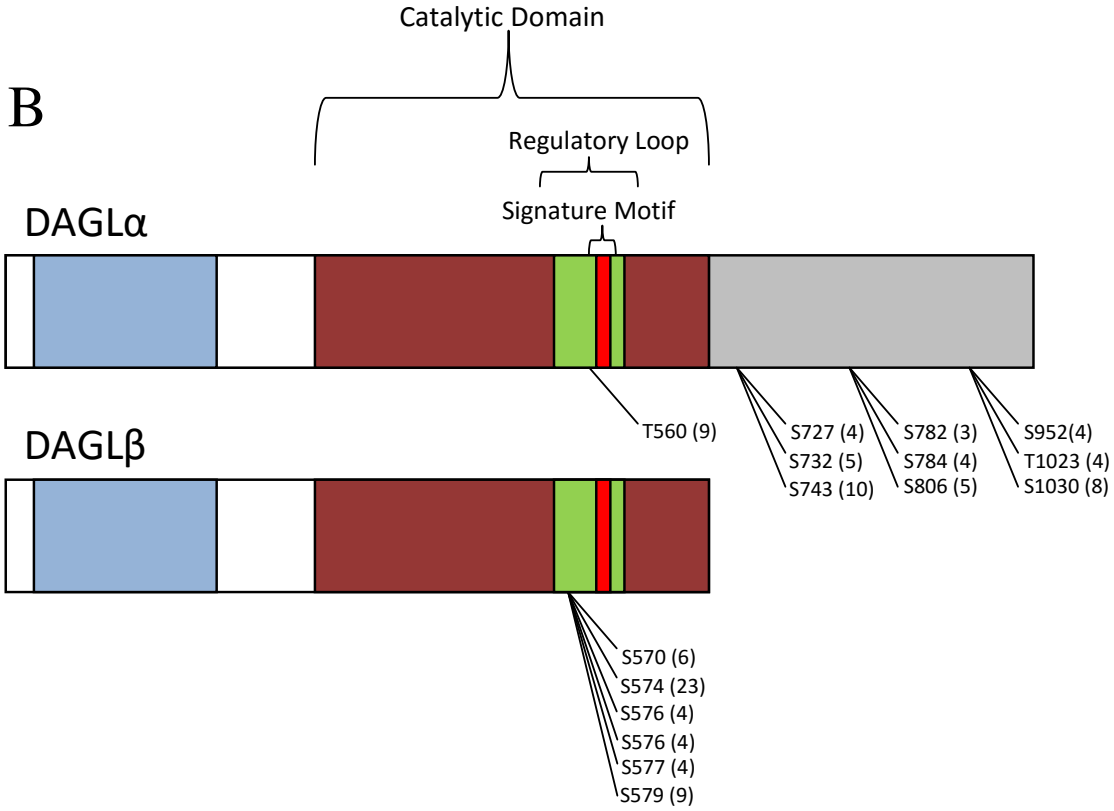
B
Catalytic Domain
Regulatory Loop
Signature Motif
DAGLα
T560 (9)
S727 (4)
S732 (5)
S743 (10)
S782 (3)
S784 (4)
S806 (5)
S952(4)
T1023 (4)
S1030 (8)
DAGLβ
S570 (6)
S574 (23)
S576 (4)
S576 (4)
S577 (4)
S579 (9)

Identification of potential phosphorylation sites for regulation of DAGL function

When considering the importance of phospho-site(s) for regulation, location and orientation at the membrane are key aspects. DAG, the substrate for the DAGLs, is generally found integrated into the cell membrane (Goni & Alonso, 1999). The DAGLs are therefore likely to be sub-localised at the membrane, via their TM domains and palmitoylation of the cysteine rich insert. This would position the enzymes close to the substrate, and may also orientate the catalytic domain to facilitate segregation of the substrate from the membrane. The membrane proximal surface of the DAGLs was identified based on the orientation of the catalytic triad, which would need to be in this position to hydrolyse DAG. Consequently, the regulatory loop is likely to be membrane (and substrate) proximal, positioning it to facilitate interfacial activation. As a result, phospho-sites involved in regulation of substrate access are more likely to also be membrane proximal. The phospho-sites (mentioned above) that were identified within the regulatory loop of DAGLα and DAGLβ are membrane proximal, posing themselves as potential regulatory candidates, and are likely to determine whether the regulatory loop is in the 'open' or 'closed' conformation.

The DAGLα tail appears to be heavily phosphorylated, but this is dispensable in terms of activity, indicating the sites in the tail do not play a direct role in regulation of the enzymatic function (Pedicord *et al.*, 2011). However, a more recent study showed that the DAGLα tail is phosphorylated by CamKIIa, resulting in inhibition of DAGLα activity by ~40% (Shonesy *et al.*, 2013). Although the mechanism underlying this inhibition is unknown, it may be due to intra-molecular interactions between the tail and the catalytic domain/lid following phosphorylation or localisation.

3.3 Summary & Conclusions

The aim of this chapter was to provide an update on the role of phosphorylation in the regulation of DAGL activity. In order to determine the role of phosphorylation (or indeed any other type of PTM), we took a bioinformatics approach to assess the wealth of information freely available and regularly updated online. We gathered this information together to determine if there is sufficient evidence for a regulatory role of phosphorylation in DAGL activity.

The structure of the catalytic domain is a member of the α/β hydrolase fold family of enzymes. Common structural features of this enzyme family can tolerate considerably sized inserts at certain locations (Nardini & Dijkstra, 1999). In the case of the DAGLs, two inserts were identified, a cysteine rich insert and a lid-like structure termed the 'regulatory loop'. The DAGLs have previously been shown to be palmitoylated (Kang *et al.*, 2008; Martin & Cravatt, 2009). Palmitoylation of the cysteine-rich insert may serve to localise the DAGLS to the membrane. The regulatory loop, on the other hand, is a 50-60 amino acid insert which has an important role in substrate access to the catalytic site. This lid is responsible for interfacial activation, a process whereby activity of lipases is enhanced upon contact with a lipid–water interface, which is believed to trigger the opening of the lid (Nardini & Dijkstra, 1999; Holmquist, 2000). The regulatory loop is in the right position to shield DAG access to the catalytic site and also contains a highly conserved 'signature motif' whose function has yet to be elucidated (Reisenberg *et al.*, 2012).

The activity of several lipases is controlled by phosphorylation (Kurat *et al.*, 2009; Gresset *et al.*, 2010; Lampidonis *et al.*, 2011). HSL, another member of the α/β hydrolase fold family, is probably the most studied in terms of phosphorylation. HSL is regulated by reversible phosphorylation on 5 critical residues by PKA, resulting in ~2fold increase in activity by displacing the regulatory lid that shields the catalytic activity (Holm *et al.*, 1994; Lampidonis *et al.*, 2011). Phosphorylation of HSL *in vitro* not only displaces the lid, it also increases the hydrophobic surface area of the

protein, probably to enhance substrate access (Krintel *et al.*, 2009; Lampidonis *et al.*, 2011). The evidence for the role of phosphorylation in regulating the activity of HSL gives us a working model for studying possible regulatory mechanisms of the DAGLs, based on its key structural features.

Through cross-examination of the DAGLs' sequences between online databases, we have identified key phospho-sites that may be important for regulation of function. These sites are explored in Tables 3.1 and 3.2 and are highlighted in the phospho-map (Figure 3.1). A total of 43 DAGLα/β phospho-sites have been reported, identified through mass spectrometry analysis of complex samples (cells/tissues), which can often result in false positives and/or negatives (Alcolea *et al.*, 2009). Therefore, phospho-sites identified 3 times or more and through the prediction tool NetPhosK 1.0 have been included on the phospho-map, as NetPhosK 1.0 has a 70-80% success rate in predicting experimentally-verified phospho-sites (Blom *et al.*, 1999; Iakoucheva *et al.*, 2004). The DAGLs are therefore potentially phosphorylated at a number of sites, and this may be important for regulation.

Glycosylation of the TM domains, and/or palmitoylation of the cysteine-rich insert, may serve to localise the DAGLs to the membrane (and thus close to their substrate DAG). However phosphorylation of the regulatory loop has positioned itself as a key potential regulatory mechanism of DAGL's activity by way of opening or closing the loop that shields the active site.

CHAPTER 4. RESULTS II – Establishing Tango cell lines stably expressing DAGLα and DAGLβ

4.1 Introduction

The main regulation point of the eCB system is the synthesis and degradation of the two eCBs, 2-AG and anandamide. These lipophillic agents are synthesised 'on-demand' from membrane components. As previously discussed, there are many reports supporting the role of 2-AG as the retrograde signalling molecule. Alongside this, the DAGLs have been implicated in a number of disease areas such as Alzheimer's disease, Parkinson's disease, obesity and pain. As a result, this project is aimed at studying the enzymes that synthesizes 2-AG, the DAGLs α and β. As discussed in the previous chapter, we believe phosphorylation to have a key regulatory function in DAGL activity, akin to HSL, whose regulatory lid is displaced upon phosphorylation (Holm, 2003)

In order to study the activation state of the DAGLs, an assay is required that can measure activity and report on functional activators and inhibitors of the enzymes. Previous reports on analytical methodologies for measuring DAGLs' activity include radio-thin layer chromatography (radio-TLC) (Majerus & Prescott, 1982; Bisogno, 2003; Bisogno *et al.*, 2006) and LC/MS (Hoover *et al.*, 2008; Pedicord *et al.*, 2011). However, detecting 2-AG production through these means has proven to be challenging and has limited screening efforts (to identify inhibitors) to small compound collections, mainly due to low throughput. This limited throughput has also led to expensive mechanism-based inhibitors (Bisogno *et al.*, 2006) that have been largely unattractive as potential candidates to put through an expensive drug discovery process. To date, only non-specific compounds have been shown to inhibit DAGL formation of 2-AG, such as RHC-80267 and the lipase inhibitor tetrahydrolipstatin (THL), also known as Orlistat®. These compounds inhibit DAGL at concentrations lower than those required to inhibit other lipases, thereby showing selectivity for the DAGLs, but not specificity (Bisogno *et al.*, 2006; Hoover *et al.*, 2008).

More recently, assays that can report on DAGL function more easily have been described, largely driven by the need of drug discovery programs for a more convenient and cost effective method to measure activity. Johnston *et al*. (2012) developed fluorescence resonance energy transfer (FRET) reporter substrates, which rely on DAGL activity to relieve internal quenching in the reporters, resulting in an increase in fluorescence (Johnston *et al.*, 2012). A commercially available fluorogenic lipase substrate, EnzChek is based on the same principle (Basu *et al.*, 2011). The study described by Pedicord *et al*. (2011) was aimed at further characterising DAGLα and to provide tools to initiate a pharmaceutical discovery effort for activators or inhibitors of the enzyme (Pedicord *et al.*, 2011). This resulted in the identification of two commercially available, non-specific substrates, that DAGLα is capable of hydrolysing *in vitro*. Using a stable HEK293F cell line expressing full length human DAGLα, the authors showed they could report on specific activity of DAGLα, compared to HEK293F wild-type control cell line, which reported little or no activity. Since the completion of this study, a natural substrate assay has been described that also allows easier detection of DAGLα activity. This assay detects production of 2-AG from 1-stearoyl-2-arachidonoyl-sn-glycerol (SAG) hydrolysis by DAGLα overexpressing membrane preparations from transiently transfected HEK293T cells. The 2-AG production is coupled to the oxidation of a commercially available peroxidase substrate, Amplifu Red, via a multi-enzyme cascade, resulting in a fluorescent signal from the dye resorufin (van der Wel *et al.*, 2015).

The two surrogate substrates described by Pedicord *et al.* (2011) were the chromogenic substrate 4-nitrophenyl butyrate (PNPB) and the fluorescent substrate 6, 8-difluoro-4-methylumbelliferyl octanoate (DiFMUO) (Pedicord *et al.*, 2011). The structures of these two substrates, as well as their products released through DAGL hydrolysis, are compared to the native substrate DAG in Figure 4.5. While these substrates are potentially useful tools for designing inhibitors of the enzymes, their limitations have meant they are unsuitable for studying DAGL regulation. For example, they are much smaller molecules than DAG, the molecular weights of PNPB and DifMUO being 209 Da and 338 Da respectively, compared to 645Da for DAG (Figure 4.5), meaning they are likely to access the catalytic site regardless of

the position of the regulatory loop; treatments aimed at increasing DAGL activity, such as kinase activation, do not result in an increase in substrate hydrolysis (work completed with Praveen Singh, unpublished data). They are also not specific substrates to the DAGLs, and so may be hydrolysed by other lipases. Furthermore, we wanted a more 'physiological' type assay that could measure an eCB-dependent CB1 response.

In this chapter, I will report on the successful adaptation of a recombinant cell line to allow measurement of DAGLα/β activity. The Tango cells are an osteosarcoma cell line (U2OS) overexpressing the human CB1 receptor. These cells can report on direct CB1 activation through β-lactamase reporter gene synthesis (van der Lee *et al.*, 2009) (discussed in more detail in chapter 4). Adaptation of the Tango cells will allow us to utilise the same cell line for measurement of DAGLα/β activity via CB1 receptor activation. We overexpressed the DAGLs in these cells to generate a 'gain of function' assay, whereby any difference between parental Tango cells and the overexpressing cells could directly be attributed to DAGLα/β activity.

Here, transgenic DAGLα/β localisation will be shown at the membrane, vital to access their native substrate, DAG, which is generally found associated to the cell membrane (Goni & Alonso, 1999). I will compare both endogenous and transgenic expression of DAGLα to DAGLβ; their relative expression will be an important factor when studying and comparing their activity in the Tango assay. We used both PNPB and DiFMUO substrates to show that DAGLα is active in membrane preparations. We also used the known DAGL inhibitors, THL, OMDM and RHC80267 to show that this activity can be inhibited. However, these substrates are not suitable for studying DAGLβ activity. Nevertheless, the fact the DAGLs can hydrolyse these substrates at different rates shows potential for specific therapeutic intervention of one DAGL over the other.

4.2 Results

Establishing Tango cell lines stably expressing DAGLα and DAGLβ at the membrane

The Tango cells (U2OS) harbour a recombinant assay system designed to specifically measure CB1 activation, known as the Tango assay. We adapted these cells to overexpress DAGLα and DAGLβ. The adapted cells could be used to study the effects of kinase activation/inhibition, based on their ability to modulate eCB-dependent CB1 signalling in the Tango assay (see chapter 5, Results II for further results and discussion).

Human DAGLα and DAGLβ constructs were cloned into the vector pcDNA6.2/V5-DEST. These vectors enabled expression of the DAGL transgenes with a C-terminus V5 tag and contained an antibiotic selection gene for blasticidin resistance; a suitable selection marker for use with the Tango cells. The constructs containing either human DAGLα or human DAGLβ (full length) were transfected into the Tango cells. Their expression was determined by immunocytochemistry using fixed cells and western blotting analysis with cell lysates, both with a V5 antibody (Dr. Fiona Howell and Dr. Praveen Singh).

Having confirmed successful expression of both constructs using transient transfection, we next used the blasticidin selection marker in these constructs to generate stable Tango cell lines expressing DAGLα (named V5α11) or DAGLβ (named V5β4). In order to confirm stable expression of the transgenes and whether our cell lines were clonal, we performed immunocytochemistry after more than 10 passages, with a V5 antibody (Figure 4.1). No V5 staining was seen in control Tango cells, showing little, if any background staining using this antibody. As expected, V5 staining can be seen throughout the membrane in V5α11 cells.

Unexpectedly, V5 staining in V5β4 cells appeared punctated and perinuclear. However, this was in line with a previous report by Piomelli's group in

overexpressing mouse neuroblastoma cells, where they observed DAGLβ to be associated with intracellular structures rather than with the plasma membrane (Jung *et al.*, 2007). After further examination, DAGLβ was found to be largely associated with the Golgi (thesis of Dr. Praveen Singh).

No difference was observed in proliferation or confluency between parental Tango cells and our overexpressing cell lines. Although DAGL has been implicated in axonal pathfinding and migration (Oudin *et al.*, 2011a; Oudin *et al.*, 2011b), the overexpressing cell lines are grown in the presence of blasticidin; the added antibiotic pressure may account for the lack of difference seen.

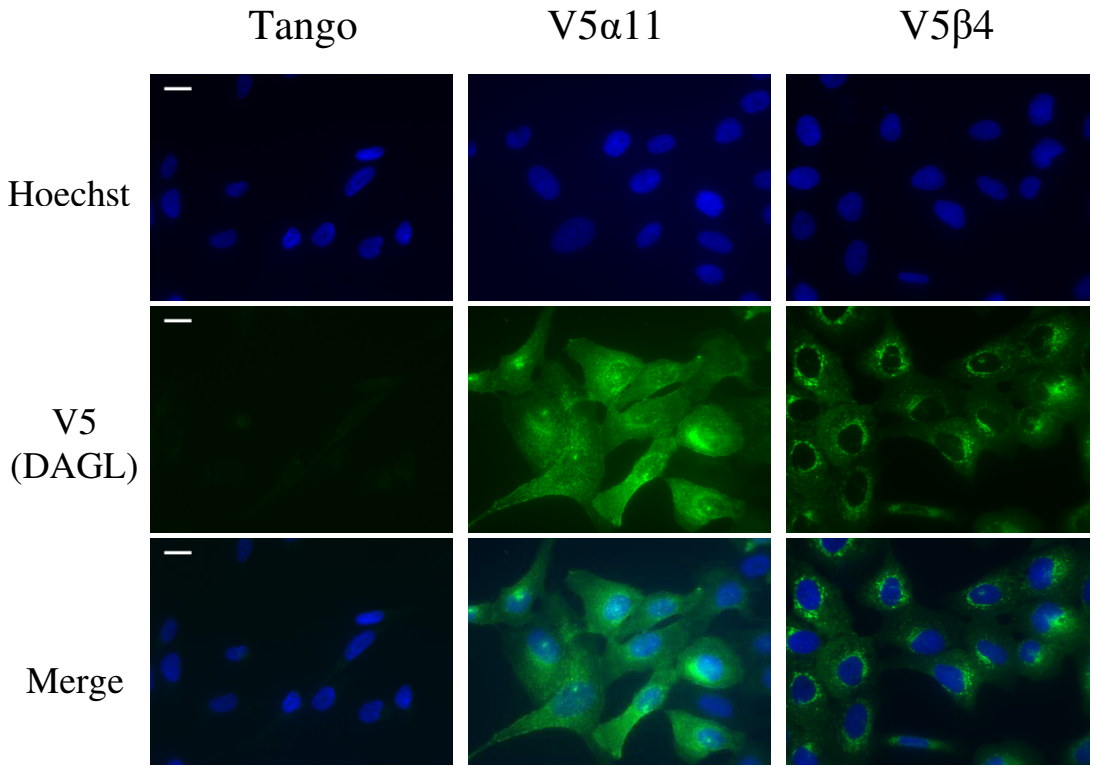

Figure 4.1 The cell lines V5α11 and V5β4 stably express human DAGLα-V5 and human DAGLβ-V5 respectively

Tango cells were transfected with either hDAGLα-V5 or hDAGLβ-V5 plasmids using lipofectamine 2000 and then grown in the presence of the selection marker blasticidin. Clones were selected and explanded and screened for stable expression of the DAGL genes by immunocytochemistry. Two clones were selected, V5α11 and V5β4 which were found to stably express hDAGLα-V5 and hDAGLβ-V5, respectively. After approximately 10 passages, cells from V5α11 and V5β4 were grown on poly-L-lysine coated coverslips and left to adhere overnight. The cells were fixed, permeabilised and stained with a V5 antibody for immunocytochemical analysis. This confirmed that the cell lines were clonal and stably expressing the transgenes. Parental Tango cells were used as control. (A: blue = hoechst; green = V5; scale bar 20 μm).

It was important to establish that there was both DAGLα and DAGLβ expression at the membrane to enable our future studies with the Tango assay. To confirm expression of the transgenes at the membrane, we used membrane preparations rather than whole cell lysates. Tango, V5α11 and V5β4 cells were grown to confluency, washed and lysed (via sucrose in the buffer). The lysed cells were removed from the culture dish with a cell scraper and homogenised (total particulate matter), followed by ultra-centrifugation to concentrate membrane protein. The supernatant was removed and the pellet / membrane fraction was re-suspended in membrane preparation buffer. The membrane protein from all cell lines was diluted to equal concentrations and loaded into wells of a western blot. Expression of the transgenes was confirmed at the membrane by probing the western with a V5 antibody. The blots were also stripped and re-probed for β-actin to control for loading (Figure 4.2 A).

The predicted molecular weights for DAGLα and DAGLβ are ~120kDa and ~75 kDa, respectively (Bisogno, 2003). Expression of the DAGL transgenes was detected at slightly larger sizes than expected when probing with a V5 antibody; but this is to be expected when considering the transgenic DAGLs have a V5 tag at their C-terminus. Therefore, we also wanted to determine their expression using a specific antibody for each DAGL and how this compared to the endogenous levels in parental Tango cells.

To do this, membranes were prepared from each of our cell lines, as described above, and analysed in a western blot using an antibody specific for each DAGL. The blots were also controlled for loading by probing for β-actin. The results for DAGLα are shown in Figure 4.2 B. There is a large band seen in V5α11 membranes with a higher molecular weight than that predicted for DAGLα, corresponding to the larger V5-tagged version of the enzyme. The band corresponding to the endogenous DAGLα is less obvious. There is a band present from all 3 cell lines at a molecular weight smaller than that predicted for DAGLα. However, this band is not enriched in membrane preparations (thesis of Praveen Singh) and is not altered following genetic disruption (discussed in more detail in chapter 6, results IV). Therefore, it is unlikely that this band is endogenous DAGLα.

When using the DAGLβ antibody, a band at the predicted molecular weight was seen for all three cell lines. We saw much greater expression in V5β4 cell membranes, thereby confirming overexpression of DAGLβ at the membrane (Figure 4.2 C). The band corresponding to DAGLβ-V5, however, was not a distinct band from the endogenous DAGLβ band suggesting that the epitope tag does not obviously affect the mobility of the enzyme. In summary, we confirmed stable expression of the transgenes in our cell lines at their predicted molecular weights and confirmed their expression at the membrane.

It was prudent at this stage to confirm whether or not our Tango cells endogenously express DAGLα, as we were unsure the DAGLα antibody was sensitive enough to pick up endogenous protein expression. Therefore, we subsequently analysed DAGLα expression at the transcript level in the Tango cells. This allowed us to compare transcripts levels of the two DAGLs, enabling us to interpret future functional studies of the enzymes.

Figure 4.2 V5α11 and V5β4 cells stably express DAGLα and DAGLβ, respectively, at greater amounts than endogenous levels

Tango, V5α11 and V5β4 cells were lysed following ~ 10 passages and 20 µg protein (membrane preparation) was analysed in a western blot using a V5 antibody (A), DAGLα antibody (B), and a DAGLβ antibody (C). The blots were stripped and re-probed for β-actin as a loading control (blot displayed under each). V5-tagged version of the DAGLs is expressed at a slightly larger molecular weight (MW), as expceted (A). The apparent endogenous DAGLα is a distinct band from the much larger DAGLα-V5, being expressed at a slightly smaller size than their predicted molecular weight of ~120 kDa, or could be running at the same MW, as indicated (B). DAGLβ-V5 was expressed at the predicted size, ~75kDa (C).

A

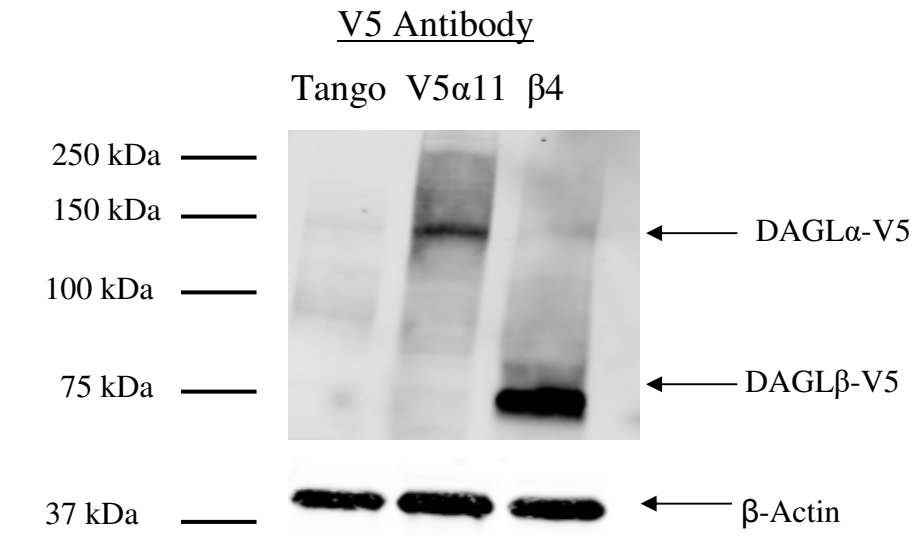
V5 Antibody
Tango V5α11 β4
250 kDa
150 kDa
100 kDa
75 kDa
37 kDa
DAGLα-V5
DAGLβ-V5
β-Actin

B

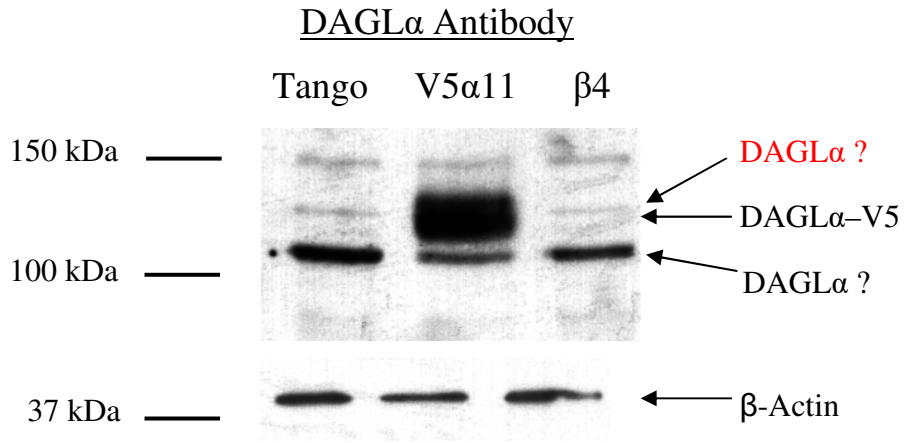
DAGLα Antibody
Tango V5α11 β4
150 kDa
100 kDa
37 kDa
DAGLα ?
DAGLα–V5
DAGLα ?
β-Actin

C

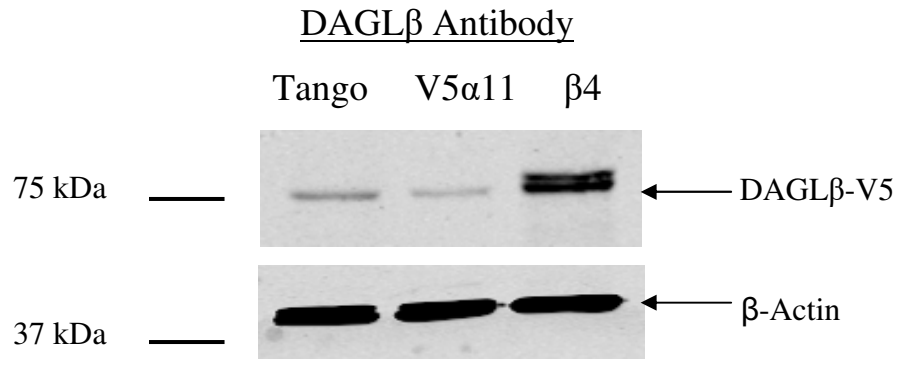
DAGLβ Antibody
Tango V5α11 β4
75 kDa
37 kDa
DAGLβ-V5
β-Actin

Taqman analysis DAGL expression in Tango cells

At this stage we had confirmed overexpression of the DAGLs in our two cell lines, V5α11 and V5β4, as well as their localisation at the membrane from the western blot. The western also indicated that the Tango cells endogenously express the DAGLβ. Using the overexpressing cells, we used real time RT-PCR to determine the relative level of endogenous DAGLβ expression and to confirm whether or not the parental Tango cells express endogenous DAGLα.

To do this, RNA from Tango, V5α11 and V5β4 cells was extracted and reverse transcribed to cDNA. The cDNA was used to perform real time RT-PCR using Taqman assays for either DAGLα or DAGLβ, where detected fluorescence is directly proportional to the amount of PCR product. Taqman assays for PPIA, GAPDH and 18S were also used as control housekeeping genes. Relative quantification relates the PCR signal of the target transcript in a group of unknown expression (Tango cells) to that of another sample which absolutely expresses the transcripts; in this case the V5α11 and V5β4 cells. The data was analysed using the $2^{-\Delta\Delta Ct}$ method, where endogenous expression is calculated as a fraction of 1; 1 being equivalent to the overexpression in V5α11 / V5β4 cells (Livak & Schmittgen, 2001).

The results confirmed endogenous expression of both DAGLα and DAGLβ transcripts in Tango cells, as seen in Figure 4.3. We also confirmed the relative level of overexpression of each enzyme, with DAGLα being expressed ~14 times more than endogenous expression in V5α11 cells, and ~7 times greater DAGLβ expression in V5β4 cells.

As this is a relative assay, we wanted to try to obtain some comparison between the transcript levels of the endogenous DAGLα to DAGLβ. To do this, we performed Taqman assay on our three cell lines, as described above, for DAGLα and DAGLβ, and the three housekeeping genes, PPIA, GAPDH and 18S. To gain an insight into the relative expression of DAGLα to DAGLβ (in all three cells lines) the data was normalised to two of the housekeeping genes and expression compared to the third housekeeping gene (using the $2^{-\Delta\Delta Ct}$ method). Data was first compared to PPIA

(Figure 4.4 A), then GAPDH (Figure 4.4 B) and finally 18S (Figure 4.4C), the values of which were all set to 1 (results excluded from graph) and DAGLα/β expression is displayed as the relative fraction.

In comparison to each of the housekeeping genes, DAGLβ transcripts appear to be expressed ~2.5 times greater than DAGLα transcripts in parental Tango cells. This is also true for the overexpressing cells lines, where DAGLβ transcripts (endogenous + overexpressed) are expressed 1-2 times greater in V5β4 cells, compared to DAGLα transcripts in V5α11 cells. Therefore, endogenous DAGLβ protein expression may be greater compared to DAGLα expression in Tango cells, and also when comparing their relative expression between V5α11 and V5β4 cells – these results are summarised in table 4.1 below.

Table 4.1 Summary of results from expression analysis using Taqman assays

DAGLβ relative expression in our overexpressing cell line (V5β4) was set to 100 (results from Fig. 4.4). The mean of the results from the other Taqman assays was set as a fraction of DAGLβ expression (100) to give an indication of the relative DAGLα and DAGLβ expression between the three cell lines, parental Tango, V5α11 and V5β4. (There are no units as this is a relative ratio compared to housekeeping gene expression.)

		Endogenous	Overexpressed
Taqman Assay	DAGLα	4	76
	DAGLβ	10	100

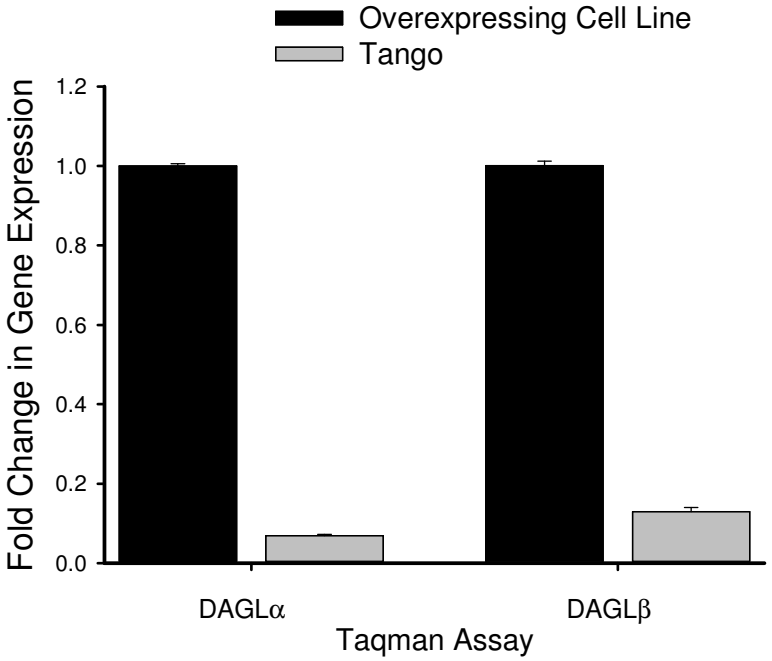

Figure 4.3 Taqman analysis reveals the relative endogenous expression of the DAGLs in Tango cells

RNA from Tango, V5α11 and V5β4 cells was extracted and reverse transcribed to cDNA. The cDNA was used to perform real time PCR with a Taqman probe. The primers in each of the Taqman assays are located in exons that span predicted splice variants of that gene. During the PCR process, bound probe is degraded by the PCR enzyme due its 5' exonuclease activity, releasing the fluorescent marker from the quencher. Detected fluorescence is directly proportional to the amount of PCR product, and therefore the amount of RNA in the original sample. The quantity detected is a relative expression, therefore endogenous expression of either DAGLα or DAGLβ is related to expression in V5α11 and V5β4 cells, respectively. Three housekeeping genes were also used; PPIA, 18S and GAPDH. Data was normalised to these genes and analysed using the $2^{-\Delta\Delta Ct}$ method ± SEM (Livak & Schmittgen, 2001). The graph is a representative from three independent experiments.

Figure 4.4 DAGLα expression relative to DAGLβ in parental Tango cells and between V5α11 and V5β4 cells

RNA from Tango, V5α11 and V5β4 cells was extracted and reverse transcribed to cDNA. The cDNA from each cell type was used to perform real time PCR with a Taqman probe for either DAGLα or DAGLβ, as described previously. Three housekeeping genes were also analysed; PPIA, GAPDH and 18S. To determine relative DAGLα expression to DAGLβ, the C_t values were first normalised to two of the housekeeping genes and then compared to the third, either PPIA (A), GAPDH (B) or 18S (C). The relative expression of the DAGLs was first compared in parental Tango cells (endogenous). DAGLα overexpression in V5α11 cells was then compared to DAGLβ overexpression in V5β4 cells (overexpression). Data was analysed using the $2^{-\Delta\Delta Ct}$ method ± SEM (Livak & Schmittgen, 2001). Data shown represents mean of three wells ± SEM, pooled from 3 independent experiments.

A

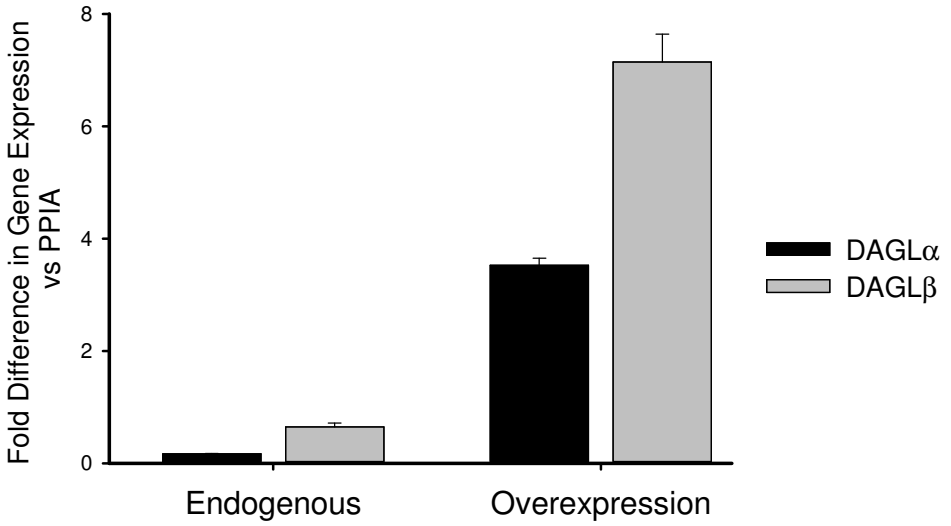
Fold Difference in Gene Expression vs PPIA
8
6
4
2
0
Endogenous
Overexpression
DAGLα
DAGLβ

B

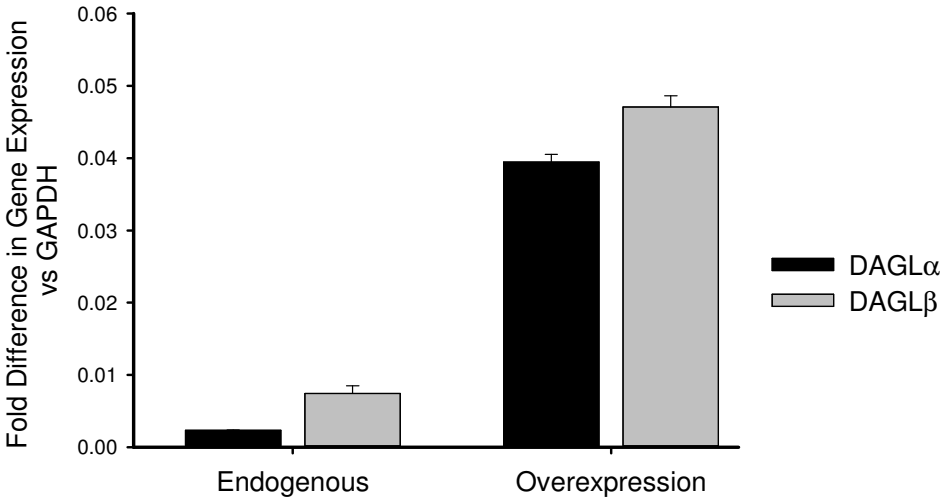
Fold Difference in Gene Expression vs GAPDH
0.06
0.05
0.04
0.03
0.02
0.01
0.00
Endogenous
Overexpression
DAGLα
DAGLβ

C

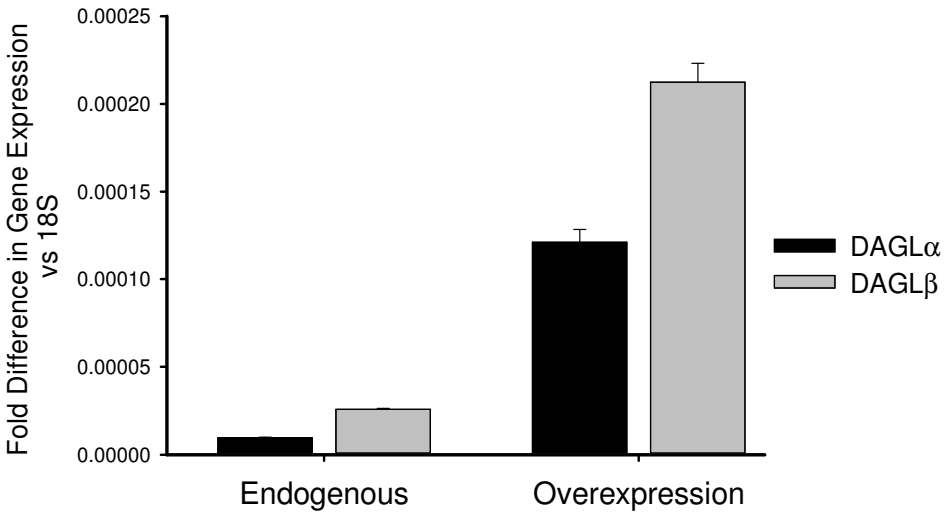
Fold Difference in Gene Expression vs 18S
0.00025
0.00020
0.00015
0.00010
0.00005
0.00000
Endogenous
Overexpression
DAGLα
DAGLβ

Determining DAGLα and DAGLβ activity using surrogate substrates

We had established DAGL expression in three cell lines – parental Tango cells, V5α11 and V5β4 cells. We next used the chromogenic substrate PNPB and fluorogenic substrate DiFMUO, as previously described (Pedicord *et al.*, 2011) to determine if the DAGLs were active in these cells. The structure of these substrates and their products were compared to the native substrate DAG in Figure 4.5.

DAGLα activity in Tango and V5α11 membranes using the chromogenic substrate PNPB

The ability of membranes from parental cells and V5α11 cells to hydrolyse a surrogate substrate was first assessed using PNPB in clear 96-well polypropylene plates. PNPB is a chromogenic substrate and hydrolysis to 4-nitrophenyl can be measured at OD_{400} on the SpectraMax (Figure 4.6). Membranes were prepared from Tango and V5α11 cells that had been in grown in McCoy's media supplemented with 10% FCS (full growth media). Membranes were prepared by mechanically lysing the cells using a homogenizer and separating the membrane enriched fraction (pellet) from the soluble cytoplasmic proteins (supernatant) by ultra-centrifugation at 100,000 g for 30 minutes, as described above. The membrane enriched fraction was then re-suspended in membrane buffer (20 mM HEPES, pH 7.2) using a homogeniser. The protein concentration of the membranes was determined and they were frozen in aliquots at a concentration of 1-2 mg/ml.

To test for hydrolytic activity, the membranes were thawed and plated at 12.5 µg/mL with 250 µM PNPB. The reaction was monitored every 12 seconds for a total of 30 minutes and a time course is shown in Figure 4.6 A. The reaction rate for V5α11 membranes is considerably higher than membranes from parental Tango cells. Moreover, this enhanced activity was suppressed by THL. Use of THL reveals the background activity, perhaps driven by other lipases and / or other enzymes. When the signal was normalised to the THL response (considered the background, non

DAGL-dependent response), the enhanced activity in the V5α11 membranes was more prominent when compared to the parental Tango membranes, suggesting that it could be attributed to the presence of the overexpressed DAGLα (Figure 4.6 B).

DAGL assay substrates	Product
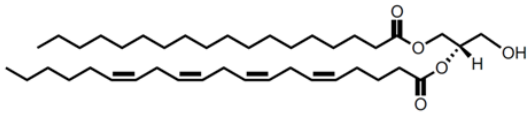 1-stearoyl-2-arachodonoyl-sn-glycerol (DAG) (645Da)	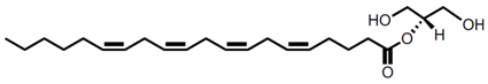 2-Arachidonoylglycerol (2-AG)
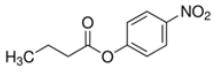 4-Nitrophenyl butyrate (PNPB) (209Da)	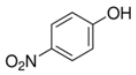 4-Nitrophenyl
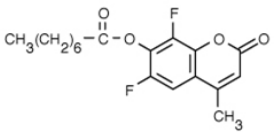 6,8-difluoro-4-methylumbelliferyl Octanoate (DiFMUO) (338Da)	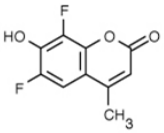 6,8-Difluoro-7-Hydroxy-4-Methylcoumarin (DiFMU)

Figure 4.5 Native and surrogate DAGL substrates

The native (DAG) and surrogate (PNPB and DiFMUO) substrates (molecular weights in brackets) of DAGL and the products generated following their hydrolysis by DAGL are presented above. PNPB is a chromogenic substrate, whereas DiFMUO is a fluorogenic substrate.

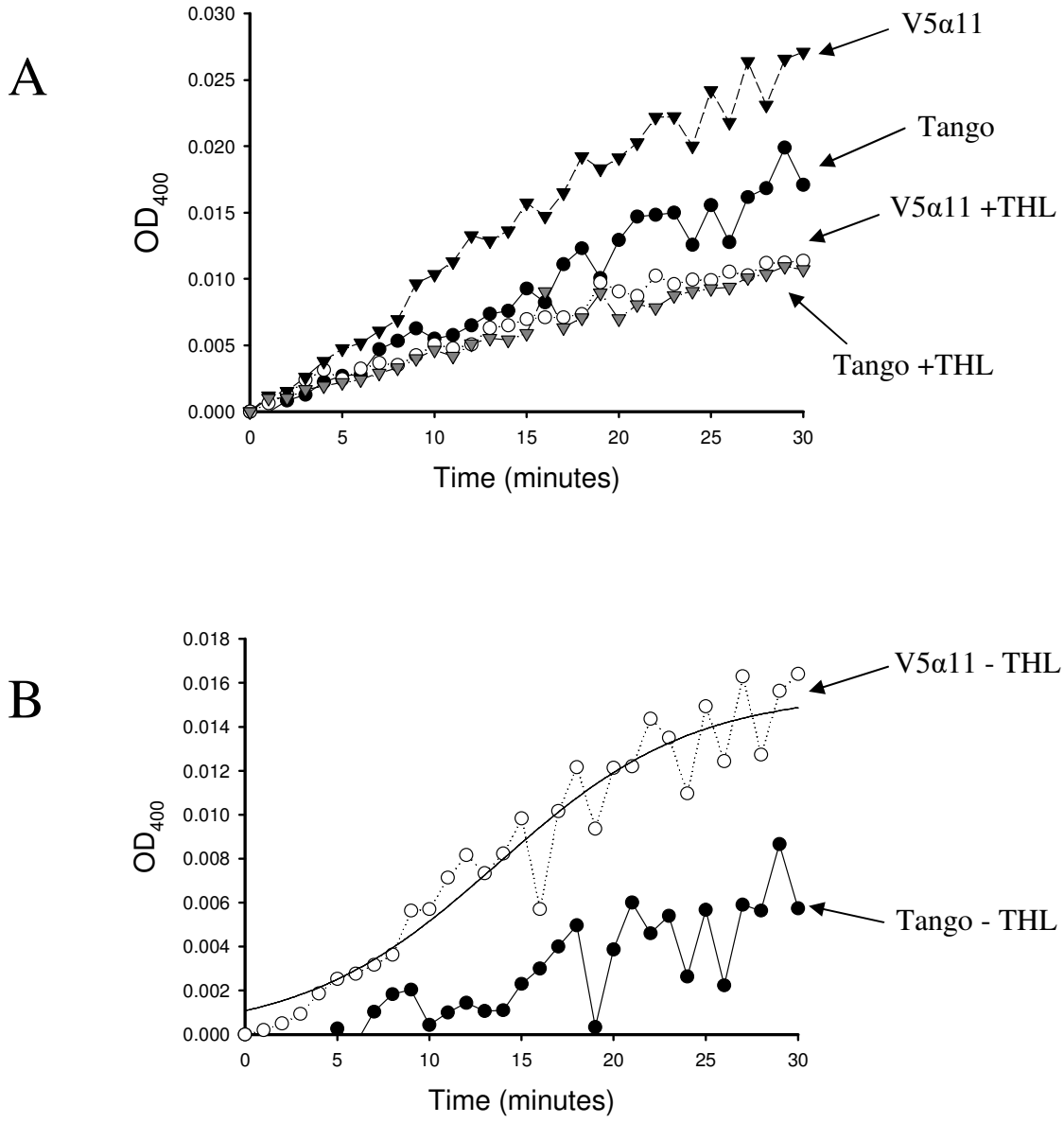

Figure 4.6 Measuring DAGL*α* activity using the chromogenic substrate PNPB in membranes from Tango and V5α11 cells

Tango and V5α11 membranes were prepared from lysed cells and used at a final concentration of 12.5 µg/ml, and PNPB was used at a concentration of 250 µM. The OD was read at 400 nM for 30 min every 12 s. The graph shown is the mean of three wells ± SEM from a single representative experiment (A). The absorbance reading measured in the presence of THL was considered as background for both membrane types and was subtracted from the absorbance signal measured for the untreated membranes (B).

The effects of varying membrane and substrate concentration in the PNPB assay were next established, and results are presented in Figure 4.7. Tango and V5α11 membranes were used at a concentration range between 0 and 15 µg/mL final assay concentration (FAC), with 250 µM PNPB. Activity was determined by measuring the rate of product formation (OD_{400} / minute) over 10 minutes using SoftMaxPro software. Increasing activity was dependent on increasing concentrations of V5α11 membranes, with little increase in hydrolysis by Tango membranes by comparison. The V5α11 membranes therefore showed more activity than the parental Tango membranes (> 6-fold) at all concentrations tested (Figure 4.7 A).

Varying concentrations of PNPB (0-8 mM FAC) showed the reaction rate was also initially linearly related to substrate concentration using V5α11 membranes. In comparison there was a much smaller increase in activity from Tango membranes (Figure 4.7 B). The response from V5α11 appears to plateau above 250 µM PNPB, perhaps reflecting the poor solubility of the substrate at higher concentrations. Even though the Tango cells clearly express endogenous DAGLβ, and possibly express endogenous DAGLα, the endogenous activity levels are relatively small in this assay. Therefore the proportion of the reaction rate seen in V5α11 membranes is most likely due to the transgenic DAGLα activity.

We tested three DAGL inhibitors, OMDM-188, THL and RHC-80267 for their ability to inhibit the hydrolytic activity associated with the V5α11 membranes. V5α11 membranes, prepared and plated as described above. 12.5 µg/ml membrane protein was pre-incubated with a concentration-response curve from each of the three inhibitor compounds for 5 minutes. For OMDM-188 and THL, 200 nM top concentration was used, diluted 1:2 (8 point curve); for RHC-80267 the top concentration used was 200 µM (1:2, 8 point curve). After 5 minutes, the reaction was initiated with 250 µM PNPB. The OD_{400} was again measured over 30 minutes and the reaction rates were calculated from the first 10 minutes.

All three compounds inhibited PNPB hydrolysis in the assay in a concentration-dependent manner (Figure 4.8 A-C). Although each inhibitor had different efficacies, the order of potency was in line with previous reports (Hoover *et al.*, 2008; Ortar *et*

al., 2008). OMDM-188 is the most potent inhibitor of the DAGLs to date (Ortar *et al.*, 2008) and it was found to be the most potent inhibitor in this assay. The approximate IC_{50} values were ~ 3 nM for OMDM-188, ~ 12.5 nM for THL and ~100 µM for RHC-80267. The fact that PNPB hydrolysis by V5α11 membranes can be fully inhibited by the three DAGL inhibitors is further evidence that this assay is measuring the activity of the transfected DAGLα.

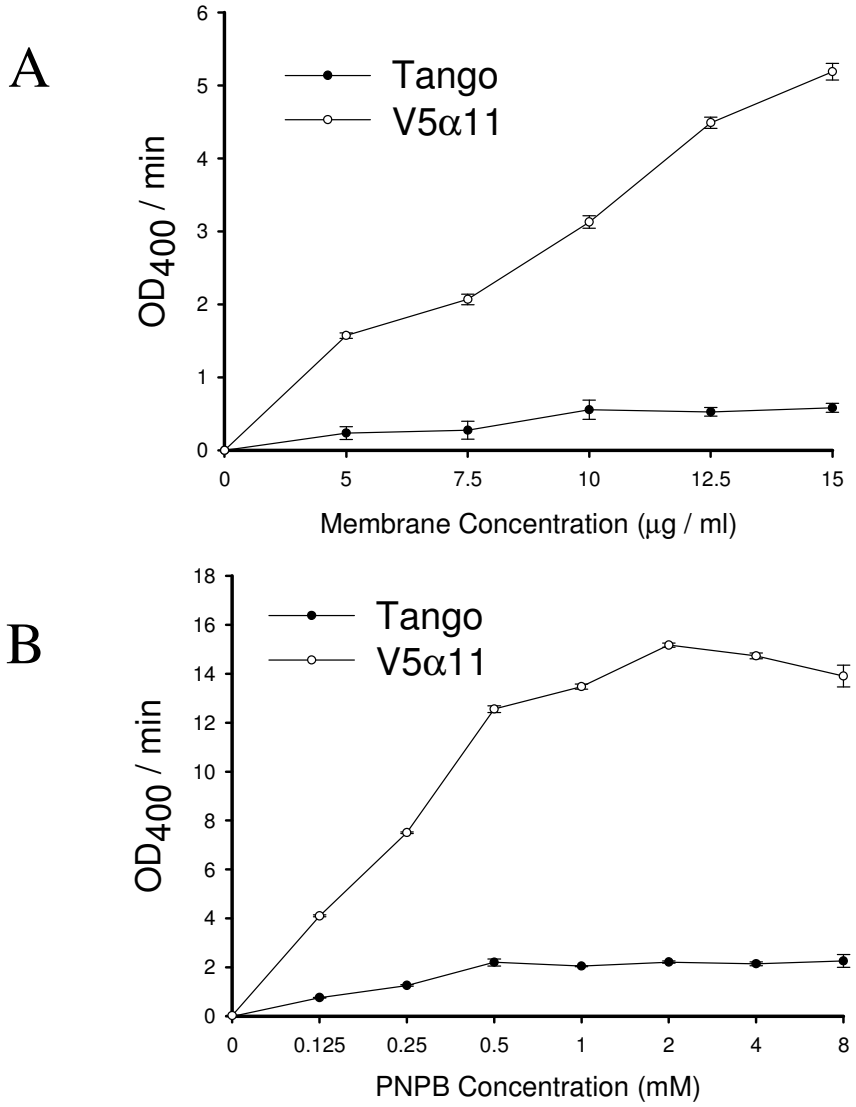

Figure 4.7 The effect of varying membrane and PNPB substrate concentration on DAGLα activity

Membranes from Tango and V5α11 cell lines were extracted and plated at varying concentrations (1.5 - 50 µg/ml FAC). PNPB was added to the plate at 250 µM FAC, before being read immediately on the SpectraMax at 400 nM. The plate was read every 12 s for a total of 30 min (A). Varying concentrations of the PNPB (0 - 8 mM FAC) were added to wells of a clear 96-well plate. The reaction was initiated with addition of 12.5 µg/ml Tango or V5α11 membranes and the plate was read immediately at OD_{400}, as described above (B). The mean of three wells ± SEM from a single representative experiment is presented in both.

Figure 4.8 DAGL*α* activity is inhibited by the three DAGL inhibitors in the PNPB Assay

Reactions were set up with inhibitors and substrate in a 96-well plate before being initiated with addition of membrane protein. Concentration response curves of OMDM-188 (200 nM top FAC), THL (200 nM top FAC) and RHC-80267 (200 µM top FAC); 1:2 dilution, 8 point curve. The inhibitor concentration responses were added to half of the wells. 250 µM PNPB was added to all wells and the reactions were initiated with 12.5 µg/ml final concentration of V5α11 membranes. Approximate IC_{50} values were ~ 3 nM for OMDM-188 (A), ~12.5 nM for THL (B) and 100 µM for RHC-80267 (C). Results show mean of three wells ± SEM from a single representative experiment.

A

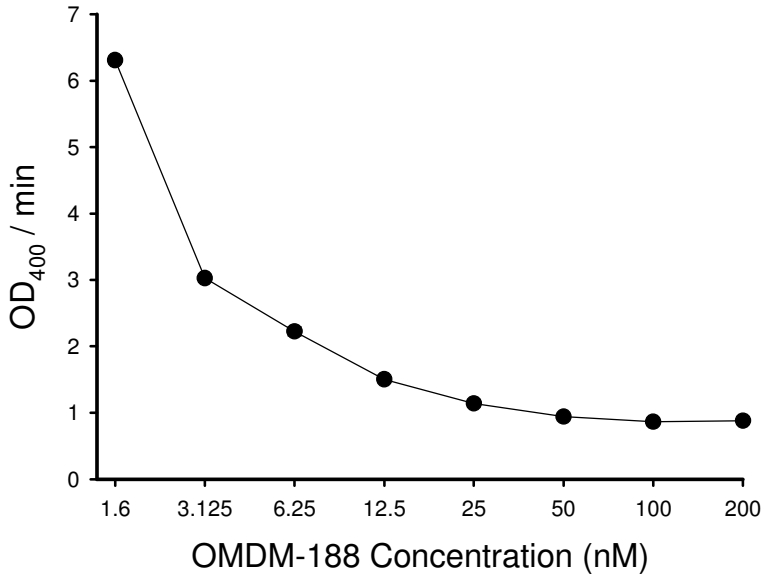
7
6
5
4
3
2
1
0
OD400 / min
1.6
3.125
6.25
12.5
25
50
100
200
OMDM-188 Concentration (nM)

B

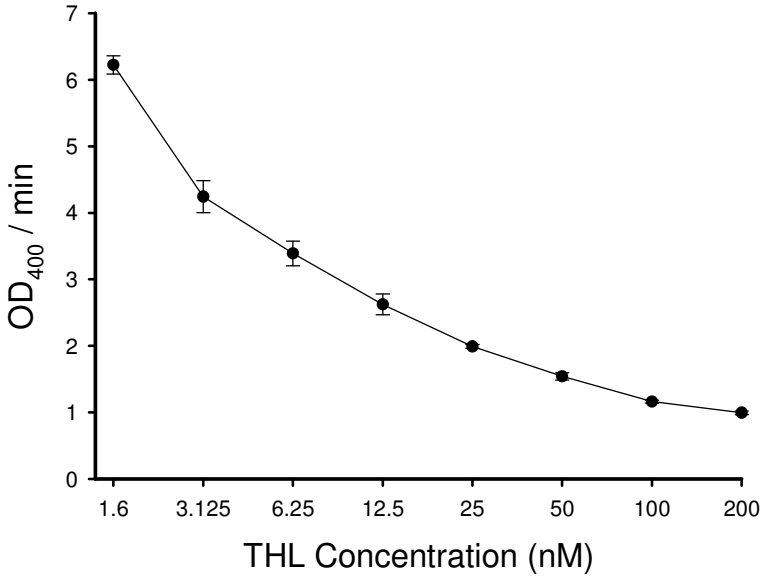
7
6
5
4
3
2
1
0
OD400 / min
1.6
3.125
6.25
12.5
25
50
100
200
THL Concentration (nM)

C

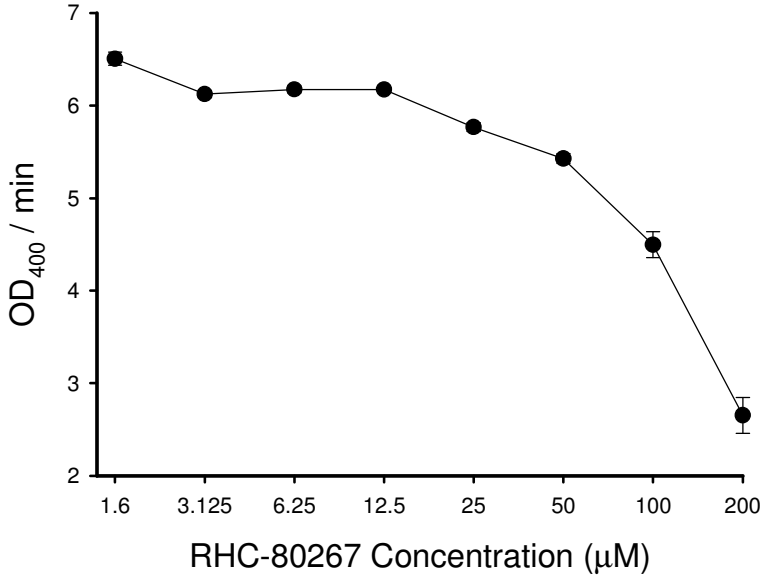
7
6
5
4
3
2
OD400 / min
1.6
3.125
6.25
12.5
25
50
100
200
RHC-80267 Concentration (μM)

DAGLα activity in membrane preparations using the fluorogenic substrate DiFMUO

We next tested the second substrate, DiFMUO which can be hydrolysed by DAGLα to the fluorescent product 6,8-Difluoro-7-Hydroxy-4-Methylcoumarin (DiFMU) (Figure 4.5) (Pedicord *et al.*, 2011). DAGLα activity can therefore be detected by measuring DiFMU at an excitation wavelength of 360 nm and an emission wavelength of 450 nm. We first set up this assay in the same manner as for the PNPB assay – 12.5 µg/ml of membranes were plated into a clear 96-well polypropylene plate. Half of the membranes were treated with 1 µM THL for 5 minutes before the reaction was initiated with 10 µM DiFMUO. The relative fluorescent units (RFU) were measured every 30 seconds for a total of 30 minutes (Figure 4.9 A). There was a considerable hydrolytic activity associated with the parental Tango membranes, but the response from V5α11 membranes was much greater; revealed by obtaining the THL-sensitive response (Figure 4.9 B). However, it was noted that the response from Tango membranes was much greater than that seen in the PNPB assay. This response was partially inhibited by THL, indicating this portion of the response may be due to endogenous DAGLα/β activity.

We next tested the effects of varying membrane and substrate concentrations. The reaction in each was monitored every 30 seconds and the rate was calculated over 10 minutes (RFU / second). Hydrolysis of DiFMUO increases with increasing membrane concentration (Figure 4.10 A). The response also plateaus above 10 µM DiFMUO, as seen in Figure 4.10 B. Again a substantial response is seen from Tango cell membranes. To determine whether this response is due to the endogenous DAGLs being active, we tested the three DAGL inhibitors, OMDM-188 (100 nM), THL (1 µM) and RHC-80267 (100 µM) (Figure 4.11). The response from Tango membranes is inhibited by both THL and OMDM-188, but not RHC-80267. RHC-80267 is known to bind to off-targets, thereby reducing potency; this may indicate that the endogenous DAGLs are active. However, DiFMUO may also be hydrolysed by other lipases at the membrane (Pedicord *et al.*, 2011). The much greater response seen from V5α11 cells is inhibited by THL and OMDM-188, which can be attributed to the transfected DAGLα.

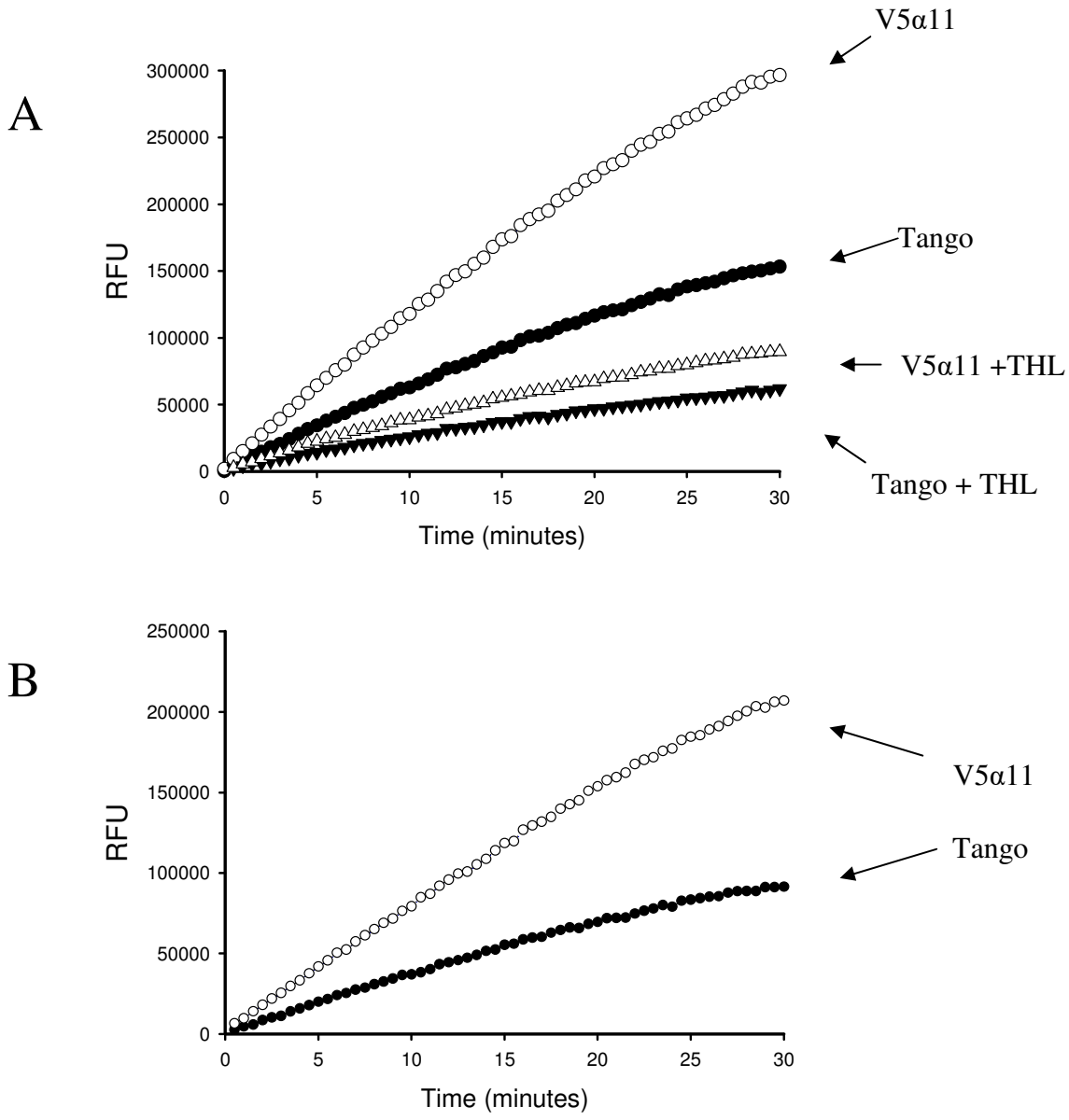

Figure 4.9 Measuring DAGL*α* activity in Tango and V5α11membranes using the fluorescent substrate DiFMUO

Tango and V5α11 membranes were plated at 12.5 µg/ml in the presence and absence of 1µM THL. The surrogate substrate DiFMUO was then added to the membranes at a FAC of 10 µM. Fluorescence was measured immediately after substrate addition for 30 min every 30 sec at an excitatory wavelength of 360 nM and an emission wavelength of 450 nM (A). The fluorescent reading measured from membranes in the presence of THL was considered as background and was subtracted from the fluorescence from the untreated membranes (B). Each time point represents the mean of 3 wells ± SEM from a single representative experiment.

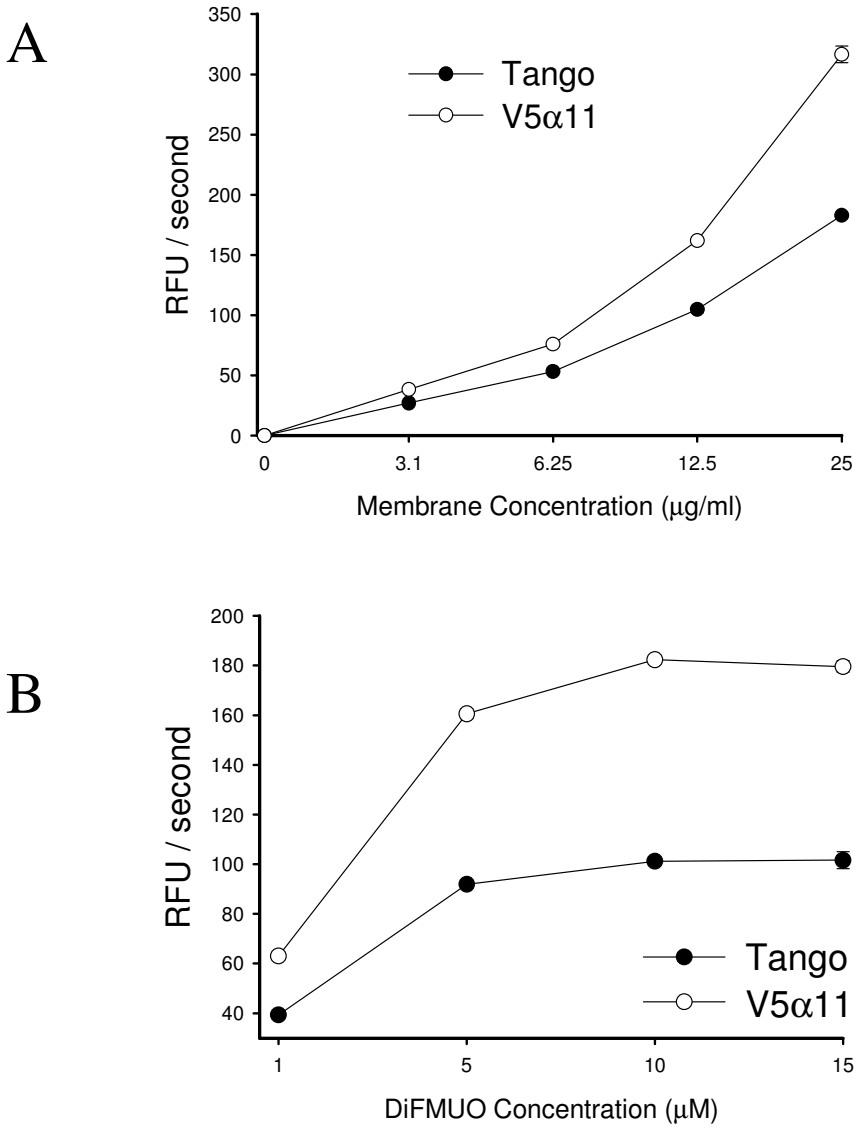

Figure 4.10 DAGL*α* activity is dependent on membrane and substrate concentration in the DiFMUO assay

Membrane protein was prepared from Tango and V5α11 cell lines. The membrane protein was plated at a top concentration of 25 µg/ml followed by a 1:2 serial dilution, 5 point curve in assay buffer (50 mM MES, pH 6.5). The reaction was initiated with 10 µM FAC DiFMUO. The plate was read immediately on the Flexstation at an excitation of 360 nM and emission of 450 nM (A). 12.5 µg/ml membrane protein were plated with varying concentrations of DiFMUO (15, 10 5 and 1 µM). The reaction was monitored as described above (B). Data shown represents the mean of three wells ± SEM from a single representative experiment for both.

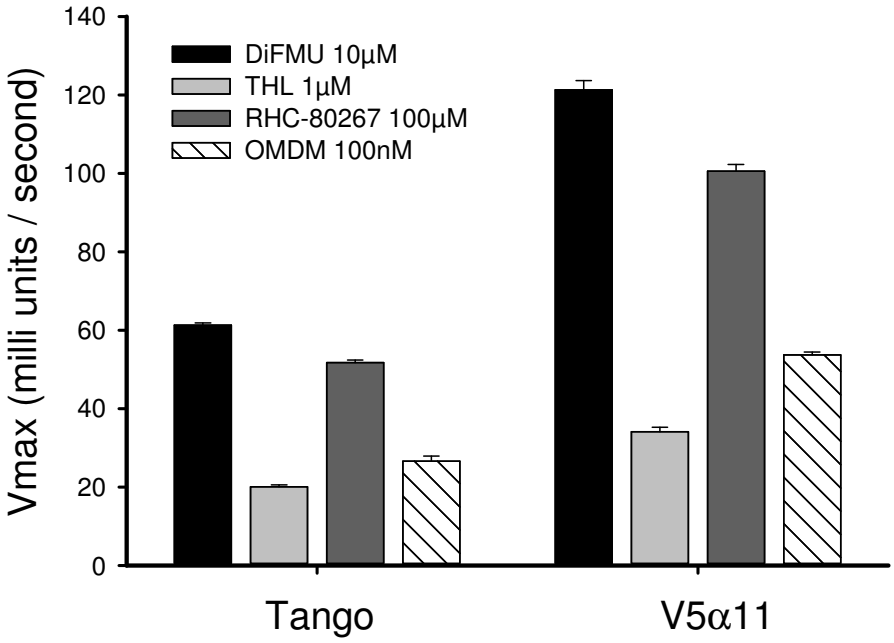

Figure 4.11 DiFMUO hydrolysis is inhibited by the DAGL inhibitors THL, RHC-80267 and OMDM-188 in both Tango and V5α11 membranes

Tango or V5α11 membranes were plated at 12.5 µg/ml into wells of a 96-well plate. Half the wells were treated for 5 minutes with the DAGL inhibitors THL (1 µM), RHC-80267 (100 µM) or OMDM-188 (100 nM). The reaction was initiated with 10 µM DiFMUO and the reaction was monitored, as described previously. Vmax represents the rate of substrate hydrolysis, calculated within the first 10 min of the assay. Results show the mean of three wells ±SEM from a single representative experiment.

As none of the inhibitors are selective for the DAGLs, we tested a full range of concentration for each compound to determine the order of potency (Figure 4.12). The approximate IC_{50} values were ~ 3 nM for OMDM-188, ~ 12 nM for THL and ~ 10 µM for RHC-80267 (see Table 4.2 below) which is in line with the PNPB assay, as well as with values reported in the literature (Hoover *et al.*, 2008; Ortar *et al.*, 2008). This clearly indicated that the response was from the transgenic DAGLα-V5, and is therefore active in our V5α11 membrane preparations.

Table 4.2 Summary of IC50 values obtained from the DAGL inhibitors and surrogate substrates

	OMDM-188	THL	RHC-80267
PNPB	3 nM	12.5 nM	100 µM
DiFMUO	3 nM	12 nM	10 µM

Figure 4.12 DAGLα-V5 activity in the membrane DiFMUO assay in inhibited by three different DAGL inhibitors

Concentration response curves of RHC-80267 (100 µM top concentration), OMDM (100nM top concentration) and THL (10 µM top concentration); 1:3 dilution, 11 point curve. Each inhibitor concentration-response curve was added to half the wells of a clear 96-well plate, before addition of 10 µM DiFMUO to all wells. The reaction was initiated by addition of 12.5 µg/ml V5α11 membranes and the plate was read immediately, as previously described. Approximate IC_{50} values were ~ 3 nM for OMDM-188 (A), ~12 nM for THL (B) and ~ 10 µM for RHC-80267 (C). Results show mean of three wells ± SEM from a single experiment.

A

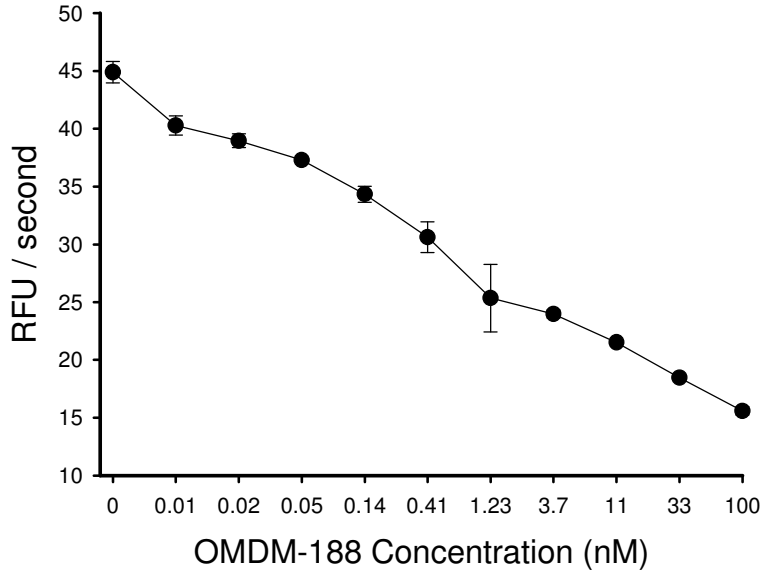
RFU / second
50
45
40
35
30
25
20
15
10
0
0.01
0.02
0.05
0.14
0.41
1.23
3.7
11
33
100
OMDM-188 Concentration (nM)

B

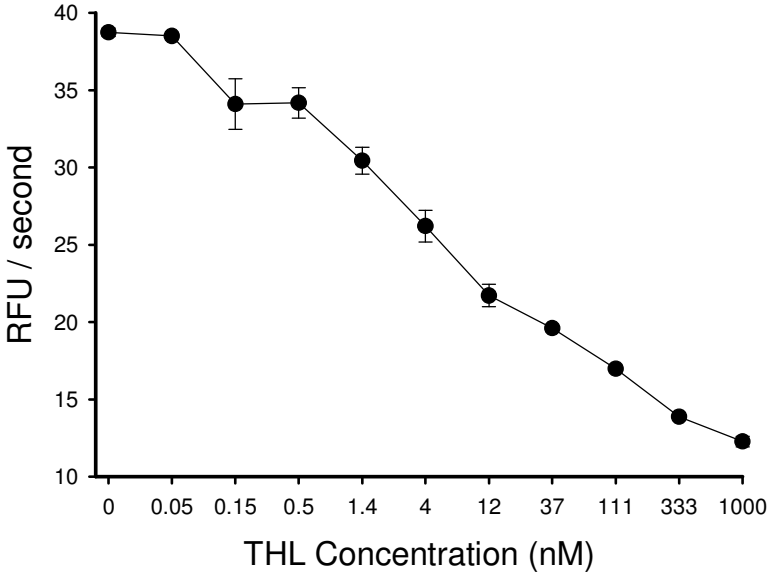
RFU / second
40
35
30
25
20
15
10
0
0.05
0.15
0.5
1.4
4
12
37
111
333
1000
THL Concentration (nM)

C

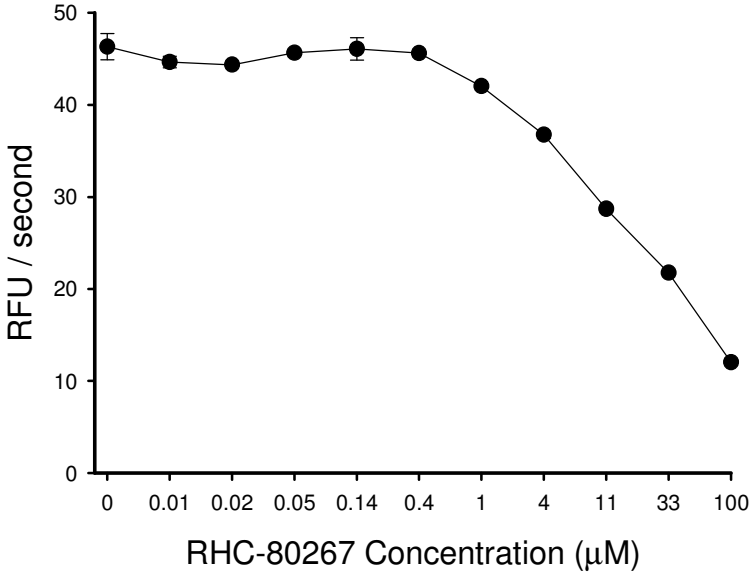
RFU / second
50
40
30
20
10
0
0
0.01
0.02
0.05
0.14
0.4
1
4
11
33
100
RHC-80267 Concentration (μM)

DAGLβ activity in V5β4 membrane preparations

We determined if we could measure DAGLβ activity in V5β4 cells. Membrane preparations were isolated from Tango and V5β4, as described above, with the membrane fraction being concentrated through ultra-centrifugation. We first tested activity against the chromogenic substrate, PNPB. Tango and V5β4 membrane protein was plated at 12.5 µg/ml in clear polypropylene 96-well plates. The membranes were incubated with 1 µM THL, before addition of 250 µM PNPB and the plate was read immediately on the SpectraMax. The reaction was monitored every 12 seconds and the reaction rate was calculated from the first 10 minutes. Surprisingly, V5β4 membranes did not hydrolyse PNPB at a greater rate than that seen with parental Tango membranes (Figure 4.13 A). We next tested the fluorogenic substrate, DiFMUO. 12.5 µg/ml of Tango and V5β4 membranes were plated as described above, before being treated for 5 minutes with 1 µM THL. The reaction was initiated with 10 µM FAC DiFMUO and was monitored on the Flexstation. As with results with PNPB, we did not see a significant level of substrate hydrolysis above Tango membrane control (Figure 4.13 B).

The level of DAGLβ expression is greater in V5β4 cells than DAGLα expression V5α11 cells. Yet it may be that the level of DAGLβ expression at the membrane may still be insufficient to hydrolyse these substrates above the level of that seen in Tango membranes.

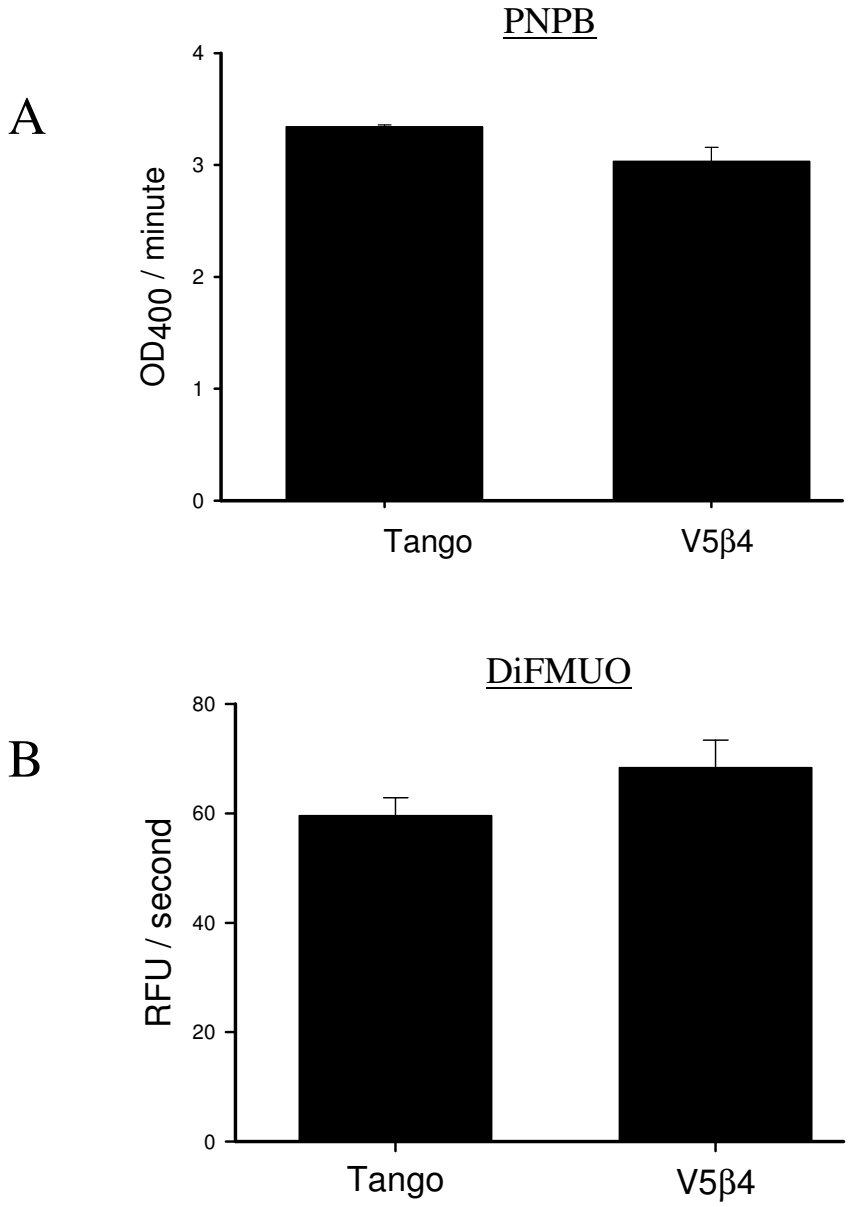

Figure 4.13 PNPB and DiFMUO are not suitable substrates to measure DAGLβ activity

The activity of membranes isolated from the V5β4 cells was measured using surrogate substrates. Membranes (12.5µg/ml) prepared from V5β4 and Tango cells were incubated in the presence or absence of THL (1µM) for 5 min. Activity was measured using PNPB (250µM) and the reaction rate was calculated over the first 10 minutes (A). Activity of the membranes was also measured using DiFMUO (10µM) as the substrate, as described above (B). The data represents the THL-sensitive activity detected and the mean of 3 wells ± SEM from a single experiment. Significance was tested using the two-sided Student's t-test.

4.3 Summary & Conclusions

In this chapter, I describe a cell line we have developed for each DAGL using the Tango (U2OS) cells. The Tango cells harbour a recombinant assay system to measure CB1 activation. Using the Tango cells allows us to develop an assay to measure eCB-dependent CB1 activation, whereby DAGLα/β hydrolysis of DAG would produce 2-AG, thereby activating the CB1 receptor. The overexpressed DAGLα/β would allow a 'gain of function' assay, whereby any increase in response over parental Tango cells could be directly attributed to the transfected DAGL, allowing us to study its function.

We successfully generated a clonal cell line for DAGLα (V5α11) and a cell line for DAGLβ (V5β4). In the last chapter, we identified structural features that are likely to orientate the DAGLs at the membrane for substrate access. As expected, DAGLα staining revealed expression throughout the cell surface, although DAGLβ expression appeared punctated and perinuclear (Figure 4.1). A portion of DAGLβ expression in our V5β4 cells is localised to the Golgi (thesis of Dr. Praveen Singh), which may be a result of an artefact of overexpressing the enzyme.

To confirm DAGLα and DAGLβ expression at the membrane we probed all three cell lines (Tango, V5α11 and V5β4) in a western blot (Figure 4.2). The resulting bands using a V5 antibody were larger than those predicted for the DAGLs (~120 kDa for DAGLα, ~75 kDa for DAGLβ) and correspond to the larger, V5-tagged version of each enzyme (Bisogno, 2003). The DAGLα was less reliable, resulting in a band at a much smaller (~110 kDa) than that predicted for DAGLα (Figure 4.2 B). On the other hand, using a DAGLβ antibody we confirmed endogenous expression of DAGLβ in the Tango cells. The Taqman assay revealed the Tango cells to have transcripts for both the DAGLs. By comparing expression to three housekeeping genes, we have shown DAGLβ expression is likely to be much greater than DAGLα expression, both endogenously in the Tango cells and between V5α11 and V5β4 cells – a point to be considered when comparing results between the 3 cell lines in the Tango assay (Figures 4.3, 4.4 and Table 4.1).

We confirmed DAGLα to be active in V5α11 cells, as hydrolysis of both PNPB and DifMUO was much greater in membranes from these cells compared to parental Tango membranes and this response could be inhibited by THL (Figure 4.6 – 4.11). However, we could not detect a greater response in V5β4 membranes over parental Tango cell membranes using these surrogate substrates (Figure 4.13), which is surprising considering the greater level of DAGLβ transcripts in these cells. This could be due to different kinetics of the DAGLs when hydrolysing these substrates. Although future studies may include DAGLβ, or indeed measuring 2-AG production by these cells lines, our initial focus is on regulation of DAGLα in the context of the CNS.

In conclusion, we have successfully developed two recombinant cell lines that overexpress DAGLα and DAGLβ, and have concluded that the transgenic DAGLα in V5α11 cells is active. There is substantial evidence that phosphorylation can change the activity of the DAGLs and that this results in increased 2-AG production. The limitations of using the surrogate substrates means we were unlikely to detect any changes in the membrane assays. However, by establishing overexpression in the Tango cells, we could develop an eCB-dependent CB1 assay using these cell lines. This assay could report on production of the endogenous ligand for CB1, 2-AG to allow us to study regulatory mechanisms of the DAGLs. The potential for this assay is explored in the next chapter.

CHAPTER 5. RESULTS III – Development of an eCB-dependent CB1 activation assay

5.1 Introduction

DAG is hydrolysed by DAGL to form the eCB 2-AG (Farooqui *et al.*, 1984; Stella *et al.*, 1997; Bisogno, 2003) and that is one of the main regulation points of the eCB system. Our focus was to measure DAGLα and/or β activity and how this can directly impact 'on demand' synthesis of 2-AG. At present, studying activity of the DAGLs relies heavily on quantifying 2-AG following cellular stimulation, or addition of synthetic DAG (Bisogno, 2003; Jung *et al.*, 2007); quantification of which relies on mass spectrometry techniques, which itself requires an expensive laboratory set up (Balgoma *et al.*, 2013). Our aim was to develop an assay to more easily study activity of the DAGLs. In this chapter, I will explain how we adapted the well-established CB1-Tango assay that measures direct activation of the CB1 receptor by pharmacological agents, in order to detect eCB-dependent CB1 activation.

The CB1-Tango assay is a recombinant assay system that reports directly on GPCR activation (summarised in Figure 5.1). A chimeric CB1 receptor is overexpressed in U2OS cells, where it is extended at the C-terminus with a non-native transcription factor, separated from the receptor by a linker containing a protease cleavage site. In addition, a chimeric version of β-Arrestin 2 is fused to a non-native protease and is also expressed. Upon CB1 activation, the recruitment of β-Arrestin 2 brings the protease into close proximity to the receptor where it acts on the cleavage site. The released transcription factor moves to the nucleus, activating a third transgene, namely a mammalian-optimised β-lactamase (*bla*) reporter gene. At the end of the treatment period, cells are loaded with a fluorescent substrate containing two fluorophores, coumarin and fluorescein. In the absence of *bla* expression, the substrate remains intact. In this state, excitation of coumarin results in FRET to the fluorescein moiety and emission of green fluorescent light. However, when *bla* is expressed the substrate is cleaved by β-lactamase. This separates the fluorophores,

disrupting energy transfer and results in a blue fluorescence signal. The resulting coumarin:fluorescein (green:blue) ratio provides a readout for activation of the CB1 receptor.

We reasoned that the CB1-Tango assay might be adaptable to report on eCB signalling via the CB1 receptor, provided that the cells have the ability to synthesise eCBs and appropriate stimulants could be identified. Unlike other neurotransmitters, lipid signalling molecules are thought to be biosynthesised by neurons at the moment of their intended action and degraded 'on-demand', rather than being stored in vesicles prior to signalling (Leung *et al.*, 2006). We hypothesised that we could stimulate 2-AG biosynthesis by activating the DAGLs, through treatments aimed at kinase activation. Consequently, CB1 activation in this instance would be indirectly reporting on DAGLα/β activity. Nonetheless, at the outset it was clear that the assay might also report on the activity of other eCBs.

Long before 2-AG was identified as an eCB, 2-AG release was examined following cell stimulation. For example, arachidonylglycerol was shown to be released from Swiss mouse 3T3 cells following stimulation by platelet-derived growth factor (Hasegawa-Sasaki, 1985). 2-AG was more recently shown to be released by other stimuli, such as the calcium ionophore ionomycin. Neuroblastoma ($N_{18}TH_2$) cells released 2-AG into the medium in a calcium-dependent fashion and in a concentration analogous to that released from 3T3 cells (Bisogno *et al.*, 1997b). Agonists for GPCRs known to be located at the postsynaptic terminal can also result in 2-AG mobilisation for retrograde activation of CB1, for example the agonist for the mGlu receptor type 1 (DHPG) in rat brain slices (Jung *et al.*, 2007). These studies have looked at stimulating cells on a broader scale for measuring 2-AG production and not on the cellular machinery that regulate its manufacture.

In Chapter 3 (Results I), I have described consensus phosphorylation sites on the regulatory loop of the DAGLs that are potentially important for regulating substrate access to the catalytic domain. Based on this, we hypothesise that the DAGLs are activated by phosphorylation by kinases such as PKA and PKC. This mechanism could explain the increase in 2-AG production from cells treated with ionomycin;

calcium influx into the cell activates various kinases, which in turn might phosphorylate the regulatory loop on the DAGLs. We sought to test this hypothesis by initially investigating the effects of activating PKA and PKC directly and how this compared to ionomycin treatment of our CB1-Tango cells.

However, as suggested above it must be noted that kinase activation might also results in anandamide being produced, which might also trigger signalling in this model. In this context, multiple synthetic pathways for anandamide synthesis have been suggested. For example, NAPE-PLD generation of anandamide (Di Marzo *et al.*, 1994; Cadas *et al.*, 1997), GDE1 hydrolysis of a glycerophospho-NAE intermediate (Simon & Cravatt, 2006; 2008) or indeed a combination of both (Simon & Cravatt, 2010b). Anandamide synthesis has also been detected in LPS-stimulated macrophages by an as yet unidentified PLC (Liu *et al.*, 2006). This is complicated further by the fact that anandamide synthesis can be stimulated by calcium (Di Marzo *et al.*, 1994; Cadas *et al.*, 1997; Schmid, 2000; Leung *et al.*, 2006). Furthermore, a number of other potential eCBs have been identified, the synthesis of which could potentially be stimulated by calcium, such as virodhamine (Porter *et al.*, 2002), NADA (Huang *et al.*, 2002), noladin ether (Hanus *et al.*, 2001; Fezza *et al.*, 2002), and the ethanolamide derivatives DHEA and EPEA (De Petrocellis *et al.*, 2000; Brown *et al.*, 2010; Yang *et al.*, 2011), although evidence for stimulation of their biosynthesis has yet to be documented. As discussed in Chapter 4 (Results II), the CB1-Tango cells endogenously express the DAGLs. We also engineered the CB1-Tango cells to overexpress either DAGLα (V5α11) or DAGLβ (V5β4). This would enable us to directly relate the difference between parental CB1-Tango cells and our overexpressing cell lines to the DAGLα/β generation of 2-AG (and not another eCB). Furthermore, overexpression of DAGLα has previously been shown to increase 2-AG levels in a recombinant system (Jung *et al.*, 2007). This 2-AG should activate the CB1 receptor, creating a DAGLα/β-dependent CB1 activation assay. Nonetheless, at the outset it was self-evident that the first objective was to identify conditions that stimulate eCB signalling in the CB1-Tango cells, with secondary objectives being to identify and isolate the responsible pathways.

The activity of eCBs can be limited by the activity of the enzymes that degrade anandamide and/or 2-AG; these are primarily FAAH (Cravatt *et al.*, 2001; Deutsch *et al.*, 2002) and MAGL (Beltramo & Piomelli, 2000; Piomelli *et al.*, 2000; Dinh *et al.*, 2002; Muccioli *et al.*, 2007; Long *et al.*, 2009a; Schlosburg *et al.*, 2010). However, 2-AG can also be hydrolyzed by FAAH or by αβ-hydrolase domain-containing protein 6 (ABHD6) (Blankman *et al.*, 2007; Long *et al.*, 2009b). To test the importance of these enzymes in limiting and/or gating eCB-CB1 activation and to determine the role of these enzymes in the CB1-Tango cells, we used a selective MAGL inhibitor, JZL184 (Long *et al.*, 2009a) and a dual MAGL/FAAH inhibitor, JZL195, that also inhibits ABHD6, albeit at a lower potency (Long *et al.*, 2009b).

In this chapter, we demonstrate the successful adaption of the CB1-Tango assay to monitor eCB activation of the CB1 receptor. At the outset of this study, there were no specific inhibitors to differentiate between DAGLα and DAGLβ, and no inhibitors of anandamide synthesis. Therefore, we recognized that a genetic intervention to delete candidate enzymes responsible for eCB synthesis would ultimately be required in order to identify pathways regulating eCB signalling in the CB1-Tango cells. However, it was important to first establish whether or not we could detect eCB-dependent CB1 activation in the CB1-Tango assay and if we could attribute this to general DAGL activity.

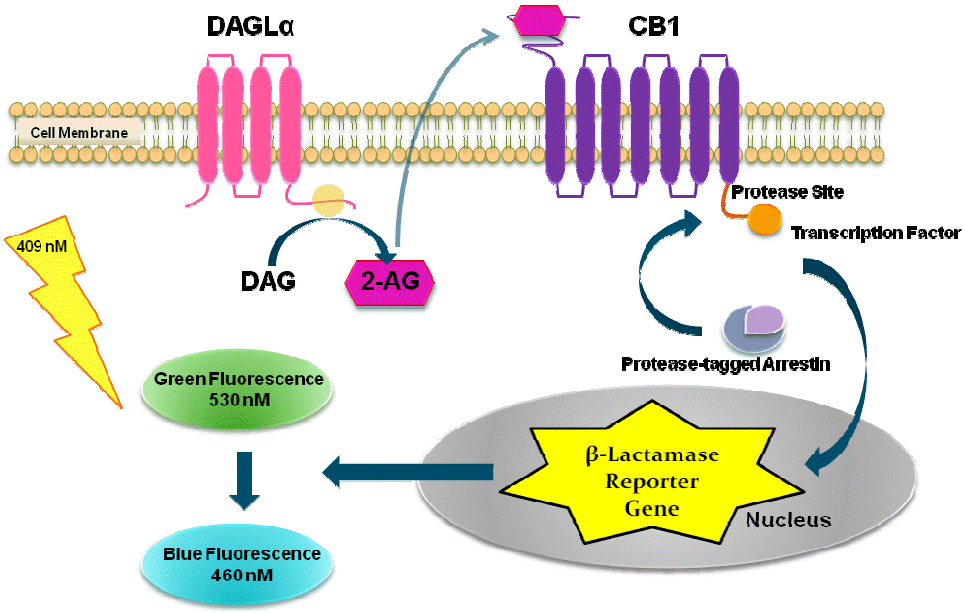

Figure 5.1 Schematic overview of the CB1-Tango Assay system

In the CB1-Tango assay, the CB1 receptor is extended at the C-terminus with a non-native transcription factor followed by a linker that contains a protease cleavage site. β-Arrestin 2 is fused to a protease. Upon CB1 activation by 2-AG, β-arrestin is recruited to the receptor. Close proximity of the protease and the cleavage site allows the transcription factor to be released, which activates β-lactamase (*bla*) reporter gene in the nucleus. During the assay, cells are loaded with a fluorescent substrate containing two fluorophores, coumarin and fluorescein. In the absence of *bla* expression, the substrate remains intact and excitation of coumarin results in FRET and emission of green fluorescent light. When *bla* is expressed, the substrate is cleaved by β-lactamase. This separates the fluorophores, disrupting energy transfer and results in a blue fluorescence signal. The resulting coumarin:fluorescein (green:blue) ratio at an excitation of 409 nM provides a normalized CB1 response. The figure highlights the role of DAGLα, but eCB signalling might also be stimulated by an increase in anandamide and/or another eCB.

5.2 Results

CB1 activation is maintained in cells overexpressing DAGLα

Having developed a cell line to overexpress DAGLα, the V5α11 cells (described in Chapter 4, Results II), our first step was to determine whether the CB1-Tango assay was still functional in these cells. To this end, we tested the standard agonist for the CB1 receptor, arachidonyl-2'-chloroethylamide (ACEA) and the standard antagonist, AM251 (as recommended by the manufacturer). To do this, we performed the CB1-Tango assay using the standard manufacturer's protocol (and as described in the methods section). 20,000 CB1-Tango and V5α11-CB1-Tango cells (hereafter just called V5α11 cells) were seeded into black, clear-bottom 96-well plates and maintained overnight in the recommended medium, Freestyle. This medium is serum free to starve the cells in order to reduce background noise in the assay. The following day, compounds were made up in the same medium. Varying concentrations of AM251 were added to half the cells (10 μM top concentration, diluted 1:2, 6 point curve), and incubated for 30 minutes. A concentration-response curve of ACEA was then made using 10 μM top concentration (diluted 1:2, 6 point curve), and was added to the second half of the plate. 2 μM ACEA was also added to the AM251 concentrations and the plate was incubated for 4 h to allow accumulation of β-lactamase expression in the cells. Expression was detected using a FRET-enable substrate ("LiveBLAzer"), which was added to the plate for 2 h. Fluorescence ratio between the green and the blue channel was detected on the Flexstation; emission and excitation filters are highlighted in Table 5.1.

Table 5.1 Excitation and emission wavelengths for the CB1-Tango assay

	Scan 1	Scan 2
Purpose	Measure fluorescence in the Blue channel	Measure FRET signal in the Green channel
Excitation filter	409/20 nm	409/20 nm
Emission filter	460/40 nm	530/30 nm

The results from each concentration curve are presented in Figure 5.2. Differences in maximal responses can be seen between the two cell lines. This might reflect the added pressure on V5α11 cells caused by the additional antibiotic for DAGLα expression in the media, or perhaps just clonal variation. The EC_{50} values for CB1-Tango and V5α11 cells were ~ 50 nM and ~ 160 nM, respectively. However, AM251 IC_{50} values of ~ 126 nM were robust and comparable between the two cell lines. Based on this, we deemed that a concentration of 1µM ACEA and 10 µM AM251 would be maximally active in both cell lines, and these concentrations were used for subsequent experiments (unless otherise stated).

Other key points to note include the observation that the addition of AM251 to control cultures does not reduce the signal below the control value in both the parental and DAGL overexpressing cell lines (background value for CB1-Tango cells was 1.4 and for V5α11 cells was 1.6). Thus under these conditions we can conclude that there is no basal eCB tone in the cultures, and on this basis conclude the simple over expression of the DAGL is not sufficient to generate a basal eCB signalling tone in cells.

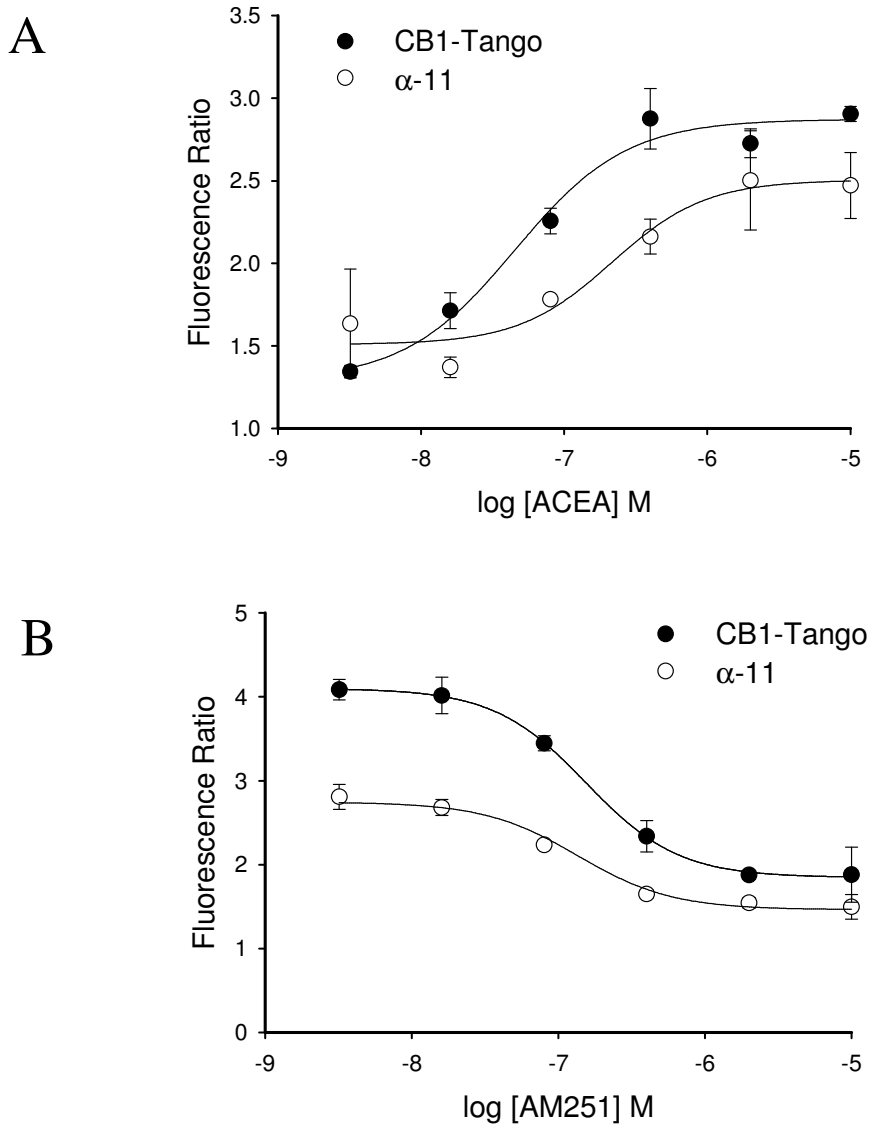

Figure 5.2 CB1-Tango activity is unaffected by the transfected DAGL*α*

20,000 Tango and V5α11 cells were seeded in Freestyle medium into black 96-well plates. The cells were treated with varying concentrations of the CB1 selective agonist, ACEA (10 µM top conc, 1:2, 5 pt curve) (A) and the standard antagonist AM251 in the presence of 1µM ACEA (10 µM top conc, 1:2 5 pt curve) (B). Compounds were incubated for 4 h. Fluorescent detection of β-lactamase reporter gene transcription was measured using a FRET-enabled substrate, as per manufacturer's protocol. Graphs show the mean of 4 wells ± SEM (n=1). ACEA CB1-Tango EC_{50} ~50 nM; V5α11 EC_{50} ~160nM; AM251 IC_{50} ~90 nM, for both cell lines.

Detection of an eCB tone using the specific MAGL inhibitor, JZL184

Next we wanted to determine if we could induce an eCB tone in the CB1-Tango cells by treating the cells with the MAGL inhibitor, JZL184 (Long *et al.*, 2009a). We reasoned that JZL184 might allow any 2-AG being produced by the DAGLs to accumulate and then signal through the CB1 receptor (Schlosburg *et al.*, 2010). An eCB tone should manifest itself as a reduction in basal response by AM251, in the presence of JZL184.

Using the standard manufacturer's protocol, CB1-Tango cells were starved in Freestyle medium for 24 h. On the day of the assay, compounds were diluted in the same medium in the presence of 100 nM JZL184, which is sufficient for maximum inhibition of MAGL (Long *et al.*, 2009a). Half the cells were treated with 10 µM AM251 for 30 minutes before addition of either Freestyle medium alone (+ JZL184) or ACEA as a positive control. The cells were treated for 4 h to allow accumulation of *Bla* expression. The FRET-enabled substrate, LiveBLAzer was used to detect fluorescence and the plate was read on the Flexstation, as described above. The results are presented in Figure 5.3.

JZL184 treatment did not stimulate an eCB tone in the assay, as AM251 did not inhibit the control response in the presence of the drug. The CB1-Tango assay is functional in the presence of JZL184, as there is a robust response seen from 1 µM ACEA. This was fully inhibited by AM251, showing the response to be through the CB1 receptor. The lack of tone in the presence of JZL184 alone is a possible indicator that the endogenous DAGLs are not active, or perhaps other enzymes can hydrolyse the basal production of 2-AG.

It has been reported that activation of PKA can lead to the synthesis of 2-AG (Vellani *et al.*, 2008). Based on this, we determined whether cAMP-dependent PKA activation, by treating the cells with forskolin, would stimulate eCB signalling. Forskolin activates adenylyl cyclase, increasing intracellular levels of cAMP which in turn activates PKA (Seamon & Daly, 1986).

Parental CB1-Tango cells were plated and starved in Freestyle medium, as described above. On the day of the assay, all compounds were made up in the same medium containing 100 nM JZL184 (in an attempt to maximise any response), and half the cells were treated with 10 μM AM251 for 30 minutes. A range of forksolin concentrations were then tested (0.08 – 10 μM FAC) in the presence and absence of AM251, and the cells were treated for 4 h. Addition of media containing JZL184 alone was used as control. Fluorescent ratio was again determined by treating the cells with the FRET-enabled substrate for 2 h, before reading the plate on the Flexstation. Results were normalised to the control, which is represented as a 100% in Figure 5.4.

Forskolin appeared to stimulate a significant CB1-Tango response over that seen from the control. This response is inhibited by AM251, and is therefore CB1-dependent. However, the forskolin response did not reach significance, as established using the one-way analysis of variance (ANOVA) (Figure 5.4).

In conclusion, a basal eCB tone is not present in parental Tango cells, nor is one revealed when MAGL is inhibited by JZL184. The forskolin response was also not significant; this could possibly be due a limiting factor, such as lack of substrate, lack of enzyme, or enzyme not being active. To determine if the lack of enzyme is a limiting factor, we looked at basal tone and responsiveness to forskolin in V5α11 cells.

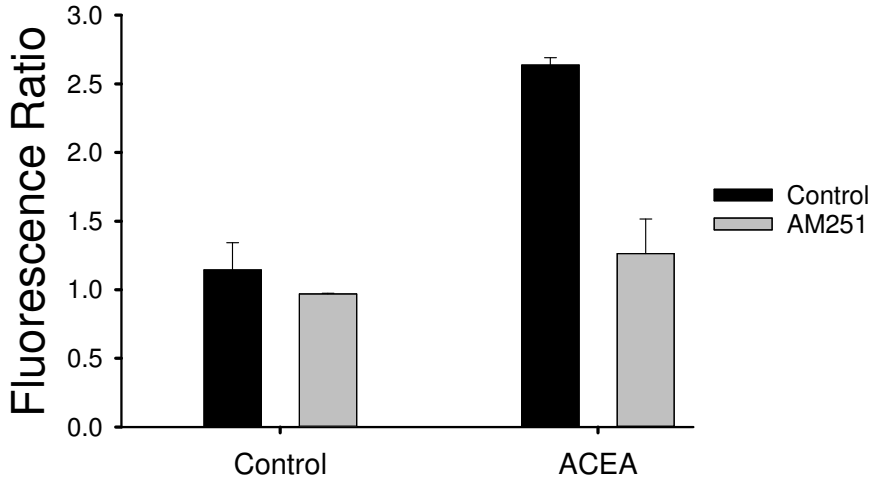

Figure 5.3 The use of the MAGL inhibitor JZL184 reveals no eCB tone in the Tango assay

20,000 parental Tango cells were plated into black, clear-bottom 96-well plates in Freestyle medium. The cells were left to adhere overnight at 37°C before assay. Compounds were made up in Freestyle medium containing 100 nM of the MAGL inhibitor, JZL184. Half of the cells were treated with 10 μM AM251 for 30 min, before addition of either Freestyle medium ('control' cells) or 1 μM ACEA. After 4 h, fluorescent detection of β-lactamase reporter gene transcription was measured using a FRET-enabled substrate, as per manufacturer's protocol. The graph shown is a representative of 3 independent experiments and is the mean of 8 replicate wells ± SEM.

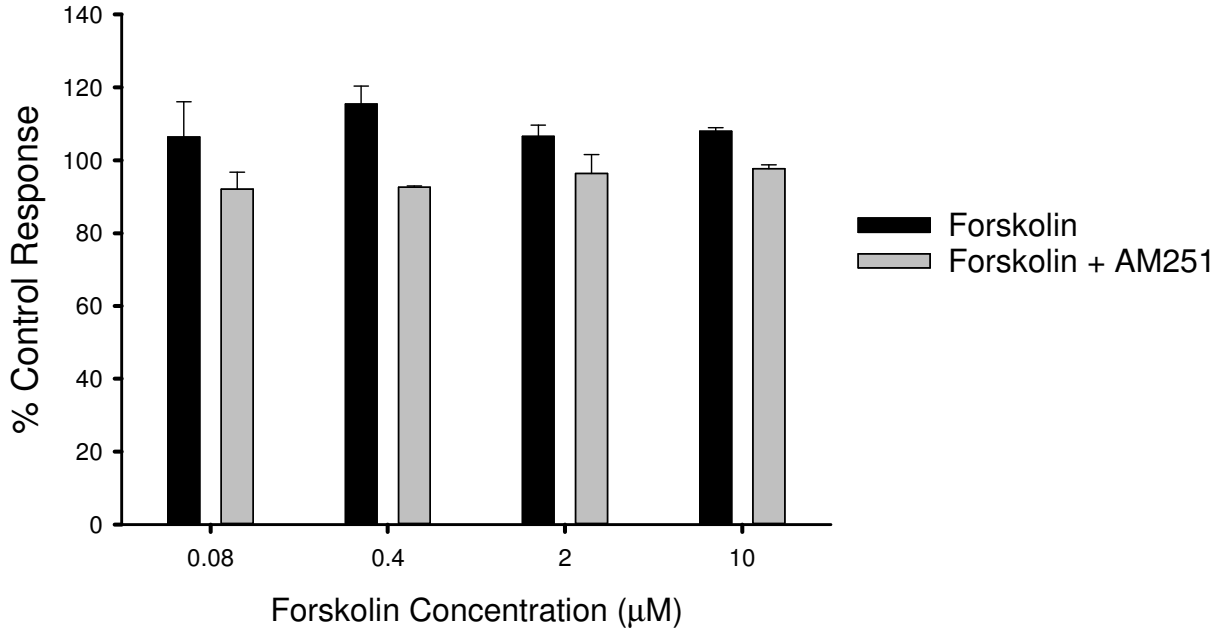

Figure 5.4 The forskolin stimulated response is not dependent on concentration

20,000 parental Tango cells were plated in black, clear-bottom 96-well plates and left to adhere overnight in Freestyle medium. The following day, compounds were diluted in Freestyle medium containing 100 nM JZL184. Half the cells were treated with 10 μM AM251 for 30 min, before addition of varying concentrations of forskolin (FSK; 0.08 – 10 μM) for 4 h to all wells. β-lactamase expression was detected by addition of a FRET-enabled substrate, as per manufacturer's protocol. The resulting data was normalised to the control background response, fixed at 100%. Data presented is pooled from 3 independent experiments, with each of these representing the mean of 8 wells ± SEM. Statistics were performed using one-way ANOVA.

Detection of an eCB tone in V5α11 cells in the presence of JZL184

To determine whether an increased level of DAGLα expression could induce an eCB tone (in the presence of JZL184), we used our DAGLα overexpressing cell line, V5α11, which were starved in Freestyle medium for 24 h. Compounds were diluted in the same medium containing 100 nM JZL184. We first treated V5α11 cells with 10 μM AM251 for 30 minutes, followed by 1 μM ACEA, or medium as control. Using AM251 alone tells us whether the CB1 receptor is being activated when JZL184 prevents 2-AG breakdown. We compared this to the ACEA response being inhibited by AM251, and results from a single representative experiment are shown in Figure 5.5.

No basal eCB tone was detected in V5α11 cells, as evident from treatment with AM251 alone, which did not reduce the background signal in the presence of JZL184. There is a robust ACEA response from these cells, which is inhibited by AM251. Again, the response from V5α11 cells is smaller than that seen from parental CB1-Tango cells, possibly reflecting the added antibiotic pressure on the cells in culture and/or simple clonal variation.

The lack of eCB tone observed in these cells might reflect a lack of substrate or perhaps substrate is available but unable to access the active site of the enzyme due to steric hindrance by the regulatory loop. Therefore, we tested responsiveness to PKA activation. To do this, V5α11 cells were plated in Freestyle media for 24 h, before addition of compounds also made up in Freestyle with 100 nM JZL184 (to again try to maximise any response). 10 μM AM251 was added to half of the cells for 30 minutes, before addition of varying concentrations of forskolin (0.08 – 10 μM FAC) for 4 h. Fluorescence was detected as described previously and read on the Flexstation. The results were normalised to the control response, which was set to 100% and results are presented in Figure 5.6.

In the presence of 10 μM forskolin, a minor yet significant response is induced that is CB1-dependent, as it is inhibited by AM251. However, as seen with parental CB1-Tango cells, the response is not concentration-dependent (over the tested range). The

response is also not significantly different from that seen from parental CB1-Tango cells, suggesting the level of enzyme expression is not rate-limiting under these conditions; lack of eCB tone might therefore be due to insufficient substrate and/or an inability of the substrate to access the active site of the enzyme.

In conclusion, after 4 h in the presence of JZL184 there was no basal eCB tone seen from either parental CB1-Tango or V5α11 CB1-Tango cells. Similarly, forskolin treatment did not induce a concentration-dependent response in the 4 h assay. A previous report has shown that increasing the compound incubation time can highlight subtle increases or decreases in CB1 activation, by allowing β-lactamase expression to accumulate (van der Lee *et al.*, 2009). It follows that increasing the length of the assay might increase sensitivity and thereby reveal tone and/or responsiveness to forskolin and as such we increased the compound incubation time with forskolin from 4 h to 18 h (overnight assay).

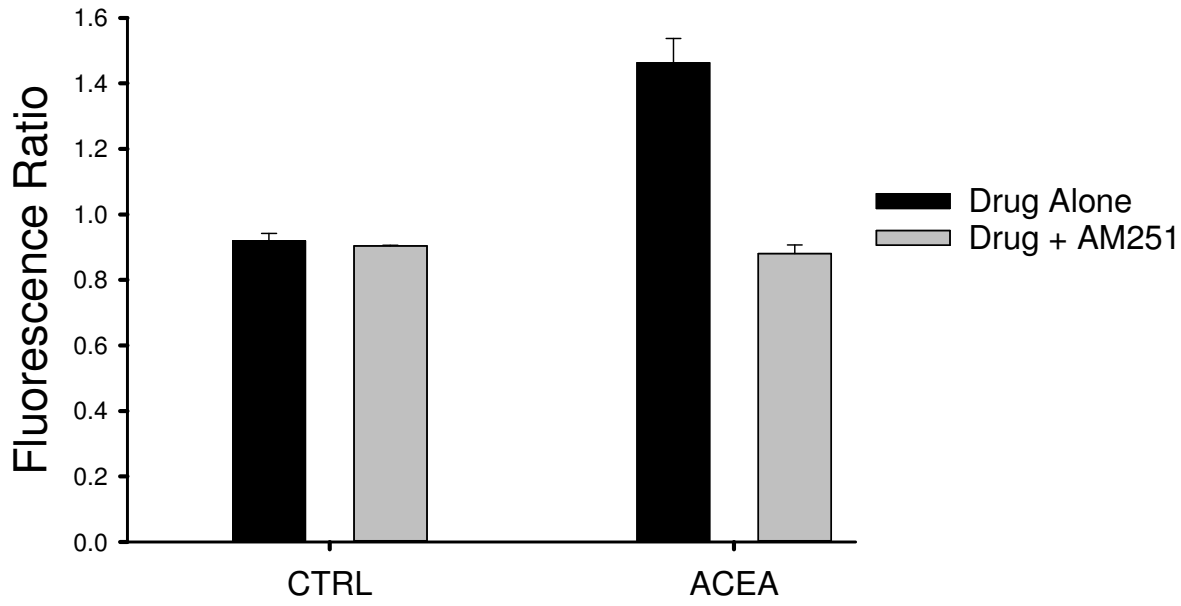

Figure 5.5 JZL184 does not reveal a basal eCB response in V5α11 cells

V5α11 cells were plated and maintained in black, clear-bottom 96-well plates in Freestyle medium at 20,000 cells per well, as previously described for the parental CB1-Tango cells. Compounds were made up in Freestyle medium containing 100 nM JZL184, and half of the cells were treated with 10 μM AM251. The cells were then treated with the same medium as control (with JZL184) or with 10 μM ACEA, for 4 h. β-lactamase expression was detected by addition of a FRET-enabled substrate, as per manufacturer's protocol. Data presented is a single representative experiment and is the mean of 8 wells ± SEM.

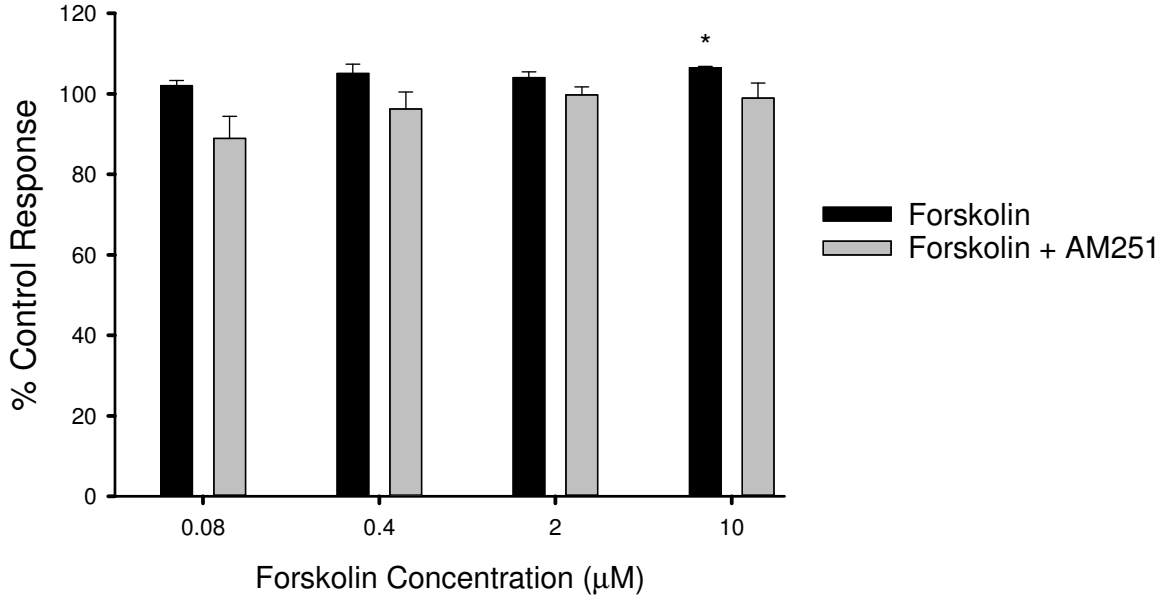

Figure 5.6 The forskolin-stimulated response in not revealed by increased DAGL*α* expression

V5α11 cells were plated and maintained in Freestyle medium, as described previously. The following day, compounds were made up in Freestyle medium containing 100 nM JZL184 and half of the cells were treated with 10 μM AM251 for 30 min. Varying concentrations of forksolin were added to the plate (0.08 – 10 μM) for 4 h and β-lactamase expression was detected using a FRET-enable substrate, as per manufacturer's protocol. The results were normalised to the control response, fixed at 100%. The data shown is from 3 independent experiments representing the mean of 8 wells ± SEM. Statistics were performed using one-way ANOVA, as indicated below.

* $p < 0.05$; one-way ANOVA

The effect of increasing compound incubation time on the response from CB1-Tango cells

We first wanted to determine the effects of increasing compound incubation time from 4 h to 18 h (overnight assay) on basal and maximal ACEA responses. The assay was run in a similar manner as before, where parental CB1-Tango cells were starved for 24 h in Freestyle medium prior to the assay (as recommended by the supplier). Compounds were made up in the same medium containing 100 nM JZL184 to maximise any response. 10 μM AM251 was added to half the cells for 30 minutes, before addition of media alone or 1 μM ACEA as a positive control. The cells were treated overnight for a total of 18 h. *Bla* expression was detected using the FRET-enabled substrate for 2 h and the plate was read on the Flexstation. No eCB tone was observed in this new assay format, as the basal signal was not reduced in the presence of AM251 (Figure 5.7). A much greater ACEA response was seen in the 18 h assay compared to the 4 h assay, indicating that increasing the compound incubation (and therefore time in starvation medium) did not have a detrimental effect on the assay and does in fact increase the response (Figure 5.7). The ACEA response was also fully inhibited by AM251. Our next step was to see whether the increased assay length could reveal a more robust forskolin-induced response in a concentration-dependent manner.

To do this, CB1-Tango cells were plated and maintained in Freestyle medium as described above. All compounds were diluted in the presence of 100 nM JZL184 and half the cells were treated with 10 μM AM251 for 30mins, before addition of varying concentrations of forskolin (0.08 – 10 μM), or medium as control. Compounds were incubated overnight, for a total of 18 h and the fluorescent ratio was calculated, as before. The results were normalised to the control response, set to 100%. Statistics were performed using one-way ANOVA and the results are shown in Figure 5.8. The response seen from 10 μM forskolin reached significance in the 18 h assay, resulting in a much greater response above control from forskolin (~ 30%) compared to that seen in the 4 h assay (~ 8%). However, and very importantly, this response was not inhibited by AM251 suggesting that it is not related to specific activation of the CB1 receptor.

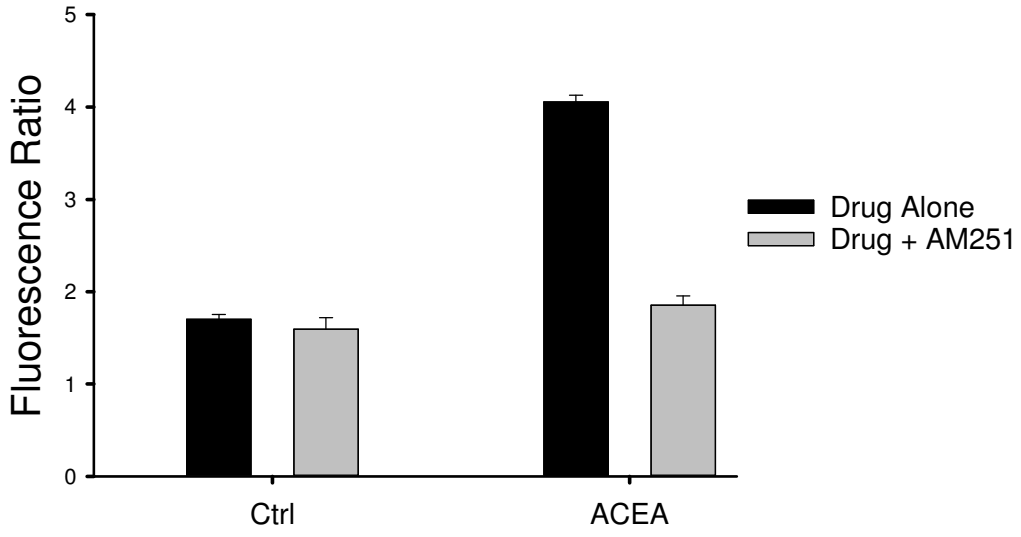

Figure 5.7 The ACEA response increases in the overnight Tango assay

Tango cells were plated and maintained in black, clear-bottom 96-well plates in freestyle medium, as previously described. Half of the cells were treated with 10 μM AM251, before addition of 10 μM ACEA or medium as control for an increased length of 18 h (overnight assay). β-lactamase expression was detected by addition of a FRET-enabled substrate, as per manufacturer's protocol. Results are pooled from 3 independent experiments, with 8 replicates used to generate the results in the individual experiments (±SEM).

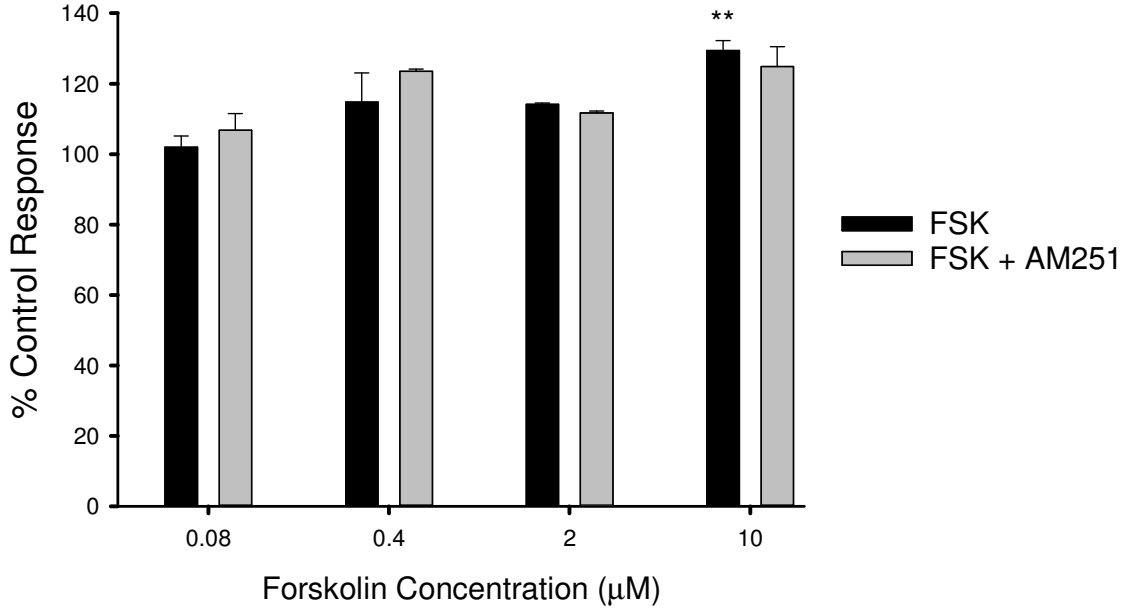

Figure 5.8 Increasing compound incubation time does not stimulate an eCB response in Tango cells

20, 000 Tango cells were plated into a black, clear-bottom 96-well plate and maintained overnight in Freestyle medium. The following day, compounds were diluted in the same medium containing 100 nM JZL184. Half the cells were treated with 10 µM AM251 for 30 min, before addition of varying concentrations of forskolin (FSK; 0.08 – 10 µM) or media as control. *Bla* expression was detected using a FRET-enabled substrate, as per manufacturer's instructions. The data was normalised to the control (fixed at 100%) and the data presented is the mean of 8 wells ± SEM pooled from 2 independent experiments. Significance was established using one-way ANOVA, as indicated below. No significant effect was found in the presence of AM251.

**$p<0.01$; one-way ANOVA

Evaluating a more physiological medium for the CB1-Tango assay

The failure to detect a substantial basal eCB signalling in cells that overexpress DAGLα in media containing JZL184 in the presence and absence forskolin was surprising given the report that PKA activation leads to 2-AG synthesis (Vellani *et al.*, 2008). The CB1-Tango assay requires the cells to be serum starved for 24 h in Freestyle medium to reduce background interference, and the manufacturers will also not reveal the composition of the Freestyle media, apart from confirming to us that it is a calcium free media. The cells are therefore cultured for a long period without serum and calcium, in media that might lack other factors required for the synthesis of 2-AG and perhaps other eCBs. Based on this it was decided to change track and determine if a CB1-Tango assay could be developed in a better defined tissue culture media.

For this reason, we decided to test McCoy's as it is the recommended growth medium for U2OS cells and it also contains 1 mM calcium. Additionally, we introduced a low concentration of FBS (1%) to ensure cell viability, while keeping it low enough as to not interfere with the assay. Low levels of serum might also increase substrate availability by stimulating various receptors in the cells. We compared these results to another media type, DMEM as a comparison and to ensure the phenol red in McCoy's medium does not interfere with the fluorescent assay. To do this, we plated parental CB1-Tango cells in DMEM 1% FBS, McCoy's 1% FBS, or Freestyle 1% FBS and tested the effects of ACEA (1μM in the same media) in a 4 h or 18 h assay. The cells were initially 'starved' for 24 h in these media. Reporter enzyme activity was determined using the standard assay protocol, as described previously, and the results are shown in Figure 5.9. In a single experiment, results for all 3 media were very similar in both 4 h and 18 h assays. The major difference observed was the background signal. The background response seen in the 4 h assay was not inhibited by AM251 giving similar values to the background response, and is therefore not CB1-dependent (data not shown). All 3 media obtained similar results from ACEA, with a much more substantial response seen in the 18 h assay, largely due to the background being greatly reduced. As McCoy's 1% FBS is a

defined medium (full contents are known), contains calcium and is the recommended medium for U2OS cells, this was used in future experiments.

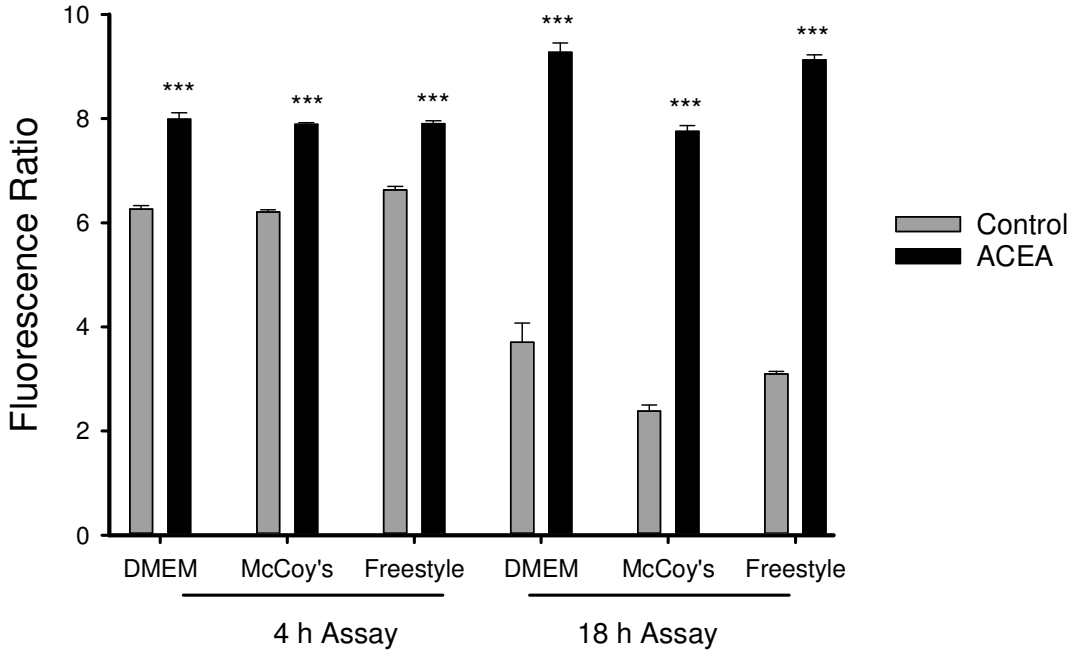

Figure 5.9 McCoy's 1% FBS is optimal as an assay medium for the CB1-Tango assay

Tango cells plated in 96-well plates at 20,000 cells/well were maintained for 24 h in different media types containing 1% FBS, as indicated. Compounds were made up in the individual media types. Half of the cells were treated with 10 µM AM251 for 30 min, followed by addition of 1 µM ACEA to all wells, for 4 h and 18 h, as indicated. (Control wells had media only.) Fluorescent detection of β-lactamase reporter gene transcription was measured using a FRET-enabled substrate, as per manufacturer's protocol. Results shown is from a single experiment and is the mean + SEM of 8 replicate wells. Significance between control and ACEA responses in each was established using the two-sided Student's t-test and is indicated as stated below.

*** $p<0.001$ Student's t-test

The effects of JZL195 on the eCB response following a 24 h 'starvation' period in McCoy's 1% FBS

When establishing whether we could detect an eCB tone in cells using McCoy's 1% FBS as the assay medium, we also included the inhibitor JZL195 in the assay. JZL195 is a dual inhibitor of the eCB-degrading enzymes MAGL and FAAH, and will also inhibit ABHD6. We decided it would be prudent to block all of these enzymes, as previous reports have shown some of these pathways are capable of crosstalk, where anandamide and 2-AG pathways can interact to regulate specific behavioural processes *in vivo* (Long *et al.*, 2009b); therefore blocking only one of these enzymes could lead to compensation by the other. For example, including JZL195 rather than JZL184 would eliminate FAAH compensating for the lack of MAGL activity.

We first established the effects of JZL195 on basal eCB tone in the 4 h and 18 h assays. To this end, parental CB1-Tango cells were plated in McCoy's 1% FBS medium. Following a 24 h 'starvation' period, compounds were made up in the same medium in the presence and absence of 100 nM JZL195. Half the cells were treated with 10 μM AM251 for 30 minutes, before addition of McCoy's 1% FBS media to all cells for either 4 h or 18 h. *Bla* expression was determined using the LiveBLAzer substrate for 2 h and the plate was read on the Flexstation, as described previously. The results are highlighted in Figure 5.10, which have been normalised to the control response in the absence of JZL195 (represented as 100%).

In both the 4h and 18 h assays, AM251 failed to significantly reduce the response below 100% in the absence of JZL195, indicating no basal eCB tone in this assay. However, there is a significant response seen over control in the presence of 100 nM JZL195. Therefore, the lack of eCB tone when JZL195 is absent might reflect MAGL/FAAH/ABHD6 acting as 'gate-keeping' enzymes, that hydrolyse 2-AG (or other eCBs) thereby preventing it from stimulating the CB1 receptor. Once these enzymes are inhibited by JZL195, β-lactamase activity increases after both 4 h and 18 h by ~15% and ~30%, respectively. This response was fully inhibited by AM251, providing evidence it is dependent on CB1 activation. Our lab has previously

established that 100 nM was a maximally active concentration of JZL195 and this has also been reported in the literature (Long *et al.*, 2009b).

Due to the eCB tone in the presence of JZL195, we determined whether the ACEA response is also potentiated when JZL195 is present. Cells were treated with ACEA +/- AM251 in control media and media supplemented with 100 nM JZL195, as described above. The results were normalised and presented as a percentage of the control response (100%) in Figure 5.11. A robust ACEA response was seen in both assays. As expected, the 18 h assay resulted in a much greater ACEA response (Figure 5.11 B). The ACEA responses were not significantly different from each other in both assays; therefore JZL195 neither potentiates nor does it add to the ACEA response. This is consistent with them operating via the same pathway (CB1 activation) and supports the view that ACEA on its own is maximally active.

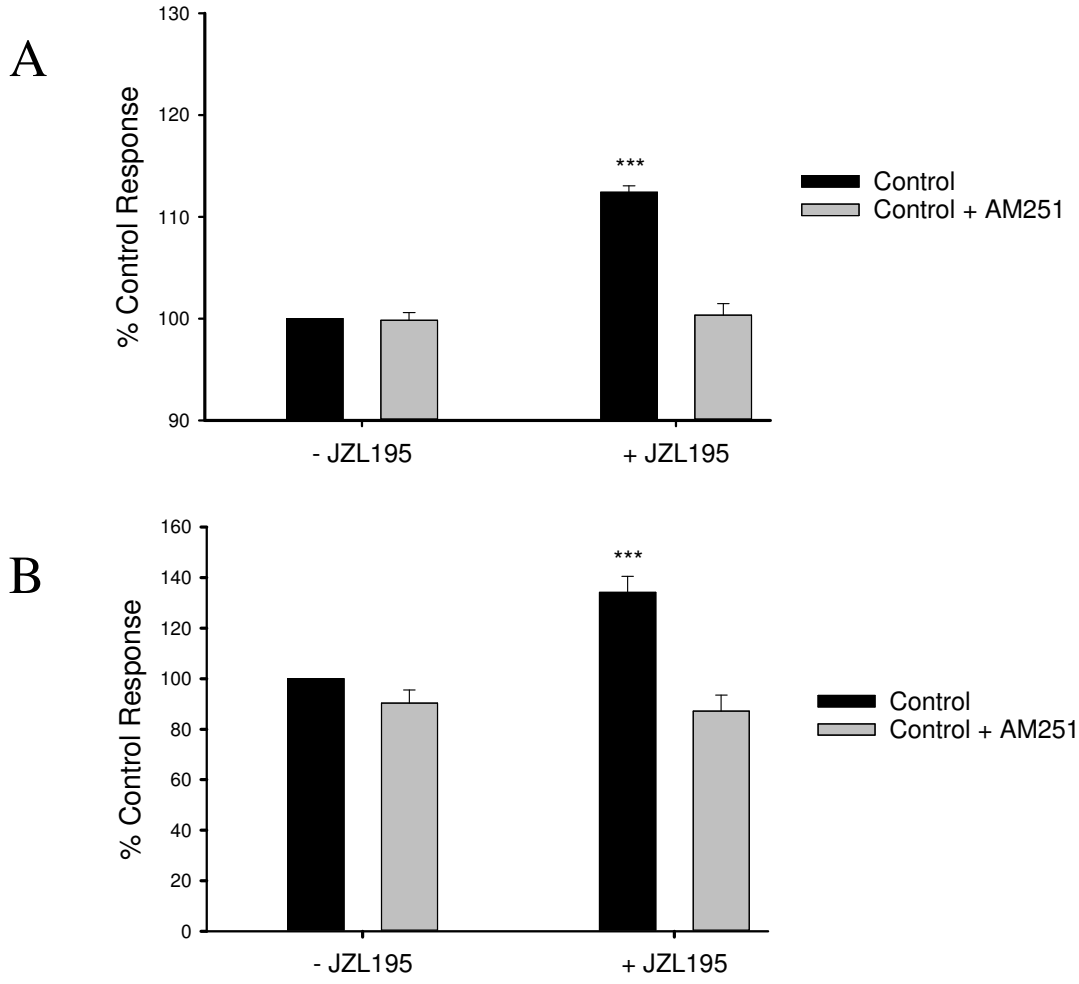

Figure 5.10 The dual MAGL/FAAH inhibitor JZL195 stimulates an eCB response following a 24-hour starvation period

20,0000 Tango cells were plated into black 96-well plates and maintained for 24 h in McCoy's 1% FBS. Compounds were made up in the same medium either in the absence (-) or presence (+) of 100 nM JZL195. Half of the cells were treated for 30 min with 10 μM AM251, before addition of control media. Compounds were incubated for either 4 h (A) or 18 h (B). Fluorescent detection of β-lactamase reporter gene transcription was measured using a FRET-enabled substrate, as per manufacturer's protocol. Data is represented as a percentage of the control response (set to 100%) and is the mean of 8 wells ± SEM from 3 pooled, independent experiments. Statistics were performed using one-way ANOVA, as indicated below. ***p<0.001; one-way ANOVA

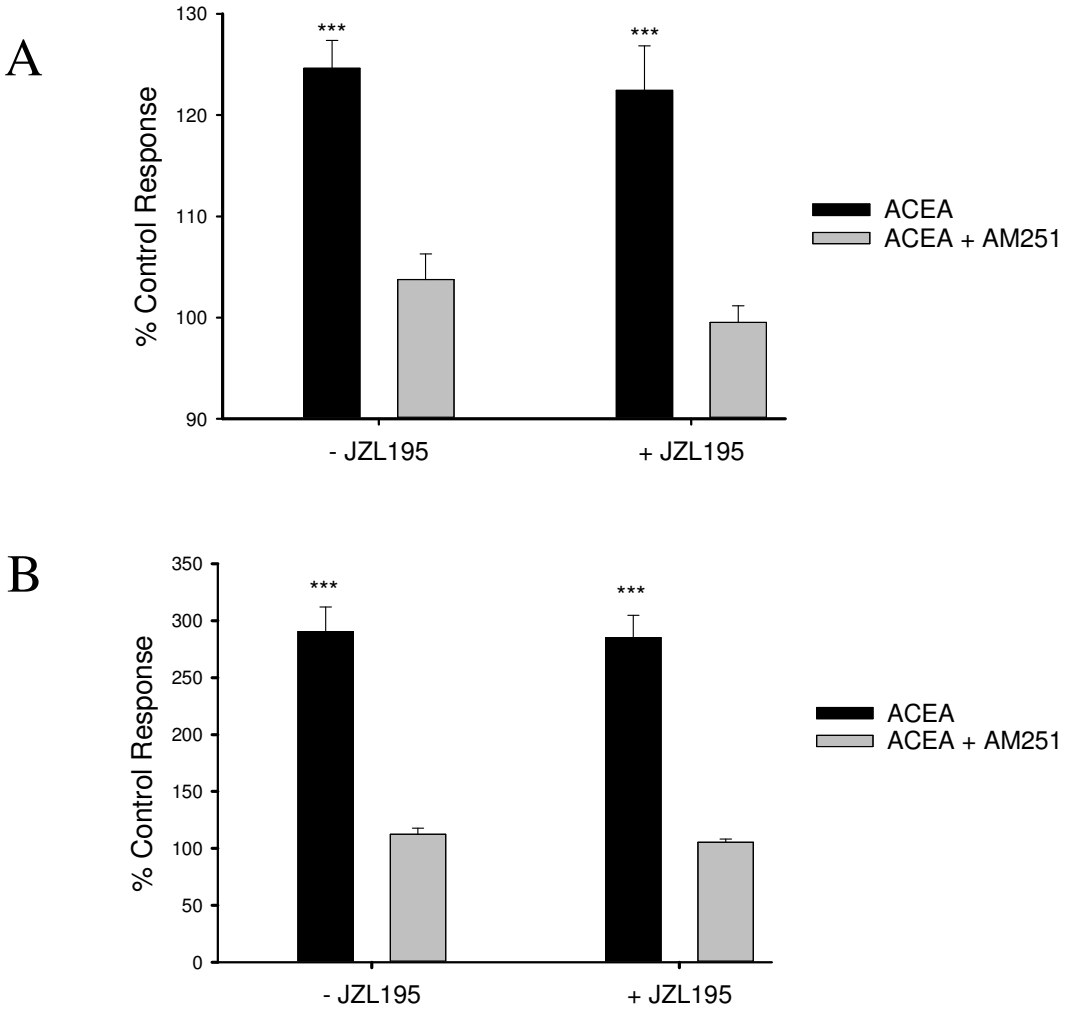

Figure 5.11 JZL195 does not have an additive effect on the ACEA response

Tango cells were plated in black 96-well plates at 20,000 cells/well and maintained for 24 h in McCoy's 1%. Compounds were made up in the same medium either in the absence (-) or presence (+) of 100 nM JZL195. Half the cells were treated for 30 min with 10 μM AM251, before addition of 1 μM ACEA for either 4 h (A) or 18 h (B). Fluorescent detection of β-lactamase reporter gene transcription was measured using a FRET-enabled substrate, as per manufacturer's protocol. The results are presented as a % of the control response, set to 100% and is the mean of 8 wells + SEM from 3 pooled, independent experiments. Statistics were performed using one-way ANOVA, as indicated below.

***p<0.001, one-way ANOVA

The effects of PKA activation in the presence of JZL195

Having established a small basal eCB with JZL195, we then determined whether we could now stimulate an eCB response from PKA activation. To this end, we treated the cells with forksolin using our new assay format. CB1-Tango cells were plated and maintained in McCoy's 1% FBS, as described above. After 24 h, compounds were made up in the same medium with and without 100 nM JZL195 and half the cells were treated with 10 µM AM251. We then treated the cells with 10 µM forskolin for 4 h and 18 h, and fluorescence ratio was calculated as before. The results were normalised to the control response (100%) and significance over the control was established.

As seen in Figure 5.12, forskolin alone stimulates an eCB tone to a similar extent as JZL195 alone, in both 4 h and 18 h assays (Figures 5.10 & 5.12). The response to these agents together is greater (and reached significance) compared to that seen with either one of them on their own (Table 5.2). The response to these agents acting together was fully inhibited by AM251 and is therefore CB1-dependent. This indicated that the forskolin-stimulated response was much greater when MAGL and FAAH, and perhaps ABHD6 are inhibited.

Overall, the above results clearly indicate that following a 24 h 'starvation' protocol, eCB tone can be generated in parental CB1-Tango cells by treating them with JZL195 or with forskolin, with a significant response seen only when both are present together. The response seen after 18 h is much greater, being ~ 2 times greater than the control response.

Our aim was to optimise this response by reducing the background signal in the presence of JZL195 alone. A response seen when MAGL and FAAH are inhibited indicates that one or both of the endogenous DAGLs could be active. Subsequently, our aim at this stage was to increase the starvation period in order to reduce this basal activity.

Table 5.2 CB1-Tango cell response (%) above control in the presence of JZL195

The Table below shows the percentage (%) response above control (background response) in the presence of JZL195 alone, in the presence of forskolin alone, or in the presence of both JZL195 and forskolin (combined).

Starvation Period	24 hour Starve		48 hour starve	
Compound Incubation	4 h	18 h	4 h	18 h
JZL195 (%)	12	34	16	31
Forskolin (%)	10	37	8	42
Combined (%)	16	96	16	162

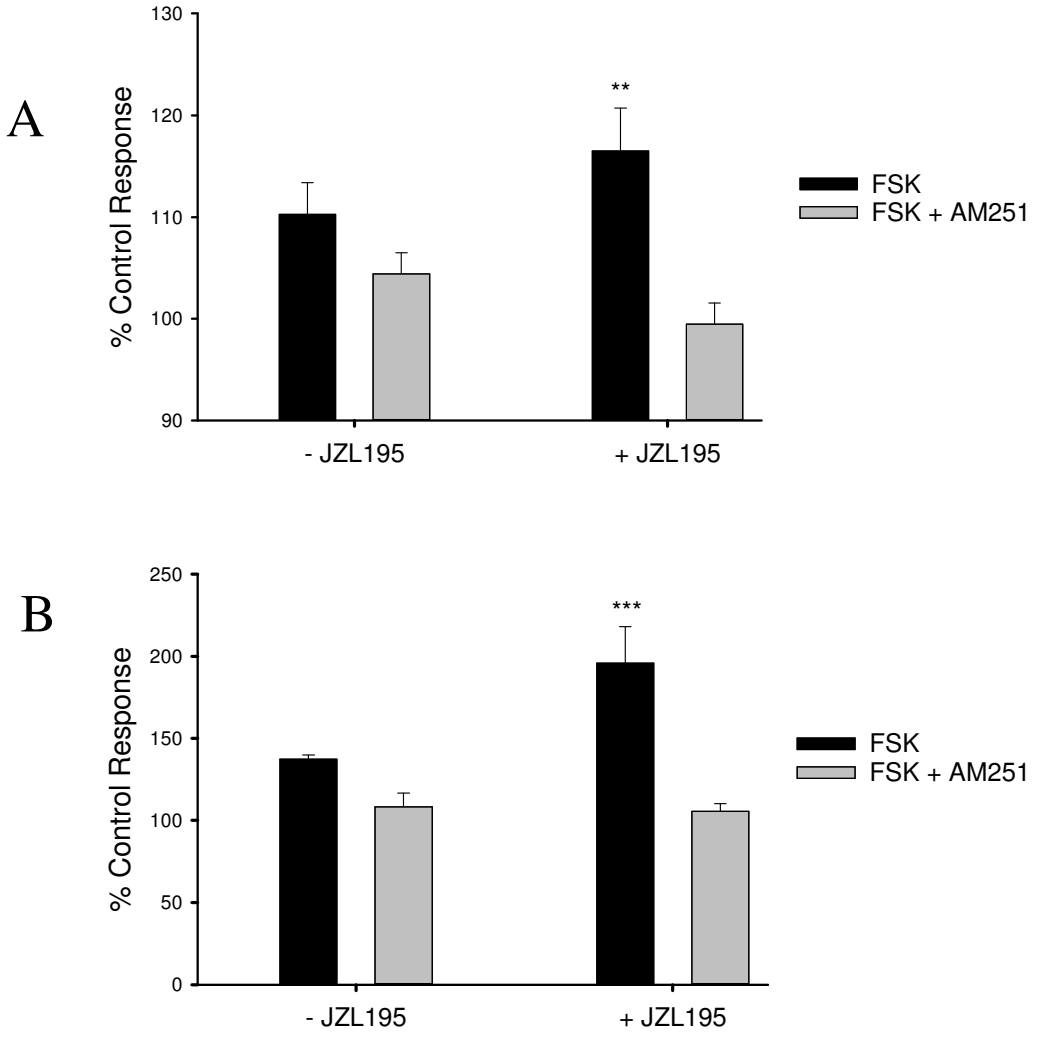

Figure 5.12 Forskolin stimulates an eCB response in Tango cells

20,000 Tango cells were plated into black 96-well plates and maintained for 24 h in McCoy's 1% FBS. Compounds were made up in the same medium either in the absence (-) or presence (+) of 100 nM JZL195. Half of the cells were treated for 30 min with 10 μM AM251, before addition of 10 μM forskolin (FSK) for either 4 h (A) or 18 h (B). Fluorescent detection of β-lactamase reporter gene transcription was measured using a FRET-enabled substrate, as per manufacturer's protocol. The results are presented as a percentage of the control response (set to 100%), pooled from 3 independent experiments, representing the mean of 8 wells + SEM. Statistics were performed using one-way ANOVA, as indicated below.

**p<0.01, ***p<0.001; One-way ANOVA

eCB tone and PKA activation following a 48 h starvation period

The aim of this part of the study was to reduce background signal seen in the presence of JZL195 alone, as this may have been due to basal activity of an eCB-synthesising pathway. To do this, we increased the 'starvation' period in McCoy's 1% FBS from 24 h to 48 h. Our first step therefore, was to determine if we could detect basal eCB tone following the increased starvation period.

Parental CB1-Tango cells were seeded in McCoy's 1% FBS in black, clear-bottom 96-well plates, as described previously. The cells were maintained for a starvation time of 48 h following which, compounds were made in the same medium in the presence or absence of 100 nM JZL195, as previously described. The cells were first treated for 30 minutes with 10 μM AM251, before addition of media containing JZL195. Compounds were then incubated for either 4 h (Figure 5.13 A) or 18 h (Figure 5.13 B). Results were normalised to the response seen from the control alone (set to 100%).

No eCB tone was seen from either 4 h or 18 h assays, which would manifest itself as inhibition below 100% in the presence of AM251 alone. There was a clear and significant response seen from JZL195 alone in the 4 h assay that was inhibited by AM251 (Figure 5.13 A). However, although significant, a much smaller CB1-dependent significant response was seen above control in the 18 h assay (Figure 5.13 B). This is could be due to the extended starvation period associated with 18 h assay and could reflect lower or absent synthesis of eCBs over this longer time period of 18 h, following a 48 h starvation period. However, it may also have been due to lack of CB1 receptor activity; therefore we next tested the response to ACEA.

To this end, CB1-Tango cells were plated and maintained in McCoy's 1% FBS for 48 h, as described above. Compounds were also made in up in a similar manner, in the presence of absence of 100 nM JZL195. The cells were treated with AM251 before addition of 1 μM ACEA for either 4 h or 18 h and fluorescence ratio was calculated, as before. The values obtained were normalised to the control response (set to 100%) and the results are presented in Figure 5.14. A robust ACEA response

was seen in both 4 h and 18 h assays, indicating the CB1-Tango assay is still functional following a 48 h starve. As seen following a 24 h starvation, JZL195 has no effect on the magnitude of the ACEA response, most probably because this represents maximal activation of the CB1 receptor pool (Figure 5.14). Therefore, increasing the starvation period to 48 h reduces the basal eCB tone in the presence of 100 nM JZL195 after 18 h, while having no effect on the ACEA response.

We next tested responsiveness to forskolin using the new assay format. CB1-Tango cells were plated, maintained and the compounds were diluted in the same way as described above. The cells were treated with 10 μM AM251, followed by 10 μM forskolin and the cells were incubated for either 4 h (Figure 5.15 A) or 18 h (Figure 5.15 B). The responses obtained were normalised to the control response in the absence of JZL195 (100%). In contrast to the results seen following a 24-hour starve, no response was seen in the presence of forskolin alone in both 4 h and 18 h assays (Figure 5.15). There is a clear and significant response seen from forskolin in the presence of JZL195, indicating that forskolin does indeed stimulate an eCB response in the CB1-Tango assay (Figure 5.15). However, this response is only revealed when the hydrolytic 'gate-keeping' action of MAGL and FAAH, and perhaps ABHD6, are inhibited. We next tested this assay format using our overexpressing cell lines to determine if we could see an increase in response from forskolin treatment when more DAGLα/β is present.

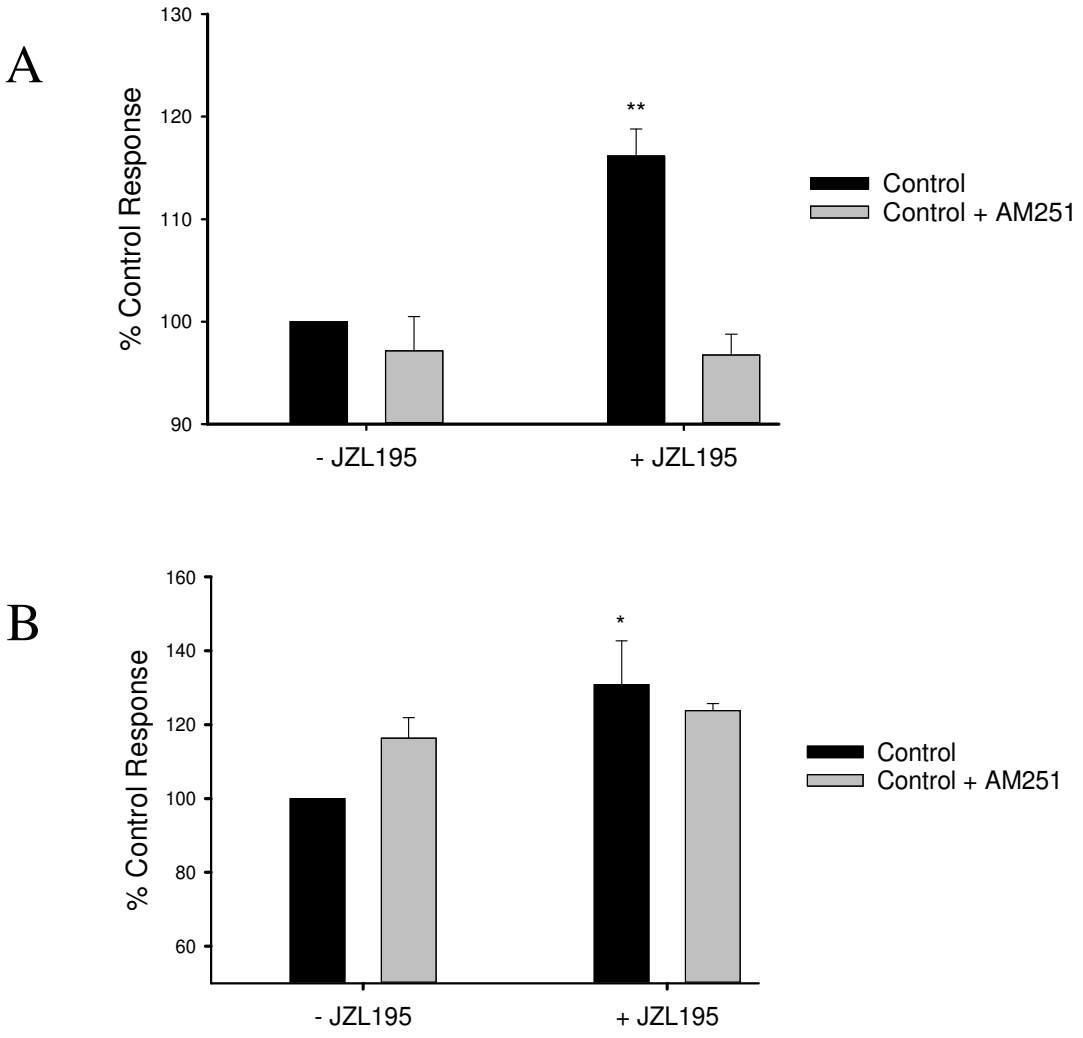

Figure 5.13 JZL195 stimulates an eCB response Tango cells

20,000 Tango cells were plated into black 96-well plates and maintained for 48 h in McCoy's 1% FBS. Compounds were made up in the same medium either in the absence (-) or presence (+) of 100 nM JZL195. Half of the cells were treated for 30 min with 10 μM AM251, before addition of control media for either 4 h (A) or 18 h (B). Fluorescent detection of β-lactamase reporter gene transcription was measured using a FRET-enabled substrate, as per manufacturer's protocol. The results are presented as a percentage of the control response (set to 100%) and are the mean of 8 wells + SEM, pooled from 3 independent experiments. Statistics was performed using one-way ANOVA, as indicated below.

*$p>0.05$, **$p<0.01$, one-way ANOVA

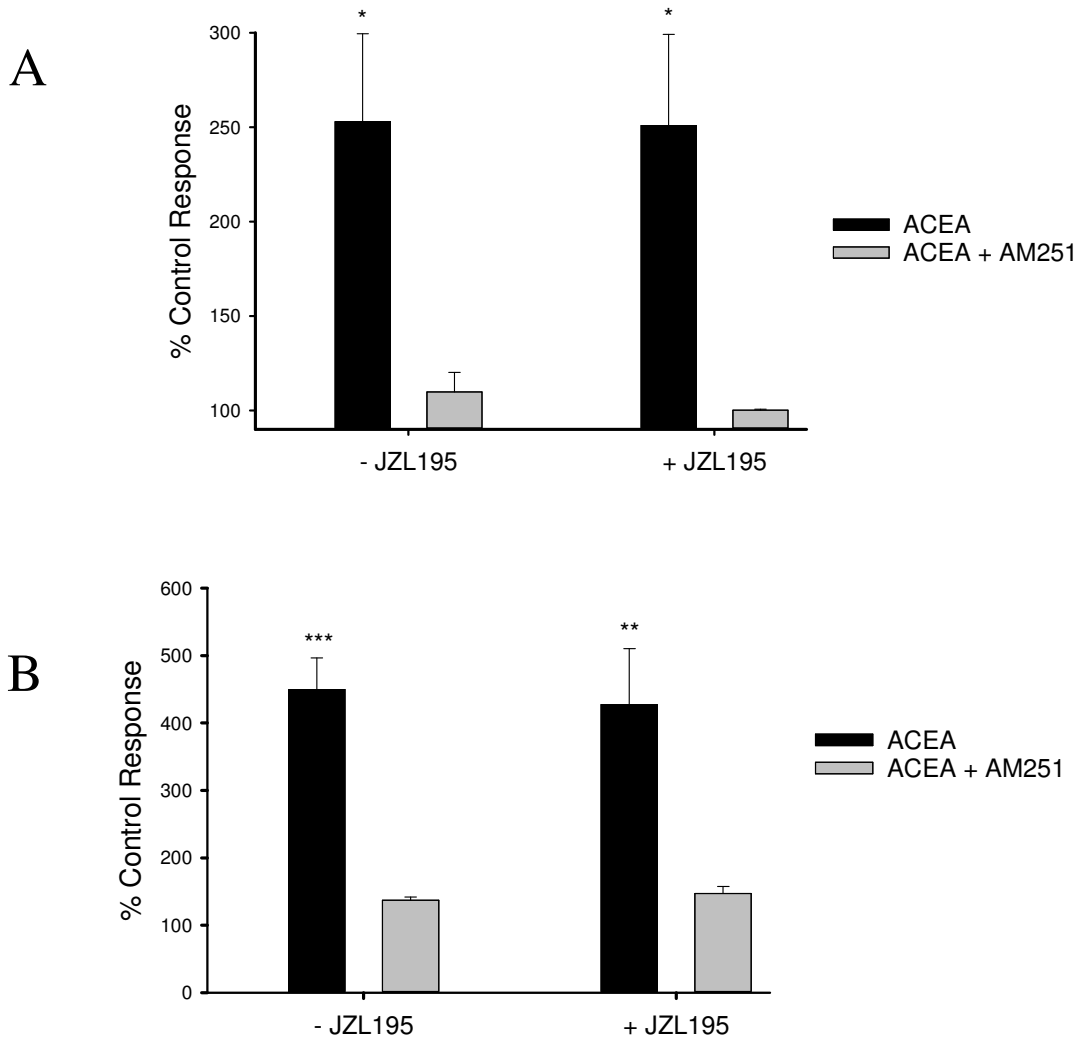

Figure 5.14 JZL195 does not potentiate the ACEA response following a 48-hour starvation period

20,000 Tango cells were plated into black 96-well plates and maintained for 48 h in McCoy's 1% FBS. Compounds were made up in the same medium either in the absence (-) or presence (+) of 100 nM JZL195. Half of the cells were treated for 30 min with 10 μM AM251, before addition of 1 μM ACEA for either 4 h (A) or 18 h (B). Fluorescent detection of β-lactamase reporter gene transcription was measured using a FRET-enabled substrate, as per manufacturer's protocol. The results are presented as a percentage of the control response (set to 100%) and are the mean of 8 wells + SEM, pooled from 3 independent experiments. Significance was established using one-way ANOVA, as indicated below.

*p<0.05, **p<0.01, ***p<0.001, one-way ANOVA

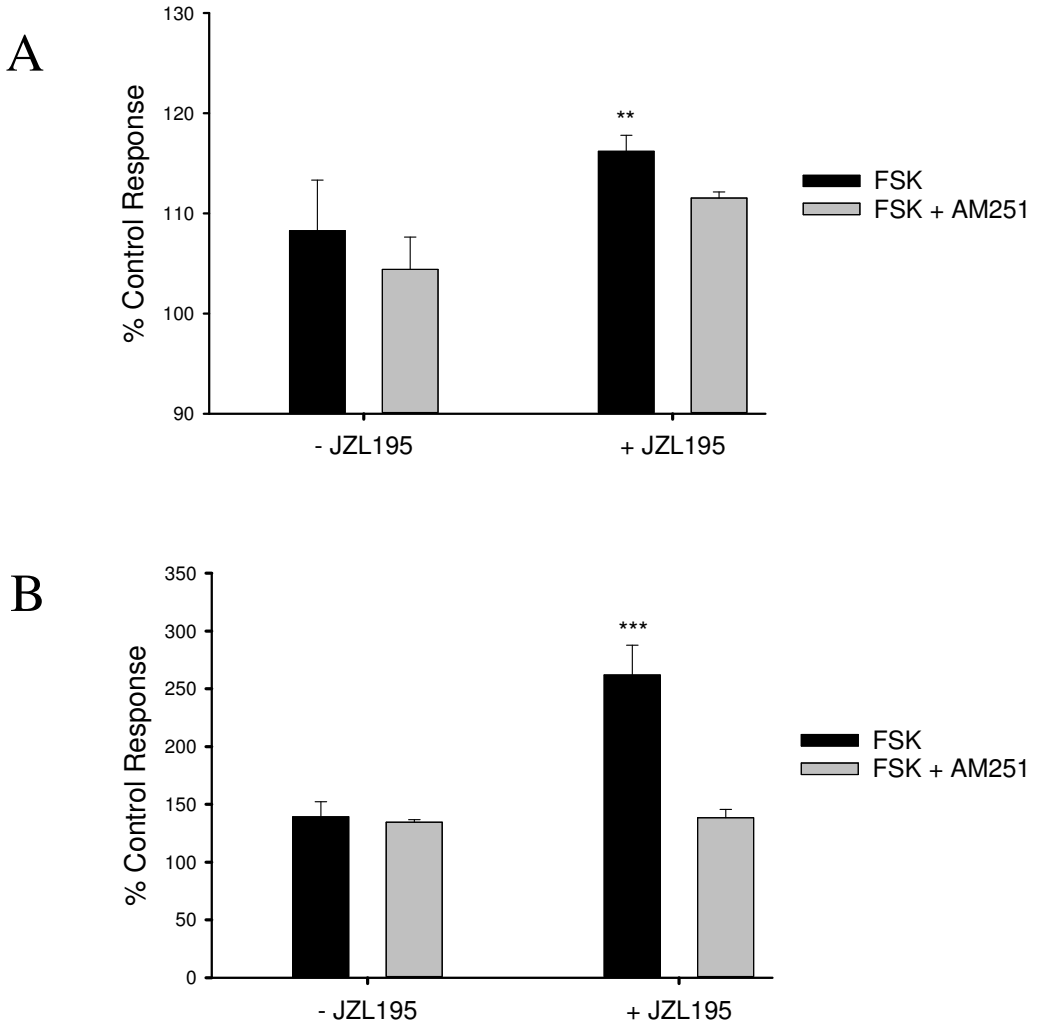

Figure 5.15 Forskolin stimulates an eCB response in the presence of JZL195 following a 48-hour starvation period

Tango cells were plated into black 96-well plates at 20,000 cells/well and maintained for 48 h in McCoy's 1% FBS. Compounds were made up in the same medium either in the absence (-) or presence (+) of 100 nM JZL195. Half of the cells were treated for 30 min with 10 μM AM251, before addition of 10 μM forskolin (FSK) for either 4 h (A) or 18 h (B). Fluorescent detection of β-lactamase reporter gene transcription was measured using a FRET-enabled substrate, as per manufacturer's protocol. The results are presented as a percentage of the control response (set to 100%) and are the mean of 8 wells + SEM, pooled from 3 independent experiments. Significance was established using one-way ANOVA, as indicated below.

**p<0.01, ***p<0.001; one-way ANOVA

eCB tone and effects of PKA activation in V5α11 and V5β4 cells

We evaluated the response from V5α11 and V5β4 cell to forskolin, with a view to determining if we could stimulate a 'gain of function' assay with these cells. We first established whether JZL195 alone could potentiate a response in the overexpressing cell lines. V5α11 and V5β4 cells were plated and maintained in McCoy's 1% FBS. After 48 h, 10 µM AM251 was added to half the cells, before addition of media in the absence or presence of 100 nM JZL195. Compounds were incubated for either 4 h or 18 h and *bla* expression was detected, as before. The results for V5α11 are presented in Figure 5.16 and for V5β4 in Figure 5.17, and were normalised to the control in each (set to 100%)

There was no eCB tone detected in V5α11 cells, as AM251 did not inhibit basal response in either the 4 h or 18 h assays. JZL195 alone stimulated a significant but small response above control in the 18 h assay (< 10 %); this potentiated response was not inhibited by AM251 and so is not CB1-dependent (Figure 5.16 B). These results suggest that the level of enzyme is not rate limiting, with the lack of eCB signalling in both absence and presence of JZL195 reflecting either a shortage of substrate and/or available substrate not accessing the active site in the catalytic domain.

A similar result was seen in V5β4 cells, whereby no eCB tone was detected and JZL195 appeared to simulate a small but significant, non CB1-dependent response after 18 h (Figure 5.17 B). So, again enzyme level is clearly not rate-limiting.

We also compared ACEA responses in all 3 of our cell lines following a 48 h starvation period. To do this, parental Tango, V5α11 and V5β4 cells were plated and maintained in McCoy's 1% FBS medium for 48 h. Compounds were made up the same medium and half of the cells were treated for 30 minutes with 10 µM AM251, before addition of either 1 µM ACEA or media as control. The cells were treated for 4 h or 18 h, before fluorescent ratio was determined, as described previously. The results were normalised to the control response (set to 100%) and are presented in Figure 5.18.

A robust ACEA response was seen from all 3 cell lines and as expected, this response was much greater after 18 h; in each case the response was fully inhibited by AM251. As a result, we could conclude that the lack of eCB tone seen in the DAGL overexpressing cell lines in both control and JZL195 containing media cannot be explained by a failure of the CB1 reporter construct.

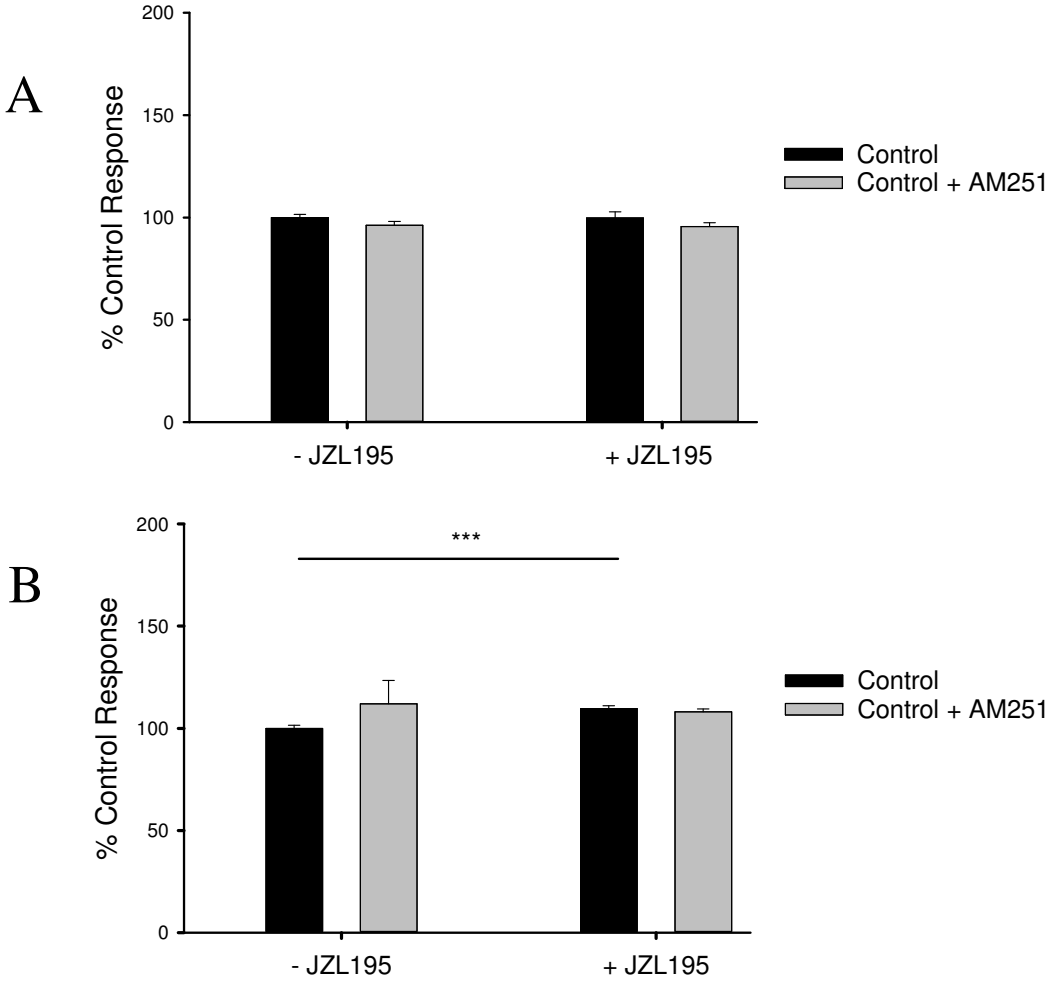

Figure 5.16 JZL195 response is not inhibited by AM251 in V5α11 cells

20,000 V5α11cells were plated into black 96-well plates and maintained for 48 h in McCoy's 1% FBS. Compounds were made up in the same medium either in the absence (-) or presence (+) of 100 nM JZL195. Half of the cells were treated for 30 min with 10 μM AM251, before addition of control media for either 4 h (A) or 18 h (B). Fluorescent detection of β-lactamase reporter gene transcription was measured using a FRET-enabled substrate, as per manufacturer's protocol. The results are presented as a percentage of the control response (set to 100%) and is the mean of 8 wells + SEM from a single representative experiment. Significance above the control response was established using the two-sided Student's t-test, as indicated below. However there was no significant inhibition of the response by AM251.

***p<0.001, Student's t-test

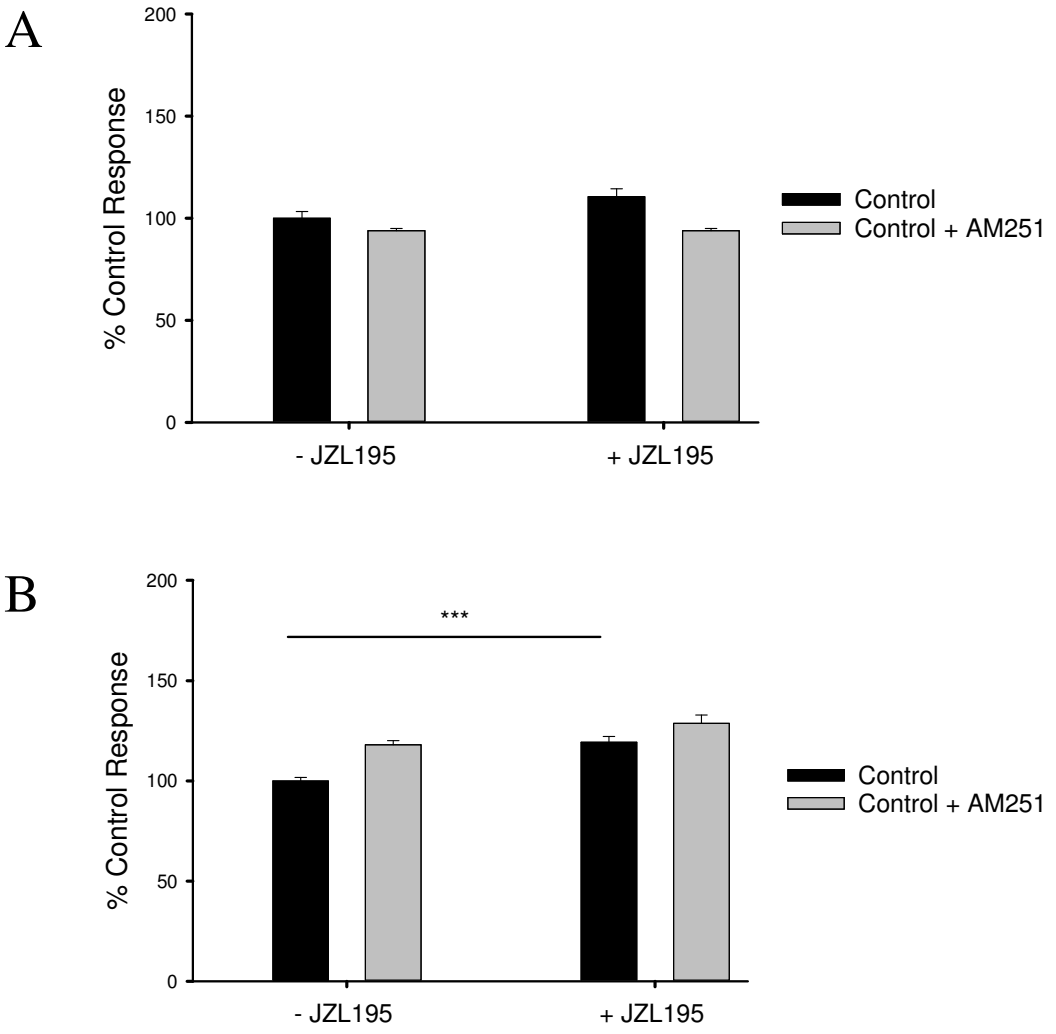

Figure 5.17 The JZL195-stimulated response in V5β4 cells is not inhibited by AM251

20,000 V5β4 were plated into black 96-well plates and maintained for 48 h in McCoy's 1% FBS. Compounds were made up in the same medium either in the absence (-) or presence (+) of 100 nM JZL195. Half of the cells were treated for 30 min with 10 μM AM251, before addition of control media for either 4 h (A) or 18 h (B). Fluorescent detection of β-lactamase reporter gene transcription was measured using a FRET-enabled substrate, as per manufacturer's protocol. The results are presented as a percentage of the control response (set to 100%) and are the mean of 8 wells + SEM of a single representative experiment. Significance above the control response was established using the two-sided Student's t-test, as indicated below. However, there was no significant inhibition of the response with AM251.

***p<0.001, Student's t-test

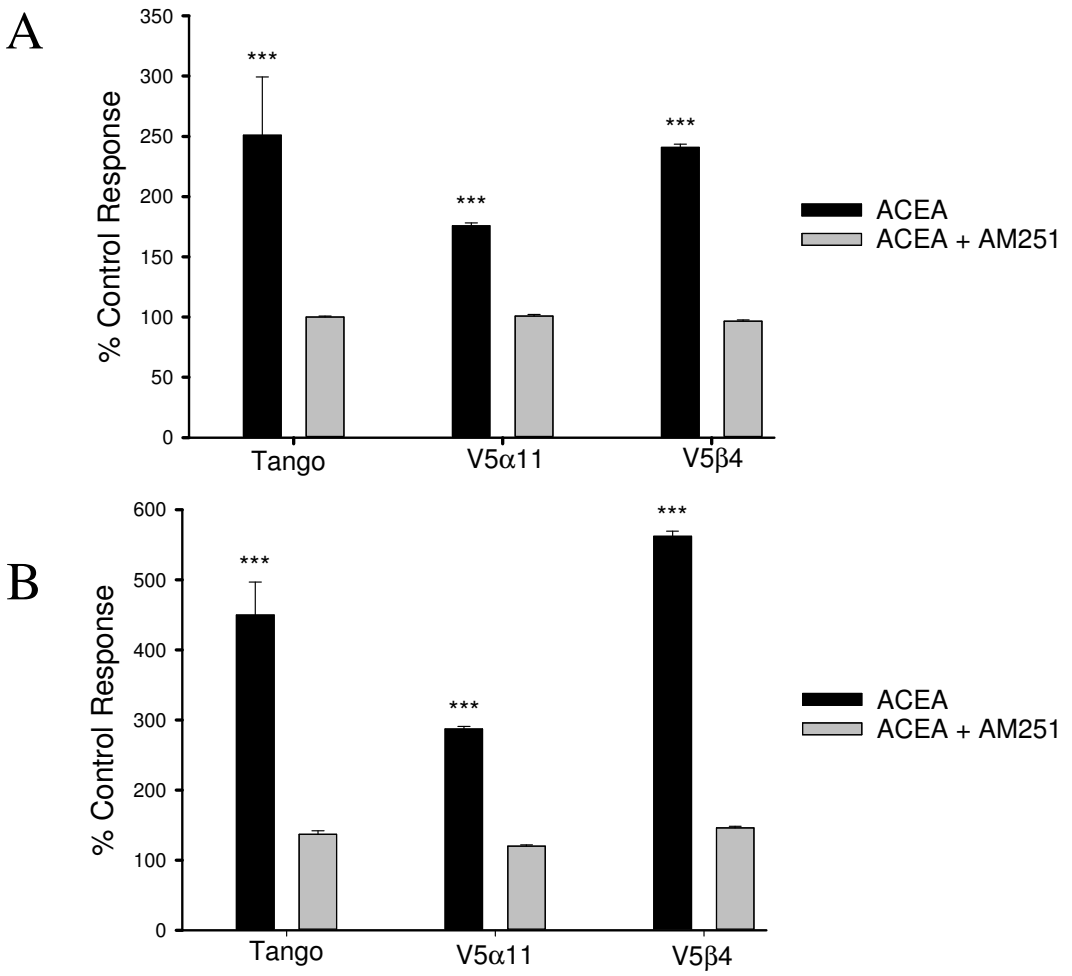

Figure 5.18 The ACEA response from all 3 cell lines is inhibited by AM251

20,000 Tango, V5α11 and V5β4 were plated into black 96-well plates and maintained for 48 h in McCoy's 1% FBS. Compounds were made up in the same medium either in the absence (-) or presence (+) of 100 nM JZL195. Half of the cells were treated for 30 min with 10 μM AM251, before addition of 1 μM ACEA (or media as control) for either 4 h (A) or 18 h (B). Fluorescent detection of β-lactamase reporter gene transcription was measured using a FRET-enabled substrate, as per manufacturer's protocol. The results are presented as a percentage of the control response (set to 100%) and are the mean of 8 wells ± SEM from a single representative experiment. Statistics were performed using one-way ANOVA, as indicated below.

***p<0.001; one-way ANOVA

We then determined if forskolin was able to stimulate eCB signalling in cells that have been starved for 48 h. To this end, V5α11 and V5β4 cells were plated and maintained in McCoy's 1% FBS medium for 48 h. Compounds were made up in McCoy's 1% FBS medium either in the absence or presence of 100 nM JZL195. The cells were first treated with AM251, before addition of 10 μM forskolin (or media as control) and incubated for 4 h and 18 h. Fluorescence was detected using the standard protocol and results were normalised to the response from media alone. The results for V5α11 are presented in Figure 5.19 and for V5β4 in Figure 5.20.

Similar to the results from parental CB1-Tango cells, no response from V5α11 cells was seen from forskolin in the 4 h assay (Figure 5.19 A). However, a significant response above control was seen from forskolin alone after 18 h, which was inhibited by AM251, and this response is much more substantial when JZL195 is present (Figure 5.19 B). The response from V5α11 cells is also similar to CB1-Tango cell response in the 18 h assay (Figure 5.15 B), indicating that the activity of the transfected DAGLα is not obviously increased following PKA activation, or that amount of enzyme is not limiting. With the DAGLβ overexpressing cell line, forskolin did not stimulate response at 4 h in control media, but interestingly, there was a significant CB1-dependent response at 4 h when JZL195 was present. However, this was a relatively small response (~20% increase over the control) (Figure 5.20 A). The response to forskolin was much more substantial in the 18 h assay, and was again clearly potentiated by JZL195 (Figure 5.20 B). For reasons that are not clear, both responses were substantially, but not fully inhibited by AM251.

The greater response seen in V5β4 cells might reflect the greater level of DAGLβ expression in these cells (compared to DAGLα expression in V5α11 cells), indicating we may have a gain-of-function assay for DAGLβ. However, the possibility remains that we are simply seeing a phenomenon related to clonal variability. No increase in response was seen from V5α11 cells which may reflect the lower level of transfected DAGLα compared to transfected DAGLβ; yet DAGLα is expressed ~ 17 times more than endogenous levels in these cells. Therefore, the reason why the response was not greater in these cells is not clear, although it may be that PKA activation alone is not sufficient for DAGLα activity.

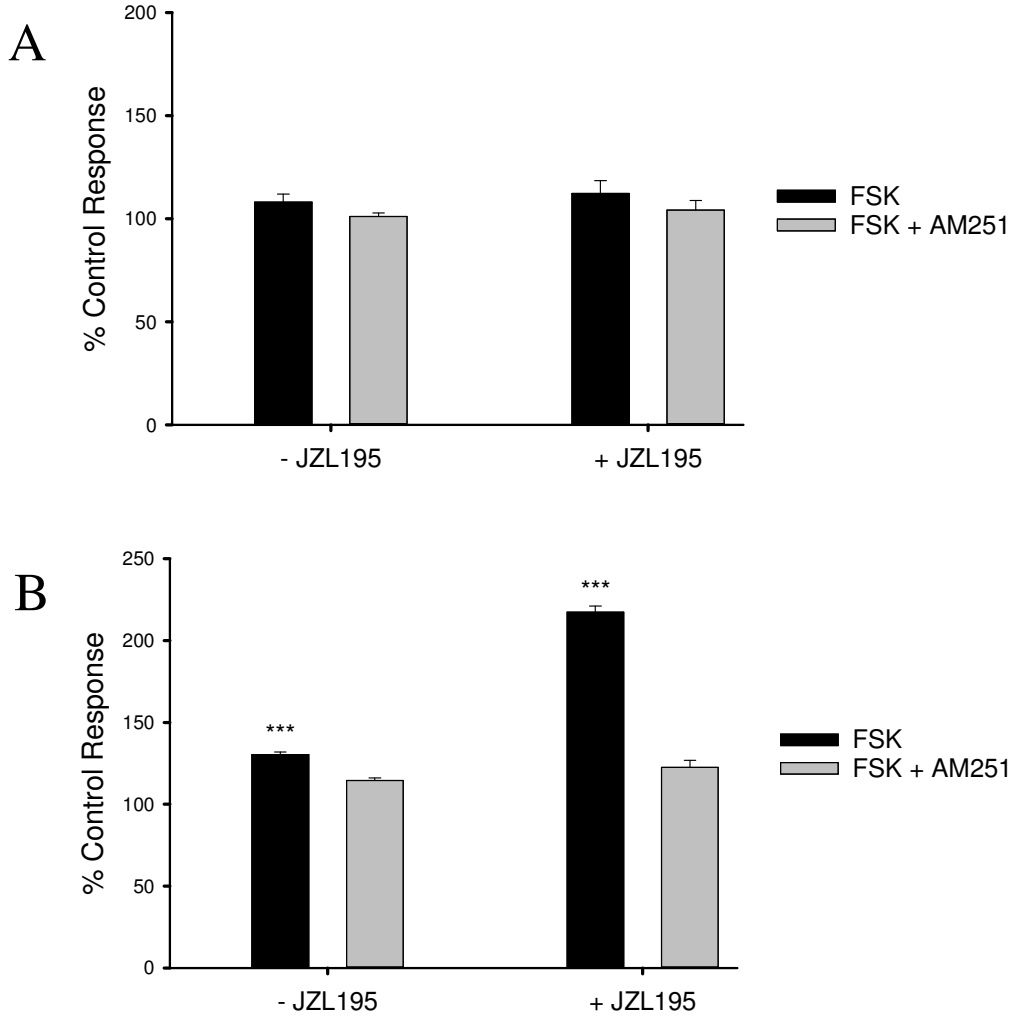

Figure 5.19 The forskolin-stimulated response in V5α11, revealed after 18 h, is much more substantial in the presence of JZL195

V5α11cells were plated into black 96-well plates at 20,000 cells/well and maintained for 48 h in McCoy's 1% FBS. Compounds were made up in the same medium either in the absence (-) or presence (+) of 100 nM JZL195. Half of the cells were treated for 30 min with 10 μM AM251, before addition of 10 μM forskolin (FSK) or media as control, for either 4 h (A) or 18 h (B). Fluorescent detection of β-lactamase reporter gene transcription was measured using a FRET-enabled substrate, as per manufacturer's protocol. The results are presented as a percentage of the control response (set to 100%) and are the mean of 8 wells + SEM of a single representative experiment. Statistics were performed using one-way ANOVA, as follows: ***$p<0.001$

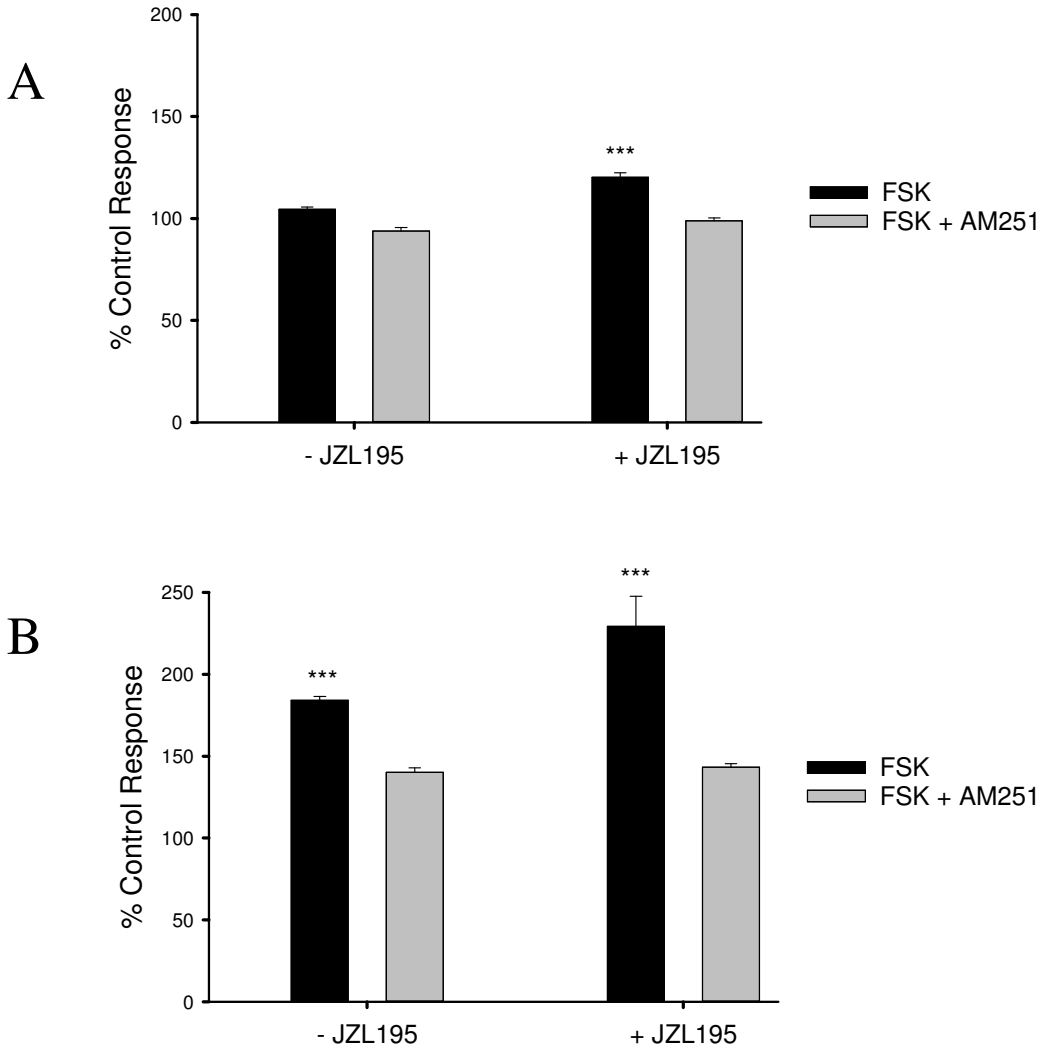

Figure 5.20 Forskolin stimulates a response in both 4 h and 18 h assay in V5β4 cells

V5β4 cells were plated into black 96-well plates at 20,000 cells/well and maintained for 48 h in McCoy's 1% FBS. Compounds were made up in the same medium either in the absence (-) or presence (+) of 100 nM JZL195. Half of the cells were treated for 30 min with 10 μM AM251, before addition of 10 μM forskolin (FSK) or media as control, for either 4 h (A) or 18 h (B). Fluorescent detection of β-lactamase reporter gene transcription was measured using a FRET-enabled substrate, as per manufacturer's protocol. The results are presented as a % of the control response (set to 100%) and are the mean of 8 wells + SEM from a single representative experiment. Statistics were performed using one-way ANOVA as follows: ***$p<0.001$.

Evaluating eCB tone following a 48 hour starvation period and PKA activation

The phorbol ester, phorbol 12-myristate 13-acetate (PMA) is an activator of protein kinase C (Castagna *et al.*, 1982). The effects of PMA on PKC result from its structural similarity to DAG, one of the natural activators of classic PKC isoforms. PKC is activated by increases in concentration of DAG or calcium ions (Ca^{2+}), and phosphorylates the hydroxyl groups of serine and threonine amino acid residues (both present on the DAGLs). We hypothesised that PMA, like forskolin, would induce a response in parental CB1-Tango cells, in the presence of 100nM JZL195. To test whether PMA can also induce an eCB tone, the CB1-Tango cells were plated as before in McCoy's 1% FBS medium for 48 h. The cells were treated with 10 µM AM251before addition of 25 nM PMA (or medium as control) for 4 h and 18 h. The results were normalised to the control resposne (100%), and are summarised in Figure 5.21 with significance over the control reponse idicated (one-way ANOVA).

In the 4 h assay, PMA has little effect on eCB signalling; note that the extremely small response of ~10% was not inhibited by AM251 and so cannot be taken as an eCB response. However, when JZL195 was present in the media, PMA stimulated a significant response (~ 45% above the control) and this was fully inhibited by AM251 (Figure 5.21 A). In the overnight assay, the results in the absence of JZL195 are not conclusive due to the relatively large variation that we observed with this set of independent experiments. However, in the presence of JZL195, there was a much greater response that reached significance and was substantially inhibited by AM251. Thus it is clear that, like activation of PKA with forskolin, stimulation of PKC with PMA can stimulate eCB signalling, but this is again only convincingly seen when JZL195 limits the breakdown of 2-AG and/or anandamide.

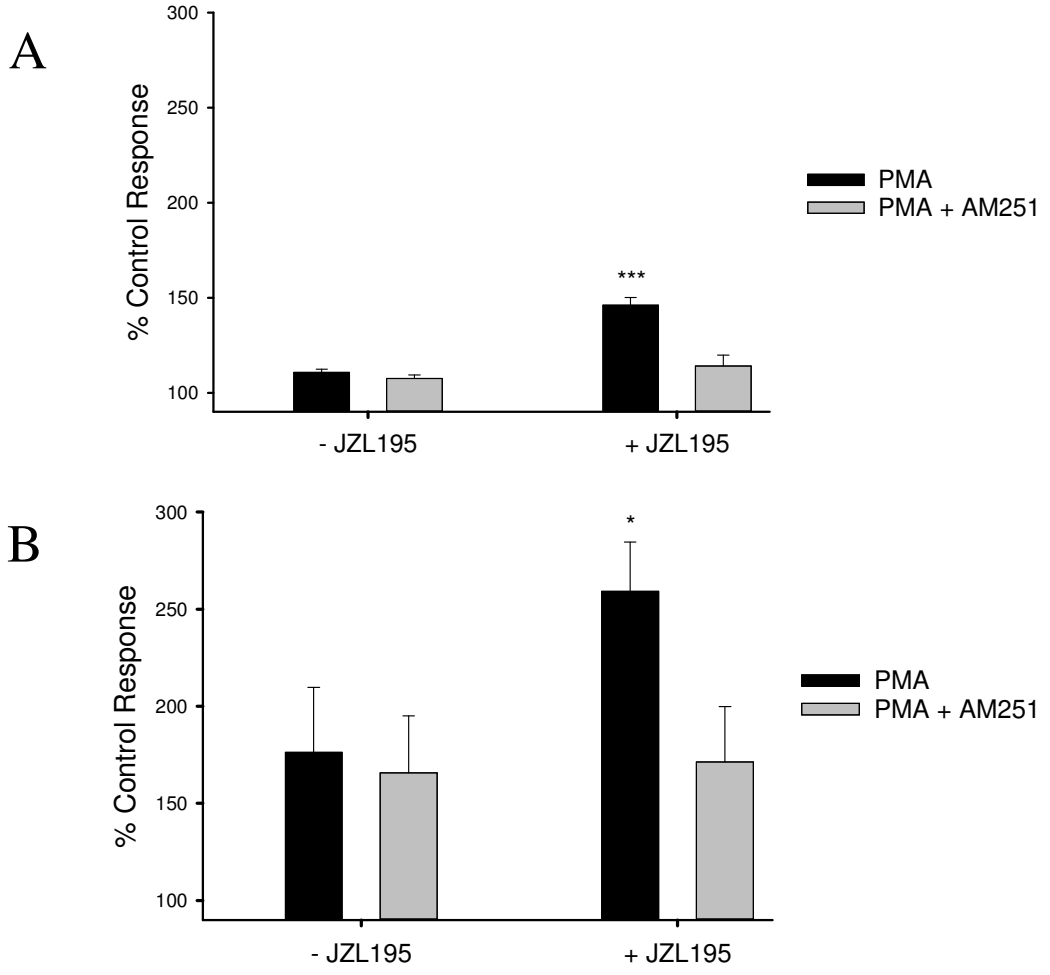

Figure 5.21 PMA can stimulate eCB signalling, but only in the presence of JZL195

CB1-Tango cells were plated in black 96-well plates at 20,000 cells/well and maintained for 48 h in McCoy's 1% FBS. Compounds were made up in the same medium either in the absence (-) or presence (+) of 100 nM JZL195. Half of the cells were treated for 30 min with 10 µM AM251, before addition of 25 nM 25 nM phorbol-12-myristate-13-acetate (PMA) for either 4 h (A) or 18 h (B). Fluorescent detection of β-lactamase reporter gene transcription was measured using a FRET-enabled substrate, as per manufacturer's protocol. The results are presented as a % of the control response (set to 100%) and represent the mean of 8 replicate wells pooled from 3 independent experiments ± SEM. Statistics were performed using one-way ANOVA, as indicated below.

* $p < 0.05$; ***$p < 0.001$; One-way ANOVA

eCB tone in CB1-Tango cells following ionomycin treatment

It has previously been shown that 2-AG biosynthesis in neurons requires calcium (Bisogno *et al.*, 1997a). Furthermore, transfected DAGLα/β led to much greater levels of 2-AG production by COS cells, which was prevented by DAGL inhibitors (Bisogno, 2003). As this assay was now developed using McCoy's 1% FBS, the assay medium now contained calcium. If this calcium was allowed to enter the cells, then we may be able to stimulate endogenous activation of protein kinases required for DAGL phosphorylation. Our next step therefore was to treat the CB1-Tango cells with ionomycin. Ionomycin is a Ca^{2+} ionophore and was added to the cells to induce an elevation of intracellular Ca^{2+} concentration. Furthermore, ionomycin-induced elevation of calcium within the cell could result in a more 'endogenous-like' activation of potential kinases essential for DAGL phosphorylation and activation.

The ionomycin treatment experiments were carried out by additional members of the lab using the same protocol as described above, and also using 30,000 cells/well in McCoy's supplemented with 0.5% FBS. The results using the two different protocols were not significantly different from each other, and so the results were collated and pooled where possible.

To test whether ionomycin could induce a response in a concentration –dependent manner, we plated 30,000 CB1-Tango cells in McCoy's 0.5% FBS medium for 48 h. Half the cells were treated for 30 minutes with 10 μM AM251, before addition of varying concentrations of ionomycin (0-4 μM), made up in the same medium. The cells were maintained for 4 h and *Bla* expression was detected by addition of the FRET-enabled substrate for 2 h, and the plate was read on the Flexstation. The results were normalized to the control response, set to 100% and the results are presented in Figure 5.22.

There was a clear and highly significant response seen from all concentrations at and above 1 μM ionomycin over the control response. Importantly, the response was inhibited by AM251, showing the response to be signalling through the CB1 receptor. The response to 4 μM ionomycin was substantially (~75%) but not fully

inhibited by AM251, which may be reflecting interference in the assay at this higher concentration. Nonetheless, there was a clear concentration-dependent response from ionomycin that is largely CB1 dependent. Therefore, our next step was to elucidate to what extent this response was due to DAGL activity by testing the inhibitor, THL.

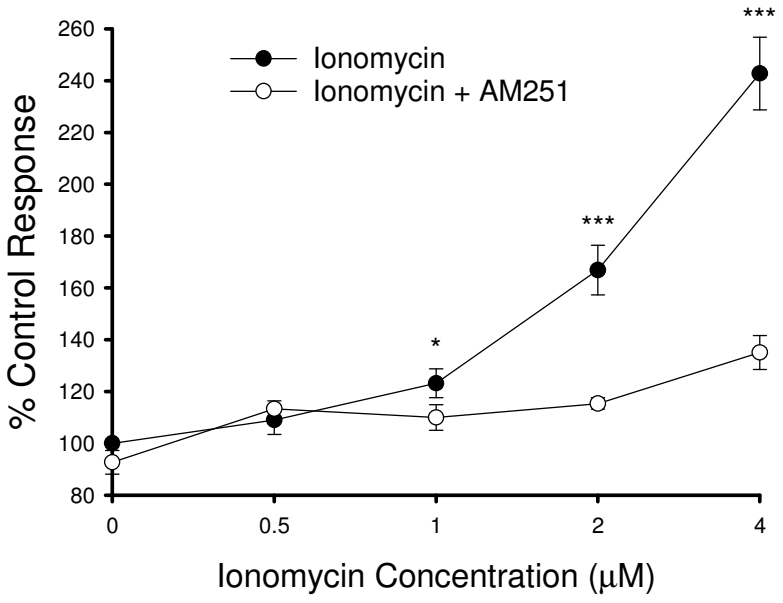

Figure 5.22 The ionomycin response is inhibited by AM251

30,000 CB1-Tango cells were plated in McCoy's medium supplemented with 0.5% FBS and maintained for 48 h. 10 µM AM251 was made up in the same medium and half the cells were treated for 30 min. Varying concentrations of ionomycin were also diluted in the same medium (4 µM top concentration, diluted 1:2, 5 point curve). The cells were treated overnight for a total of 4 h. *Bla* expression was detected using the FRET enabled substrate, as described previously. The data presented has been normalised to the control response (set at 100%) and represents the mean of 8 wells from *n* independent experiments ± SEM (for 4 µM and 0.5 µM *n*=5; for 2 µM *n*=17; for 1 µM *n*= 8). Significant difference was established using the two-sided Student's t-test, as indicated below.

* p< 0.05; ***p<0.001, Student's t-test

The DAGL component of the ionomycin response in CB1-Tango cells

Ionomycin has been shown to induce 2-AG production, as well as anandamide (Di Marzo *et al.*, 1994; Bisogno *et al.*, 1997b; Cadas *et al.*, 1997; Schmid, 2000; Leung *et al.*, 2006). We wanted to determine to what extent DAGL was responsible for the ionomycin response in CB1-Tango cells.

To this end, we plated 30,000 CB1-Tango cells in McCoy's 0.5% medium for 48 h. Varying concentrations of THL were diluted in the same medium (0-20 μM), which was then added to the cells for 30 minutes, before addition of 2 μM ionomycin for a further 4 h. Fluorescent ratio was determined by adding the FRET-enabled substrate for 2 h and reading the plate on the Flexstation. The results were normalized to the ionomycin response ('0 μM', set to 100%) and the results are presented in Figure 5.23.

The ionomycin response was not significantly reduced by THL at any concentration. The response in the presence of 5 μM THL or greater was only inhibited by ~ 15-20%, indicating that ~80% of the ionomycin response may not be due to DAGL activity. It was noted that THL on its own did not reduce basal tone in these cells (data not shown). As these experiments were carried out in the absence of JZL195, it may be that the 'gate keeping' activity of MAGL and FAAH was reducing the detectable DAGL activity from ionomycin treatment. Therefore, it was important to test whether we could to determine the relative contribution of the hydrolytic activity of MAGL and FAAH.

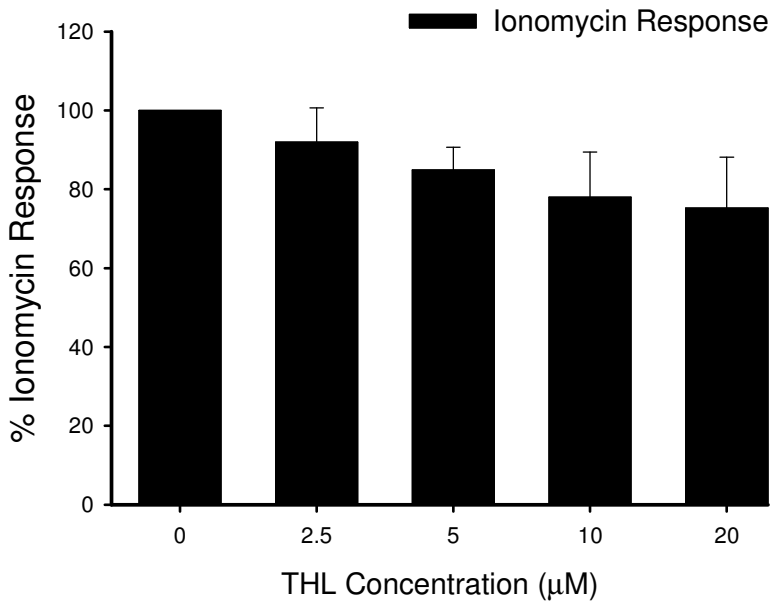

Figure 5.23 The ionomycin response can be inhibited by THL

30,000 CB1-Tango cells were plated and maintained in McCoy's medium containing 0.5% FBS for 48 h. Half the cells were treated with varying concentrations of THL (0-20 µM) for 30 min, before addition of 2 µM ionomycin for a further 4 h. *Bla* expression was detected using a FRET-enabled substrate, as described previously. The data was normalised to the response from ionomycin alone (set to 100%). The graph represents the mean of 8 wells pooled from *n* independent experiments (for 0 µM *n*=5; for 20 µM *n*=6; for 10 & 5 µM *n*= 3; for 2.5 µM *n*=2). Statistics were performed using one-way ANOVA.

The effects of inhibiting MAGL and/or FAAH on the ionomycin response in CB1-Tango cells

Our previous results have shown that by inhibiting MAGL and FAAH, a much greater response is revealed from kinase activation (Figures 5.15, 5.19, 5.20 and 5.21). To determine whether the ionomycin response could be potentiated, we used the dual MAGL/FAAH inhibitor, JZL195. To understand the relative contribution of MAGL and FAAH, we also tested JZL184 (MAGL inhibitor) and the specific FAAH inhibitor, URB597 (Mor *et al.*, 2004; Alexander & Cravatt, 2005). To do this, we plated 30,000 CB1-Tango cells in McCoy's 5% medium for 48 h. The cells were then treated for 30 minutes with either 100 nM JZL195 (Figure 5.24 A), 1 μM JZL184 (Figure 5.24 B) or with 100 nM URB597 (Figure 5.24 C) The cells were then treated with the same medium as control, or with either 1 μM or 2 μM ionomycin for a further 4 h. *Bla* expression was detected, as described previously and the data was normalized to the control response in the absence of drug, set to 100%. JZL195 induces a basal eCB tone, as seen when treated alone. Similarly, the ionomycin response from both 1 and 2 μM is much greater in the presence of JZL195 (Figure 5.24 A). In contrast, neither JZL184 nor URB597 increased basal eCB tone or potentiated the ionomycin response (Figure 5.24 B & C), indicating that inhibiting either MAGL or FAAH alone is not sufficient to potentiate the eCB response in CB1-Tango cells; the response is greater only when the hydrolytic activity of both of these enzymes is inhibited, thereby allowing eCBs being produced to signal through the CB1 receptor.

Next, we compared the concentration response from ionomycin in the absence and presence of JZL195. It was also important to assess whether this response could be inhibited by AM251, to determine if the response was CB1-dependent. To this end, CB1-Tango cells were plated and maintained as described above. Half of the cells were first treated with 10 μM AM251 for 30 minutes, before addition of varying concentrations of ionomycin (0.5-4 μM) +/- 100 nM JZL195 for a further 4 h. *Bla* expression was detected as described previously and the results were normalized to the control response in the absence of JZL195, set to 100%. There was a clear and concentration-dependent response from ionomycin alone in the absence of JZL195

(Fig 25A), which was consistent with our previous results (Figure 5.22). However in the presence of 100 nM JZL195, this response is much greater and is highly significant compared to response in the absence of JZL195 at all concentrations of ionomycin below 4 μM. The responses from 4 μM are similar, which may indicate the level of eCB production is sufficient to signal through the CB1 receptor, regardless of MAGL/FAAH activity. Importantly, these responses were fully inhibited by AM251 at all concentrations and were therefore signalling through the CB1 receptor (Figure 5.25 B).

Figure 5.24 Basal eCB tone and ionomycin response from CB1-Tango cells is potentiated by JZL195, but not by JZL184 or URB597

30,000 CB1-Tango cells were plated and maintained in McCoy's medium containing 0.5% FBS for 48 h. Half the cells were treated with either 100 nM JZL195 (A), 1 µM JZL184 (B), or 100 nM URB597 (C) for 30 min, before addition of either media alone (control) or varying concentrations of ionomycin, as indicated (either 1 µM or 2 µM) for 4 h. *Bla* expression was detected using a FRET-enabled substrate, as per manufacturer's protocol. The data was normalised to the control response (in the absence of drug, set to 100%). Graphs represent the mean of 8 replicate wells pooled from 4 independent experiments (7 for JZL195) ± SEM. Significance was established using the two-sided Student's t-test, as indicated below.

* $p < 0.05$; ** $p<0.01$; *** $p<0.001$ Student's t-test

A

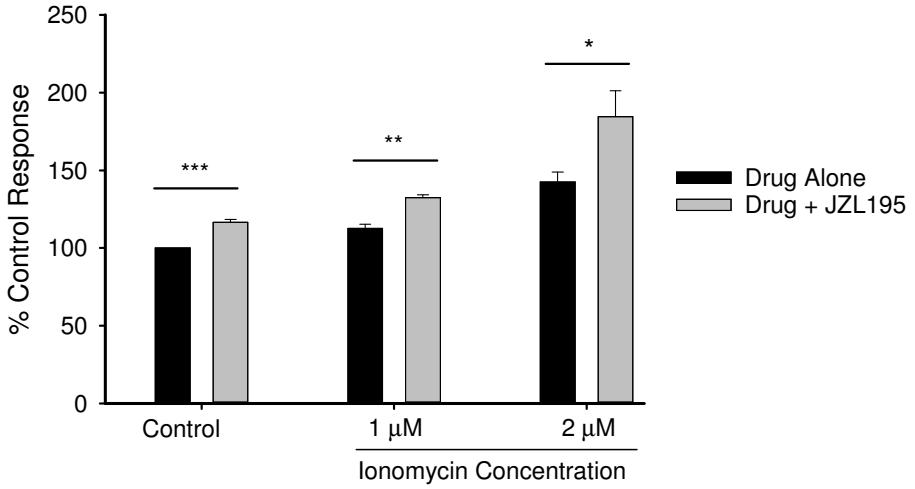
250
200
150
100
50
0
% Control Response
***
**
*
Control
1 μM
2 μM
Ionomycin Concentration
Drug Alone
Drug + JZL195

B

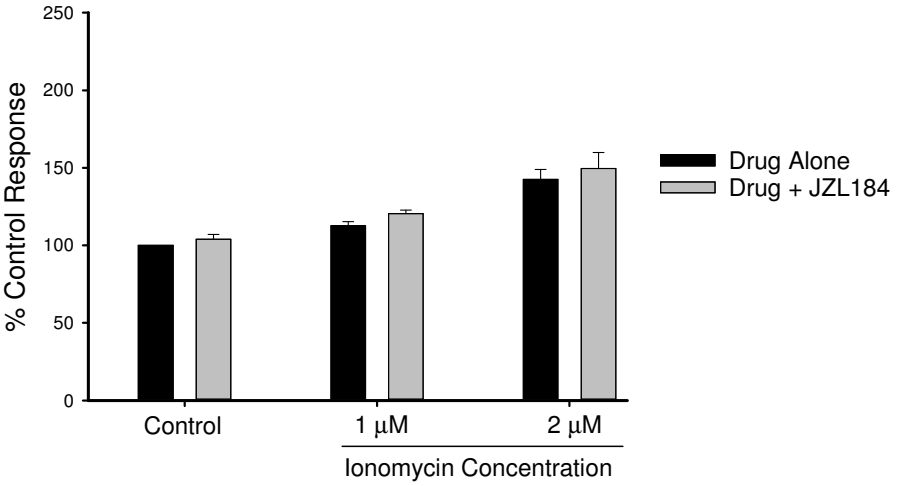
250
200
150
100
50
0
% Control Response
Control
1 μM
2 μM
Ionomycin Concentration
Drug Alone
Drug + JZL184

C

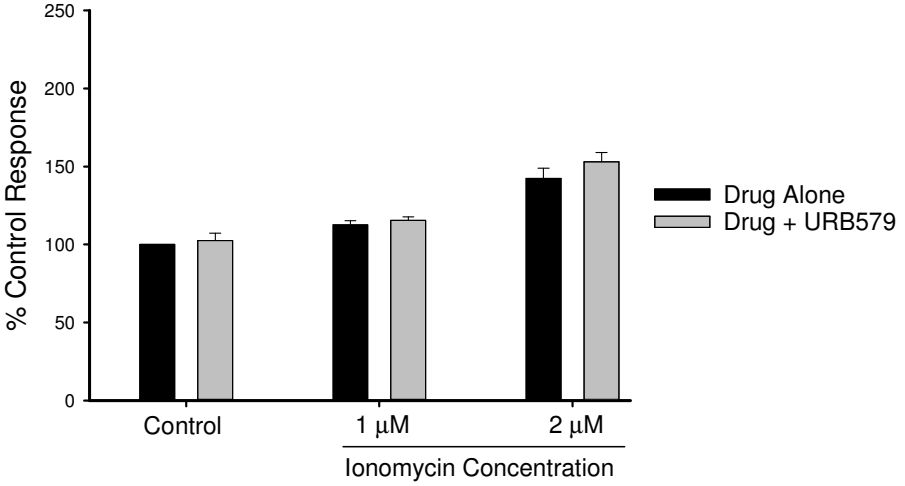
250
200
150
100
50
0
% Control Response
Control
1 μM
2 μM
Ionomycin Concentration
Drug Alone
Drug + URB579

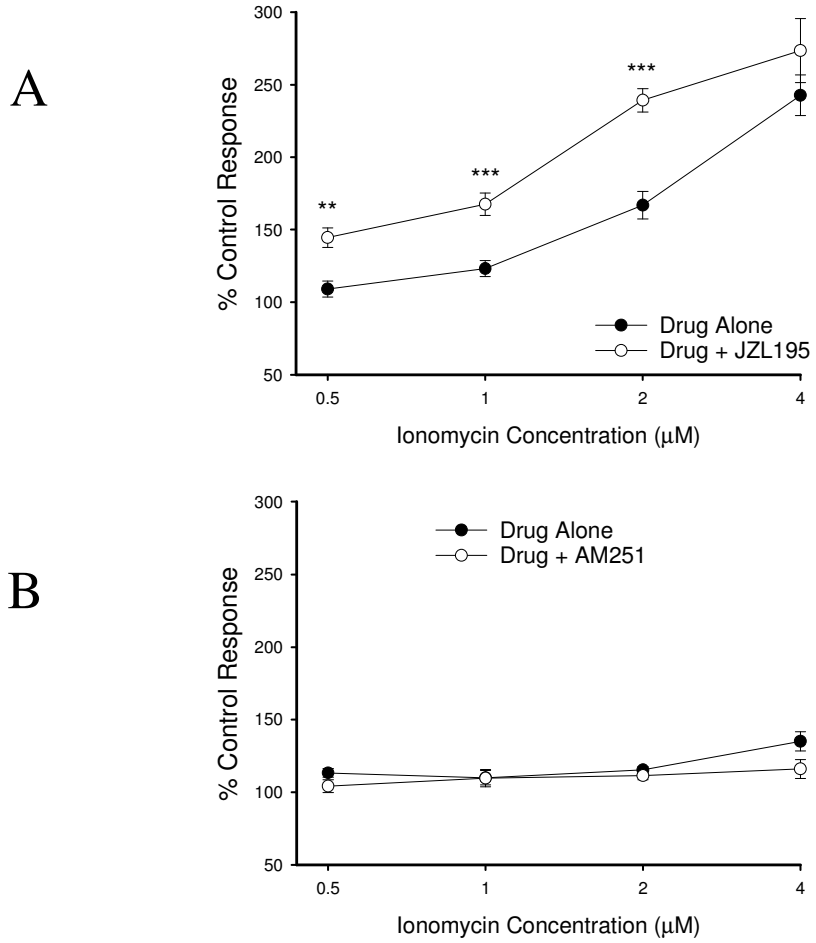

Figure 5.25 The ionomycin response is potentiated in the presence of the dual MAGL/FAAH inhibitor, JZL195

CB1-Tango (20,000 or 30,000) cells were plated and maintained in McCoy's media, containing either 0.5% or 1% FBS, for 48 h. Half the cells were treated with 10 μM AM251 for 30 min. Varying concentrations of ionomycin were diluted in the same medium +/-100 nM JZL195, which were added to all wells for 4 h. *Bla* expression was detected, as described previously. Data was normalised to the control response in the absence of JZL195 (set to 100%). Ionomycin concentration-response curve is presented in A, and in the presence of AM251 in B. Each graph represents the mean of 8 replicates pooled from 5-20 independent experiments, performed by all members of the lab (using different cell number / FBS concentrations, as stated above); the data was not significantly different using the two protocols and data was pooled. Significance was established using the two-sided Student's t-test, as indicated below.

*p<0.05; **p<0.01, Student's t-test

The effects of the DAGL inhibitors, THL and OMDM-188 on the ionomycin response in CB1-Tango cells

As we had seen in the above results, ionomycin could significantly induce a response in CB1-Tango cells, and this is much greater in the presence of JZL195 (Figure 5.25). To determine what extent this enhanced response was due to DAGL activity, we tested whether the DAGL inhibitors, THL and OMDM-188 could inhibit this response. While neither of these compounds is a specific inhibitor for the DAGLs, these enzymes are the only targets these compounds have in common (Hoover *et al.*, 2008; Ortar *et al.*, 2008). Therefore, using these inhibitors in combination provides evidence as to which portion of the ionomycin response is DAGL-dependent. We also used these compounds to determine if the eCB tone seen in the presence of JZL195 alone can be attributed to DAGL activity. To do this, CB1-Tango cells were plated and maintained in McCoy's 1% for 48 h. All compounds were made up in the same medium in the presence of 100 nM JZL195. The cells were then treated with either 2 µM OMDM-188 or 20 µM THL for 30 minutes, followed by media (+ JZL195, 'control') or 2 µM ionomycin, for a further 4 h. *Bla* expression was detected using the FRET-enabled substrate for 2 h, as described previously. The results were normalized to the control response in the absence of drug, set to 100%.

Both OMDM-188 and THL significantly reduced the basal response in these cells by ~20%, which may indicate basal DAGL activity revealed by the presence of JZL195 (Figure 5.26 A). As seen before, 2 µM ionomycin significantly induces a response above control (~140%) in the presence of JZL195. The ionomycin response in the presence of either OMDM-188 or THL is increased from a reduced baseline of ~70% to a response of ~150% and so these compounds inhibit the ionomycin response by ~ 50%. Therefore, in the presence of JZL195, ~50% of the ionomycin response may be a result of DAGL activity (Figure 5.26 B).

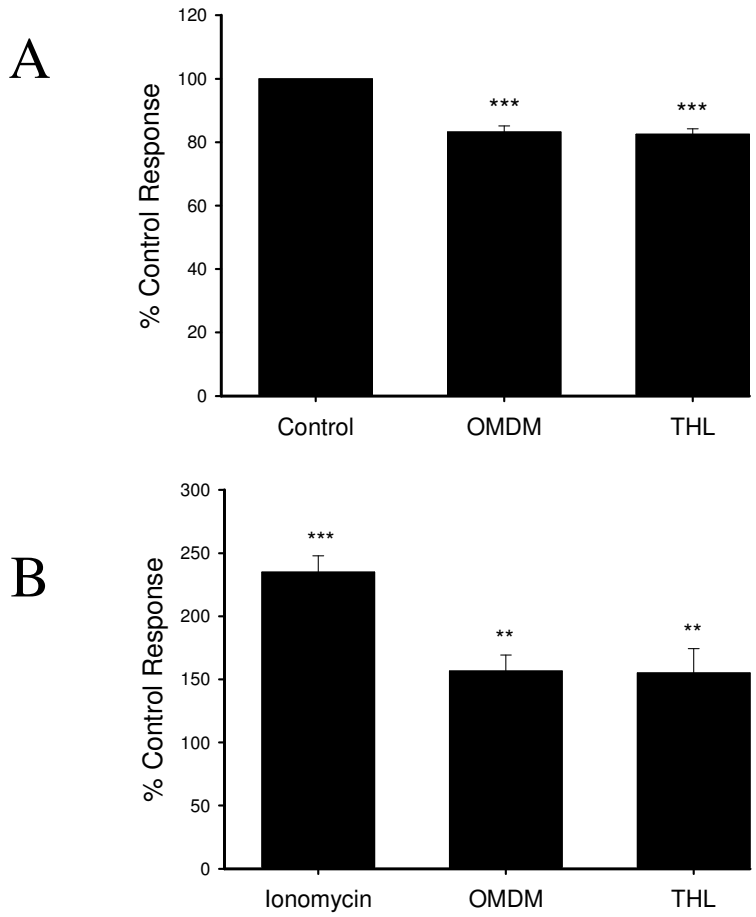

Figure 5.26 The DAGL inhibitors OMDM-188 and THL reduce basal eCB tone and inhibit the ionomycin response, in the presence of JZL195

20,000 CB1-Tango and V5α11 cells were plated and maintained in McCoy's medium containing 1% FBS for 48 h. Compounds were made up in the same medium, containing 100 nM JZL195. The cells were treated with either 2 µM OMDM or 20 µM THL for 30 min, before addition of control media ('control', A) or 2 µM ionomycin (B). *Bla* expression was detected using the standard manufacturer's protocol, as described previously. The data was normalised to the control response (set to 100%) and the graphs represent the mean of 8 replicates ± SEM pooled from 5 independent experiments. Significant difference was established from the control response or from the ionomycin response for OMDM and THL in B, using the one-way ANOVA, as indicated below.

**p<0.01; ***p<0.001, One-way ANOVA

The ionomycin response in CB1-Tango, V5α11 and V5β4 cells

In examining whether we had a 'gain of function' assay, we treated our V5α11 cells with ionomycin, in the presence of JZL195. Two in-house protocols were used; one using 20,000 cells plated in McCoy's 1% and the other using 30,000 cells plated in McCoy's 0.5%. As results from either protocol were not statistically different from each other (data not shown), the data was collated and pooled. In summary, CB1-Tango and V5α11 cells were 'starved' for 48 h. Half the cells were treated with 10 μM AM251 for 30 minutes, before addition of varying concentration of ionomycin (0.25 - 2 μM) for a further 4 h. Fluorescent ratio was determined as described previosuly, and the data was normalised to the control in the absence of drug, set to 100%. The data presented in Figure 5.27 shows that there was no significant difference in the ionomycin response seen between CB1-Tango and V5α11 cells, indicating that the level of enzyme expression is not limiting. Most of the responses seen were fully inhibited by AM251. The response in the presence of 2 μM ionomycin seen from V5α11 cells was significantly above the control response, but was still inhibited by > 95% (Figure 5.27 B).

Finally, we wanted to compare the ionomycin response from CB1-Tango and V5α11 cells to ionomycin treatment of V5β4 cells in the presence of JZL195. To this end, 20,000 parental Tango, V5α11 and V5β4 cells were plated as described before, in McCoy's 1% for 48 h. The cells were treated with 0.1 μM and 1 μM ionomycin (or medium as control) in the presence of 100nM JZL195. The cells were incubated overnight for a total of 4 h, and fluorescence was detected as described previously, and the results were normalised to the control response (100%).

The results in Figure 5.28 show a significant response from both concentrations of ionomycin, and this is true for all 3 cell lines. Furthermore, the ionomycin response was greater in all cell lines than either forkolin or PMA treatments (Table 5.3), possibly indicating different activity levels of the DAGLs. However, the response obtained from the overexpressing cell lines was not obviously greater than that seen in parental CB1-Tango cells. In fact, from 3 independent experiements the resposne from CB1-Tango cells was greater than the overexpressing cell lines (Table 5.3). This may be because the level of DAGLα/β is not rate-limiting and may be due to

insufficient substrate; or it may be because the DAGLs are not active, with the ionomycin response being a result of another eCB being produced in response to the calcium influx.

Table 5.3 Comparison of % response to FSK, PMA and ionomycin (48 h starve, + JZL195)

The table below show the % response above control (background) response in all three cell lines in response to forskolin, PMA and ionomycin treatment, in both 4 h and 18 h assays.

Treatment	Forskolin		PMA		Ionomycin
Compound Incubation	4h	18h	4h	18h	4h
Tango (%)	4	26	46	162	146
V5α11 (%)	8	30	56	-	86
V5β4 (%)	8	84	22	-	88

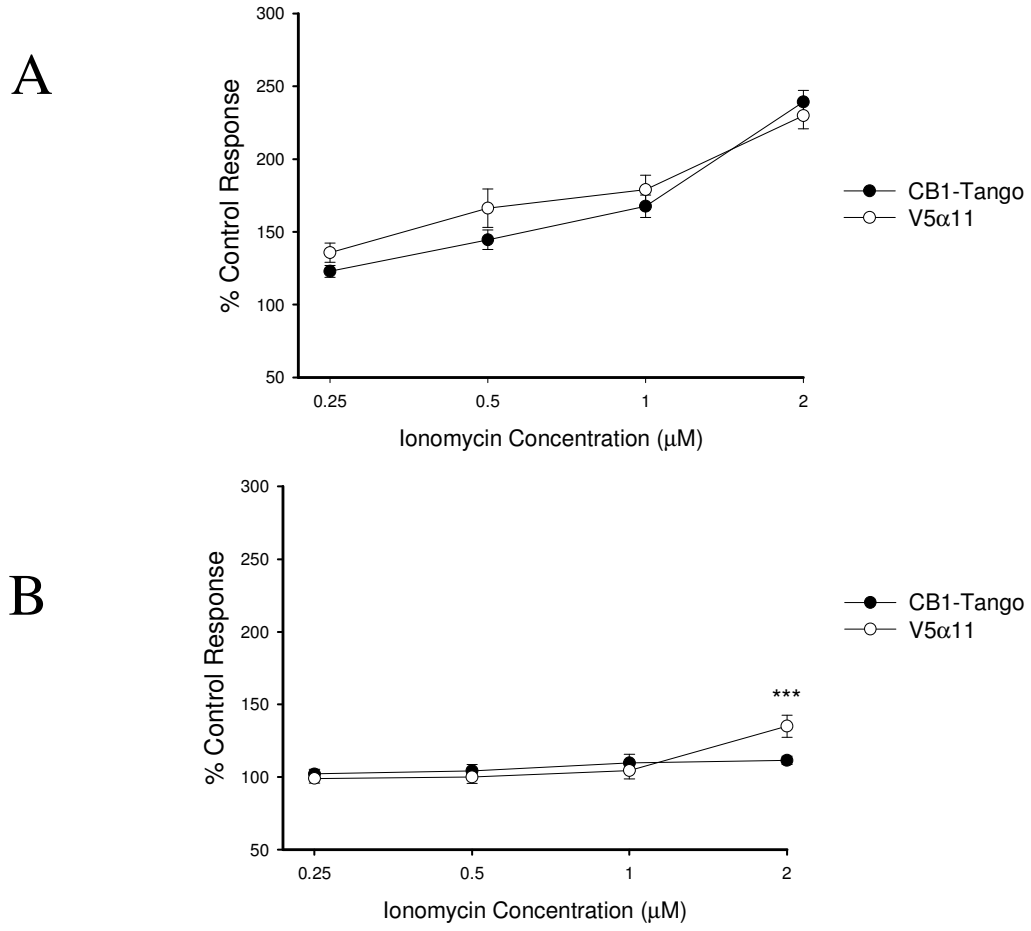

Figure 5.27 The ionomycin response is not increased when DAGLα is overexpressed in CB1-Tango cells

CB1-Tango and V5α11 (20,000 or 30,000) cells were plated and maintained in McCoy's media, containing either 0.5% or 1% FBS, for 48 h. Half the cells were treated with 10 μM AM251 for 30 min. Varying concentrations of ionomycin were diluted in the same medium containing 100 nM JZL195, which was added to all wells for 4 h. *Bla* expression was detected, as described previously. Data was normalised to the control response in the absence of JZL195 (set to 100%). Ionomycin concentration-response curve is presented in A, and in the presence of AM251 in B. Each graph represents the mean of 8 replicate wells pooled from 2-16 independent experiments, performed by all members of the lab (using different cell number / FBS concentrations, as stated above); the data was not significantly different using the two protocols and the data was pooled. Significance was established using the two-sided Student's t-test, as indicated below.

***$p<0.001$ Student's t-test

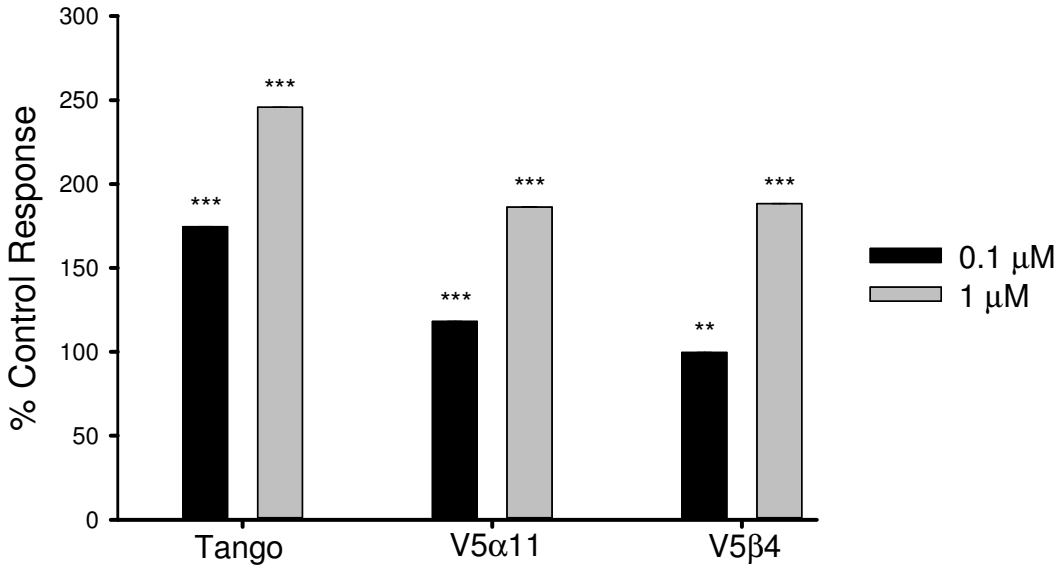

Figure 5.28 Ionomycin stimulates an eCB response in the 4 h Tango assay

20,000 Tango, V5α11 and V5β4 cells were plated and maintained in 96-well plates in McCoy's 1% medium, as described previously. After 48 h, compounds were diluted in the same medium containing 100 nM JZL195. The cells were treated with two concentrations of ionomycin (0.1 μM and 1 μM), or media as control for 4 h. *Bla* expression was detected using a FRET-enabled substrate, as per manufacturer's protocol. The results were normalised to the control response (set at 100%). Data presented represents the mean of 8 wells ± SEM pooled from *n* independent experiments (0.1 μM *n*=2; 1 μM *n*=3). Significance above the control response was established using one-way ANOVA, as indicated below.

**p<0.01; ***p<0.001, one-way ANOVA

5.3 Summary & Conclusions

The aim of this study was determine if we could establish a simple model to easily stimulate eCB signalling by adapting a CB1-Tango cell assay, with a view to determining the contribution that either one of the DAGLs make to the response. In this context, we have developed the CB1-Tango assay in McCoy's 1% medium to maintain viability and so the full contents of the medium are known, including the presence of 1 mM calcium. We have shown that PKA and PKC activation can stimulate eCB signalling, but robust responses are only seen when JZL195 is included in the media. Ionomycin treatment also stimulated a robust response, with more subtle differences highlighted in the presence of JZL195. Responses are only revealed by dual blockade of MAGL and FAAH (and possibly ABHD6 activity) and not when either one of these agents are inhibited alone; this was in line with previous reports (Long *et al.*, 2009b).

By using our overexpressing cell lines, we have tested whether the level of these enzymes are "rate-limiting" for a number of stimuli, whereby an increase in response could be directly related to the transfected DAGL. However, no obvious increase in response was seen using V5α11 or V5β4 cells (Figures 5.26 & 5.27). As mentioned earlier, this may be because the level of enzyme expression is not limiting, and may be due to insufficient substrate. It may also be it is not likely due to a lack of enzyme activity, as the DAGLs do appear to be active in response to forskolin, PMA and ionomycin treatment. Since the completion of this part of the study, others in our lab have shown that the PKA and PKC responses to be largely inhibited by the DAGL inhibitors (Emma Williams, unpublished data). Furthermore, almost 50% of the ionomycin response is inhibited by OMDM-188 and THL, which may reflect a large portion of these responses to be a result of DAGL activity. However, production of other eCBs following these treatments is possible and is most likely contributing to the residual clear response that is seen in the presence of OMDM and THL.

Given that there were no specific inhibitors for DAGLα or DAGLβ at the time of this study, and the fact there are no inhibitors for anandamide production, we

recognised that a genetic intervention in the production of these eCBs was required to further elucidate the pathways governing the responses to forskolin, PMA and the calcium ionophore. A cell line lacking eCB-producing activity would allow us to think about gain-of-function and structure/function experiments with wild-type and mutated versions of the DAGLs. We initially focussed on a "feasibility" study to determine if the recently described CRISPR/Cas9 can readily be applied to knockout the DAGLs and/or to introduce mutations that would disrupt the catalytic activity of the enzymes. This work would serve as a prelude to future gain of function studies that unfortunately are out with the remit/timeframe of the thesis.

CHAPTER 6. RESULTS IV – Generating a DAGL-inactive Tango cell line mediated by the CRISPR/Cas9 System

6.1 Introduction

As we saw in chapter 3 (Results I), the human DAGLs have similar structural features and their catalytic domain is a member of the α/β hydrolase fold family. The activity of another member of this family, hormone sensitive lipase (HSL) is protected by a regulatory lid, which shields the catalytic domain from substrate access. Upon phosphorylation, this lid is displaced and the substrate can access the catalytic site for hydrolysis (Holm, 2003). Through homology modelling with fungal and drosophila DAGL, our group identified a similar insert in human DAGL, termed the 'regulatory loop'. We have identified phosphorylation as a potential regulatory mechanism for the DAGLs which we believe displaces the regulatory loop to allow access of DAG to the catalytic domain, akin to HSL. To study which phosphorylation sites are key to DAGL function, we require a simple assay that is amenable to structure/function studies.

To this end, we have developed the CB1-Tango assay to measure an eCB response. In chapter 4 (Results II), we showed the Tango cells to endogenously express transcripts for both the DAGLs, with DAGLβ protein also readily detectable (the case for DAGLα is still uncertain). The eCB tone in the CB1-Tango assay can be stimulated when PKA or PKC are activated or following treatment with ionomycin, presumably as a consequence of calcium influx into the cell (Chapter 5, Results III). These stimuli will all activate kinases and our data is consistent with, but does not prove, a role for DAGL phosphorylation in eCB generation. Data presented on the ionomycin response shows that it is in part dependent on DAGL activity, but it is unclear as to whether this reflects DAGLα or DAGLβ activity, as at the outset of this study there were no specific inhibitors for either of the DAGLs. Our results with cells that overexpress DAGL constructs, that we have shown to be enzymatically active against surrogate substrates in the case of DAGLα, have failed to show a

"gain-of-function" phenotype in response to any stimuli, suggesting that the level of enzyme is not rate limiting. Furthermore, the eCB response was only seen in the presence of the dual MAGL/FAAH inhibitor, JZL195 and not when MAGL was inhibited alone; possibly due to compensation by FAAH, as shown in previous reports (Long *et al.*, 2009b).

Based on the above we have decided that a radically different strategy is required in order to fully exploit the potential of the CB1-Tango cells as a vehicle for dissecting out the structure/function activity of the individual DAGLs. In brief, this strategy involves genetic manipulation to strip back the ability of the parental cells to respond to the three stimuli mentioned above, by the systematic elimination of enzymes likely to be responsible for the generation of the eCBs. Our initial aim was to eliminate DAGLα and DAGLβ activity, with a view to then taking on the perhaps more challenging task of "eliminating" the DAGL-independent response. If this can be achieved, we will be in a position to reconstruct both DAGLα– and DAGLβ–dependent eCB pathways for detailed structure/function studies and so disrupting DAGL would be the first step in eliminating eCB generation in these cells.

We used the CRISPR/Cas9 system to mediate this intervention, as presented in the introduction, which can effectively be used to make precise genome modifications in mammalian cell lines (Jinek *et al.*, 2013). This system is a cost effective and efficient method to disrupt the gene of interest. Cas9 is an endonuclease that is guided by a gRNA sequence to the target DNA. The resulting DSB can be repaired by indel-forming NHEJ or by HDR using a donor template (Valerie & Povirk, 2003; Gaj *et al.*, 2013). A mutant form of Cas9 allows single-strand cleavage capability to facilitate "nicking" and is termed Cas9 nickase (Cas9n). Using two Cas9ns can radically reduce off-target effects and is an effective method for HDR repair at the specific site (Jinek *et al.*, 2012).

In this chapter, I will report on the successful use of the novel CRISPR/Cas9 system to introduce mutations into both alleles in the DAGLα and DAGLβ genes that should disrupt correct protein translation and therefore eliminate DAGL activity in

the Tango cells. I will discuss the obstacles encountered in our initial strategy to target both the DAGLs simultaneously, highlighting the challenges associated with disrupting a relatively large gene. I will present on the use of Cas9n as an effective method to leverage HDR repair. Finally, I will present an alternative strategy to eliminate DAGL activity. We applied the CRISPR/Cas9 system to effectively target the catalytic domain of the DAGLs, thereby generating a Tango cell line that does not express functional variants of the DAGLs. This is the first step in eliminating eCB production in Tango cells. Next steps to disrupt other eCB-generating enzymes will be discussed.

6.2 Results

Targeting expression of the DAGLs using the site specific endonuclease, Cas9

Design of strategy to target DAGLα by CRISPR/Cas9

Our aim was to target both the DAGLs in CB1-Tango cells using the CRISPR/Cas9 system. It is important to design gRNA sequences that target all predicted splice variants for the gene of interest. Splice variants for each enzyme were analysed using data available on Ensembl Genome Browser (ensembl.org). For DAGLα, there are 2 predicted variants and for DAGLβ there are 7. We selected exon 3 for targeting DAGLα and exon 7 for targeting DAGLβ, with a view to targeting the most upstream exon to disrupt all potential splice variants. By targeting each gene towards the 5' end, our aim was to stimulate NHEJ to disrupt translation of the rest of the sequence downstream from the target site.

Construction of expression vectors and Generation of Tango KO cell lines

In order to apply the CRISPR/Cas9 system to the Tango cells, we used Cas9 vectors that contained genes for all the essential components (Cong *et al.*, 2013); Cas9 gene (4272 bp) with nuclear localization signal for eukaryotic expression, U6 promoter and tracrRNA, as well as vectors which also had the fluorescent markers GFP and mCherry – all of which were a kind gift from Marcello Maresca, Astra Zeneca (prior to any patent laws) (Mali *et al.*, 2013b). We designed gRNAs specifically targeting DAGLα, as well as DAGLβ (Figure 6.1 & Figure 6.2). These sequences were ordered as two single oligonucleotide strands and were designed such that, once annealed, the double-stranded DNA had overhangs compatible with AarI restriction digest of our vectors. 20 nucleotide sequences were selected using software available on ww.zifit.org and in line with the criteria described previously (Hwang *et al.*,

2013; Mali *et al.*, 2013b). The sequences also began with G for U6 promoter recognition. For DAGLα, 4 sequences were chosen from exon 3 (Figure 6.1). For DAGLβ, 6 sequences were chosen from exon 7 and from the introns just upstream and downstream of this exon (Figure 6.2). To test the efficiency of each gRNA we designed, we first constructed these vectors to contain our custom oligonucleotides into the gRNA cassette.

To do this, the Cas9 vector was digested with AarI and separated on agarose gel. The digested vector was purified from the gel, dephosphorylated and ligated with each of our gRNAs. Once each construct was generated, transient expression of each Cas9/gRNA construct for DAGLα and DAGLβ (double transfection) was achieved via Fugene HD, using the manufacturer's protocol. After approximately 48 h, DNA from these heterogeneous cells was extracted and amplified by PCR, using primers flanking the CRISPR/Cas9 cutting site; for DAGLα, the forward primer was 5'– GCTAGTAGCATCTCGAGGTACAGG –3' and the reverse primer was 5'– CGTAGAGCACGTACTGCATGG –3', which amplified a 266 bp product for the wild type (WT) allele. For DAGLβ, the forward primer was 5'– CACCTT GTCATGGAAGCTGA –3' and reverse primer was 5'– TCCTG AGAATTGTCCGCTCT –3', amplifying a 262 bp product. The PCR products now contained a heterogeneous pool of WT DNA, as well as DNA containing insertions/deletions (indels) following Cas9 cutting and subsequent NHEJ repair. The PCR products were boiled and re-annealed to form mismatched heteroduplexes. Mismatched DNA is recognized and cleaved by the SURVEYOR Cel 1 mismatch-specific endonuclease and can be visualized as a smaller band on an acrylamide gel (as described in the methods section, Chapter 2).

Figure 6.3 shows the results from the different gRNA sequences tested. An empty Cas9 vector did not generate any fragment following Cel I digestion in either DAGLα or DAGLβ ('ctrl', Figure 6.3 A); a single larger dark band can be seen, indicating the presence of WT / matching DNA only. However, two smaller bands can clearly be seen in the presence of gRNA plasmids containing CRISPR sequences 1 (cr 1) and 2 (cr 2) for DAGLα and also CRISPR sequence 2 (cr 2) for DAGLβ. Cr 1 did not appear to result in efficient guiding of Cas9 to exon 7 of DAGLβ, indicated

by the lack of a smaller fragment in this column. We also tested digestion of AAVS1 locus as a control, where two smaller bands can clearly be seen following Cas9 activity (Figure 6.3 A, 'cr'). We then tested the other sequences designed for the DAGLs (Figure 6.1 & 6.2) in the SURVEYOR Cel I assay. Figure 6.3 C shows that the sequences cr 3 and cr 4 for DAGLα were also efficient at guiding Cas9. Therefore any of these sequences could be used for future experiments. In the case of DAGLβ, sequence cr 6 resulted in a smaller fragment in the Cel I assay, but is less obvious than the fragment from cr 7. Therefore, cr 7 was selected as a backup for cr 2 to knockout (KO) DAGLβ translation in the CB1-Tango cells.

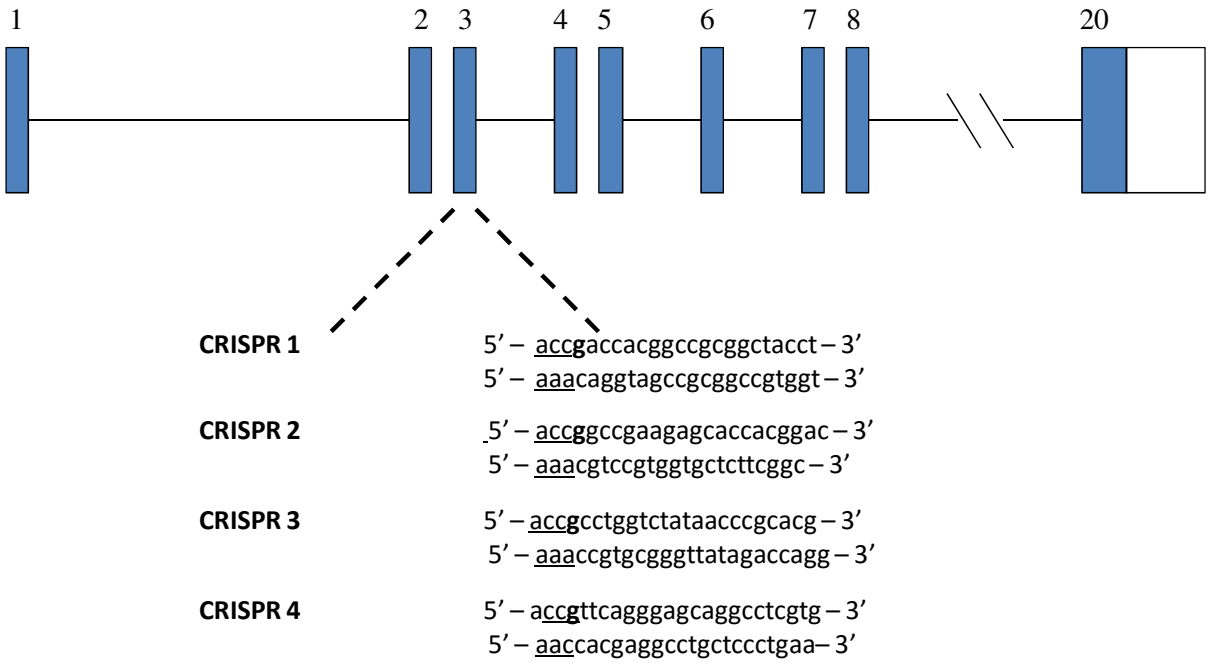

Figure 6.1 Design of gRNAs to guide Cas9 to cut DAGLα DNA sequence at Exon 3

Schematic representation of the human DAGLα sequence, indicating exons 1 – 20 (blue). Three sequences were selected using software available on ww.zifit.org. Each gRNA sequence selected was located in exon 3 of the hDAGLα gene and begin with G (bold) for U6 promotor recognition. Sequences show sense and antisense strands with overhangs present at the 5'-end (underlined), which are compatible with AarI restriction digest of the Cas9 vector.

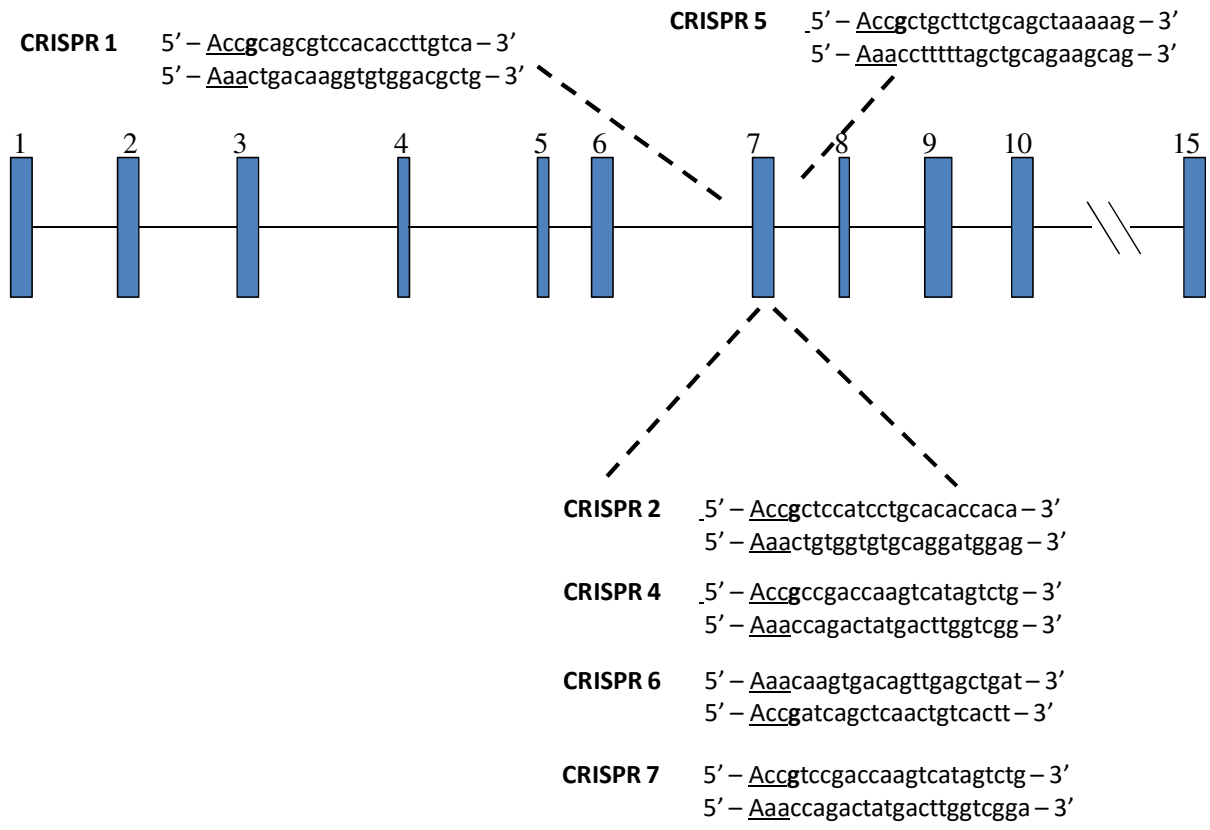

Figure 6.2 Selection of oligonucleotide sequences for synthesis of gRNA for Cas9 recognition of the DAGLβ gene

Schematic representation of the human DAGLβ sequence, indicating exons 1 – 12 (blue). There are many predicted splice variants of DAGLβ with this diagram representing the longest predicted transcript. Sequences for gRNAs were selected from exon 7 which is the one predicted to cross all splice variants and begin with G (bold) for U6 promotor recognition. CRISPR 1 and 5 are partially outside the boundaries of exon 7. Sequences show sense and antisense strands with overhangs present at the 5'-end (underlined), which are compatible with AarI restriction digest of the Cas9 vector.

Figure 6.3 SURVEYOR Cel I assay showing Cas9-mediated cleavage at the target locus in Tango cells using the different CRISPR sequences

Tango cells were transfected with Cas9 nuclease vectors containing gRNA sequences detailed in figures 6.1 & 6.2 (CRISPR 1 = cr1, etc.). DNA from the transfected cells was extracted; DAGLα / DAGLβ DNA were PCR-amplified using primers flanking the gRNA recognition site. The PCR product contained a hetergenous population including modified as well as unmodified DNA, which were reannealed slowly to generate heteroduplexes. The reannealed heteroduplexes are cleaved by SURVEYOR Cel I nuclease, whereas homoduplexes are left intact.

(A) CRISPR 2 (cr2) is effective in guiding Cas9 to cleave the target DNA sequence in both for DAGLα and DAGLβ, as indicated by the prominent smaller bands (*).

(B) Cells were transfected with Cas9 vector containing a GFP marker. Cell pools were enriched for positive Cas9 transfection by FACs sorting for GFP, thereby increasing chances for selecting cell lines with indel formation (as seen here by a more prominent smaller band when compared to the same one seen in A).

(C) Identification of efficiency of the other CRISPR sequences designed, as highlighted in figure 6.1 and 6.2, through analysis in the Cel 1 assay. For DAGLα (top) CRISPR 5 and 6 both are effective at guiding Cas9 to cut the target sequence, but not as effciently as CRISPR 1 or 2 seen in A. DAGLβ CRISPR 7 is much more efficient than CRISPR 6 at cutting the target sequence (as highlighted by *)

A

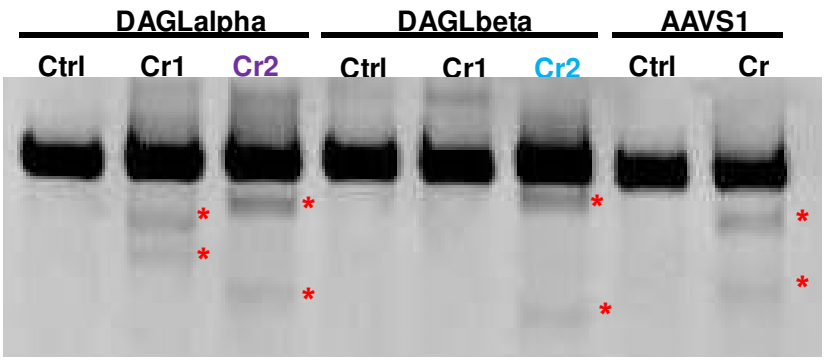

B

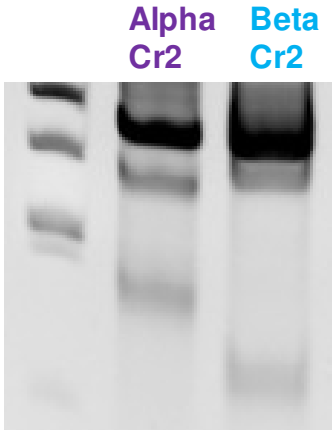

C

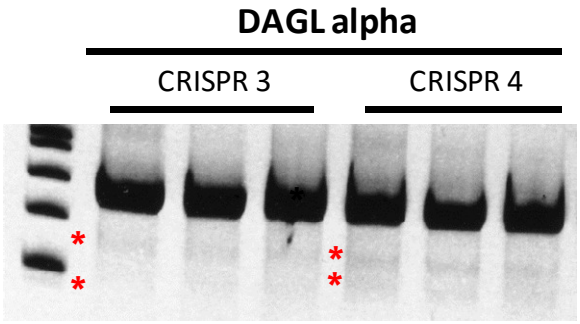

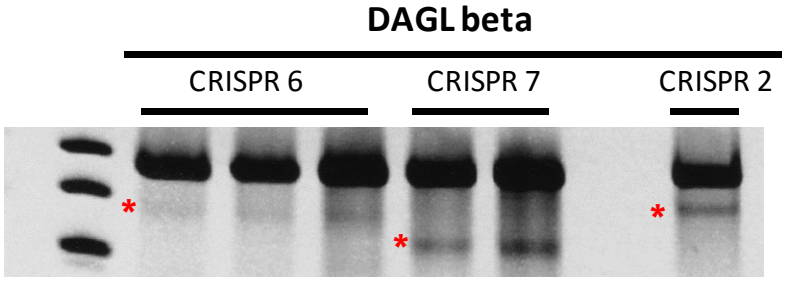

* Indicates cutting at the particular locus

Targeting the DAGLs using Cas9 endonuclease

In order to enrich for Cas9 transfected cells and therefore cells with higher potential for DAGLα/β KO, we used the fluorescent markers GFP and mCherry. Vectors containing either of these fluorescent markers were digested and purified as described above. Our selected gRNAs, cr2 for DAGLα and cr2 for DAGLβ were cloned into Cas9-GFP and Cas9-mCherry, respectively. Cells expressing the fluorescent markers were selected from heterogeneous pools using fluorescence-activated cell sorting (FACS). This allowed us to detect co-transfection of the two constructs. However, it was noted that cell viability following sorting was very poor and cell number was vastly reduced as a result.

In order to determine if FACS had enriched for expressing cells, we performed the Cel I assay on fluorescent pools of cells to detect mutated DAGLα and DAGLβ DNA, as before. Figure 6.3 B shows the gRNA sequences cr2 for targeting DAGLα and DAGLβ resulted in a darker band than that seen in Figure 6.3 A. This selection process therefore resulted in enrichment of cells that had taken up the Cas9 vectors. Individual cell colonies were isolated by first diluting the fluorescent pools into a large 15 cm dish, allowing single cells to grow separately from each other. Individual cell colonies were isolated with a cloning disc and expanded for further analysis.

Sequencing of the CRISPR/Cas9 cell lines

To detect small modifications (indels) in the sequence of either of the DAGLs' alleles, DNA was analysed using Sanger Sequencing. To do this, DNA from each of the candidate KO cell lines was isolated using Puregene core kit. PCR was performed on each sample using Taq Polymerase (AmpliTaq Gold® DNA Polymerase). *Taq* polymerase has a nontemplate-dependent terminal transferase activity that adds a single deoxyadenosine (A) to the 3´ ends of PCR products. The primers flanking the targeted regions for both DAGLα and DAGLβ were used for the PCR, as described above. The PCR products were cloned into a TOPO-cloning vectors, which is already linerised with overhanging 3´ deoxythymidine (T) residues,

allowing our PCR inserts to be ligated efficiently into the TOPO-cloning vector at room temperature. The ligated PCR products were then transformed into DH5α competent *E. coli* cells. The next day, positive bacterial colonies were selected using blue/white screening and ten bacterial colonies were selected for each DAGL candidate KO cell line. DNA was isolated from each of the bacterial colonies using a miniprep kit (Qiagen) and sequencing analysis was performed using the BigDye terminator method (Sanger Sequencing). The sequencing results from each cell line are summarised in Table 6.1. From these results, cell lines 1, 3, 7 and 10 appeared to be a potential KO for both DAGLα and DAGLβ. (Note: As cell line 1 grew much more slowly and appeared less healthy than the other cell lines, this was not selected for further analysis). It was noted that cell line number 7 may contain a mixed population of cells and may need to be subjected to further clonal selection.

Table 6.1 Summary of sequencing of DAGLα and DAGLβ double KO efforts using Cas9 endonuclease

DNA from Tango cell KO cell lines was extracted, PCR-amplified using Taq Polymerase and cloned into a TOPO cloning vector. The vectors were then transformed into DH5α cells where positive cones were selected using blue/white screening. DNA was isolated from 10 bacterial colonies (for each cell line) and sequenced using Sanger Sequencing. Results were 'blasted' against WT DAGL sequence to check for indel formation, as highlighted below.

Clone #	DAGLα	DAGLβ
1	Possible double KO (3 different results for β)	
3 *	Possible double KO	
4	WT	1 allele KO
5	WT	Both allele KO
6	WT	Both allele KO
7 *	Possible double KO – mixed population for α	
8	1 allele KO	1 allele KO
9	WT	Both allele KO
10 *	WT	Both allele KO

qPCR on the CRISPR/Cas9 Cell lines

To determine how the sequencing results related to the transcript level, we performed qPCR experiments on the cell lines 3, 7 and 10. To do this, RNA from each of the cell lines was extracted and reverse transcribed to cDNA. We used 'best coverage' Taqman assays for the DAGLs, which contain primers that span exon 3 and therefore our CRISPR cutting sites, and so were deemed suitable assays for KO detection. PPIA was used as the endogenous control. C_t values for all assays were calculated using Bio-Rad CFX software. Fold change in transcript level was determined using the $2^{-\Delta\Delta Ct}$ method, as described in Chapter 4 (Results II) (Livak & Schmittgen, 2001). The results from each cell line were compared to transcript levels in parental Tango cells and are presented in Figure 6.4 A-C.

DAGLα transcripts appeared to be reduced by ~ 60 % in cells from lines 7 & 10, while being unaffected in cell line 3. DAGLβ transcripts were much more affected, being reduced by ~ 80% in cell line 3, by ~ 90% in 7 and by ~ 60% in 10. However, no cell line showed a complete KO of transcripts. Therefore, it was necessary to determine how this related to protein expression. In spite of the unreliability of the DAGLα antibody, we used it to determine if we could detect disurpted protein expression relative to WT Tango cells. However, no difference was seen in any of the selected cell lines (Figure 6.4). It was noted that the band detected in the western blot is smaller than that predicted for WT DAGLa (~ 120 kDa) and so this band appears to be non-specific (Bisogno, 2003).

In conclusion, Cas9 is efficient at creating mutations within the DAGL sequence, as evident from the Cel I assay results (Figure 6.3). From the sequencing it looked as though these mutations would be sufficient to cause a frameshift in the sequence of the DAGLs, yet transcripts were not reduced by > 50% in our selected cell lines. The reason for this was unclear. While screening for successful transfection may be done through the fluorescent markers GFP and mCherry, FACS sorting appeared to be detrimental to cell viability. Furthermore, this may not be sufficient for detecting successful Cas9 cutting of the sequence, thereby resulting in a number of WT transcripts in our selected cell lines, especially in the case of DAGLα and we may

not have detected these transcripts in the sequence analysis. In addition, the double transfection of constructs to target both the DAGLs simultaneously may have interfered with one another, as co-transfection is known to reduce efficiency and can depend on the ratio of the DNA concentration between the two constructs (Hannig, 2013). In our next step, we used Cas9n and initially focussed on disrupting DAGLα, with a view to subsequently disrupting DAGLβ. By using Cas9n we can insert a gene coding for a resistance marker, through introducing a donor DNA template, thereby stimulating the HDR pathway.

Figure 6.4 Analysis of the candidate KO cell lines 3, 7 and 10 using Taqman Assay and Western Blot.

Tango cells as well as the candidate DAGL KO cell lines 3, 7 and 10 were grown to confluency in 2 x 10 cm dishes. 1 dish was using for RNA isolation, the other was used for membrane preparation.

(A-C) RNA was isolated from cell lines 3, 7 and 10 and reverse transcribed to cDNA. The cDNA was used to perform real-time PCR reaction with a Taqman probe spanning the CRISPR cutting site for both DAGLα and DAGLβ. PPIA was used as a housekeeping gene. Data was analysed using the $2^{-\Delta\Delta C}{}_t$ method previously described (Livak & Schmittgen, 2001). The Taqman assay revealed that line 3 is a possible KO of DAGLβ, but not of DAGLα **(A).** Cell line 7 is a knockdown of DAGLα and possible KO of DAGLβ **(B)** and cell line 10 has both DAGLα and DAGLβ knocked down **(C).**

(D) Membranes were prepared from cell lines 3, 7 and 10. 20 µg of the membrane protein was analysed in a western blot using a DAGLα antibody, revealing a band at the predicted molecular weight (~120 kDa) for all three cell lines, indicating that none of these cell lines are a KO for DAGLα.

A

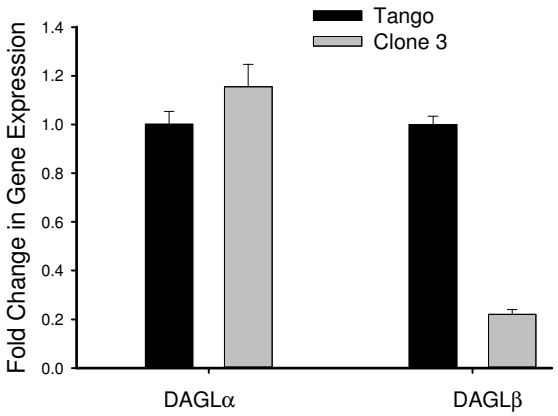
Tango
Clone 3
Fold Change in Gene Expression
1.4
1.2
1.0
0.8
0.6
0.4
0.2
0.0
DAGLα
DAGLβ

B

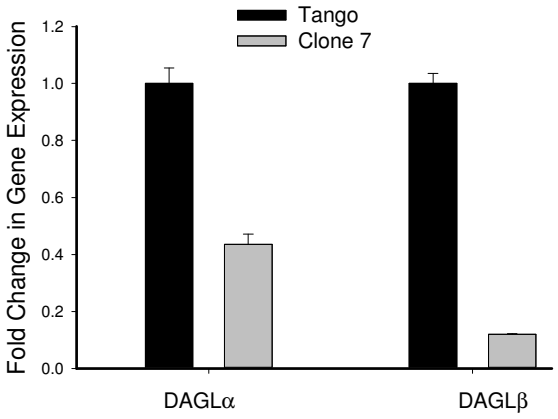
Tango
Clone 7
Fold Change in Gene Expression
1.2
1.0
0.8
0.6
0.4
0.2
0.0
DAGLα
DAGLβ

C

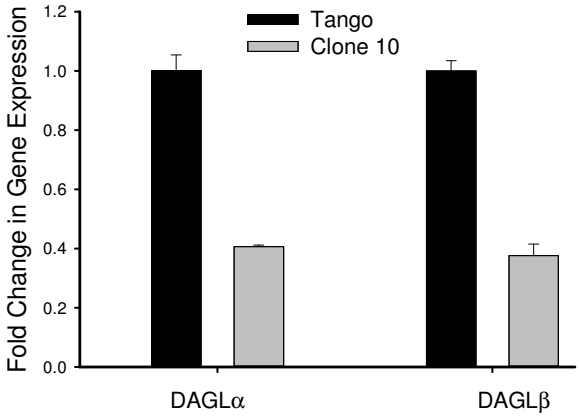
Tango
Clone 10
Fold Change in Gene Expression
1.2
1.0
0.8
0.6
0.4
0.2
0.0
DAGLα
DAGLβ

D

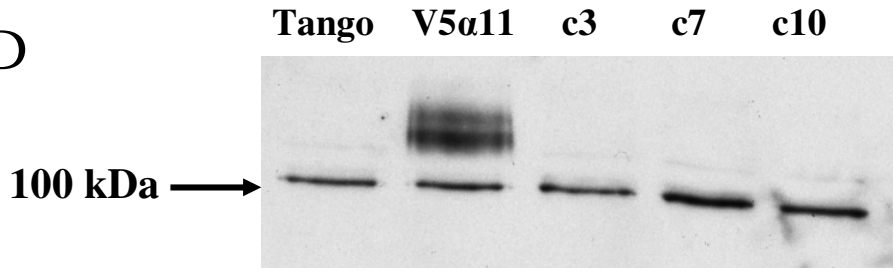
Tango
V5α11
c3
c7
c10
100 kDa

Double nicking strategy target the DAGLs and stimulate HDR repair in Tango cells

Due to the difficulties experienced with our initial strategy to target both the DAGLs in Tango cells, our next approach was to use a pair of Cas9ns. An aspartate-to-alanine (D10A) mutation in the RuvC catalytic domain allows Cas9n mutant to nick, rather than cleave DNA, yielding single-stranded breaks (Sapranauskas *et al.*, 2011; Gasiunas *et al.*, 2012; Jinek *et al.*, 2012). Using a pair of Cas9ns greatly reduces off-target effects, which we may have been picking up in the Cel1 assay. Following the DSB, the introduction of a donor repair template stimulates the HDR repair pathway (Ran *et al.*, 2013a).

Design of repair template

Large modifications can be made at a target sequence by using plasmid-based donor repair templates that contain homology arms flanking the target sequence (Smithies *et al.*, 1985; Thomas *et al.*, 1986). The offset (distance) between our two gRNA sequences, cr2 and cr3 was -2 bp, which was well within the optimal range of -4 to 20 bp (Figure 6.5 A) (Ran *et al.*, 2013a; Ran *et al.*, 2013b). We introduced plasmid DNA into our parental Tango cells containing a blasticidin-resistance gene (Life Technologies), with homology arms flanking the target sequence in exon 3 of the DAGLα sequence (Figure 6.5 B). This was transfected into the Tango cells alongside two Cas9n constructs, one containing gRNA sequence cr 2 and the other containing the sequence cr 3, which already had been functionally tested in the SURVEYOR Cel I assay (Figure 6.3). The blasticidin resistance gene had a promotor directing translation in the reverse to prevent translation of an unwanted protein, followed by a stop codon (Figure 6.5 C). Successful integration of our donor plasmid was detected by treating the Tango cells with blasticidin, which we viewed as toxic to parental Tango cells at 4 mg/ml. Blasticidin was kept in the media at this concentration following transfection. Single cell colonies were selected with a cloning disc, expanded and analysed for indel formation.

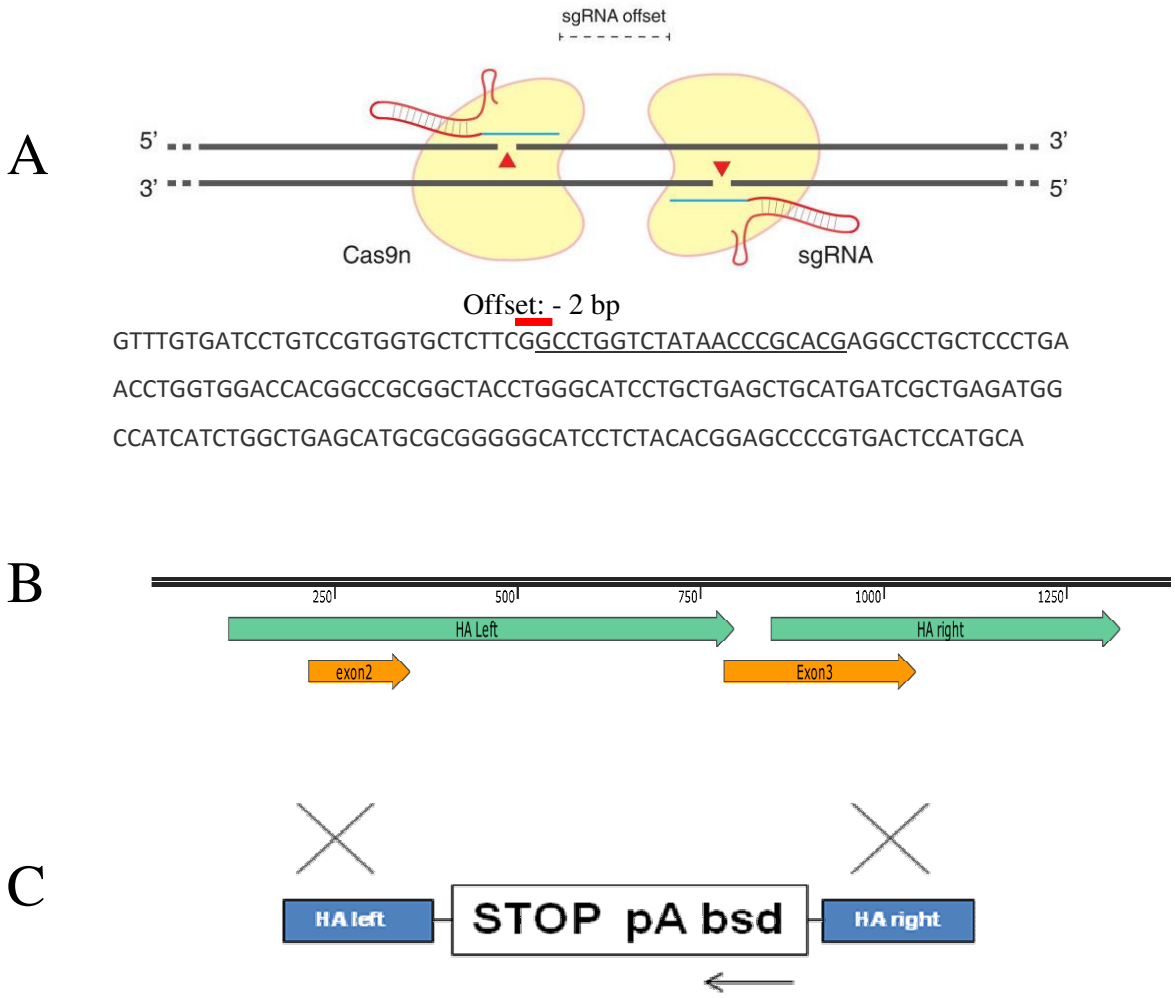

Figure 6.5 Double nicking facilitates HDR and incorporation of blasticidin resistance gene

(A) Schematic illustrating DSBs caused by two Cas9ns with different gRNA sequences – one for the sense- (CRISPR 3) and antisense-strand (CRISPR 2). Below are the two gRNA sequences to target DAGLα (CRISPR 2, yellow; CRISPR 3, underlined) located in exon 3, highlighting offset of -2 bp. (B) Design of homology arms (HA) to flank the CRISPR cutting sites (highlighted in green on DAGLα sequence). (C) Design of donor template DNA, with blasticidin resistance gene (bsd) flanked by homology arm (HA) DNA. The promotor is in the reverse (arrow), followed by a stop codon.

Figure A adapted from Ran et. al., 2013.

Transcript levels in the nickase/ blasticidin resistant cell lines

To determine the relative expression of DAGLα in our nickase cell lines compared to endogenous expression in the parental Tango cells, we performed Taqman analysis. To do this, our nickase cell lines were grown in the presence of blasticidin and lysed. RNA was extracted and converted to cDNA. Three housekeeping genes were used, PPIA, GAPDH and 18S. Relative fold change to WT Tango cells was analysed using the $2^{-\Delta\Delta Ct}$ method, as described above. Relative transcript levels are presented in Figure 6.6 A.

While none of the cell lines resulted in an apparent complete KO of DAGLα, B, C and X3 appeared to have a reduced level of transcripts and these cell lines were selected for further analysis (as indicated in Figure 6.6 A). Membrane protein from these cells was prepared and analysed in a western blot using the DAGLα antibody. As described above, this antibody is not entirely reliable, often resulting in non-specific bands. However, we wanted to know if we could detect any changes when compared to parental Tango cells. However, no band that was detected in Tango cell membrane protein was absent or disrupted in these cells (Figure 6.6 B).

The Taqman assay we used is a 'best coverage' assay from Life Technologies, as described before. This assay may have a variety of primers to cover the two predicted splice variants of DAGLα, but these may also be outside the locus of the blasticidin resistance gene. To gain a better understanding of what disruption had occurred followed treatment with our Cas9n constructs, we designed our own primers to perform RT-PCR. The forward primer selected was 5'–GCTAGTAGCATCTCGAGGTACAGG –3' and the reverse primer was 5'–CGTAGAGCACGTACTGCATGG –3'; we used these primers to amplify the cDNA already extracted from our nickase cell lines, as described above. WT DAGLα cDNA would result in a band size of 266 bp. Insertion of our donor template would result in a band > 2 kb. The results from the RT-PCR are shown Figure 6.7.

DNA from parental Tango cells (T) was at the predicted band size of 266 bp. This band is also present in some of the nickase cell lines, for example A and C, indicating that these cell lines still contain WT DAGLα transcripts. A large insert

can be seen in other cell lines, whose size corresponds to the blasticidin resistance gene. Where this is present and the 'T' band is absent, we predicted it to be successful disruption of the DAGLα gene in both alleles; this can be seen in the results from J. We selected this cell line for further analysis in a western blot with the DAGLα antibody, as described previously. The results can also be seen in Figure 6.7 (below the RT-PCR results), where a clear, undisrupted band can be seen for J.

It was unclear at this stage how these cells acquired blasticidin resistance without disruption to DAGLα transcription or translation. However, it may have been that one allele was undisrupted, while the other allele contained the blasticidin resistance gene, thereby affording them immunity to the antibiotic. However, this does not explain the results for cell line J. Bearing in mind the unreliability of the DAGLα antibody and the fact that cell line J clearly had a large insertion, we investigated the nickase disruption further by amplifying the catalytic domain. If the catalytic domain was still present, then DAGLα activity would be undisrupted.

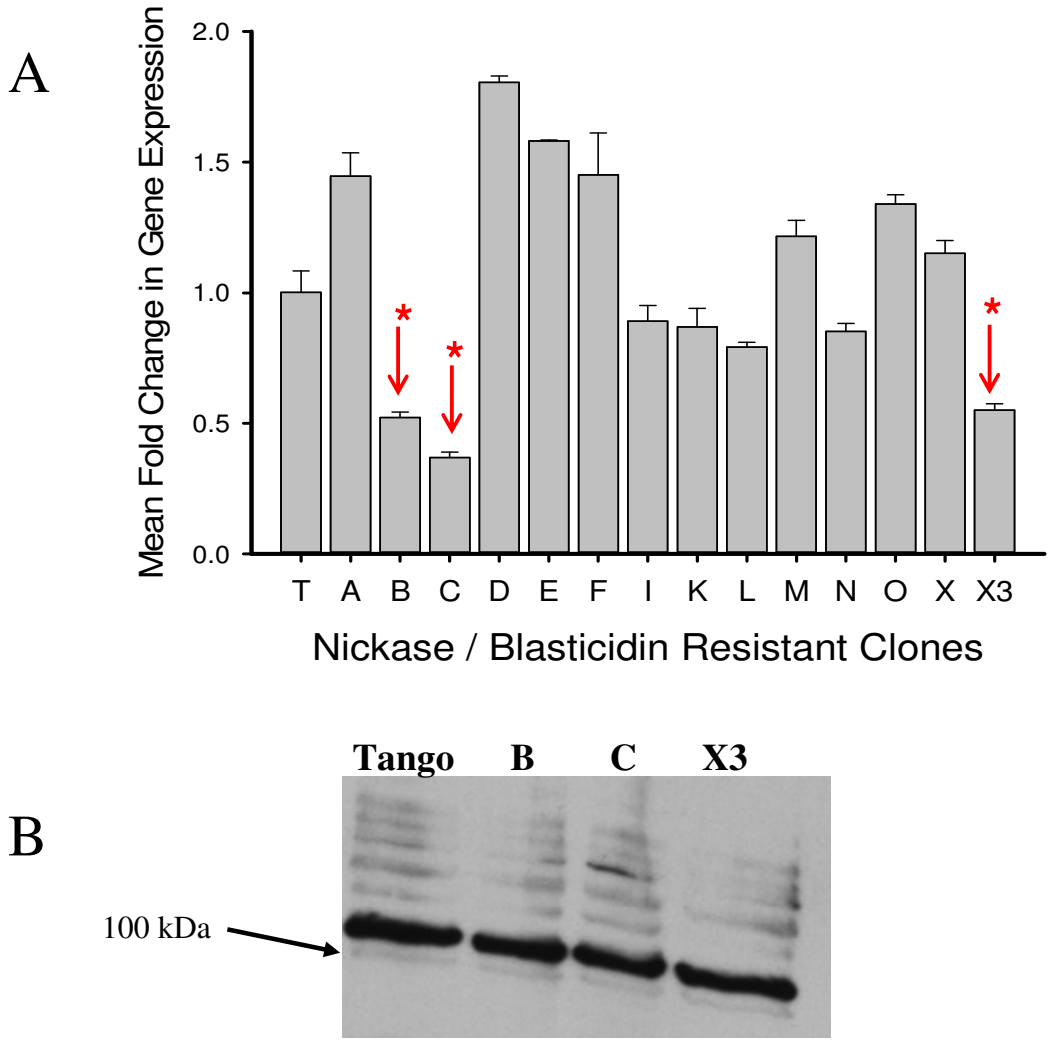

Figure 6.6 Taqman and western blot analysis of DAGLα expression in blasticidin-resistant cell lines

(A) DAGLα RNA transcripts were analysed using a Taqman assay, as described previously, and compared to endogenous DAGLα expression in parental Tango cells. PPIA was used as a housekeeping gene. Data was analysed using the $2^{-\Delta\Delta C}{}_t$ method previously described (Livak & Schmittgen, 2001). Cell lines B, C and X3 (red arrows) appeared to have fewer DAGLα RNA transcripts than Tango cells, and were selected for further investigation. (B) Membrane protein from B, C and X3 cells were analysed in a western blot using a DAGLα antibody, which indicated that DAGLα protein expression may still be translated in these cell lines, as all bands detected in Tango cell membranes were still present in our potential KO cell lines. However, we cannot exclude the possibility that the antibody picking up a protein other than DAGLα.

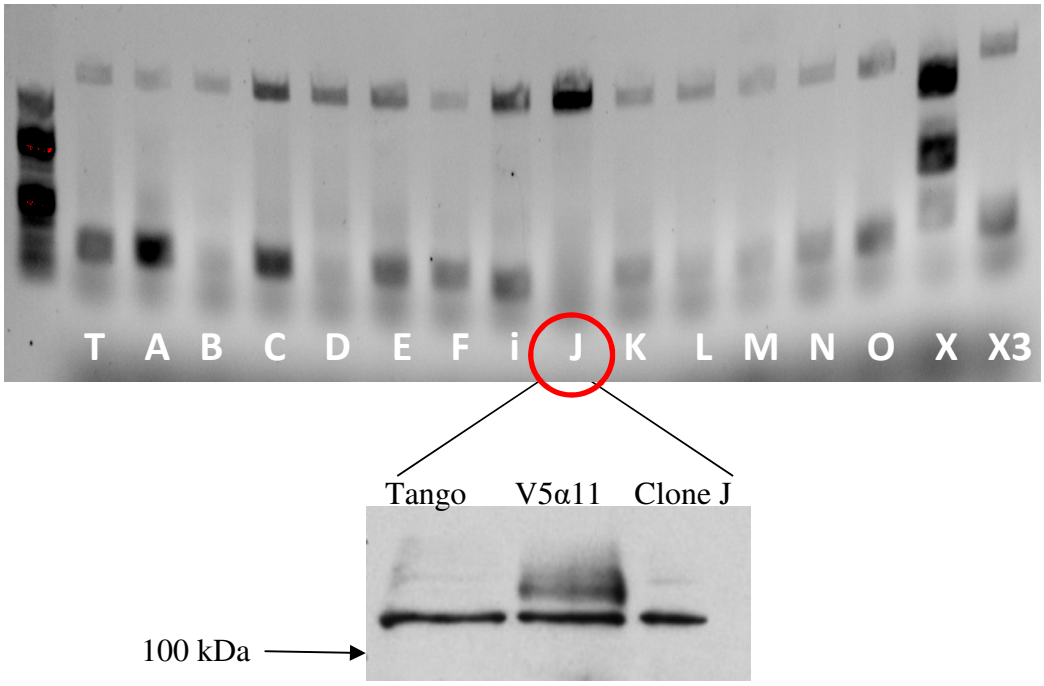

Figure 6.7 RT-PCR and western blot analysis of blasticidin-resistant cell lines

PCR was performed on cDNA from each of our blasticidin-resistant cell lines using primers flanking the CRISPR cutting site and locus of blasticidin resistant gene insertion. Cell line J appeared to be the most likely disrupted candidate, as WT band was absent from the expected size (~200 bp) with a much larger insertion, corresponding to the blasticidin-resistance gene. Membrane preparations from J were subsequently analysed in a western blot using a DAGLα antibody, and compared to Tango and V5α11 cell membranes, revealing the presence of a band at the predicted size for DAGLα (~120 kDa); However, as discussed previously the specificity of the antibody is questionable.

Amplification of DAGLα catalytic domain

In order to determine whether the catalytic domain of DAGLα was disrupted in our nickase cell line J, we performed RT-PCR using primers designed within the catalytic domain. To do this, RNA was extracted from both parental Tango cells and from J cells and reverse transcribed to cDNA. The cDNA was PCR-amplified using two sets of primers. The first set of primers designed flanked the CRISPR cutting site and locus of the blasticidin resistance gene. The forward primer used was 5'–GCTAGTAGCATCTCGAGGTACAGG –3' and the reverse was 5'–CGTAGAGCACGTACTGCATGG –3', which amplified a 266 bp product (as described previously). The second set of primers used were designed within the catalytic domain; the forward was located in exon 15 (5'–AGACAGCTCCTGGATGTCCT –3') and the reverse in exon 18 (5'–GAGTCAGGTCCACCTCGGTA –3') which amplified a 324 bp product. The results were analysed on an agarose gel and are shown in Figure 6.8.

The disruption of DAGLα in exon 3 is clearly evident in the first gel ('Primers 1 – spanning CRISPR site'), indicated by the lack of product at the predicted size, which can clearly be seen in parental Tango cells. Instead a much larger PCR product can be seen for J and this correlates with the predicted size of the blasticidin resistance gene (~ 2.8 kB), and our previous results seen in Figure 6.7. This confirmed insertion of our repair template via HDR at this locus. The second gel ('Primers 2 – DAGLα catalytic domain') is a repeat of the first, but using the second set of primers located within the catalytic domain. No difference was seen between the cDNA from parental Tango DNA and that from J; indicating that transcripts for the catalytic domain was still present in our J cell line.

We were not sure at this point why the full DAGLα gene was not disrupted in our nickase cell line J. We hypothesised that there may have been a splicing event across the site of disruption by Cas9n (Black, 2003), especially considering the relatively large size of DAGLα transcript (~ 5,700 bp) and the fact that it contains 20 exons. The DAGLα has been raised against a peptide encoded within exon 20, the last exon in the sequence, and if there is splicing around the disrupted exon 3, this might explain why we still see a band in the western blot. However, we did not see an

expected shift in mw of the band recognised by the antibody, suggesting that the band might not be DAGLα. In any case, it was clear that whatever way the DNA had been repaired, transcripts encoding for the catalytic domain are still present, and on that basis active enzyme might still be expressed in these cells. As a result, we deemed it to be prudent to redesign our CRISPR strategy to directly target the catalytic domain of DAGLα. This strategy might result in the expression of a protein, but given our understanding of the catalytic triad, this protein would not be enzymatically active (Bisogno, 2003; Pedicord *et al.*, 2011). However, we were concerned that the presence of a catalytically-dead DAGLα in the Tango cells may act as a dominant negative and we evaluated whether this was the case.

A. Primers 1 – spanning CRISPR site

B. Primers 2 – DAGLα catalytic domain

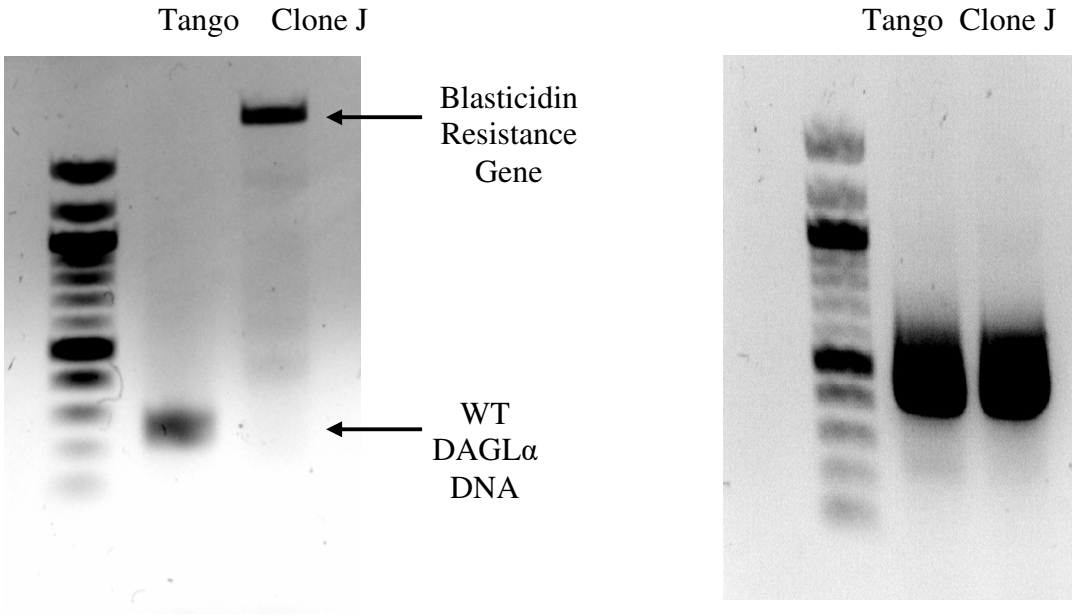

Figure 6.8 RT-PCR using RNA from Tango and Clone J cells reveals the presence of DAGLα catalytic domain

RNA from each cell line was extracted and reverse transcribed to cDNA. RT-PCR was performed on cDNA from both parental Tango cells and Clone J cells using two sets of primers. The first set of primers flank the CRISPR site and locus of blasticidin resistance gene, revealing the disruption of WT DAGLα DNA and presence of the gene at the expected locus (exon 3) (A) . The second set of primers used amplifies the catalytic domain, which is present in both cells types (B).

Expression of a catalytically-dead DAGLα and activity in the PNPB membrane assay

A 'dominant negative' form of a protein can be a useful tool in testing the function of the native WT counterpart; this is enabled by proteins that need to assemble into multimers in order to function (Sheppard, 1994), or by competing for ligand binding. For example, a catalytically-dead version of the FGFR acts as a dominant negative by competing out ligand binding to the WT receptor (Saffell *et al.*, 1997). It was important to determine if a catalytically-dead version of DAGLα interferes with the activity of WT or mutated DAGLα that is re-introduced back into the cells for mutagenesis studies. To this end, we used the PNPB membrane assay (described in results chapter II) to determine if the presence of a catalytically-dead version of the enzyme interferes with substrate hydrolysis driven by the WT enzyme.

We first introduced a mutant, catalytically-dead version of DAGLα into our DAGLα overexpressing cells, V5α11 (see Chapter 4, Results II for details). V5α11 cells were transiently transfected with GFP alone (control), or with a second vector containing either an epitope-tagged DAGLα–V5 (wtDAGLα) or with an epitope-tagged catalytically-dead DAGLα-V5 (cdDAGLα), whereby a mutation within the catalytic domain has rendered it inactive. These constructs were introduced into the Tango cells via Fugene HD (as described before). After approximately 48 h, successful transfection was confirmed by examining the cells for GFP expression under a fluorescent microscope. Membrane protein from each transfection was then extracted. Equal expression of both wtDAGLα and cdDAGLα was confirmed by western blot and densitometry analysis using a V5 antibody and odyssey software, respectively. Results obtained were compared to V5α11 cells transfected with GFP alone (control), showing overexpression of each construct (Figure 6.9).

We then tested the activity of the transfected V5α11 cells in the membrane protein PNPB assay. Membranes were plated at 12.5 µg/ml in a polypropylene 96-well plate, in the presence and absence of 1 µM THL. 250 µM of PNPB was then added per well and the plate was read immediately at 400 nM on the Spectramax, (as described in Chapter 4, Results II). Figure 6.10 shows there was clear hydrolysis of PNPB by

V5α11 cells, acting as a control for our assay. There was a much larger rate of PNPB hydrolysis when more DAGLα–V5 is present (wtDAGLα), which reached significance compared to the control. The presence of cdDAGLα does not reduce the rate of PNPB hydrolysis, and results were similar to V5α11 cells transfected with GFP alone, a comparison made much clearer when the responses are normalised to the THL response (Figure 6.10 B). It appeared that the presence of an inactive form of DAGLα does not interfere with the activity of the active form of the enzyme; therefore the catalytically-dead DAGLα does not act as a dominant negative.

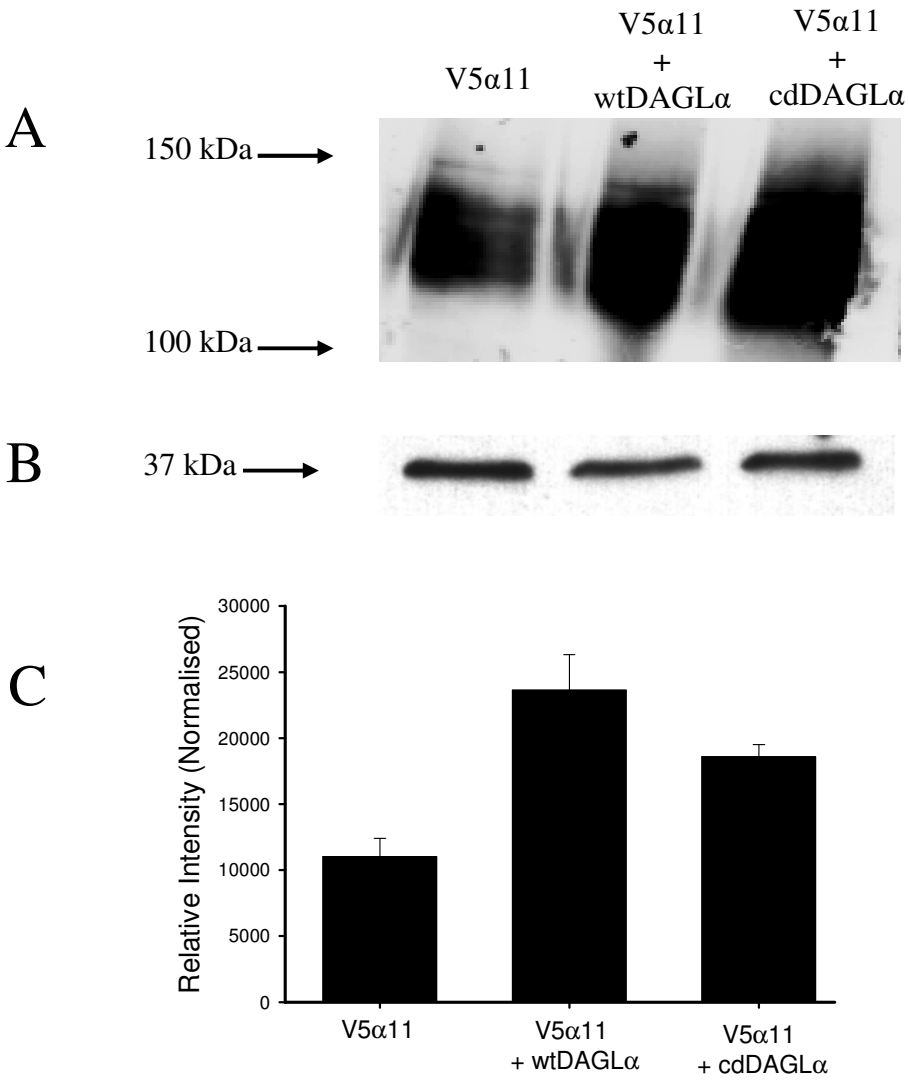

Figure 6.9 Expression of a catalytically dead DAGLα-V5 in the Tango cells compared with αV5 cells

Stable V5α11 cells were transiently transfected with either GFP alone as control (V5α11), epitope-tagged DAGLα (wtDAGLα) and GFP, or with an epitope-tagged DAGLα whose catalytic domain is inactive (cdDAGLα) and GFP. Transfection was deemed successful by viewing GFP expression under a fluorescent microscope. The cells were expanded, protein extracted and used at equal amounts for western blot analysis with a V5 antibody to confirm expression of both constructs (A) and actin was used as loading control (B). This was repeated in 3 independent experiments and the average intensity (normalised to actin) from three blots ± SEM is presented, which were not statistically different from each other (Student's t-test) (C).

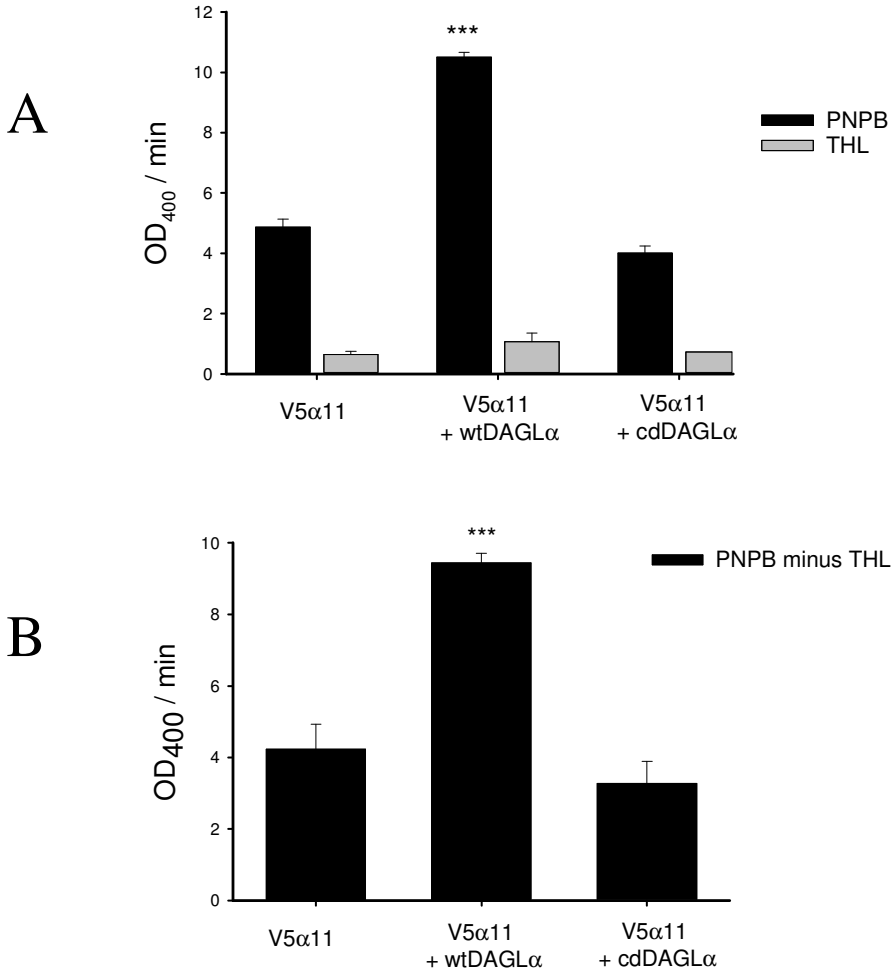

Figure 6.10 The catalytically dead version does not display different activity to that seen from DAGLα- in the PNPB membrane assay

Stable V5α11 cells were transfected with either GFP alone (V5α11), with an epitope-tagged DAGLα (wtDAGLα) and GFP, or with a catalytically-dead DAGLα (cdDAGLα) and GFP. Successful transfection was determined by examining GFP expression under a fluorescent microscope. Membrane protein from each transfection was extracted and plated at 12.5 µg/ml into a 96-well plate. Half of the membranes were treated with 1 µM THL and 250 µM PNPB was used as substrate. The absorbance was read at 400 nM for 10 min (A). Significance compared to V5α11 cells was established using the two-sided Student's t-test (indicated below). The cdDAGLα response was not significantly different, indicating that DAGLα does not act as a multimer, as evident from the THL-sensitive response (B). Results presented are the mean of 3 wells from 3 independent experiments ± SEM.

*** p>0.001 Student's t-test

Targeting DAGLα catalytic domain with Cas9 endonuclease

gRNA design to target DAGLα catalytic domain

The DAGLs' catalytic triad activity consists of a serine in exon 14, histidine in exon 15 and aspartic acid in exon 18 (see Fig 3.3, Results I). As the serine is the most upstream of the amino acids, we took the sequence from exon 14 and designed 3 new gRNA sequences, as a frameshift downstream of this site would also disrupt the histidine and aspartic acid. However, a simple disruption of the serine would also render DAGLα catalytically dead, as a mutation in one member of the catalytic triad disrupts activity (Bisogno, 2003; Pedicord *et al.*, 2011). CRISPR 2 therefore had a high probability of disrupting DAGLα activity, as this sequence cuts directly at the serine codon (Figure 6.11). We inserted our gRNA sequences into our Cas9 vectors, containing the necessary components for CRISPR/Cas9 system, as described previously. We used Cas9 vectors available from Addgene to allow our cells to have temporary puromycin antibiotic resistance following transfection (Ran *et al.*, 2013b). We confirmed that our new gRNA sequences could effectively guide Cas9 to induce indels by testing in the SURVEYOR Cel I assay, as described previously (Figure 6.11 B).

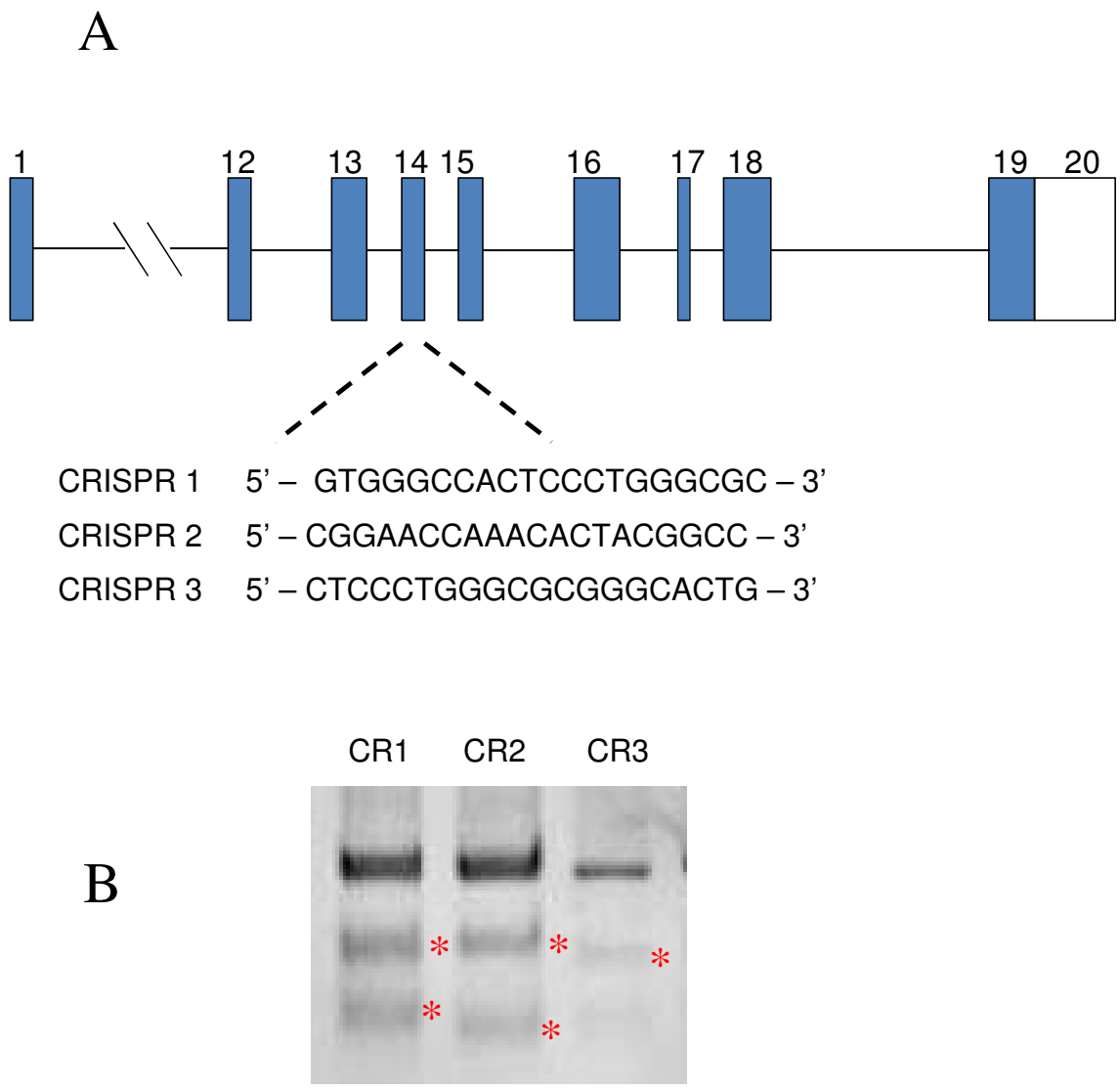

Figure 6.11 Custom gRNAs can effectively target DAGLα catalytic domain

Schematic representation of the human DAGLα sequence, indicating exons 1, 12 – 20 (A: blue). Three CRISPR sequences were selected using software on www.zifit.org. Each gRNA sequence is located in exon 14 of the hDAGLα gene, which contains the code for the catalytic serine. Tango cells were transfected with Cas9 nuclease vectors containing each of the 3 gRNA sequences and DNA from these cells was analyzed using the SURVEYOR Cel 1 nuclease assay, which detects indel formations, cleaving the DNA at this site. Agarose gel shows cutting at a particular locus (*) thereby confirming effective Cas9 guiding by the gRNA sequences (B).

Generation and genotyping of DAGLα-inactive Tango cell lines

Following selection of cell lines transfected with our custom gRNA-Cas9 vectors, we wanted to determine any gross changes in transcript size via RT-PCR. To do this, we took our three custom gRNA sequences (CRISPR 1-3) inserted into the Cas9 vector and transfected them into the Tango cells via Fugene HD. The cells were maintained for ~ 24 h before addition of 1mg/ml of puromycin to the media for a further 24 h, to enrich for cells containing our CRISPR/Cas9 constructs. The cells were then diluted and spread into a large 10 cm dish to allow individual cell colonies to grow before being selected and expanded. RNA was extracted from each of the cell lines, which was reverse transcribed to cDNA and amplified using primers spanning the CRISPR cutting site. The forward primer, located in exon 12 was 5'–GATGCCCTGACTGACCTGAC –3' and the reverse, located in exon 15 was 5'–GAGTCAGGTCCACCTCGG –3', which amplified an 856 bp product. The PCR products were analysed in an agarose gel and the results from CRISPR sequences 1, 2 and 3 are shown in Figure 6.12.

The results from the three CRISPR sequences were very different. No major changes in transcript size were seen in cell lines treated with CRISPRs 1 and 3. Cell line 1A may have one disrupted allele, as indicated by a smaller band seen compared to the WT band, but there is also a band at the expected WT size. Similarly, cells from 3E and 3F resulted in a fainter band compared to the WT DNA. This may be a result of knockdown, or may simply be an issue with quantity of cDNA prior to PCR. Interestingly, CRISPR 2 resulted in a variety of disrupted transcripts. The cell line 2B appeared to have a sizeable deletion, resulting in only one band that was much smaller than the WT transcript. RNA from 2I also appeared to contain less WT transcript. However, the lack of a clear band in the gel raises the possibility of an issue with the PCR reaction as opposed to major gene disruption. Other cell lines showed evidence for major disruptions to one transcript alongside a WT–sized transcript; for example 2D may have one allele with a deletion, while 2R could have an allele with an insertion. 2B appeared to have the largest deletion out of all the cell lines selected following CRISPR 2 treatment, while also missing a band at the expected WT size. As the results were much clearer for 2B, transcripts were amplified for sequencing.

Figure 6.12 RT-PCR analysis of DAGL*α* CRISPR cell lines highlights gross transcript changes following Cas9 targeting to the catalytic site

RNA from the candidate DAGLα KO cell lines from each of the CRISPR sequences was extracted and reverse transcribed to cDNA. The cDNA was amplified using PCR with primers flanking the CRISPR cutting sites, and compared with non-transfected Tango cell cDNA as a control. Cell lines isolated following treatment of each of our gRNA sequences (CRISPR 1-3) are indicated.

CRISPR 1 Clones

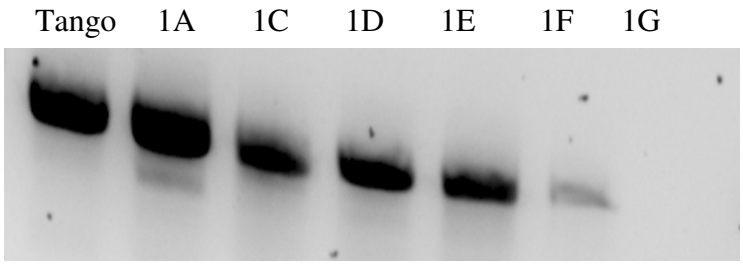

CRISPR 2 Clones

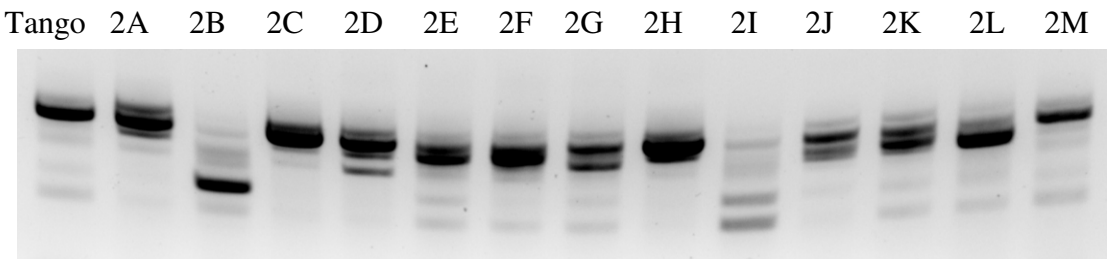

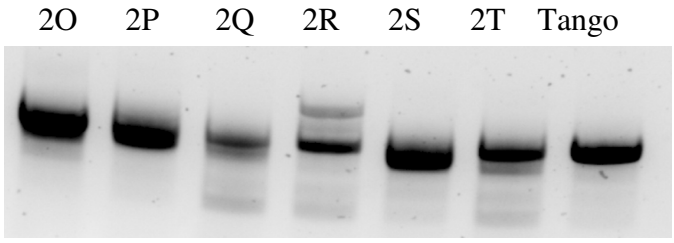

CRISPR 3 Clones

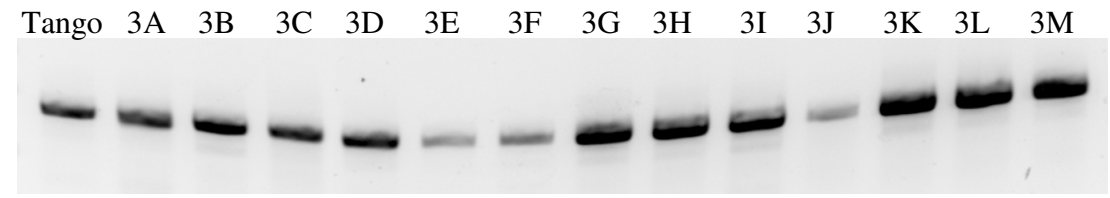

Sequencing of 2B cells

2B looked like the most promising cell line to follow up and it was important to obtain the sequence of both alleles. Therefore, we extracted RNA from 2B, reversed transcribed it to cDNA and PCR-amplified the catalytic domain using the primers above and Taq polymerase. The addition of an 'A' on the end of the sequence by Taq allowed us to TOPO clone and transform into *E.Coli*, as described previously (and in the methods section, Chapter 2). 48 colonies were selected and sent to GATC Biotech (Konstanz, Germany) for sequencing. The sequence of each allele was aligned with WT DAGLα sequence and the results are presented in Figures 6.13 & 6.14. The two alleles are aligned to WT DAGLα in the diagram in Figure 6.15, showing the locus of the catalytic triad and the resulting disruptions.

'Allele 1' had a 2 bp deletion within exon 14 and had the whole of exon 17 deleted; exon 17 harbours the histidine of the catalytic triad (Figure 6.13). The 2 bp deletion causes a frameshift in the rest of the sequence downstream, resulting in a KO of the catalytic triad. 'Allele 2' had exons 13-16 deleted, which is in frame but results in a KO of the serine and the aspartic acid of the catalytic triad (Figure 6.14).

The translation of sequences from each allele were aligned to WT DAGLα and are shown in Figure 6.16 and Figure 6.17, highlighting the 3 amino acids of the catalytic triad (blue) and the disruption in each allele caused by Cas9 and NHEJ repair. The section of disrupted sequence that has been deleted is highlighted in yellow. In 'Allele 1', the initial 2 bp deletion causes a frameshift in the downstream sequence; DAGLα protein translated from this sequence would be missing all three amino acids of the catalytic triad (Figure 6.16). In 'Allele 2', the translated sequence is lacking both the serine and aspartic acid of the catalytic triad (Figure 6.17). These two results indicated that in 2B, both DAGLα alleles have been seriously disrupted and can no longer express a catalytically active enzyme (hereafter termed α2B).

Figure 6.13 Alignment of DAGLα catalytic domain in Tango cells with one allele of the DAGLα-inactive cell line, α2B

RNA from Tango and DAGLα-inactive cell line, 2B was extracted and reverse transcribed to cDNA. The catalytic domain was amplified using primers (green) flanking the CRISPR cutting site (red) and the catalytic triad. Sequence analysis was performed using TOPO cloning and Sanger sequencing (Source Bioscience; accounted for 97% of results; 32% successful sequence results). Sequence alignment was performed using CLUSTAL W, highlighting a 2 bp deletion in exon 14 and deletion of exon 17 (yellow).

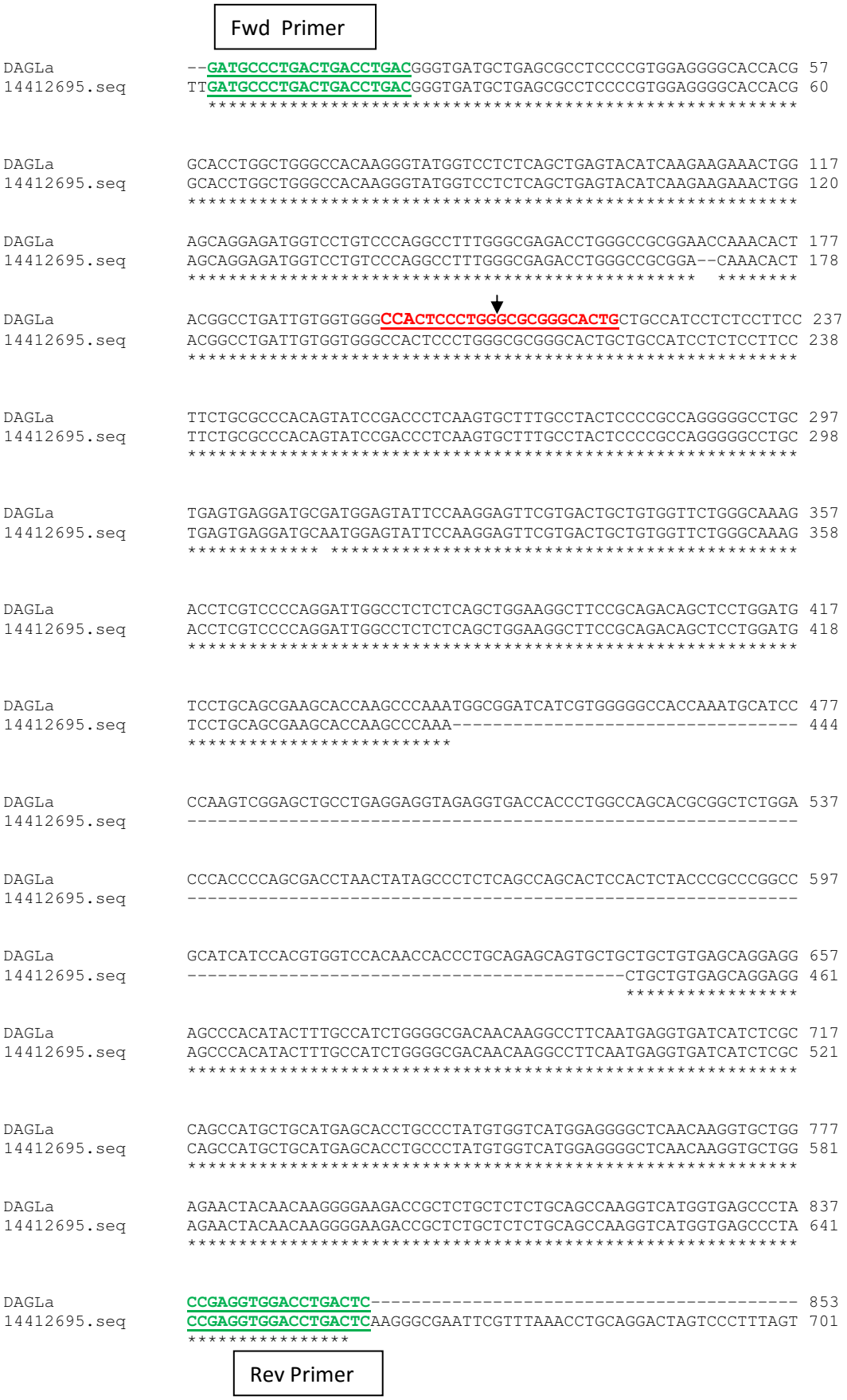
Fwd Primer
DAGLa --GATGCCCTGACTGACCTGACGGGTGATGCTGAGCGCCTCCCCGTGGAGGGGCACCACG 57
14412695.seq TTGATGCCCTGACTGACCTGACGGGTGATGCTGAGCGCCTCCCCGTGGAGGGGCACCACG 60
DAGLa GCACCTGGCTGGGCCACAAGGGTATGGTCCTCTCAGCTGAGTACATCAAGAAGAAACTGG 117
14412695.seq GCACCTGGCTGGGCCACAAGGGTATGGTCCTCTCAGCTGAGTACATCAAGAAGAAACTGG 120
DAGLa AGCAGGAGATGGTCCTGTCCCAGGCCTTTGGGCGAGACCTGGGCCGCGGAACCAAACACT 177
14412695.seq AGCAGGAGATGGTCCTGTCCCAGGCCTTTGGGCGAGACCTGGGCCGCGGA--CAAACACT 178
DAGLa ACGGCCTGATTGTGGTGGGCCACTCCCTGGGCGCGGGCACTGCTGCCATCCTCTCCTTCC 237
14412695.seq ACGGCCTGATTGTGGTGGGCCACTCCCTGGGCGCGGGCACTGCTGCCATCCTCTCCTTCC 238
DAGLa TTCTGCGCCCACAGTATCCGACCCTCAAGTGCTTTGCCTACTCCCCGCCAGGGGGCCTGC 297
14412695.seq TTCTGCGCCCACAGTATCCGACCCTCAAGTGCTTTGCCTACTCCCCGCCAGGGGGCCTGC 298
DAGLa TGAGTGAGGATGCGATGGAGTATTCCAAGGAGTTCGTGACTGCTGTGGTTCTGGGCAAAG 357
14412695.seq TGAGTGAGGATGCAATGGAGTATTCCAAGGAGTTCGTGACTGCTGTGGTTCTGGGCAAAG 358
DAGLa ACCTCGTCCCCAGGATTGGCCTCTCTCAGCTGGAAGGCTTCCGCAGACAGCTCCTGGATG 417
14412695.seq ACCTCGTCCCCAGGATTGGCCTCTCTCAGCTGGAAGGCTTCCGCAGACAGCTCCTGGATG 418
DAGLa TCCTGCAGCGAAGCACCAAGCCCAAATGGCGGATCATCGTGGGGGCCACCAAATGCATCC 477
14412695.seq TCCTGCAGCGAAGCACCAAGCCCAAA---------- 444
DAGLa CCAAGTCGGAGCTGCCTGAGGAGGTAGAGGTGACCACCCTGGCCAGCACGCGGCTCTGGA 537
14412695.seq ----------
DAGLa CCCACCCCAGCGACCTAACTATAGCCCTCTCAGCCAGCACTCCACTCTACCCGCCCGGCC 597
14412695.seq ----------
DAGLa GCATCATCCACGTGGTCCACAACCACCCTGCAGAGCAGTGCTGCTGCTGTGAGCAGGAGG 657
14412695.seq ----------CTGCTGTGAGCAGGAGG 461
DAGLa AGCCCACATACTTTGCCATCTGGGGCGACAACAAGGCCTTCAATGAGGTGATCATCTCGC 717
14412695.seq AGCCCACATACTTTGCCATCTGGGGCGACAACAAGGCCTTCAATGAGGTGATCATCTCGC 521
DAGLa CAGCCATGCTGCATGAGCACCTGCCCTATGTGGTCATGGAGGGGCTCAACAAGGTGCTGG 777
14412695.seq CAGCCATGCTGCATGAGCACCTGCCCTATGTGGTCATGGAGGGGCTCAACAAGGTGCTGG 581
DAGLa AGAACTACAACAAGGGGAAGACCGCTCTGCTCTCTGCAGCCAAGGTCATGGTGAGCCCTA 837
14412695.seq AGAACTACAACAAGGGGAAGACCGCTCTGCTCTCTGCAGCCAAGGTCATGGTGAGCCCTA 641
DAGLa CCGAGGTGGACCTGACTC---------- 853
14412695.seq CCGAGGTGGACCTGACTCAAGGGCGAATTCGTTTAAACCTGCAGGACTAGTCCCTTTAGT 701
Rev Primer

Figure 6.14 Alignment of the nucleotide sequence of DAGLα catalytic domain in Tango cells with the second allele of the DAGLα-inactive cell line, α2B

RNA from Tango and DAGLα-inactive cell line, 2B was extracted and reverse transcribed to cDNA. The catalytic domain was amplified using primers (green) flanking the CRISPR cutting site (red) and the catalytic triad. Sequence analysis was performed using TOPO cloning and Sanger sequencing (Source Bioscience; accounted for 6% of results; 32% successful sequence results). Sequence alignment was performed using CLUSTAL W, highlighting deletion of exons 13-16 (yellow).

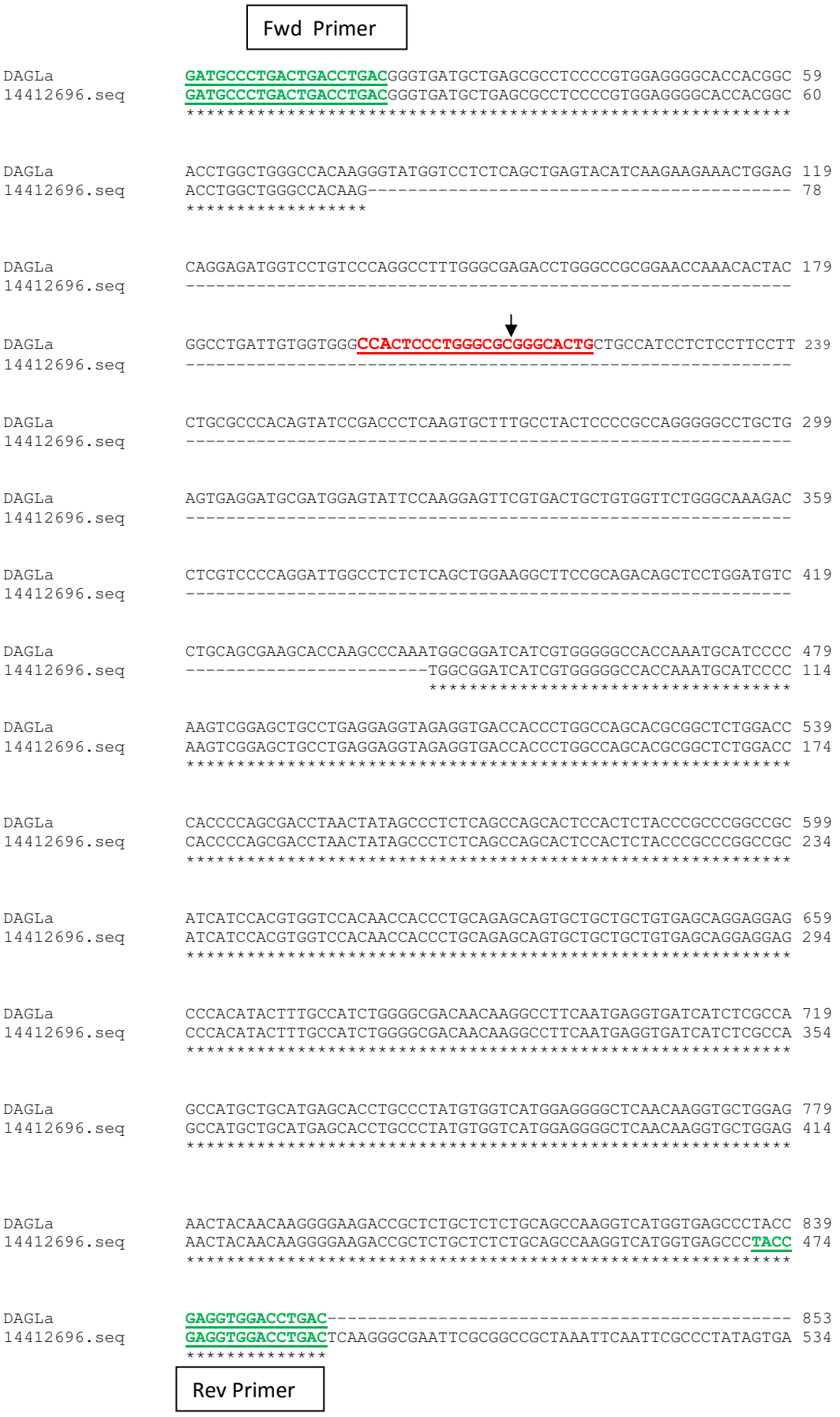
Fwd Primer
DAGLa GATGCCCTGACTGACCTGACGGGTGATGCTGAGCGCCTCCCCGTGGAGGGGCACCACGGC 59
14412696.seq GATGCCCTGACTGACCTGACGGGTGATGCTGAGCGCCTCCCCGTGGAGGGGCACCACGGC 60
DAGLa ACCTGGCTGGGCCACAAGGGTATGGTCCTCTCAGCTGAGTACATCAAGAAGAAACTGGAG 119
14412696.seq ACCTGGCTGGGCCACAAG---------- 78
DAGLa CAGGAGATGGTCCTGTCCCAGGCCTTTGGGCGAGACCTGGGCCGCGGAACCAAACACTAC 179
14412696.seq ----------
DAGLa GGCCTGATTGTGGTGGGCCACTCCCTGGGCGCGGGCACTGCTGCCATCCTCTCCTTCCTT 239
14412696.seq ----------
DAGLa CTGCGCCCACAGTATCCGACCCTCAAGTGCTTTGCCTACTCCCCGCCAGGGGGCCTGCTG 299
14412696.seq ----------
DAGLa AGTGAGGATGCGATGGAGTATTCCAAGGAGTTCGTGACTGCTGTGGTTCTGGGCAAAGAC 359
14412696.seq ----------
DAGLa CTCGTCCCCAGGATTGGCCTCTCTCAGCTGGAAGGCTTCCGCAGACAGCTCCTGGATGTC 419
14412696.seq ----------
DAGLa CTGCAGCGAAGCACCAAGCCCAAATGGCGGATCATCGTGGGGGCCACCAAATGCATCCCC 479
14412696.seq ----------TGGCGGATCATCGTGGGGGCCACCAAATGCATCCCC 114
DAGLa AAGTCGGAGCTGCCTGAGGAGGTAGAGGTGACCACCCTGGCCAGCACGCGGCTCTGGACC 539
14412696.seq AAGTCGGAGCTGCCTGAGGAGGTAGAGGTGACCACCCTGGCCAGCACGCGGCTCTGGACC 174
DAGLa CACCCCAGCGACCTAACTATAGCCCTCTCAGCCAGCACTCCACTCTACCCGCCCGGCCGC 599
14412696.seq CACCCCAGCGACCTAACTATAGCCCTCTCAGCCAGCACTCCACTCTACCCGCCCGGCCGC 234
DAGLa ATCATCCACGTGGTCCACAACCACCCTGCAGAGCAGTGCTGCTGCTGTGAGCAGGAGGAG 659
14412696.seq ATCATCCACGTGGTCCACAACCACCCTGCAGAGCAGTGCTGCTGCTGTGAGCAGGAGGAG 294
DAGLa CCCACATACTTTGCCATCTGGGGCGACAACAAGGCCTTCAATGAGGTGATCATCTCGCCA 719
14412696.seq CCCACATACTTTGCCATCTGGGGCGACAACAAGGCCTTCAATGAGGTGATCATCTCGCCA 354
DAGLa GCCATGCTGCATGAGCACCTGCCCTATGTGGTCATGGAGGGGCTCAACAAGGTGCTGGAG 779
14412696.seq GCCATGCTGCATGAGCACCTGCCCTATGTGGTCATGGAGGGGCTCAACAAGGTGCTGGAG 414
DAGLa AACTACAACAAGGGGAAGACCGCTCTGCTCTCTGCAGCCAAGGTCATGGTGAGCCCTACC 839
14412696.seq AACTACAACAAGGGGAAGACCGCTCTGCTCTCTGCAGCCAAGGTCATGGTGAGCCCTACC 474
DAGLa GAGGTGGACCTGAC---------- 853
14412696.seq GAGGTGGACCTGACTCAAGGGCGAATTCGCGGCCGCTAAATTCAATTCGCCCTATAGTGA 534
Rev Primer

Figure 6.15 Diagrammatic representation of each allele from the DAGLα-inactive cell line, α2B

The amplified nucleotide sequence of each allele from α2B is compared to WT DAGLα sequence. Features highlighted include the gRNA sequence ('CRISPR', red), CRISPR cutting site (arrow), the catalytic residues (blue), missing exons following Cas9 treatment (yellow) and location of primers (purple), using software available from Snapgene.


Cas9 cutting site
DAGLα
Fwd Primer
Rev Primer
200
400
600
800
Exon 12
Exon 13
Exon 14
Exon 15
Exon 16
Exon 17
Exon 18
Exon 19
CRISPR
Aspartic Acid
Histidine
Serine
Clone α2b
Allele 1
2 bp Deletion
Clone α2b
Allele 2

```
DAGLa           DALTDLTGDAERLPVE  420
C03             DALTDLTGDAERLPVE  16
                ****************
```

Out of Frame

```
DAGLa           GHHGTWLGHKGMVLSAEYIKKKLEQEMVLSQAFGRDLGRGTKHYGLIVVGHSLGAGTAAI 480
C03             GHHGTWLGHKGMVLSAEYIKKKLEQEMVLSQAFGRDLGRGQTLRPDCGG---------- 65
                ************************************* .

DAGLa           LSFLLRPQYPTLKCFAYSPPGGLLSEDAMEYSKEFVTAVVLGKDLVPRIGLSQLEGFRRQ 540
C03             ------------------------------------------------------------

DAGLa           LLDVLQRSTKPKWRIIVGATKCIPKSELPEEVEVTTLASTRLWTHPSDLTIALSASTPLY 600
C03             ------------------------------------------------------------

DAGLa           PPGRIIHVVHNHPAEQCCCCEQEEPTYFAIWGDNKAFNEVIISPAMLHEHLPYVVMEGLN 660
C03             -------------------------------------PLPGRGHCCHPLLPSAPTVSDP 87

DAGLa           KVLENYNKGKTALLSAAKVMVSPTEVDLT 720
C03             QVLCLLPARGPAE-GCNGVFQGVRDCCGS 146
```

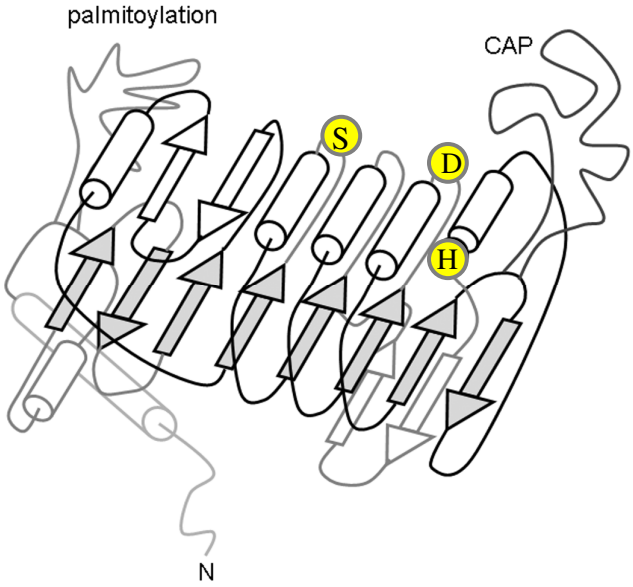

Figure 6.16 Amino acid translation of 'Allele 1' from α2B cells

The sequencing results from 'allele 1' of α2B cells following CRISPR (red) treatment were translated and aligned with the amino acid sequence of WT DAGLα. Allele 1 had a 2bp deletion, resulting in a frameshift of the amino acid sequence (highlighted in yellow). The frameshift disrupts all three amino acids of the catalytic triad, as indicated in yellow in the figure below the sequence.

```
DAGLa           DALTDLTGDAERLPVE   420
D03             DALTDLTGDAERLPVE   16
                ****************

DAGLa           GHHGTWLGHKGMVLSAEYIKKKLEQEMVLSQAFGRDLGRGTKHYGLIVVGHSLGAGTAAI 480
D03             GHHGTWLGHK---------------------------------------------------- 26
                **********

DAGLa           LSFLLRPQYPTLKCFAYSPPGGLLSEDAMEYSKEFVTAVVLGKDLVPRIGLSQLEGFRRQ 540
D03             ------------------------------------------------------------

DAGLa           LLDVLQRSTKPKWRIIVGATKCIPKSELPEEVEVTTLASTRLWTHPSDLTIALSASTPLY 600
D03             ------------WRIIVGATKCIPKSELPEEVEVTTLASTRLWTHPSDLTIALSASTPLY 74
                            **********************************************

DAGLa           PPGRIIHVVHNHPAEQCCCCEQEEPTYFAIWGDNKAFNEVIISPAMLHEHLPYVVMEGLN 660
D03             PPGRIIHVVHNHPAEQCCCCEQEEPTYFAIWGDNKAFNEVIISPAMLHEHLPYVVMEGLN 134
                ************************************************************

DAGLa           KVLENYNKGKTALLSAAKVMVSPTEVDLT 720
D03             KVLENYNKGKTALLSAAKVMVSPTEVDLT 190
                ******************************
```

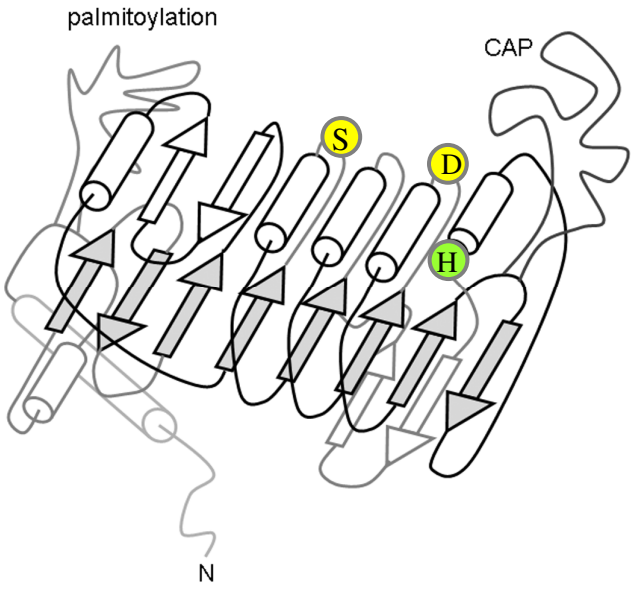

Figure 6.17 Amino acid translation of 'Allele 2' from α2B cells

The sequencing results from 'allele 2' of α2B cells following CRISPR (red) treatment were translated and aligned with the amino acid sequence of WT DAGLα. The primers used to amplify this sequence are in green. Allele 2 had a specific region deleted, which harbours the serine and aspartic acid of the catalytic triad, as highlighted in yellow in the figure below, rendering DAGLα translated from this allele catalytically dead.

Targeting DAGLβ catalytic activity in α2B cells

gRNA design to target DAGLβ activity

Having disrupted both DAGLα alleles in α2B cells, we next turned our attention to disrupting the DAGLβ alleles in the same cell line. To ensure we obtained a gRNA sequence that can effectively guide Cas9, we designed a total of 9 gRNAs to target exons 9, 10 and 11 of DAGLβ.

To do this, we used software available on zifit.org and compared the results with those obtained from DNA 2.0 software (Figure 6.18 A). Each of the sequences were ordered as single nucleotide strands, with overhangs compatible with our vector and annealed to form double-stranded oligonucleotides, as described previously. We inserted our custom gRNA sequences into the Cas9 vector backbone (Ran *et al.*, 2013b). To test their efficiency, Tango cells were transfected with each of the vectors and treated with puromycin for 24 h, as described above. DNA from the transfected cells was extracted and amplified using primers flanking each of the CRISPR cutting sites and analysed in the SURVEYOR Cel I assay, as described previously.

The results are shown in Figure 6.18 B. Sequence numbers 1, 2, 4, 6 and 8 appeared to have resulted in indel formations, as detected and cleaved by the Cel I endonuclease. Sequence number 2 resulted in two separate and darker bands and so this was selected for the DAGLβ targeting studies.

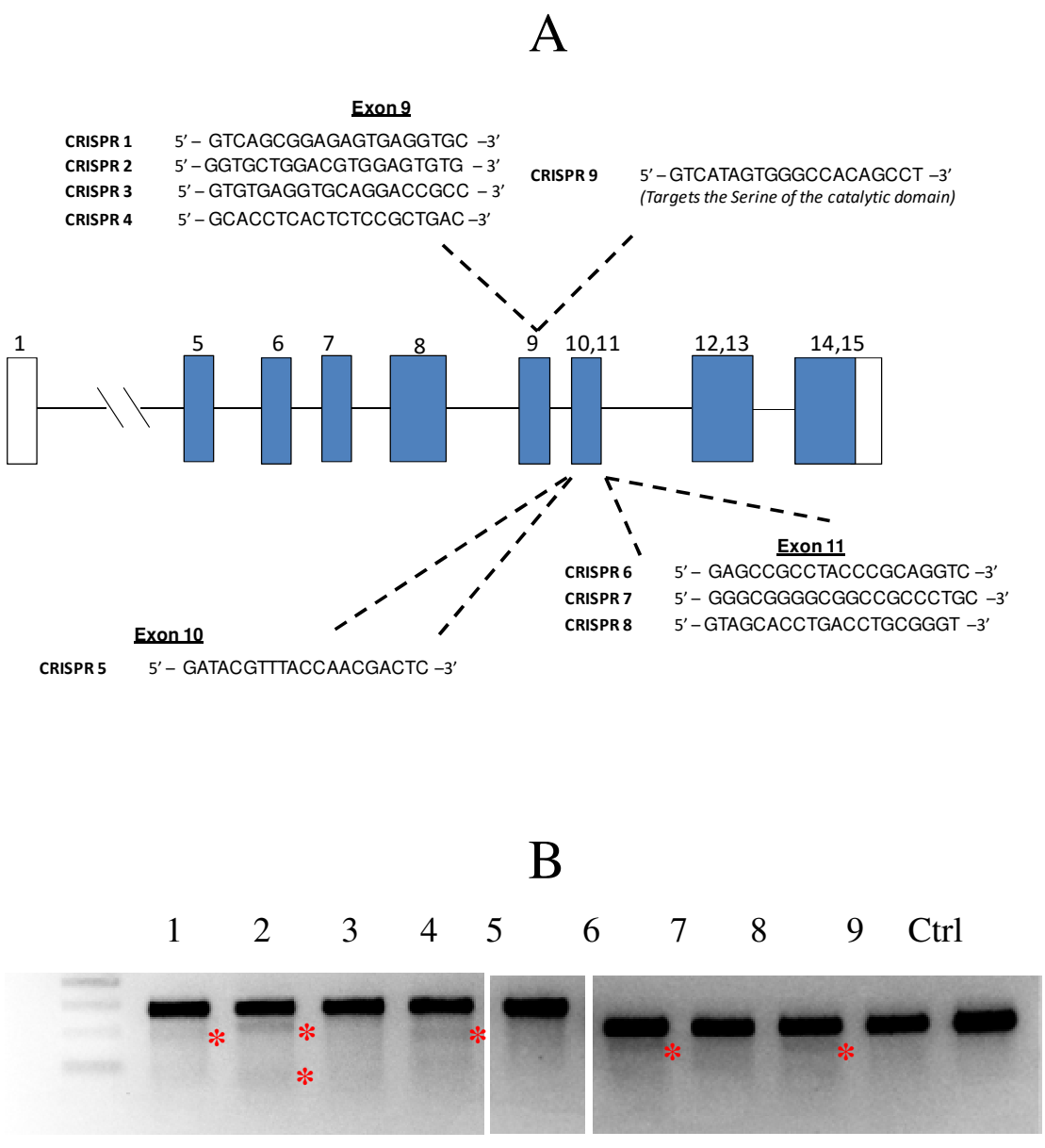

Figure 6.18 Design of gRNA sequences that target DAGLβ catalytic domain

Schematic representation of the human DAGLβ sequence, indicating exons 1, 5 – 20 (A: blue). 9 CRISPR (gRNA) sequences were selected using software on ww.zifit.org. The gRNA sequences are located in exons 9, 10 and 11 which harbour the residues encoding the catalytic triad of the enzyme (A). Tango cells were transfected with Cas9 vectors containing each of our custom gRNA sequences. DNA from these cell pools was analyzed using the SURVEYOR Cel I assay, which detects any mutations or indel formations, cleaving the DNA at this site. Agarose gel shows cutting at a particular locus (*) thereby confirming effective Cas9 guiding by the gRNA sequence (B).

Generation and genotyping of DAGLβ-targeted Tango cell lines

Next, we wanted to generate a double DAGLα and DAGLβ inactive cell line. We generated cell lines following transfection with our Cas9 vector containing our custom gRNA sequence 2 (located in exon 9) and determined any gross changes to the catalytic domain of DAGLβ via RT-PCR, as described before.

To do this we transfected α2B cells with gRNA2/Cas9 vector via Fugene HD. The cells were maintained for ~ 24 h, before addition of 1mg/ml of puromycin to the media for a further 24 h, to enrich for cells containing our CRISPR/Cas9 construct. The cells were then diluted and spread into a large 10 cm dish and colonies picked ~ 10 days later. Following this, individual cell lines were selected and expanded. RNA was extracted from each of the cell lines, which was reverse transcribed to cDNA and amplified using primers spanning the CRISPR cutting site. The forward primer used was 5'– AGTCTGTTGTGGTCGCTGTG – 3' (exon 8) and the reverse primer was 5' – CGTCGTTGATGAGTCGTTGG – 3' (exon 10). PCR products were analysed on an agarose gel and compared with cDNA from parental Tango cells (Figure 6.19).

Disruptions can be seen in transcripts from a number of the cell lines generated following CRISPR/Cas9 treatment. Interestingly, there appeared to be a number of candidate cell lines with insertions (rather than deletions) at the target site; for example, B, P, R and most prominently in 1E. As we had a very reliable antibody for DAGLβ, we decided to analyse those cell lines with an apparent disruption to both transcripts for protein expression in a western blot.

To do this, membrane protein was extracted from the cell lines B, P, R, V, U, 1B, 1E, 1I, 1L, 1M, 1U, 1V and 1W. We also extracted parental Tango cell membranes to act as a control. We analysed for DAGLβ expression using a DAGLβ antibody (cell signalling) in a western blot. This antibody was raised against a peptide corresponding to the N-terminus of the enzyme, which is further downstream than the CRISPR target locus. Therefore, any disruption from NHEJ repair that leads to a frameshift in the sequence would result in an absent band in the western blot. As seen in Figure 6.20, there was a clear band at the expected size of ~ 74 kDa from

parental Tango cell membranes. None of the cell lines tested resulted in the WT band, or any band of a different size, indicating a high hit rate of DAGLβ disruption in these cell lines. Actin was used as a loading control, showing most of the membrane protein to be present (except clone 1M), albeit at different concentrations. However, none of the cell lines were loaded at concentrations lower than the control.

These results point towards our selected DAGLβ-inactive cell lines having a gross mutation in their DAGLβ sequence, which has probably led to a frameshift downstream of the target site, as evident from the absent band in the western blot. It was important at this stage to understand what effect these mutations have in the CB1-Tango assay. We therefore selected 4 cell lines (1B, 1E, 1I and 1U) to determine if firstly they maintained a Tango assay response to ACEA and secondly, whether we could stimulate eCB production in response to forskolin treatment.

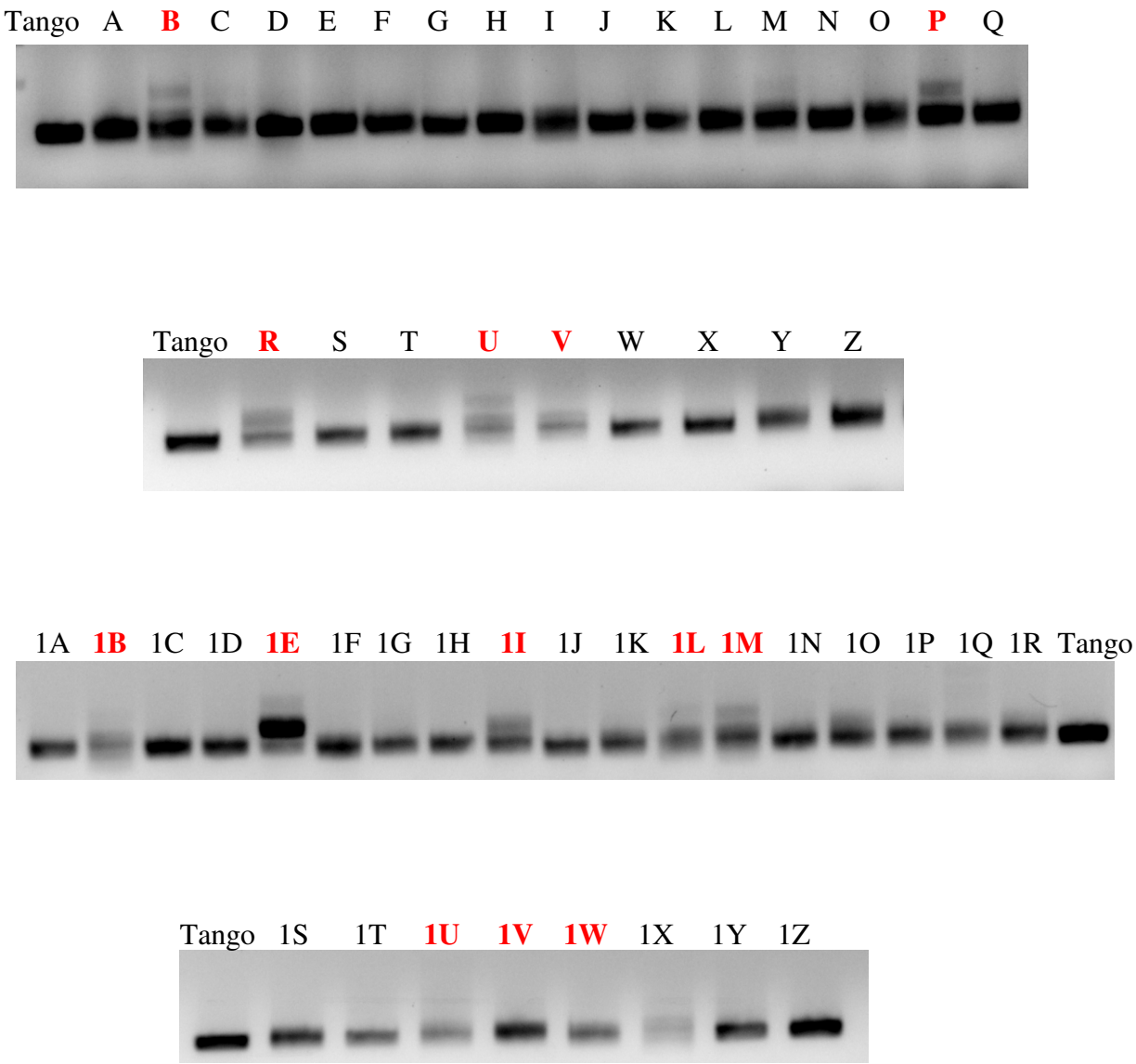

Figure 6.19 RT-PCR analysis of DAGLβ CRISPR cell lines highlights gross changes following Cas9 cutting at the targeted catalytic domain

RNA from candidate DAGLβ KO cell lines from each of the CRISPR sequences was extracted and reverse transcribed to cDNA. The cDNA was amplified using PCR and primers flanking the CRISPR cutting sites (as indicated below) and compared with control cell cDNA (Tango) in an agarose gel. Selected cell lines were chosen for further analysis in a western blot (red).

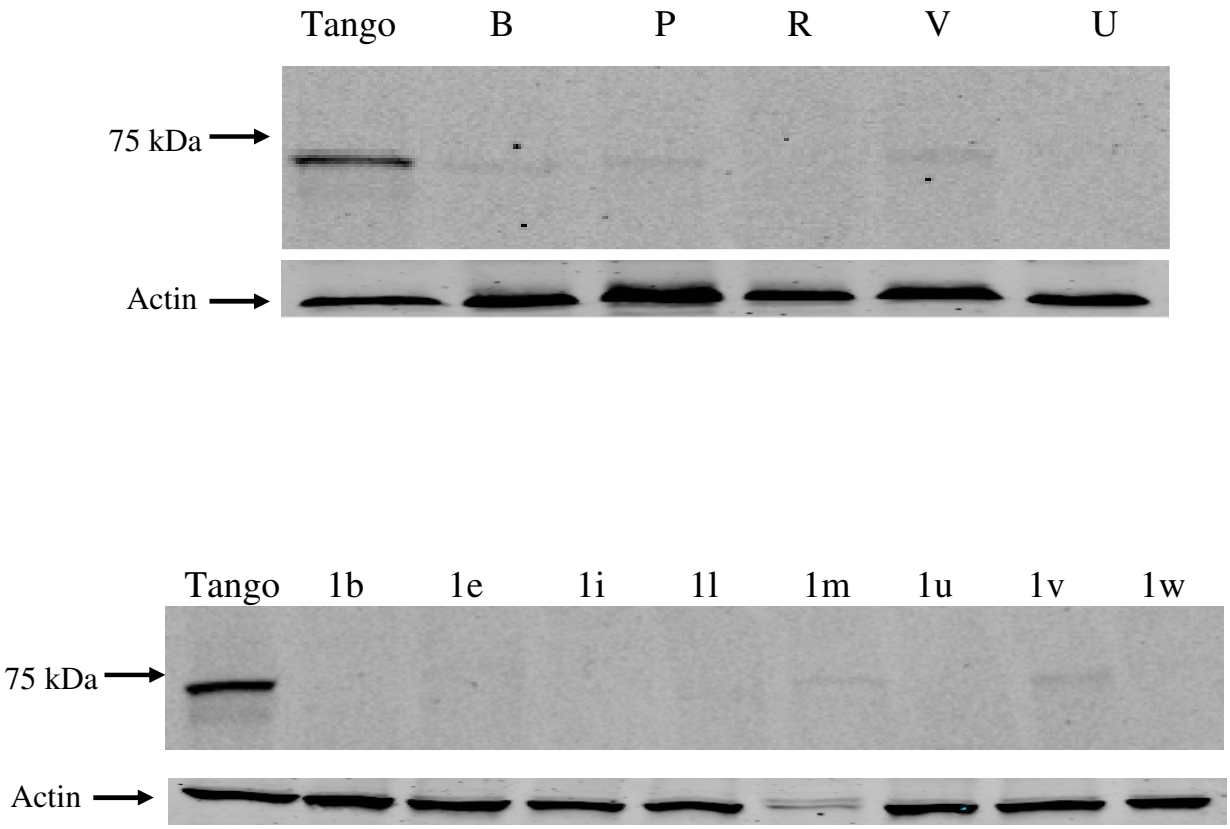

Figure 6.20 The DAGLβ antibody highlights the disruption caused by Cas9 in our candidate DAGLβ KO cell lines

Membrane protein was extracted from our candidate DAGLβ KO cell lines and from Tango cells as control. 20 µg of protein was analysed in a western blot and probed with a DAGLβ antibody (Cell Signalling). The blots were stripped and re-probed for actin to act as loading control (displayed under each blot). Control Tango membranes have a clear band at the expected size (~74 kDa), which is reduced or absent in all cell lines.

The CB1-Tango assay in the CRISPR/Cas9-treated cell lines

We had successfully disrupted the DAGLα catalytic triad in α2B cells. We also had apparently disrupted the catalytic domain of DAGLβ in these cells, as evident from the western blot. Therefore, we ensured that the Tango assay was still functional in these cell lines. To do this, 20,000 parental Tango, α2B and our candidate DAGLβ-inactive cell lines (1B, 1E, 1I and 1U) were plated in McCoy's medium containing 1% FBS for 48 h. Compounds were made up in the same medium containing 100 nM JZL195. Half the cells were treated with 10 μM AM251 for 30 minutes, before addition of 1 μM ACEA or media as control (+ JZL195) for a further 4 h. Fluorescence was detected using a FRET-enabled substrate, as described previously. The results were normalised to the control response in the presence of JZL195, set to 100%. Significant difference between the response and that in the presence of AM251 is indicated in Figure 6.21.

There was a substantial and highly significant response seen from ACEA in all cell lines. Importantly, the Tango assay response was maintained following disruption of both DAGLs. The background response in the presence of JZL195 appears greatly reduced in the case of the cell line 1B, which may indicate a reduction in eCB production. Therefore, how this affects eCB synthesis in response to forskolin treatment was next evaluated.

Figure 6.21 The background and ACEA responses in the Tango assay from our DAGL KO cells

20,000 cells (parental Tango, α2B and cells from 1B, 1E, 1I and 1U, as indicated) were plated in McCoy's medium containing 1% FBS and maintained for 48 h. Compounds were diluted in the same medium containing 100 nM JZL195. Half the cells were treated with 10 μM AM251 for 30 min before addition of control medium or 1 μM ACEA for a further 4 h. *Bla* expression was detected using a FRET enabled substrate, as per manufacturer's protocol. The results were normalised to the control response in the presence of JZL195, set to 100%. The data presented represents the mean of 8 replicate wells from 2 independent experiments ± SEM. Significant difference from the response in the presence of AM251 was established using the two-sided Student's t-test, as indicated below.

$p>0.05$*; $p>0.01$**; $p<0.001$, *** Student's t-test

Tango

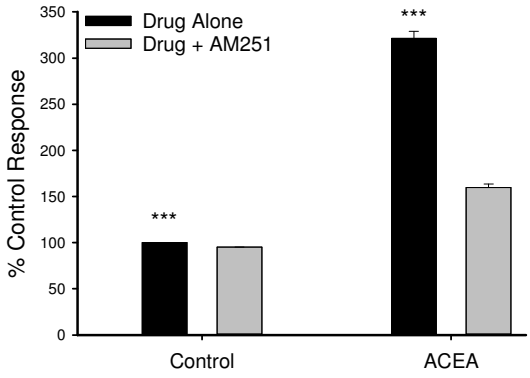

α2B

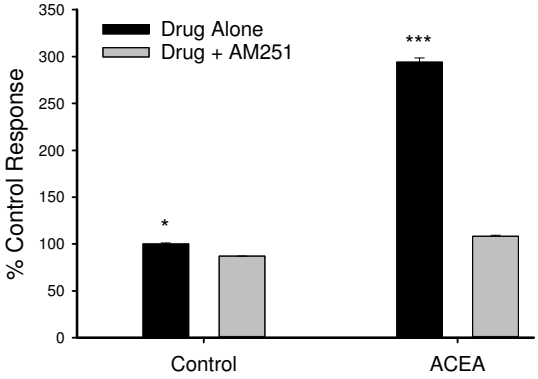

1B

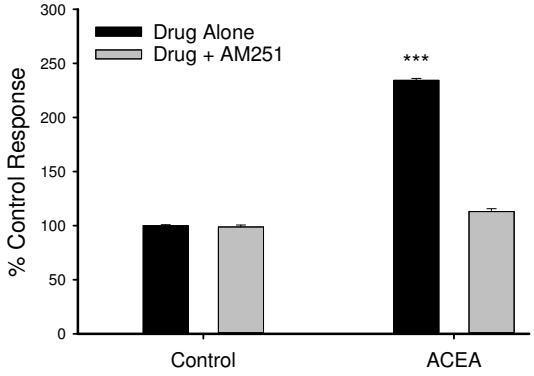

1E

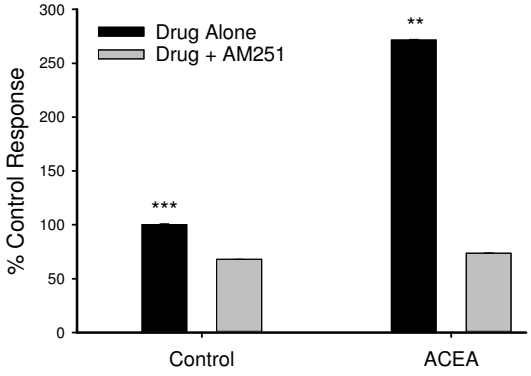

1I

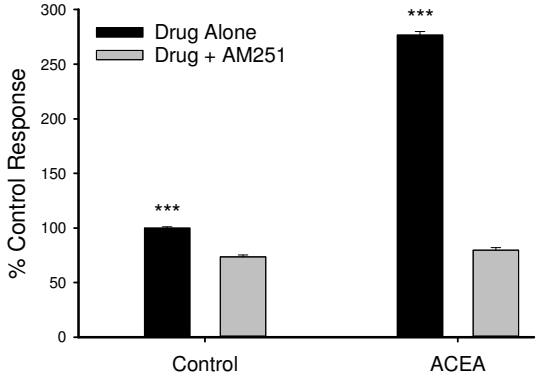

1U

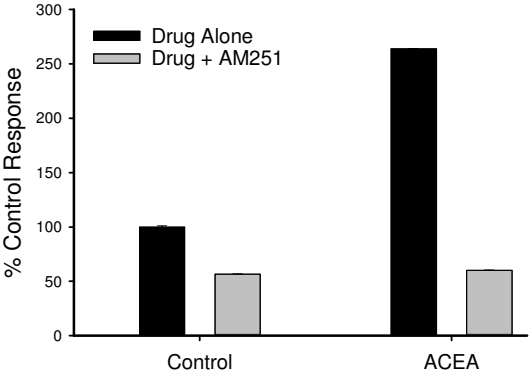

Response of the candidate DAGL-inactive cell lines to PKA activation

In order to determine the level of CB1 activation in response to PKA activation in our candidate cell lines, 20,000 Tango cells and cells from 1B, 1E, 1I and 1U were plated and maintained for 48 h, as described above. Compounds were diluted in McCoy's 1% medium containing 100 nM JZL195. Half the cells were treated with 10 μM AM251 for 30 minutes before addition of 10 μM forskolin to all wells for a further 4 h. Fluorescence was detected, as described above and the data was normalised to the control response, set to 100%.

As expected, there was a clear and highly significant response seen from parental Tango cells to forskolin, in the presence of JZL195 (Figure 6.22). In comparison, the response from 1B, albeit significant above the control response, was markedly reduced. The responses seen from the other cell lines, 1E, 1I and 1U were still > 50% of that from parental Tango cells. This may be a variation of cell line selection, or it may be that these cell lines are not clonal and still contain WT DAGLα / DAGLβ. To determine if WT transcripts were still present in our candidate cell lines, we performed sequence analysis of the Cas9 disruptions to the DNA.

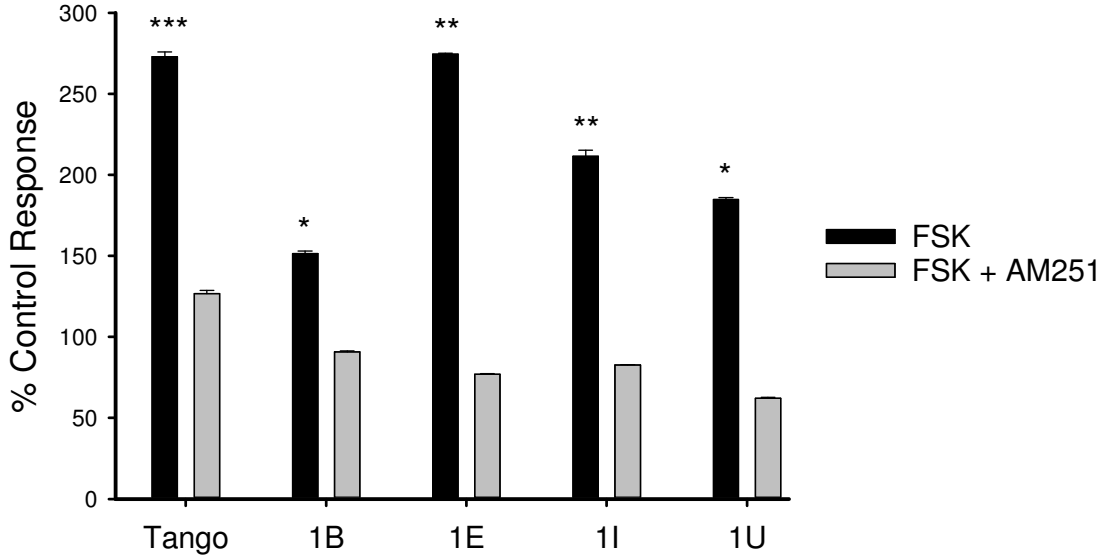

Figure 6.22 The candidate double DAGL KO cell lines still respond to forskolin in the presence of JZL195

20,000 cells (parental Tango cells and cell lines 1B, 1E, 1I and 1U, as indicated) were plated in McCoy's medium containing 1% FBS and maintained for 48 h. Compounds were diluted in the same medium containing 100 nM JZL195. Half the cells were treated with 10 µM AM251 for 30 min before addition of 10 µM forskolin (FSK) for a further 4 h. *Bla* expression was detected using a FRET enabled substrate, as per manufacturer's protocol. The results were normalised to the control response, set to 100%. The data presented represents the mean of 8 replicate wells from 2 independent experiments ± SEM. Significance was established using the two-sided Student's t-test, as indicated below.

$p<0.05$*; $p<0.01$**; $p<0.001$ ***; Student's t-test

Sequencing of the DAGL-inactive candidate cell lines

To understand how the forskolin responses in the Tango assay related to the disruptions caused by Cas9, we sequenced the DNA from each of the candidate cell lines 1B, 1E, 1I and 1U. To do this, we extracted RNA from these cells, reverse transcribed to cDNA and PCR-amplified the catalytic domain using the forward primer 5'– GGCTCTGGATCACAGGAAAG–3' (exon 8), the reverse primer 5'– GGAGACCCCTTGTGCTGGAC– 3' (exon 15) and Taq polymerase. The addition of a 'A' on the end of the sequence by Taq allowed us to TOPO clone and transform into *E.Coli*, as described previously (and in the methods section). 24 colonies were selected and sent to Source Bioscience for sequencing. The sequence of each allele was aligned with DAGLα WT sequence and the results are summarised in Table 6.2 – 6.5.

There were a large number of disruptions seen from treating the Tango cells with CRISPR/Cas9, demonstrating the efficiency of this genome editing technique. However, none of the cell lines we selected for sequencing were clonal, as each cell line had more than 2 sequencing results. Importantly, only clone 1I had results that aligned with WT DAGLβ (Table 6.4). Therefore, the response to forskolin in the other cell lines may have been due to the activity of eCB-producing enzymes other than the DAGLs.

It was clear that clone 1B's response to forskolin was greatly reduced in the Tango assay compared to parental Tango cells (Figure 6.22). From the sequencing results, it was apparent that this cell line did not contain any WT DAGLβ DNA (Table 6.2). Furthermore, most of the disruptions seen from the sequencing results caused frameshift mutations within the catalytic domain, except for the 78 bp deletion. This deletion is located in exon 9 of DAGLβ, which harbours the serine of the catalytic triad; therefore this disruption and all other disruptions seen render DAGLβ catalytically dead in these cells. As 1B showed a reduction in response to PKA activation, and had the least number of results from sequencing, this cell line will be subjected to further clonal selection. However, timeline for generating a clonal cell line and further testing was beyond the scope of this thesis.

Table 6.2 Summary of sequencing results from 1B cells

Clone 1B	# Results
1 bp insertion; 82 bp insertion	2
4 bp deletion; 128 bp deletion	1
4 bp deletion only	2
78 bp deletion	5
128 bp deletion	2
1 bp deletion	8
No alignment with WT DAGLβ, align with each other	2

Table 6.3 Summary of sequencing results from 1E cells

Clone 1E	# Results
6 bp Deletion	1
120bp insertion	3
120bp insertion; 128bp deletion	1
94bp insertion	1
1bp insertion; 128bp deletion	1
1bp insertion	6
128 bp deletion	1
1bp insertion; 82bp insertion	1
1bp insertion; 209bp insertion	1
78bp deletion	2
120bp insertion; 86bp insertion	3

Table 6.4 Summary of sequencing results from 1I cells

Clone 1I	# Results
Misalignment / 84 bp deletion	1
1bp insertion; 128 bp deletion	4
1bp insertion	8
1bp insertion; 41 bp deletion	1
14bp deletion; 128 bp deletion	2
WT	4
78bp deletion	2

Table 6.5 Summary of sequencing results from 1X cells

Clone 1X	# Results
No alignment at beginning (align with each other)	7
78bp deletion	3
1bp insertion	5
40bp insertion	2
1 bp insertion; 209 bp deletion	1
2 bp insertion	1

6.3 Summary & Conclusions

We have previously shown that we can report on eCB-dependent CB1 activation in the Tango assay. These cells express transcripts for both the DAGLs and are likely to also express other eCB-synthesising enzymes. The aim of this section therefore was to disrupt transcripts for each of the DAGL genes, with a view to also disrupting the non-DAGL component of the responses seen to forskolin, PMA and ionomycin in the Tango assay. Eliminating the activity of these enzymes and the DAGLs would provide us with a convenient method to study the structure-function relationship to DAGL activity and regulation.

There a number of tools currently used to disrupt gene expression, which traditionally has been achieved in cultured cells through RNA interference (RNAi). RNAi represses gene expression through sequence-specific degradation of mRNA. However, RNAi is limited by its off-target effects and by the partial and / or transient nature of gene suppression, which is often insufficient to create noticeable changes in phenotype (Qiu *et al.*, 2005; Gupta & Musunuru, 2014). Consequently, the ability to precisely edit DNA sequences specifically has obvious advantages.

As presented in the general introduction, 'precise genome editing' or 'genome engineering' is currently achieved through one of three techniques; ZFNs, TALENs and CRISPR/Cas9. ZFNs and TALENs comprise chimeric nucleases, composed of sequence-specific DNA-binding modules linked to a nonspecific DNA cleavage (Fok1) domain (Gaj *et al.*, 2013). In contrast, CRISPR/Cas9 is guided by small gRNAs to a specific target locus. This technology is derived from the type II CRISPR/Cas9 system, an adaptive immune response in bacteria which functions by Cas9 recognizing and cleaving foreign DNA through gRNAs (Horvath & Barrangou, 2010; Jinek *et al.*, 2012; Wiedenheft *et al.*, 2012). The system has been manipulated to target mammalian genes (Cho *et al.*, 2013; Mali *et al.*, 2013b) and has successfully been used to disrupt specific DNA sequences, both in human and non-human cell lines (Cho *et al.*, 2013; Jinek *et al.*, 2013; Yang *et al.*, 2014) and more recently in U2OS cells (Feng *et al.*, 2015). New CRISPR/Cas9 complexes can be

prepared simply by replacing the gRNA sequence; therefore this is a markedly easier and cheaper method than ZFNs or TALENs and is why we choose this method to disrupt DAGL activity in the Tango cells.

Our initial approach was to use CRISPR/Cas9 to target both the DAGLs simultaneously. From the gRNA sequences we designed, cr2 was deemed the most successful to target both DAGLα and DAGLβ through examination in the SURVEYOR Cel I assay (Figure 6.3). Even though we stimulated NHEJ at the 5' end of the sequence, none of the cell lines had complete KO of DAGL transcripts in the Taqman assay (Figure 6.4).

At the time this study began, CRISPR/Cas9 was a relatively new genome editing technique and there was little evidence for the effective use of CRISPR/Cas9 in U20S cells, although at the time specific gene disruption had been achieved in Human Embryonic Kidney (HEK) cells (Cho *et al.*, 2013; Cong *et al.*, 2013; Jinek *et al.*, 2013; Mali *et al.*, 2013b). To explore the capabilities of CRISPR/Cas9 and stimulating the HDR DNA repair pathway, we did a parallel study using a 'nickase' strategy. This involved a 'double-nicking' approach, consisting of using a D10A mutant Cas9 (Cas9n) which renders it as a single-strand endonuclease. NHEJ can be stimulated using a pair of offset gRNAs, appropriately positioned at the target sequence (Jinek *et al.*, 2012; Shen *et al.*, 2014) and introduction of a repair template stimulates the HDR repair pathway (Smithies *et al.*, 1985; Thomas *et al.*, 1986; Ran *et al.*, 2013b). Although WT Cas9 is more efficient at mediating homologous recombination than Cas9n, at the time of this study, HDR had only detected in HUES9 cells when using a pair of Cas9ns (and not WT Cas9) (Ran *et al.*, 2013b). Due to the lack of literature and experience using CRISPR/Cas9 in U2OS cells, we used Cas9n to ensure stimulation of the HDR pathway and subsequent introduction of a resistance gene to the antibiotic, blasticidin. Therefore, our nickase strategy not only allowed us to disrupt DAGLα, it also allowed us to positively select cell lines through introduction of blasticidin into the medium (Figure 6.5).

Through analysis in the Taqman assay and western blot, we saw similar results to our initial strategy, whereby the selected cell lines that appeared to have reduced DAGLα transcripts (B, C and X3) still had apparent undisrupted protein translation, albeit with an unreliable DAGLα antibody (Figure 6.6 B).

The Taqman assay provided by Life Technologies is a 'best coverage' assay. This is used to detect transcripts of all predicted splice variants of the gene of interest, and so the primer sequences for the real-time PCR reaction are not specified. To investigate our cell lines further, we designed primers flanking the insertion site of the blasticidin-resistance gene. The results from the RT-PCR on DNA from the cell line J gave us the most confidence. Firstly, there was a large insertion (corresponding to the blasticidin-resistance gene). Importantly, there was no resulting band at the predicted WT size, indicating both alleles had been disrupted in this cell line. However, analysis in a western blot revealed that all the bands detected in WT Tango cells were undisrupted in cell membranes from J (Figure 6.7). Furthermore, transcripts encoding for the catalytic domain were still present (Figure 6.8 B). We hypothesised that there may be a splicing event occurring across the site of the inserted gene, which would allow the downstream sequence to be translated.

Considering the difficulties we were experiencing in disrupting the full length DAGL sequence downstream of the CRISPR targeting site, we re-focussed our efforts to target the catalytic domain. We proposed that if we targeted just one of the amino acids of the catalytic triad, then DAGL activity would be eliminated and this has been shown in previous reports (Bisogno, 2003; Pedicord *et al.*, 2011). By using the PNPB membrane assay we confirmed that DAGLα is unaffected in the presence of a catalytically-dead version of DAGLα (Figure 6.10) and therefore this strategy should not interfere with future mutagenesis studies.

We targeted DAGLα catalytic domain using 3 new gRNA sequences (Figure 6.11) and CRISPR 2 cuts directly at the serine of the catalytic triad. It may be that targeting Cas9 to a critical residue for a protein's function results in more severe forms of NHEJ, as this gRNA resulted in the highest number of obvious disruptions

by Cas9 (Figure 6.12). As a result, we selected 2B (termed α2B) for sequencing, which had both alleles disrupted to eliminate DAGLα activity (Figure 6.13 – 6.16).

To generate a DAGL-inactive cell line, we targeted the catalytic domain of DAGLβ in α2B cells. Through screening the selected cell lines treated with CRISPR/Cas9 using RT-PCR (Figure 6.19) and subsequently western blot analysis (Figure 6.20), we selected 4 cell lines to test in the Tango assay. The eCB tone (as evident from a lack of reduction seen in the presence of AM251) seen in 1E, 1I and 1U cells appeared greater than that in parental Tango cells, which may be a result of cell line selection or possibly the presence of WT transcripts (Figure 6.21). While all cell lines maintained a robust response from ACEA, only 1B showed a reduction in eCB tone. 1B also resulted in a reduced response from PKA activation, which was ~ 50% of that seen in control Tango cells (Figure 6.22). This may indicate a lack of DAGL activity, with the forskolin response seen possibly being a result of the activity of other eCB-synthesising enzymes.

The DNA from these cell lines was analysed by Sanger sequencing, which lead to a number of results for each, indicating none of the cell lines selected were clonal (Table 6.2 – Table 6.5). From these results, only 1I contained WT DAGLβ transcripts. Results from 1B indicated that these cells had the least number of transcripts, indicating that generating a clonal cell line from this pool may be achieved relatively easily. These cells also had the largest decrease in basal eCB tone and response to forskolin treatment in comparison to parental Tango cells. Therefore, next steps following this study would be to isolate a single clonal cell line from 1B for further investigations, with a view to disrupting the other aforementioned eCB-producing enzymes to completely remove the eCB response (to forskolin, PMA and ionomycin) in CB1-Tango cells. This would provide us with a 'parent' cell line in order to study the structure of DAGL in relation to its function; these points are explored in more detail in the general discussion.

CHAPTER 7. DISCUSSION

7.1 Therapeutic potential of the eCB system

Until recently, research into the CB system was a relatively small field. The first breakthrough that opened the field was the discovery of the major psychoactive component of the cannabis plant, Δ^9-THC about 50 years ago (Mechoulam & Gaoni, 1965). However, it is only in the last two-three decades that great advances have been made, such as the identification and cloning of the receptors activated by Δ^9-THC, CB1 and CB2 (Matsuda *et al.*, 1990; Munro *et al.*, 1993), followed by the isolation of endogenous ligands that activate them, 2-AG and anandamide (Devane *et al.*, 1992; Mechoulam *et al.*, 1995). This has led to an increased interest in specifically targeting the eCB system for therapeutic purposes, particularly as cannabis was known to induce anti-nociception or analgesia. However, targeting the eCB system has proved difficult due to the widespread expression of the CB receptors throughout the body. For example, an anti-obesity drug SR141716A, a CB1 antagonist commercially known as Rimonabant (Pertwee, 2005; Le Foll *et al.*, 2009), was withdrawn from the market following links with anxiety and suicide, demonstrating the severity of undesired effects associated with targeting the CB1 receptors in the CNS (Le Foll *et al.*, 2009). However, the therapeutic potential of the eCB system is still generating a great deal of interest for areas such as neuropathic pain (Lau & Vaughan, 2014), liver disease (Basu *et al.*, 2014) and for the eCB's anti-proliferative effects in cancer (Mimeault *et al.*, 2003), with the idea of designing more specific drugs to minimize unwanted effects.

The enzymes responsible for the synthesis of 2-AG, the DAGLs, have been cloned (Bisogno, 2003) and deleted in transgenic mice (Gao *et al.*, 2010; Tanimura *et al.*, 2010), which has helped establish these enzymes as regulators within the eCB system. These efforts were also important in establishing DAGLα as being responsible for virtually all the 2-AG in the brain, as well as DAGLβ generating

more than 90% of 2-AG in the liver (Gao *et al.*, 2010). The specificity of the individual DAGLs over the control of 2-AG synthesis is in vast contrast to anandamide, as identifying a specific enzyme for anandamide's production has remained elusive; no significant reduction in anandamide was seen in animals lacking enzymes thought to be responsible for anandamide synthesis, such as knockouts of NAPE-PLD, GDE1 or both (Leung *et al.*, 2006; Simon & Cravatt, 2010b).

2-AG is produced following elevations in calcium in the postsynaptic neuron by hydrolysis of DAG by the action of the DAGLs. The released 2-AG acts retrogradely to activate the presynaptic CB1 receptor to suppress further neurotransmitter (NT) release. DAGL-generated 2-AG also plays a role in fasciculated axonal growth in the developing brain (Berghuis *et al.*, 2007; Keimpema *et al.*, 2010; Wu *et al.*, 2010), as well as in adult neurogenesis (Goncalves *et al.*, 2008; Gao *et al.*, 2010). 2-AG is then degraded by the action of MAGL, although the action of COX-2 may also play a role (Beltramo & Piomelli, 2000; Kozak *et al.*, 2000; Piomelli *et al.*, 2000; Dinh *et al.*, 2002; Muccioli *et al.*, 2007; Long *et al.*, 2009a; Schlosburg *et al.*, 2010). FAAH and ABHD12 have also been shown to have 2-AG hydrolytic activity (Long *et al.*, 2009a; Long *et al.*, 2009b). However, there remains stronger evidence for a role for ABHD6 alongside that of MAGL. For example, ABHD6 knockdown has been shown to increase the efficacy of 2-AG to stimulate CB2-mediated cell migration in a microglial cell line. Immunohistochemical studies revealed ABHD6 localizes to sites of 2-AG generation, including post-synaptic dendrites of glutamatergic neurones and some GABAergic interneurones (Marrs *et al.*, 2010). Being a member of the α/β-hydrolase fold family, the active site of ABHD6 is predicted to face the cell interior and is therefore well suited to guard the intracellular pool of 2-AG. This been suggested to provide the eCB system with a greater capacity to control the duration and magnitude of 2-AG signalling (Savinainen *et al.*, 2012).

In DAGL KO animals, there was a parallel reduction in AA alongside 2-AG. AA acts as a precursor for the production of the major eicosanoids (prostaglandins, leukotrienes, thromboxanes), which are potent inducers of inflammation (Srinivasan & Kulkarni, 1989; Tilley *et al.*, 2001; Kozak *et al.*, 2002). MAGL hydrolysis of 2-

AG generates an arachidonate precursor pool for neuroinflammatory prostaglandins which have been shown to promote neuroinflammation (Nomura *et al.*, 2011), a process associated with a number of neurodegenerative diseases, including Alzheimer's disease (AD), Parkinson's disease (PD) and multiple sclerosis (MS) (reviewed in (Glass *et al.*, 2010)). In fact, activation of CB receptors has been associated with anti-inflammatory and neuroprotective effects on the level of neurodegeneration that occurs as a result of the inflammatory insults seen in MS (Baker & Pryce, 2008). Furthermore, pharmacological or genetic inhibition of MAGL that increases 2-AG, with parallel reductions in AA and eicosanoid production, has highlighted non-eCB roles for the DAGLs in the context of neuroinflammation (Schlosburg *et al.*, 2010; Nomura *et al.*, 2011). For example, in mouse models of AD, MAGL KO animals had decreased AA and eicosanoid levels, as well as a reduction in microglia and astrocyte activation, inflammatory cytokines and amyloid plaques (the latter being one of the hallmarks of the disease), where MAGL inhibition exhibited its effects through a reduction in prostaglandin production, rather than through enhanced eCB signalling (Piro *et al.*, 2012).

Similarly in PD, genetic or pharmacological inhibition of MAGL prevents MPTP increases in AA and eicosanoids as well as neuronal loss, showing that in the brain, the production of pro-inflammatory prostaglandins is controlled by hydrolysis of 2-AG by MAGL (Nomura *et al.*, 2011). However, prolonged MAGL inactivation causes profound alterations to the brain eCB system, including physical dependence, impaired eCB-dependent synaptic plasticity and desensitised brain CB1 receptors (Schlosburg *et al.*, 2010). Genetic or pharmacological DAGLβ inactivation resulted in elevated 2-AG and corresponding reductions in AA, demonstrating 2-AG synthesis as a major precursor pro-inflammatory eicosanoids in the brain and peritoneal macrophages (Hsu *et al.*, 2012). Therefore, the DAGLs may be better targets for therapeutic intervention.

The potential benefit of enhancing DAGL activity was highlighted in a study examining Fragile X retardation protein, which has linked the eCB system to autism. 2-AG, enhanced by MAGL inhibition, repaired synaptic defects seen in Fragile X KO mice (Jung *et al.*, 2012). Beyond the nervous system, increased CB1 and

DAGLβ expression, alongside 2-AG levels were seen in the liver of mice in a model of alcohol-induced liver steatosis, also known as fatty liver disease. When the CB1 receptor was disrupted either pharmacologically or genetically, these effects were reduced (Jeong *et al.*, 2008). As DAGLβ activity accounts for the majority of 2-AG produced in the liver (Gao *et al.*, 2010), targeting DAGLβ may have therapeutic benefit in fatty acid liver disease.

These studies have highlighted the role of the DAGLs in regulating eCB function and also AA and eicosanoid production. However, very little is known about the regulatory mechanisms that affect their ability to hydrolyse DAG in order to provide 2-AG as a precursor for AA synthesis, as well as the endogenous ligand for CB1 activation. Studying regulation of the DAGLs will further our knowledge of their physiological and possible patho-physiological roles in both the CNS and the periphery. As the DAGLs demonstrate different tissue contributions towards 2-AG production (Gao *et al.*, 2010), targeting them individually may be ideal to alter their activity in a specific tissue relating to a disease. Recently, a compound was developed known as KT109, which displays more than 50 times greater potency for DAGLβ over DAGLα, highlighting that differences between the two enzymes could be exploited for a therapeutic strategy (Hsu *et al.*, 2012). Therefore, understanding how their structure relates to their function and whether/how they are regulated, could allow design of specific therapeutics.

7.2 Identifying structural features of the DAGLs and their functions

As presented in this thesis, we examined the structure of the DAGLs in order to determine the role of a post-translational modification (PTM) in regulating activity. We took a bioinformatics approach to assess the wealth of information freely available online. We gathered this information together to determine if there is sufficient evidence for a regulatory role of phosphorylation (or other type of PTM) in DAGL activity.

Through homology modelling of the crystallised fungal DAGL to drosophila, and drosophila to the human DAGL, our group identified 4 TM domains, linked by helices (2 intracellular and 2 extracellular). The TM domains lead onto an intracellular catalytic domain, whose structure is a member of the α/β hydrolase fold family of enzymes (Reisenberg *et al.*, 2012). Common structural features of this enzyme family can tolerate considerable-sized inserts at certain locations (Nardini & Dijkstra, 1999). In the case of the DAGLs, two substantial inserts were identified; a cysteine-rich insert and a lid-like structure that we have termed the 'regulatory loop'.

The cysteine rich insert is a potential palmitoylation site and evidence for palmitoylation of the DAGLs was provided in rat brain synaptosomes, rat cortical neurons and Jurkat cells (Kang *et al.*, 2008; Martin & Cravatt, 2009). This insert therefore may act to regulate DAGL activity by affecting its localization at the membrane, and subsequent access to the substrate. The second insert, the regulatory loop, may constitute a common lid-like feature that is seen in many lipases of the α/β hydrolase fold family of enzymes, where it is responsible for interfacial activation, a process whereby activity of lipases is enhanced upon contact with a lipid–water interface and is believed to trigger the opening of the lid (Nardini & Dijkstra, 1999; Holmquist, 2000). The regulatory loop is in the right position to shield DAG access to the catalytic site and also harbours a highly conserved 'signature motif' (Reisenberg *et al.*, 2012).

7.3 Regulatory mechanisms for the DAGLs

We have proposed phosphorylation as a regulator of DAGL activity that determines the position of the regulatory loop in the 'open' or 'closed' conformation. The activity of many lipases is controlled by phosphorylation (Kurat *et al.*, 2009; Gresset *et al.*, 2010; Lampidonis *et al.*, 2011) by increasing/decreasing an enzyme's activity, or affecting protein-protein interactions (Johnson & Lewis, 2001; Salazar & Hofer, 2009). For example, HSL is phosphorylated by PKA, resulting in ~ 2-fold increase in

activity and all phospho-sites are located within the regulatory lid. This has led to the model whereby, at least *in vitro*, HSL is phosphorylated by PKA in response to certain stimuli (Holm *et al.*, 1994; Krintel *et al.*, 2009; Lampidonis *et al.*, 2011).

The evidence for the role of phosphorylation in regulating the activity of HSL gives us a working model for studying possible regulatory mechanisms of the DAGLs, based on its key structural features. Furthermore, there is ample evidence for the role of PKA and PKC in 2-AG generation. For example, DAGL from brain microsomes was shown to be phosphorylated by PKA (Rosenberger *et al.*, 2007) and phosphorylation of bovine rod membranes by PKA resulted in a ~70% increase in DAGL activity (Perez Roque *et al.*, 1998). Similarly, PKA and PKC activation stimulated 2-AG synthesis (Vellani *et al.*, 2008).

We have identified key phospho-sites through cross-examination of the DAGLs' sequences between different online databases. All of those identified in DAGLβ are within the catalytic domain and are therefore well positioned to regulate activity. Surprisingly, these sites are not conserved in the sequence of DAGLα. However, 5 of the 15 amino acids in the corresponding region are serine/threonine and so this does not rule out identification of phosphorylation sites within this region in the future. In the case of DAGLα, only one site was identified within the regulatory loop (T560), while the rest are located within the tail domain. While the tail is dispensable in terms of activity, it may still serve to regulate positioning of the regulatory loop, as one report showed that phosphorylation by CaMKII decreased DAGLα activity by ~ 40% (Shonesy *et al.*, 2013). This is surprising considering that previous reports have shown phosphorylation to increase DAGLα activity. However, CaMKII signalling has been shown to allow stimuli-specific spatiotemporal patterns, which may be important for synapse-specificity of synaptic plasticity. CaMKII therefore may exert its activity to control DAGLα activity at specific synapses (Lee *et al.*, 2009). However, the role of CaMKII in the regulation of DAGLα in a more physiological context remains to be seen.

The DAGLs are therefore potentially phosphorylated at a number of sites, and this may be important for regulation. Furthermore, stimuli observed to increase

production of 2-AG levels in cells/tissues can also activate various kinases, as discussed below.

7.4 2-AG levels increase following stimuli that activate protein kinases

There have been numerous reports demonstrating an increase in 2-AG production following various stimuli. For example, cerebellar granular neurons increased their 2-AG synthesis in response to ethanol, ionomycin and glutamate (Basavarajappa *et al.*, 2000). 2-AG synthesis was enhanced in astrocytes by endothelin 1, ionomycin and ATP (Walter & Stella, 2003; Walter *et al.*, 2004). Stimulation was also seen in cortical neurons in response to glutamate and NMDA (Stella *et al.*, 1997; Stella & Piomelli, 2001), as well as by ionomycin in neuroblastoma cells (Bisogno *et al.*, 1997a). The DAGLs are the principle enzymes responsible for 2-AG synthesis (Gao *et al.*, 2010; Tanimura *et al.*, 2010) and are therefore the likely enzymes to be responsible for this increase in 2-AG.

The calcium ionophore, ionomycin (and other stimuli) is likely to be mimicking the increase in intracellular calcium seen as a result of specific signals which open calcium channels either in the cell membrane or in the endoplasmic reticulum. Activated GPCRs, such group 1 and 5 mGluRs, form GTP-Gαq complexes (Willard & Koochekpour, 2013). The canonical effector of Gαq signalling is the activation of PLCβ, although the βγ subunits of G proteins can also stimulate PLCβ (Rozengurt, 2007). Active PLCβ catalyses the hydrolysis of PIP_2 to produce inositol 1,4,5-triphosphate (IP_3) and DAG. DAG activates PKC, while IP_3 triggers calcium mobilization from endoplasmic reticulum stores leading to an increase of intracellular calcium concentration (Parekh & Putney, 2005; Cattaneo *et al.*, 2014) However, a recent review has commented on there being one or more Gαq-dependent, PLCβ-independent effectors (Sanchez-Fernandez *et al.*, 2014). For example, the activation of the glycogen synthase kinase-3 (GSK-3) has been shown to be promoted by Gαq independently of PLCβ (Fan *et al.*, 2003). However, other

PLCβ-independent effectors have yet to be identified (Sanchez-Fernandez *et al.*, 2014). Gαq signalling might stimulate these other effectors as well as increase intracellular calcium in tandem to mediate its effects. This PLCβ-independent element of Gαq signalling may encompass the unidentified signalling pathway that results in phosphorylation of the DAGLs.

7.5 Establishing CB1-Tango cell lines stably expressing DAGLα and DAGLβ

The eCB system is regulated at the level of synthesis and degradation of the eCBs, and our aim was to study the regulatory mechanisms of the DAGLs. Activity of the DAGLs is commonly assessed by measuring the production of 2-AG. However, this is challenging for a few reasons; for example, 2-AG isomerizes spontaneously to its biologically inactive analogue 1-arachidonoyl glycerol (1-AG) (Zoerner *et al.*, 2012; Balgoma *et al.*, 2013). It also requires an expensive and elaborate laboratory setup for LC/MS, as well as user expertise (Balgoma *et al.*, 2013). Other groups have shown that, in general, to be able to measure robust activity there is a requirement to overexpress the DAGLs (Bisogno, 2003; Shonesy *et al.*, 2013; van der Wel *et al.*, 2015). These assays have generally been limited to studies that aim to directly measure DAGL activity for the purpose of developing new inhibitors (Hoover *et al.*, 2008; Ortar *et al.*, 2008; Bisogno *et al.*, 2009; Hsu *et al.*, 2012; Bisogno *et al.*, 2013)

As described in the thesis, we have developed a CB1-Tango (U2OS) cell line to over express DAGLα and DAGLβ. The Tango cells harbour a recombinant assay system to measure CB1 activation. Using the Tango cells allows us to try to develop an assay to measure DAGL-dependent CB1 activation. Provided an appropriate stimulus is given, theoretically DAGLα/β hydrolysis of DAG would produce 2-AG thereby activating the CB1 receptor. The overexpressed DAGLα/β may or may not be required to measure this response as there are endogenous DAGLs expressed in the cells and enzyme levels may not be rate-limiting. However, given that this in itself is an important question, we decided to generate the overexpressing cell lines.

Previous attempts to reconstitute eCB-mediated CB1 activation was shown in isolated rat sympathetic neurons. Transfected mGluR5a and CB1 produced modest, but variable intracellular calcium inhibition (in the same neuron) following L-glutamate application. However, when DAGLα was recombinantly expressed, L-glutamate resulted in robust intracellular calcium influx inhibition, consistent with mGluR5-mediated 2-AG biosynthesis, transport, and subsequent activation of CB1 receptor (Won *et al.*, 2009). This study demonstrated a gain of function assay, whereby the transfected DAGLα resulted in a larger and more robust response to L-glutamate compared to control cells. Similarly, we generated a Tango cell line overexpressing DAGLα (V5α11) and a cell line overexpressing DAGLβ (V5β4) to determine if we could measure a gain of function response in the Tango assay.

The natural substrate, DAG is generally found associated to the membrane (Goni & Alonso, 1999). Consequently, the DAGLs are likely to orientate themselves at the membrane to increase accessibility of their substrate to the catalytic domain. When assessing expression patterns of the transfected DAGLs, DAGLα staining revealed expression throughout the cell surface. Surprisingly, DAGLβ expression appeared punctated and perinuclear. This observation was also made by Piomelli's group, where overexpression in mouse neuroblastoma cells showed DAGLβ to be associated to intracellular structures, rather than at the plasma membrane (Jung *et al.*, 2007). We confirmed the location of DAGLβ in our V5β4 cells to be localised to the Golgi (thesis of Praveen Singh, Prof. Doherty lab). The functional significance of this, and relevance to 2-AG mobilisation, is unknown. However, DAGLβ localisation in V5β4 cells may also be due to an artefact of overexpressing the enzyme.

When confirming DAGLα and DAGLβ expression at the membrane, the bands detected in a western blot were at slightly larger molecular weights than is predicted for each DAGL (~120 kDa for DAGLα, ~75 kDa for DAGLβ) (Bisogno, 2003), perhaps owing to their V5 tag. However, a previous study using a V5-tagged version of DAGLα revealed a band at ~ 116 kDa, albeit in HEK293 cells (Shonesy *et al.*, 2013). Although the DAGLα antibody did not reliably detect endogenous

expression, we concluded that the Tango cells express DAGLβ as well as RNA transcripts for both the DAGLs.

Previously, a membrane assay was developed as a convenient method to screen for inhibitors of DAGLα (Pedicord *et al.*, 2011). Using the reported surrogate substrates, PNPB and DiFMUO, we showed we could measure activity from the transfected DAGLα and that this could be inhibited by the DAGL inhibitors THL, OMDM and RHC-80267, with the only target these inhibitors compounds having in common being DAGL (Ortar *et al.*, 2003; Hoover *et al.*, 2008; Ortar *et al.*, 2008). Although these substrates did not report on activity of the transfected DAGLβ, another surrogate substrate, Enzchek has been reported that may detect activity of this enzyme (Basu *et al.*, 2011). Further development of the membrane assay would be to determine whether these substrates could report on DAGL in the context of a live cell. This would enable direct measurement of DAGL activity in both live cells as well as in membrane preparations, allowing aspects such as membrane permeability to be factored into kinetics of the different synthetic substrates. Work on developing this assay in our lab is ongoing.

Although we could measure activity from the transfected DAGLα, the size of the substrates meant they might not report on the position of the regulatory loop. The surrogate substrates are substantially smaller than DAG and may be able to access the active site irrespective of the loop's conformational position. In support of this, treatments aimed at phosphorylating the DAGLs, such as kinase activation, did not alter hydrolysis of either substrate in a live cell assay (data not shown; work completed with Dr. Praveen Singh, unpublished data). Therefore it appears that the catalytic site of DAGLα is consistently active, and shielding by the regulatory loop is what regulates DAG hydrolysis, akin to the active catalytic site of GL, where substrate access is limited by the position of the regulatory lid (Miled *et al.*, 2003).

The fact that no transgenic DAGLβ activity could be detected using these substrates was surprising considering that DAGLβ is more highly expressed in V5β4 cells than DAGLα is in V5α11 cells. This might demonstrate different kinetics between the two enzymes, whereby DAGLα is capable of hydrolysing these substrates and

DAGLβ is not. If this were the case then there is certainly potential for specific therapeutic intervention of one DAGL over the other. This potential was highlighted by the discovery of two compounds, KT109 and KT172. These compounds were shown to lower 2-AG, as well as AA and eicosanoids, in mouse peritoneal macrophages. IC_{50} values of 2.3 and 0.14 μM were reported for inhibition of recombinant DAGLα by KT109 and KT172, respectively. In comparison, IC_{50} values of 0.04 and 0.06 μM for KT109 and KT172 respectively were reported for DAGLβ inhibition. KT109 can therefore be considered an isoform-selective inhibitor of DAGLβ, whereas KT172 exhibits similar activity against both DAGLα and DAGLβ (Hsu *et al.*, 2012). As the DAGLs are expressed at different levels by different tissues, developing specific compounds could lead to therapeutic intervention with less undesired effects.

As discussed, there is substantial evidence that phosphorylation can change the activity of the DAGLs and that this results in an increase in 2-AG production. The limitations of using the surrogate substrates means we were unlikely to detect any changes in DAGL activity in the membrane assays. However, by establishing their overexpression in the Tango cells, we intend to develop a DAGL-dependent CB1 activation assay using these cell lines in the future.

7.6 Detecting eCB activation of CB1

At the outset of the project we recognised that eCBs other than 2-AG might be active in the CB1-Tango assay. Based on this our strategy was to try to establish a robust eCB-dependent response in the cells with a view to then determining which (if any) of the known eCB synthesising enzymes mediated the response. In this context, the relationship between 2-AG synthesis and CB receptor activation is not well established and might be governed by other factors, such as rapid 2-AG hydrolysis by MAGL and/or ABHD6.

Recently a natural substrate assay has been developed, whereby 2-AG production is measured as a result of DAGLα hydrolysis of SAG (van der Wel *et al.*, 2015). At the outset of this study we wanted to develop an assay that measures eCB-dependent activation of the CB1 receptor, rather than eCB production per se. This is because it is likely that there are metabolic as well as signalling pools of the eCBs, and we wanted to focus on the signalling pools. For this purpose, we used the CB1-Tango assay. This assay uses U2OS cells (osteosarcoma cell line) overexpressing the CB1 receptor, which has been fused to a non-native transcription factor at its C-terminus. This is separated from the receptor by a linker containing a protease cleavage site. Upon receptor activation, β-Arrestin 2, fused to a non-native protease, is recruited. The protease acts on the cleavage site releasing the transcription factor, activating a mammalian-optimised β-lactamase (*bla*) reporter gene in the nucleus (Barnea *et al.*, 2008; van der Lee *et al.*, 2009). β-lactamase activity is then monitored using a FRET–enabled substrate (Zlokarnik *et al.*, 1998), thereby directly reporting on CB1 activation.

By establishing CB1-Tango cell lines that stably and robustly express the DAGL transgenes (V5α11 and V5β4), our aim was not only to increase our chances of being able to measure DAGL-dependent CB1 activation, but to also address the question as to whether the enzyme level is rate limiting. This is similar to an approach described previously, where reconstitution of DAGLα provided a gain-of-function assay, thereby demonstrating eCB-mediated signalling in rat neurons (Won *et al.*, 2009). However, reconstituting the pathway in primary neurons is not amenable to moderate throughput assays, which we developed to evaluate various stimuli that could potentially induce eCB-CB1 activation.

PKA and PKC are two kinases implicated in stimulating 2-AG synthesis in cells and they can be activated synthetically through treatment with forskolin and PMA respectively. 2-AG levels increased approximately 3-fold when HEK293 cells were treated with forskolin or PMA, a response that was blocked when these kinases were inhibited (Vellani *et al.*, 2008). However, these stimuli can also result in production of anandamide. For example, glucocorticoids cause rapid synthesis of both anandamide and 2-AG in neuroendocrine cells of the hypothalamus (Di *et al.*, 2003;

Malcher-Lopes *et al.*, 2006). Moreover, anandamide synthesis can also be stimulated by calcium (Di Marzo *et al.*, 1994; Cadas *et al.*, 1997; Schmid, 2000; Leung *et al.*, 2006). We therefore sought to determine whether we could stimulate eCB activation of CB1, with a view to extrapolating the DAGL-dependent portion of the response.

No basal eCB tone was detected in this assay, nor was one revealed when MAGL was inhibited by JZL184. The lack of eCB tone observed in these cells might reflect a lack of substrate, or perhaps substrate is available but unable to access the active site of the enzyme due to steric hindrance by the regulatory loop. However, the forskolin response, although significant at certain concentrations, was not concentration-dependent and was relatively small; this could be due to lack of substrate or possibly another limiting factor such as lack of enzyme, or enzyme not being active. However, even the relatively large overexpression of enzyme did not reveal tone, showing that enzyme level is not limiting.

The failure to detect a substantial basal eCB tone, in cells that overexpress DAGLα in media containing JZL184 and in the presence and absence forskolin, was surprising given the report that PKA activation leads to 2-AG synthesis (Vellani *et al.*, 2008). Due to constraints of the assay format, whereby the full contents of Freestyle starvation medium were undisclosed, we optimised the assay in McCoy's medium supplemented with 1% FBS. This ensured that all factors that are likely to be required for the synthesis of 2-AG (and perhaps other eCBs), including calcium, were present in the culture media.

JZL195 is a dual MAGL/FAAH inhibitor that also displays some activity against ABHD6 (Long *et al.*, 2009b). We included this inhibitor in the assay as a previous report demonstrated cross talk between MAGL and FAAH pathways, where one enzyme had the ability to compensate when the other was inhibited (Long *et al.*, 2009b). Furthermore, JZL184 has not been reported to have activity against ABHD6 (Long *et al.*, 2009b). A small eCB tone was detected in the presence of JZL195, which was absent when JZL195 was not present. The lack of eCB tone when JZL195 is absent might reflect MAGL/FAAH/ABHD6 acting as 'gate-keeping' enzymes, which hydrolyse 2-AG (or other eCBs) thereby preventing it from stimulating the

CB1 receptor. Once these enzymes are inhibited by JZL195, β-lactamase activity increases after both 4 h and 18 h by ~ 15% and ~ 30%, respectively. This response was fully inhibited by AM251, providing evidence it is dependent on CB1 activation. This 'gate-keeping' activity is similar to that seen in developing axon, whereby MAGL is restricted from the motile tip of the growth cone, being confined further back along the axon, thereby allowing 2-AG to be available to activate CB1 in a highly restricted manner and this is required for axonal growth (Keimpema *et al.*, 2010). In adult synapses, MAGL is expressed on the presynaptic neuron (with DAGL expressed on the postsynaptic neuron), which is in keeping with MAGL's function to terminate the signal, rather than preventing the DAGL-produced 2-AG to reach the presynaptic CB1 receptor (Bisogno, 2003; Yoshida *et al.*, 2006; Hashimotodani *et al.*, 2007).

By allowing calcium to be present in the culture medium, we found that forskolin alone could stimulate an eCB tone to a similar extent as JZL195 alone, in both 4 h and 18 h assays. The response to these agents together is greater than that seen from either one of them on their own and were inhibited by AM251. This indicated that the forskolin-stimulated response was much greater when MAGL and FAAH, and perhaps ABHD6 are inhibited, indicating that possibly one or both of the endogenous DAGLs could be active. Following a 48 h starvation period, no response was detected in the presence of forskolin alone and was only revealed in the presence of JZL195. Similarly, stimulation of PKC with PMA stimulated eCB signalling and this again was only convincingly seen when JZL195 limited the breakdown of 2-AG and/or anadamide (and possibly some other eCB).

A clear and concentration-dependent increase in response was seen in the presence of ionomycin alone. This response was significantly reduced in the presence of either 5 or 10 μM THL. However, this only reached 15-20% inhibition, indicating that ~80% of the ionomycin response may not be due to DAGL activity. (It was noted that THL on its own did not reduce basal tone in these cells.) The fact that ionomycin could stimulate a response in the absence of JZL195 might be a result of the activation of more than one component necessary for eCB production. In the case of the DAGLs, it might be that more than one kinase is important for regualtion of

activity. In the presence of JZL195, the level of the ionomycin-simulated CB1 activation is much greater, with the response from 2 μM being increased by ~ 50% . In contrast, neither JZL184 nor URB597 increased basal eCB tone or potentiated the ionomycin response, indicating that inhibiting either MAGL or FAAH alone is not sufficient to potentiate the eCB response in CB1-Tango cells; the response is greater only when the hydrolytic activity of both of these enzymes (and possibly ABHD6) is inhibited, thereby allowing eCBs being produced to signal through the CB1 receptor. Again this may have been that FAAH was compensating for the lack of activity of MAGL, and vice versa. Dual blockade of FAAH/MAGL (and not when MAGL was inhibited alone) has been shown to produce THC-like responses that were reversed by a CB1 antagonist, indicating these pathways display a degree of crosstalk and may not be mutually exclusive (Long *et al.*, 2009b). Furthermore, JZL195 can also inhibit ABHD6, an enzyme previously shown to contribute to 2-AG hydrolysis in mouse brain which also appears to play a role in efficacy of 2-AG to activate CB1, being suggested as a rate-limiting step for 2-AG signalling (Blankman *et al.*, 2007; Marrs *et al.*, 2010).

Our overexpressing cell lines did not show an obvious 'gain of function' phenotype. However, this may be possible in the future by further optimising assay conditions, but as yet we have not seen substantive evidence; although it may also be an indication that substrate is a limiting factor. DAGL (as well as other eCB producing enzymes) activity may be controlled at the level of substrate availability as well as phosphorylation and as such, the availability of DAG has been implicated as another regulatory mechanism for the activity of the enzymes. For example, an increase in PLCγ activity is likely to hydrolyse phospholipids and DAG levels, thereby upregulating DAGL activity, 2-AG and subsequent CB1 activation. This pathway has been suggested in FGFR driven neurite outgrowth in cerebellar neurons in culture (Saffell *et al.*, 1997; Bisogno, 2003; Williams *et al.*, 2003). Furthermore, increased PLCβ activity has been shown to upregulate DAGL-dependent 2-AG synaptic signalling (Hashimotodani *et al.*, 2005; Tanimura *et al.*, 2010). Consequently, post-synaptic receptor activation, resulting in an increase in intracellular calcium, activates PLCβ and increases DAG levels, DAGL activity and 2-AG production. Nonetheless, it was essential to eliminate eCB production in the

Tango cells to accommodate future structure-function studies of the DAGLs and also study the non-DAGL component of the responses seen. As at the outset of this study, there were no specific inhibitors for the enzymes and so it was apparent that a genetic intervention tool was required.

7.7 Precise genome editing with CRISPR/Cas9

The above results have started to give us clear insights into some of the factors governing eCB signalling, and there is no doubt that much more could be learned by utilising simple pharmacological approaches. In a recent commentary, the late Alan Hall discussed several reasons for the increase in irreproducibility seen across the field of science. One such explanation was that small molecules described as 'specific' are never truly so and one should exploit the power of genetics to target the specific protein in question (Yamada & Hall, 2015). However, there is also a high degree of irreproducibility associated with the use of RNA interference (RNAi), a technique used to repress gene expression through sequence-specific degradation of mRNA. RNAi is limited by its off-target effects and by the partial and / or transient nature of gene suppression, which is often insufficient to create noticeable changes in phenotype (Qiu *et al.*, 2005; Gupta & Musunuru, 2014). Consequently, the ability to precisely edit specific DNA sequences has obvious advantages. Until recently, this was typically achieved through ZFNs or TALENs. These technologies comprise chimeric nucleases, composed of sequence-specific DNA-binding modules linked to a nonspecific DNA cleavage (Fok1) domain (Gaj *et al.*, 2013); because a new chimeric protein needs to be generated for each new target, both of these methodologies are time-consuming and expensive.

Three years ago, CRISPR hit the radar screen (Jinek *et al.*, 2012). This gave us the opportunity to explore this technology in the context of DAGL function. This technique was derived from the type II CRISPR-Cas9 system, an adaptive immune response in bacteria and archaea, which functions by Cas9 recognizing and cleaving foreign DNA (viruses or plasmids) through gRNAs, whose sequences are partially

derived from the invaders (Horvath & Barrangou, 2010; Jinek *et al.*, 2012; Wiedenheft *et al.*, 2012). The system has been manipulated to target mammalian genes (Cho *et al.*, 2013; Mali *et al.*, 2013b) and has successfully been used to disrupt specific DNA sequences, both in human and non-human cell lines (Cho *et al.*, 2013; Cong *et al.*, 2013; Mali *et al.*, 2013a; Yang *et al.*, 2014) and more recently, in U2OS cells (Feng *et al.*, 2015). New CRISPR/Cas9 complexes can be prepared simply by replacing the gRNA sequence; therefore it is a markedly easier and cheaper method than ZFNs or TALENs and is the method we chose to KO the DAGLs.

We used three different approaches to target DAGL activity in the Tango cells with CRISPR/Cas9. Initially we attempted to disrupt the most upstream exon to hit any predicted splice variants of each enzyme; we targeted exon 3 in DAGLα and exon 7 in DAGLβ. At the same time, we exploited the D10A mutant version of Cas9, Cas9 nickase to limit off-target effects and introduce a blasticidin resistance gene through the HDR DNA repair pathway (at the same locus in each gene). Although we were aware of the unreliability of the DAGLα antibody, neither method gave us confidence that we were disrupting the full length gene downstream of the CRISPR targeting site. Inducing a DSB in a DNA sequence has been known to effectively create a frameshift or premature stop codon in the downstream sequence (Perez *et al.*, 2008) and from the sequencing it looked as though the mutations in our selected cell lines would be sufficient to cause a frameshift in the DAGLs' sequences; yet transcripts were not reduced by > 50% in our selected cell lines.

We questioned whether the relatively large length of the DAGL genes was providing a mechanism to splice across the CRISPR cutting site. More recently, a report has demonstrated that by using two gRNAs coupled with Cas9 efficiently generates DNA deletions of up to 10 kb in human cells through introduction of a repair template, thereby stimulating HDR repair pathway (Zheng et al., 2014). Furthermore, a single Cas9-gRNA complex was used to effectively disrupt CDK11 gene (~20 kb) in U2OS cells (Feng *et al.*, 2015). However, the DAGLα gene consists of ~ 67 kb and DAGLβ gene ~ 65 kb and there are no reports to date on using CRISPR/Cas9 to disrupt a gene of a similar size. Therefore, it is unclear if one Cas9-gRNA complex alone (or two in the case of our nickase strategy) can efficiently

disrupt this size without pairing it with another complex. More than one gene can be disrupted by 'multiplexing' two Cas9-gRNA complexes simultaneously (Cong *et al.*, 2013; Yan *et al.*, 2014). Using two or more Cas9-gRNA complexes to target different loci on the DAGL sequence could be a more effective method to disrupt the full length gene.

When using CRISPR/Cas9 technology, it is important to have appropriate screening methods for selecting a knockout cell line. For this purpose, we targeted DAGLα and DAGLβ simultaneously, with vectors containing GFP and mCherry, respectively. While screening for successful transfection may be done through these fluorescent markers, FACS sorting appeared to be detrimental to cell viability. Furthermore, this may not be sufficient for detecting successful Cas9 cutting of the sequence, thereby resulting in a number of WT transcripts in our selected cell lines. This was especially true in the case of DAGLα, where we may not have detected these WT transcripts in the sequence analysis. In addition, the double transfection of constructs to target both the DAGLs simultaneously may have interfered with one another, as co-transfection is known to reduce efficiency and can depend on the ratio of the DNA concentration between the two constructs (Hannig, 2013). In deciphering whether WT transcripts for DAGLα's catalytic domain were still present, we screened the blasticidin-resistant cell line J using RT-PCR. This provided a much more efficient and higher throughput method to detect WT or disrupted DAGL transcripts.

One clearly has to consider the limitations of CRISPR, such as mosaicism seen in mice, whereby a mutant allele in only some of their cells may be produced (Long *et al.*, 2014). This has been one issue we encountered when attempting to generate a clonal DAGL-inactive cell line. Furthermore, earlier reports of the aforementioned off-targeting events reported a number of tolerated mismatches between the gRNA sequence and the target locus (Fu *et al.*, 2013). However, off-target effects are only a concern for us if they interfere with the Tango assay system, and to this end we have very clear controls in place; for example, ensuring the Tango cells maintained maximal ACEA responses that can be inhibited by AM251. As we could show that DAGLα activity is not interfered by the presence of a catalytically-dead version of the enzyme, by re-focussing our efforts to disrupt the catalytic domain and therefore

activity of the DAGLs, we could show the efficiency of Cas9 in disrupting a target DNA locus. The simplicity of the technology allowed us to generate cell lines with various disruptions within catalytic domain of each of the DAGLs and these may be of interest in future studies. As a result, our Tango cell lines contained disruptions to both genes that should eliminate DAGLα and DAGLβ activity in the same cell line. However, as expected these cells responded significantly to PKA activation, indicating other eCBs are likely to be contributing to the response.

More than 1,000 reports have been published since the explosion of CRISPR/Cas9 onto the genome modifying market and the genomes of virtually all model animals and plants have been successfully edited by the technology (Sternberg & Doudna, 2015). However researchers are continuing to adapt the CRISPR/Cas9 system to suit their needs. For example, it has been used to generate chromosomal rearrangements, similar to those found in tumours, in both human and primary cell lines (Choi & Meyerson, 2014; Torres *et al.*, 2014). In addition, a catalytically-dead version of Cas9 (dCas9) has been used to study gene regulation, by fusing dCas9 to transcription activators or repressors, which are guided to a specific genomic locus via the gRNA (Gilbert *et al.*, 2013; Maeder *et al.*, 2013; Perez-Pinera *et al.*, 2013), which could of interest in studying DAGL phosphorylation and regulation in the future.

Although many hurdles still exist for clinical use, the therapeutic potential of CRISPR/Cas9 is becoming more evident for treatment of genetic disease. For example, CRISPR/Cas9-mediated correction of a Fah mutation seen in the metabolic hereditary disorder, tyrosinemia resulted in rescue of the body weight loss phenotype in a mouse model of the disease, demonstrating that genome editing is possible in adult animals (Yin *et al.*, 2014). In addition, Duchenne muscular dystrophy was prevented by injection of CRISPR/Cas9 components directly into the mouse germline (Long *et al.*, 2014). These examples highlight the potential of CRISPR/Cas9 to one day treat disease-causing mutations.

7.8 Future Directions

Before continuing with disruption of other eCB synthetic pathways, it would be prudent to isolate a clonal cell line from the DAGL-inactive Tango cells, in order to study the non-DAGL pathway. In designing a strategy to KO anandamide biosynthesis, one has to take into account the numerous pathways that have been described. For example, in NAPE-PLD KO mouse (Leung *et al.*, 2006), GDE1 KO mouse or mice lacking both GDE1 and NAPE-PLD activity (Simon & Cravatt, 2010b) there were no significant reductions in anandamide levels, indicating that more than one synthetic pathway can account for anandamide synthesis *in vivo*. However, one could eliminate one pathway at a time in the Tango cells and therefore decipher the most important pathway or combination of pathways for anandamide biosynthesis, at least *in vitro.*

A cell line lacking eCB synthesis would act as a 'parent' cell line for the generation of cells that have a single gain-of-function pathway, e.g. DAGLα, DAGLβ and possibly an anandamide pathway for detailed studies on factors that can stimulate their activity. Another advantage to obtaining a cell line that in itself cannot mount an eCB response would be to use it as a reporter in co-culture assays with, for example, neurons, to monitor their ability to release eCBs via CB1 activation in our parent cell line. Co-cultures have previously been used to demonstrate that developing acetylcholinergic basal forebrain neurons are attracted to COS-7 cells overexpressing DAGLα, termed "2-AG hotspots"

We would then perform structure-function studies on each of the DAGL enzymes, for example mutagenesis, to determine which phospho-sites that we have identified are important for their function. One such method to re-introduce a mutated version of DAGL would be CRISPR/Cas9, which has previously been shown to be an effective method to insert DNA at a target locus in mammalian cells via the HDR pathway (Lee *et al.*, 2015).

Following on from this study, it would be interesting to see the effects of knocking out the DAGLs in induced pluripotent stem (iPS) cells, a type of cell that can be

generated from adult cells. One caveat of researching in cell lines or in animal models is translating the information into human; therefore, if we could determine the effects resulting from a lack of DAGL activity in human cells, especially those that can differentiate into different cell types, this may give us a better understanding of the different functions between DAGLα and DAGLβ that occur in the human. For example, we could reintroduce DAGLβ back into these cells followed by differentiation into neurons and determine whether DAGLβ is located in post-synaptic densities, a function associated to the tail in DAGLα. In addition, DAGLα could be reintroduced before differentiation into immune cells and determine whether they retain anti-inflammatory properties. For example, would DAGLα expression in these cells, or a lack of 2-AG production (double KO) result in an increase in cytokines, or result in an increase in microglial activation? These processes have previously been shown to be suppressed by an increase in 2-AG production, via MAGL inhibition (Ramirez *et al.*, 2005; Nomura *et al.*, 2011). Similarly, if they were differentiated into macrophages, how would they compare to a mouse (RAW 264.7) or human (U937) macrophage cell line, or primary animal/human macrophage cells? If one could extrapolate the exact reason for the difference in expression and function between DAGLα and DAGLβ then this would allow a greater understanding of how the eCB system in regulated, as well as more selective therapeutic targeting.

Understanding the different functions as well as their regulatory mechanisms is crucial if these enzymes are to become attractive drug targets in the future. If the activity of these enzymes can be targeted therapeutically, there is great potential for treatment of disease associated with synaptic dysfunction, such as depression or obesity. Furthermore, if the elusive cure is discovered for neurodegenerative diseases such as Alzheimer's or Parkinson's, there will still be a need to repair the damage caused in time to diagnosis. The role of the DAGLs in neurogenesis may prove crucial in order to generate new neurons to innervate the damaged areas. Finally, as they also appear to play a crucial role in regulation of inflammatory processes, the DAGLs may also be a target for treatment of diseases where inflammation plays a major role, such as in autoimmune disease, or in diseases that contain an inflammatory component, such as MS or AD.

CHAPTER 8. BIBLIOGRAPHY

Aguado, T., Monory, K., Palazuelos, J., Stella, N., Cravatt, B., Lutz, B., Marsicano, G., Kokaia, Z., Guzman, M. & Galve-Roperh, I. (2005) The endocannabinoid system drives neural progenitor proliferation. *FASEB J*, **19**, 1704-1706.

Aguado, T., Palazuelos, J., Monory, K., Stella, N., Cravatt, B., Lutz, B., Marsicano, G., Kokaia, Z., Guzman, M. & Galve-Roperh, I. (2006) The endocannabinoid system promotes astroglial differentiation by acting on neural progenitor cells. *J Neurosci*, **26**, 1551-1561.

Ahn, K., Johnson, D.S., Mileni, M., Beidler, D., Long, J.Z., McKinney, M.K., Weerapana, E., Sadagopan, N., Liimatta, M., Smith, S.E., Lazerwith, S., Stiff, C., Kamtekar, S., Bhattacharya, K., Zhang, Y., Swaney, S., Van Becelaere, K., Stevens, R.C. & Cravatt, B.F. (2009) Discovery and characterization of a highly selective FAAH inhibitor that reduces inflammatory pain. *Chem Biol*, **16**, 411-420.

Alcolea, M.P., Kleiner, O. & Cutillas, P.R. (2009) Increased confidence in large-scale phosphoproteomics data by complementary mass spectrometric techniques and matching of phosphopeptide data sets. *J Proteome Res*, **8**, 3808-3815.

Alexander, J.P. & Cravatt, B.F. (2005) Mechanism of carbamate inactivation of FAAH: implications for the design of covalent inhibitors and in vivo functional probes for enzymes. *Chem Biol*, **12**, 1179-1187.

Alexander, S.P. & Kendall, D.A. (2007) The complications of promiscuity: endocannabinoid action and metabolism. *Br J Pharmacol*, **152**, 602-623.

Alger, B.E. (2002) Retrograde signaling in the regulation of synaptic transmission: focus on endocannabinoids. *Prog Neurobiol*, **68**, 247-286.

Alger, B.E. & Pitler, T.A. (1995) Retrograde signaling at GABAA-receptor synapses in the mammalian CNS. *Trends Neurosci*, **18**, 333-340.

Allen, A.C., Gammon, C.M., Ousley, A.H., McCarthy, K.D. & Morell, P. (1992) Bradykinin stimulates arachidonic acid release through the sequential actions of an sn-1 diacylglycerol lipase and a monoacylglycerol lipase. *J Neurochem*, **58**, 1130-1139.

Altman, J. (1962) Are new neurons formed in the brains of adult mammals? *Science*, **135**, 1127-1128.

Alvarez-Buylla, A. & Garcia-Verdugo, J.M. (2002) Neurogenesis in adult subventricular zone. *J Neurosci*, **22**, 629-634.

Aso, E. & Ferrer, I. (2014) Cannabinoids for treatment of Alzheimer's disease: moving toward the clinic. *Front Pharmacol.*, **5**, 37.

Auclair, N., Otani, S., Soubrie, P. & Crepel, F. (2000) Cannabinoids modulate synaptic strength and plasticity at glutamatergic synapses of rat prefrontal cortex pyramidal neurons. *J Neurophysiol*, **83**, 3287-3293.

Baker, D., Jackson, S.J. & Pryce, G. (2007) Cannabinoid control of neuroinflammation related to multiple sclerosis. *Br J Pharmacol*, **152**, 649-654.

Baker, D. & Pryce, G. (2008) The endocannabinoid system and multiple sclerosis. *Curr Pharm Des*, **14**, 2326-2336.

Baker, D., Pryce, G., Croxford, J.L., Brown, P., Pertwee, R.G., Huffman, J.W. & Layward, L. (2000) Cannabinoids control spasticity and tremor in a multiple sclerosis model. *Nature*, **404**, 84-87.

Baker, D., Pryce, G., Davies, W.L. & Hiley, C.R. (2006) In silico patent searching reveals a new cannabinoid receptor. *Trends Pharmacol Sci*, **27**, 1-4.

Balgoma, D., Checa, A., Sar, D.G., Snowden, S. & Wheelock, C.E. (2013) Quantitative metabolic profiling of lipid mediators. *Mol Nutr Food Res*, **57**, 1359-1377.

Barnea, G., Strapps, W., Herrada, G., Berman, Y., Ong, J., Kloss, B., Axel, R. & Lee, K.J. (2008) The genetic design of signaling cascades to record receptor activation. *Proc Natl Acad Sci U S A*, **105**, 64-69.

Barrangou, R., Fremaux, C., Deveau, H., Richards, M., Boyaval, P., Moineau, S., Romero, D.A. & Horvath, P. (2007) CRISPR provides acquired resistance against viruses in prokaryotes. *Science*, **315**, 1709-1712.

Basavarajappa, B.S., Saito, M., Cooper, T.B. & Hungund, B.L. (2000) Stimulation of cannabinoid receptor agonist 2-arachidonylglycerol by chronic ethanol and its modulation by specific neuromodulators in cerebellar granule neurons. *Biochim Biophys Acta*, **1535**, 78-86.

Basu, D., Manjur, J. & Jin, W. (2011) Determination of lipoprotein lipase activity using a novel fluorescent lipase assay. *J Lipid Res*, **52**, 826-832.

Basu, P.P., Aloysius, M.M., Shah, N.J. & Brown, R.S., Jr. (2014) Review article: the endocannabinoid system in liver disease, a potential therapeutic target. *Aliment Pharmacol Ther*, **39**, 790-801.

Begbie, J., Doherty, P. & Graham, A. (2004) Cannabinoid receptor, CB1, expression follows neuronal differentiation in the early chick embryo. *J Anat*, **205**, 213-218.

Bell, R.L., Kennerly, D.A., Stanford, N. & Majerus, P.W. (1979) Diglyceride lipase: a pathway for arachidonate release from human platelets. *Proc Natl Acad Sci U S A*, **76**, 3238-3241.

Beltramo, M. & Piomelli, D. (2000) Carrier-mediated transport and enzymatic hydrolysis of the endogenous cannabinoid 2-arachidonylglycerol. *Neuroreport*, **11**, 1231-1235.

Beltramo, M., Stella, N., Calignano, A., Lin, S.Y., Makriyannis, A. & Piomelli, D. (1997) Functional role of high-affinity anandamide transport, as revealed by selective inhibition. *Science*, **277**, 1094-1097.

Berghuis, P., Dobszay, M.B., Wang, X., Spano, S., Ledda, F., Sousa, K.M., Schulte, G., Ernfors, P., Mackie, K., Paratcha, G., Hurd, Y.L. & Harkany, T. (2005) Endocannabinoids regulate interneuron migration and morphogenesis by transactivating the TrkB receptor. *Proc Natl Acad Sci U S A*, **102**, 19115-19120.

Berghuis, P., Rajnicek, A.M., Morozov, Y.M., Ross, R.A., Mulder, J., Urban, G.M., Monory, K., Marsicano, G., Matteoli, M., Canty, A., Irving, A.J., Katona, I., Yanagawa, Y., Rakic, P., Lutz, B., Mackie, K. & Harkany, T. (2007) Hardwiring the brain: endocannabinoids shape neuronal connectivity. *Science*, **316**, 1212-1216.

Bhaya, D., Davison, M. & Barrangou, R. (2011) CRISPR-Cas systems in bacteria and archaea: versatile small RNAs for adaptive defense and regulation. *Annu Rev Genet*, **45**, 273-297.

Bisogno, T. (2003) Cloning of the first sn1-DAG lipases points to the spatial and temporal regulation of endocannabinoid signaling in the brain. *J Cell Biol*, **163**, 463-468.

Bisogno, T., Berrendero, F., Ambrosino, G., Cebeira, M., Ramos, J.A., Fernandez-Ruiz, J.J. & Di Marzo, V. (1999) Brain regional distribution of endocannabinoids: implications for their biosynthesis and biological function. *Biochem Biophys Res Commun*, **256**, 377-380.

Bisogno, T., Cascio, M.G., Saha, B., Mahadevan, A., Urbani, P., Minassi, A., Appendino, G., Saturnino, C., Martin, B., Razdan, R. & Di Marzo, V. (2006) Development of the first potent and specific inhibitors of endocannabinoid biosynthesis. *Biochim Biophys Acta*, **1761**, 205-212.

Bisogno, T., Mahadevan, A., Coccurello, R., Chang, J.W., Allara, M., Chen, Y., Giacovazzo, G., Lichtman, A., Cravatt, B., Moles, A. & Di Marzo, V. (2013) A novel fluorophosphonate inhibitor of the biosynthesis of the endocannabinoid 2-arachidonoylglycerol with potential anti-obesity effects. *Br J Pharmacol*, **169**, 784-793.

Bisogno, T., Melck, D., Bobrov, M., Gretskaya, N.M., Bezuglov, V.V., De Petrocellis, L. & Di Marzo, V. (2000) N-acyl-dopamines: novel synthetic CB(1) cannabinoid-receptor ligands and inhibitors of anandamide inactivation with cannabimimetic activity in vitro and in vivo. *Biochem J*, **351**, 817-824.

Bisogno, T., Ortar, G., Petrosino, S., Morera, E., Palazzo, E., Nalli, M., Maione, S. & Di Marzo, V. (2009) Development of a potent inhibitor of 2-arachidonoylglycerol hydrolysis with antinociceptive activity in vivo. *Biochim Biophys acta*, **1791**, 53-60.

Bisogno, T., Sepe, N., De Petrocellis, L. & Di Marzo, V. (1997a) Biosynthesis of 2-arachidonoyl-glycerol, a novel cannabimimetic eicosanoid, in mouse neuroblastoma cells. *Adv Exp Med Biol*, **433**, 201-204.

Bisogno, T., Sepe, N., Melck, D., Maurelli, S., De Petrocellis, L. & Di Marzo, V. (1997b) Biosynthesis, release and degradation of the novel endogenous cannabimimetic metabolite 2-arachidonoylglycerol in mouse neuroblastoma cells. *Biochem J*, **322** 671-677.

Black, D.L. (2003) Mechanisms of alternative pre-messenger RNA splicing. *Annu Rev Biochem*, **72**, 291-336.

Blankman, J.L., Simon, G.M. & Cravatt, B.F. (2007) A comprehensive profile of brain enzymes that hydrolyze the endocannabinoid 2-arachidonoylglycerol. *Chem Biol*, **14**, 1347-1356.

Blom, N., Gammeltoft, S. & Brunak, S. (1999) Sequence and structure-based prediction of eukaryotic protein phosphorylation sites. *J Mol Biol*, **294**, 1351-1362.

Brenowitz, S.D. & Regehr, W.G. (2003) Calcium dependence of retrograde inhibition by endocannabinoids at synapses onto Purkinje cells. *J Neurosci*, **23**, 6373-6384.

Brittis, P.A., Silver, J., Walsh, F.S. & Doherty, P. (1996) Fibroblast Growth Factor Receptor Function Is Required for the Orderly Projection of Ganglion Cell Axons in the Developing Mammalian Retina. *Mol Cell Neurosci*, **8**, 120-128.

Brose, N., Betz, A. & Wegmeyer, H. (2004) Divergent and convergent signaling by the diacylglycerol second messenger pathway in mammals. *Curr Opin Neurobiol*, **14**, 328-340.

Brown, A.J. (2007) Novel cannabinoid receptors. *Br J Pharmacol*, **152**, 567-575.

Brown, I., Cascio, M.G., Wahle, K.W., Smoum, R., Mechoulam, R., Ross, R.A., Pertwee, R.G. & Heys, S.D. (2010) Cannabinoid receptor-dependent and -independent anti-proliferative effects of omega-3 ethanolamides in androgen receptor-positive and -negative prostate cancer cell lines. *Carcinogenesis*, **31**, 1584-1591.

Buckley, N.E., McCoy, K.L., Mezey, E., Bonner, T., Zimmer, A., Felder, C.C., Glass, M. & Zimmer, A. (2000) Immunomodulation by cannabinoids is absent in mice deficient for the cannabinoid CB(2) receptor. *Eur J Pharmacol*, **396**, 141-149.

Burstein, S. (2005) PPAR-gamma: a nuclear receptor with affinity for cannabinoids. *Life Sci*, **77**, 1674-1684.

Burstein, S.H., Karst, M., Schneider, U. & Zurier, R.B. (2004) Ajulemic acid: A novel cannabinoid produces analgesia without a "high". *Life Sci*, **75**, 1513-1522.

Butler, R.K., Rea, K., Lang, Y., Gavin, A.M. & Finn, D.P. (2008) Endocannabinoid-mediated enhancement of fear-conditioned analgesia in rats: opioid receptor dependency and molecular correlates. *Pain*, **140**, 491-500.

Cadas, H., di Tomaso, E. & Piomelli, D. (1997) Occurrence and biosynthesis of endogenous cannabinoid precursor, N-arachidonoyl phosphatidylethanolamine, in rat brain. *J Neurosci* **17**, 1226-1242.

Cadogan, A.K., Alexander, S.P., Boyd, E.A. & Kendall, D.A. (1997) Influence of cannabinoids on electrically evoked dopamine release and cyclic AMP generation in the rat striatum. *J Neurochem*, **69**, 1131-1137.

Canaan, S., Roussel, A., Verger, R. & Cambillau, C. (1999) Gastric lipase: crystal structure and activity. *Biochim Biophys Acta*, **1441**, 197-204.

Carpenter, E.P., Beis, K., Cameron, A.D. & Iwata, S. (2008) Overcoming the challenges of membrane protein crystallography. *Curr Opin Struct Biol*, **18**, 581-586.

Carta, G., Nava, F. & Gessa, G.L. (1998) Inhibition of hippocampal acetylcholine release after acute and repeated Delta9-tetrahydrocannabinol in rats. *Brain Res*, **809**, 1-4.

Castagna, M., Takai, Y., Kaibuchi, K., Sano, K., Kikkawa, U. & Nishizuka, Y. (1982) Direct activation of calcium-activated, phospholipid-dependent protein kinase by tumor-promoting phorbol esters. *J Biol Chem*, **257**, 7847-7851.

Cattaneo, F., Guerra, G., Parisi, M., De Marinis, M., Tafuri, D., Cinelli, M. & Ammendola, R. (2014) Cell-surface receptors transactivation mediated by g protein-coupled receptors. *Int J Mol Sci*, **15**, 19700-19728.

Chanda, P.K., Gao, Y., Mark, L., Btesh, J., Strassle, B.W., Lu, P., Piesla, M.J., Zhang, M.Y., Bingham, B., Uveges, A., Kowal, D., Garbe, D., Kouranova, E.V., Ring, R.H., Bates, B., Pangalos, M.N., Kennedy, J.D., Whiteside, G.T. & Samad, T.A. (2010) Monoacylglycerol lipase activity is a critical modulator of the tone and integrity of the endocannabinoid system. *Mol Pharmacol*, **78**, 996-1003.

Chen, R., Zhang, J., Wu, Y., Wang, D., Feng, G., Tang, Y.P., Teng, Z. & Chen, C. (2012) Monoacylglycerol lipase is a therapeutic target for Alzheimer's disease. *Cell Rep*, **2**, 1329-1339.

Cho, S.W., Kim, S., Kim, J.M. & Kim, J.S. (2013) Targeted genome engineering in human cells with the Cas9 RNA-guided endonuclease. *Nat Biotechnol*, **31**, 230-232.

Cho, S.W., Kim, S., Kim, Y., Kweon, J., Kim, H.S., Bae, S. & Kim, J.S. (2014) Analysis of off-target effects of CRISPR/Cas-derived RNA-guided endonucleases and nickases. *Genome Res*, **24**, 132-141.

Choi, P.S. & Meyerson, M. (2014) Targeted genomic rearrangements using CRISPR/Cas technology. *Nat Commun*, **5**, 3728.

Compston, A. & Coles, A. (2002) Multiple sclerosis. *Lancet*, **359**, 1221-1231.

Cong, L., Ran, F.A., Cox, D., Lin, S., Barretto, R., Habib, N., Hsu, P.D., Wu, X., Jiang, W., Marraffini, L.A. & Zhang, F. (2013) Multiplex genome engineering using CRISPR/Cas systems. *Science*, **339**, 819-823.

Cravatt, B.F., Demarest, K., Patricelli, M.P., Bracey, M.H., Giang, D.K., Martin, B.R. & Lichtman, A.H. (2001) Supersensitivity to anandamide and enhanced endogenous cannabinoid signaling in mice lacking fatty acid amide hydrolase. *Proc Natl Acad Sci U S A*, **98**, 9371-9376.

Cravatt, B.F., Giang, D.K., Mayfield, S.P., Boger, D.L., Lerner, R.A. & Gilula, N.B. (1996) Molecular characterization of an enzyme that degrades neuromodulatory fatty-acid amides. *Nature*, **384**, 83-87.

Cravatt, B.F. & Lichtman, A.H. (2002) The enzymatic inactivation of the fatty acid amide class of signaling lipids. *Chem Phys Lipids*, **121**, 135-148.

Daniel, H. & Crepel, F. (2001) Control of Ca(2+) influx by cannabinoid and metabotropic glutamate receptors in rat cerebellar cortex requires K(+) channels. *J Physiol*, **537**, 793-800.

De Petrocellis, L., Melck, D., Bisogno, T. & Di Marzo, V. (2000) Endocannabinoids and fatty acid amides in cancer, inflammation and related disorders. *Chem Phys Lipids*, **108**, 191-209.

Deltcheva, E., Chylinski, K., Sharma, C.M., Gonzales, K., Chao, Y., Pirzada, Z.A., Eckert, M.R., Vogel, J. & Charpentier, E. (2011) CRISPR RNA maturation by trans-encoded small RNA and host factor RNase III. *Nature*, **471**, 602-607.

Derewenda, U., Swenson, L., Green, R., Wei, Y., Dodson, G.G., Yamaguchi, S., Haas, M.J. & Derewenda, Z.S. (1994) An unusual buried polar cluster in a family of fungal lipases. *Nature Struct Biol*, **1**, 36-47.

Deutsch, D.G. & Chin, S.A. (1993) Enzymatic synthesis and degradation of anandamide, a cannabinoid receptor agonist. *Biochem Pharmacol*, **46**, 791-796.

Deutsch, D.G., Ueda, N. & Yamamoto, S. (2002) The fatty acid amide hydrolase (FAAH). *Prostaglandins Leukot Essent Fatty Acids*, **66**, 201-210.

Devane, W.A., Dysarz, F.A., 3rd, Johnson, M.R., Melvin, L.S. & Howlett, A.C. (1988) Determination and characterization of a cannabinoid receptor in rat brain. *Mol Pharmacol*, **34**, 605-613.

Devane, W.A., Hanus, L., Breuer, A., Pertwee, R.G., Stevenson, L.A., Griffin, G., Gibson, D., Mandelbaum, A., Etinger, A. & Mechoulam, R. (1992) Isolation and structure of a brain constituent that binds to the cannabinoid receptor. *Science*, **258**, 1946-1949.

Deveau, H., Barrangou, R., Garneau, J.E., Labonte, J., Fremaux, C., Boyaval, P., Romero, D.A., Horvath, P. & Moineau, S. (2008) Phage response to CRISPR-encoded resistance in Streptococcus thermophilus. *J Bacteriol*, **190**, 1390-1400.

Devinsky, O., Cilio, M.R., Cross, H., Fernandez-Ruiz, J., French, J., Hill, C., Katz, R., Di Marzo, V., Jutras-Aswad, D., Notcutt, W.G., Martinez-Orgado, J., Robson, P.J., Rohrback, B.G., Thiele, E., Whalley, B. & Friedman, D. (2014) Cannabidiol: Pharmacology and potential therapeutic role in epilepsy and other neuropsychiatric disorders. *Epilepsia*, **55**, 791-802.

Di Marzo, V. (2006) A brief history of cannabinoid and endocannabinoid pharmacology as inspired by the work of British scientists. *Trends Pharmacol Sci*, **27**, 134-140.

Di Marzo, V. (2008) Targeting the endocannabinoid system: to enhance or reduce? *Nat Rev Drug Discov*, **7**, 438-455.

Di Marzo, V. (2011) Endocannabinoid signaling in the brain: biosynthetic mechanisms in the limelight. *Nat Neurosci*, **14**, 9-15.

Di Marzo, V., Bisogno, T., Melck, D., Ross, R., Brockie, H., Stevenson, L., Pertwee, R. & De Petrocellis, L. (1998) Interactions between synthetic vanilloids and the endogenous cannabinoid system. *FEBS J*, **436**, 449-454.

Di Marzo, V., Fontana, A., Cadas, H., Schinelli, S., Cimino, G., Schwartz, J.C. & Piomelli, D. (1994) Formation and inactivation of endogenous cannabinoid anandamide in central neurons. *Nature*, **372**, 686-691.

Di Marzo, V., Hill, M.P., Bisogno, T., Crossman, A.R. & Brotchie, J.M. (2000) Enhanced levels of endogenous cannabinoids in the globus pallidus are associated with a reduction in movement in an animal model of Parkinson's disease. *FASEB J*, **14**, 1432-1438.

Di, S., Malcher-Lopes, R., Halmos, K.C. & Tasker, J.G. (2003) Nongenomic glucocorticoid inhibition via endocannabinoid release in the hypothalamus: a fast feedback mechanism. *J Neurosci*, **23**, 4850-4857.

Dianov, G.L. & Hubscher, U. (2013) Mammalian base excision repair: the forgotten archangel. *Nucleic Acids Res*, **41**, 3483-3490.

Dinh, T.P., Freund, T.F. & Piomelli, D. (2002) A role for monoglyceride lipase in 2-arachidonoylglycerol inactivation. *Chem Phys Lipids*, **121**, 149-158.

Dowie, M.J., Bradshaw, H.B., Howard, M.L., Nicholson, L.F., Faull, R.L., Hannan, A.J. & Glass, M. (2009) Altered CB1 receptor and endocannabinoid levels precede motor symptom onset in a transgenic mouse model of Huntington's disease. *Neuroscience*, **163**, 456-465.

Du, G., Altshuller, Y.M., Vitale, N., Huang, P., Chasserot-Golaz, S., Morris, A.J., Bader, M.F. & Frohman, M.A. (2003) Regulation of phospholipase D1 subcellular cycling through coordination of multiple membrane association motifs. *J Cell Biol*, **162**, 305-315.

Egertova, M., Cravatt, B.F. & Elphick, M.R. (2003) Comparative analysis of fatty acid amide hydrolase and cb(1) cannabinoid receptor expression in the mouse brain: evidence of a widespread role for fatty acid amide hydrolase in regulation of endocannabinoid signaling. *Neuroscience*, **119**, 481-496.

Egertova, M. & Elphick, M.R. (2000) Localisation of cannabinoid receptors in the rat brain using antibodies to the intracellular C-terminal tail of CB. *J Comp Neurol*, **422**, 159-171.

Eljaschewitsch, E., Witting, A., Mawrin, C., Lee, T., Schmidt, P.M., Wolf, S., Hoertnagl, H., Raine, C.S., Schneider-Stock, R., Nitsch, R. & Ullrich, O. (2006) The endocannabinoid anandamide protects neurons during CNS inflammation by induction of MKP-1 in microglial cells. *Neuron*, **49**, 67-79.

Elphick, M.R. & Egertova, M. (2001) The neurobiology and evolution of cannabinoid signalling. *Philos Trans R Soc Lond B Biol Sci*, **356**, 381-408.

Fan, G., Ballou, L.M. & Lin, R.Z. (2003) Phospholipase C-independent activation of glycogen synthase kinase-3beta and C-terminal Src kinase by Galphaq. *J Biol Chem*, **278**, 52432-52436.

Farooqui, A.A., Taylor, W.A. & Horrocks, L.A. (1984) Separation of bovine brain mono- and diacylglycerol lipases by heparin sepharose affinity chromatography. *Biochem Biophys Res Commun*, **122**, 1241-1246.

Farooqui, A.A., Taylor, W.A. & Horrocks, L.A. (1986) Characterization and solubilization of membrane bound diacylglycerol lipases from bovine brain. *Int J Biochem*, **18**, 991-997.

Felder, C.C. & Glass, M. (1998) Cannabinoid receptors and their endogenous agonists. *Annu Rev Pharmacol Toxicol*, **38**, 179-200.

Feng, Y., Sassi, S., Shen, J.K., Yang, X., Gao, Y., Osaka, E., Zhang, J., Yang, S., Yang, C., Mankin, H.J., Hornicek, F.J. & Duan, Z. (2015) Targeting CDK11 in osteosarcoma cells using the CRISPR-Cas9 system. *J Orthop Res*, **33**, 199-207.

Fernandez-Ruiz, J., Lastres-Becker, I., Cabranes, A., Gonzalez, S. & Ramos, J.A. (2002) Endocannabinoids and basal ganglia functionality. *Prostaglandins Leukot Essent Fatty Acids*, **66**, 257-267.

Ferraro, L., Tomasini, M.C., Cassano, T., Bebe, B.W., Siniscalchi, A., O'Connor, W.T., Magee, P., Tanganelli, S., Cuomo, V. & Antonelli, T. (2001) Cannabinoid receptor agonist WIN 55,212-2 inhibits rat cortical dialysate gamma-aminobutyric acid levels. *J Neurosci Res*, **66**, 298-302.

Ferrer, B., Asbrock, N., Kathuria, S., Piomelli, D. & Giuffrida, A. (2003) Effects of levodopa on endocannabinoid levels in rat basal ganglia: implications for the treatment of levodopa-induced dyskinesias. *Eur J Neurosci*, **18**, 1607-1614.

Fezza, F., Bisogno, T., Minassi, A., Appendino, G., Mechoulam, R. & Di Marzo, V. (2002) Noladin ether, a putative novel endocannabinoid: inactivation mechanisms and a sensitive method for its quantification in rat tissues. *FEBS Lett*, **513**, 294-298.

Flachenecker, P. (2013) A new multiple sclerosis spasticity treatment option: effect in everyday clinical practice and cost-effectiveness in Germany. *Expert Rev Neurother*, **13**, 15-19.

Fu, J., Bottegoni, G., Sasso, O., Bertorelli, R., Rocchia, W., Masetti, M., Guijarro, A., Lodola, A., Armirotti, A., Garau, G., Bandiera, T., Reggiani, A., Mor, M., Cavalli, A. & Piomelli, D. (2012) A catalytically silent FAAH-1 variant drives anandamide transport in neurons. *Nature Neurosci*, **15**, 64-69.

Fu, Y., Foden, J.A., Khayter, C., Maeder, M.L., Reyon, D., Joung, J.K. & Sander, J.D. (2013) High-frequency off-target mutagenesis induced by CRISPR-Cas nucleases in human cells. *Nat Biotechnol*, **31**, 822-826.

Gage, F.H., Coates, P.W., Palmer, T.D., Kuhn, H.G., Fisher, L.J., Suhonen, J.O., Peterson, D.A., Suhr, S.T. & Ray, J. (1995) Survival and differentiation of adult neuronal progenitor cells transplanted to the adult brain. *Proc Natl Acad Sci U S A*, **92**, 11879-11883.

Gaj, T., Gersbach, C.A. & Barbas, C.F., 3rd (2013) ZFN, TALEN, and CRISPR/Cas-based methods for genome engineering. *Trends Biotechnol*, **31**, 397-405.

Galiegue, S., Mary, S., Marchand, J., Dussossoy, D., Carriere, D., Carayon, P., Bouaboula, M., Shire, D., Le Fur, G. & Casellas, P. (1995) Expression of central and peripheral cannabinoid receptors in human immune tissues and leukocyte subpopulations. *Eur J Biochem*, **232**, 54-61.

Gammon, C.M., Allen, A.C. & Morell, P. (1989) Bradykinin stimulates phosphoinositide hydrolysis and mobilization of arachidonic acid in dorsal root ganglion neurons. *J Neurochem*, **53**, 95-101.

Gantz, I., Muraoka, A., Yang, Y.K., Samuelson, L.C., Zimmerman, E.M., Cook, H. & Yamada, T. (1997) Cloning and chromosomal localization of a gene (GPR18) encoding a novel seven transmembrane receptor highly expressed in spleen and testis. *Genomics*, **42**, 462-466.

Gao, Y., Vasilyev, D.V., Goncalves, M.B., Howell, F.V., Hobbs, C., Reisenberg, M., Shen, R., Zhang, M.Y., Strassle, B.W., Lu, P., Mark, L., Piesla, M.J., Deng, K., Kouranova, E.V., Ring, R.H., Whiteside, G.T., Bates, B., Walsh, F.S., Williams, G., Pangalos, M.N., Samad, T.A. & Doherty, P. (2010) Loss of retrograde endocannabinoid signaling and reduced adult neurogenesis in diacylglycerol lipase knock-out mice. *J Neurosci*, **30**, 2017-2024.

Gaoni, Y. & Mechoulam, R. (1964) Isolation, Structure, and Partial Synthesis of an Active Constituent of Hashish. *J. Am. Chem. Soc.*, **86**, 1646–1647.

Garneau, J.E., Dupuis, M.E., Villion, M., Romero, D.A., Barrangou, R., Boyaval, P., Fremaux, C., Horvath, P., Magadan, A.H. & Moineau, S. (2010) The CRISPR/Cas bacterial immune system cleaves bacteriophage and plasmid DNA. *Nature*, **468**, 67-71.

Gasiunas, G., Barrangou, R., Horvath, P. & Siksnys, V. (2012) Cas9-crRNA ribonucleoprotein complex mediates specific DNA cleavage for adaptive immunity in bacteria. *Proc Natl Acad Sci U S A*, **109**, E2579-2586.

Gerdeman, G.L., Ronesi, J. & Lovinger, D.M. (2002) Postsynaptic endocannabinoid release is critical to long-term depression in the striatum. *Nature Neurosci*, **5**, 446-451.

Gessa, G.L., Casu, M.A., Carta, G. & Mascia, M.S. (1998) Cannabinoids decrease acetylcholine release in the medial-prefrontal cortex and hippocampus, reversal by SR 141716A. *Eur J Pharmacol*, **355**, 119-124.

Gilbert, L.A., Larson, M.H., Morsut, L., Liu, Z., Brar, G.A., Torres, S.E., Stern-Ginossar, N., Brandman, O., Whitehead, E.H., Doudna, J.A., Lim, W.A., Weissman, J.S. & Qi, L.S. (2013) CRISPR-mediated modular RNA-guided regulation of transcription in eukaryotes. *Cell*, **154**, 442-451.

Gill, E.W., Paton, W.D. & Pertwee, R.G. (1970) Preliminary experiments on the chemistry and pharmacology of cannabis. *Nature*, **228**, 134-136.

Glass, C.K., Saijo, K., Winner, B., Marchetto, M.C. & Gage, F.H. (2010) Mechanisms underlying inflammation in neurodegeneration. *Cell*, **140**, 918-934.

Gobel, I., Trendelenburg, A.U., Cox, S.L., Meyer, A. & Starke, K. (2000) Electrically evoked release of [(3)H]noradrenaline from mouse cultured sympathetic neurons: release-modulating heteroreceptors. *J Neurochem*, **75**, 2087-2094.

Goncalves, M.B., Suetterlin, P., Yip, P., Molina-Holgado, F., Walker, D.J., Oudin, M.J., Zentar, M.P., Pollard, S., Yanez-Munoz, R.J., Williams, G., Walsh, F.S., Pangalos, M.N. & Doherty, P. (2008) A diacylglycerol lipase-CB2 cannabinoid pathway regulates adult subventricular zone neurogenesis in an age-dependent manner. *Mol Cell Neurosci*, **38**, 526-536.

Goni, F.M. & Alonso, A. (1999) Structure and functional properties of diacylglycerols in membranes. *Prog Lipid Res*, **38**, 1-48.

Gonzalez-Montelongo, M.C., Marin, R., Perez, J.A., Gomez, T. & Diaz, M. (2013) Polyamines transduce the nongenomic, androgen-induced calcium sensitization in intestinal smooth muscle. *Mol Endocrinol*, **27**, 1603-1616.

Gottesman, S. (2011) Microbiology: Dicing defence in bacteria. *Nature*, **471**, 588-589.

Gresset, A., Hicks, S.N., Harden, T.K. & Sondek, J. (2010) Mechanism of phosphorylation-induced activation of phospholipase C-gamma isozymes. *J Biol Chem*, **285**, 35836-35847.

Gupta, R.M. & Musunuru, K. (2014) Expanding the genetic editing tool kit: ZFNs, TALENs, and CRISPR-Cas9. *J Clin Invest*, **124**, 4154-4161.

Guzman, M., Sanchez, C. & Galve-Roperh, I. (2002) Cannabinoids and cell fate. *Pharmacol Ther*, **95**, 175-184.

Hadvary, P., Sidler, W., Meister, W., Vetter, W. & Wolfer, H. (1991) The lipase inhibitor tetrahydrolipstatin binds covalently to the putative active site serine of pancreatic lipase. *J Biol Chem*, **266**, 2021-2027.

Hall, J.L. & van Teijlingen, E.R. (2006) A qualitative study of an integrated maternity, drugs and social care service for drug-using women. *BMC Pregnancy Childbirth*, **6**, 19.

Hannig, G., Jany, C. (2013) Co-transfection of Plasmid DNA. *Biotechniques*, **54**, 47.

Hansen, H.H., Schmid, P.C., Bittigau, P., Lastres-Becker, I., Berrendero, F., Manzanares, J., Ikonomidou, C., Schmid, H.H., Fernandez-Ruiz, J.J. & Hansen, H.S. (2001) Anandamide, but not 2-arachidonoylglycerol, accumulates during in vivo neurodegeneration. *J Neurochem*, **78**, 1415-1427.

Hanus, L., Abu-Lafi, S., Fride, E., Breuer, A., Vogel, Z., Shalev, D.E., Kustanovich, I. & Mechoulam, R. (2001) 2-arachidonyl glyceryl ether, an endogenous agonist of the cannabinoid CB1 receptor. *Proc Natl Acad Sci U S A*, **98**, 3662-3665.

Hasegawa-Sasaki, H. (1985) Early changes in inositol lipids and their metabolites induced by platelet-derived growth factor in quiescent Swiss mouse 3T3 cells. *Biochem J*, **232**, 99-109.

Hashimotodani, Y., Ohno-Shosaku, T. & Kano, M. (2007) Presynaptic monoacylglycerol lipase activity determines basal endocannabinoid tone and terminates retrograde endocannabinoid signaling in the hippocampus. *J Neurosci*, **27**, 1211-1219.

Hashimotodani, Y., Ohno-Shosaku, T., Tanimura, A., Kita, Y., Sano, Y., Shimizu, T., Di Marzo, V. & Kano, M. (2013) Acute inhibition of diacylglycerol lipase blocks endocannabinoid-mediated retrograde signalling: evidence for on-demand biosynthesis of 2-arachidonoylglycerol. *J Physiol*, **591**, 4765-4776.

Hashimotodani, Y., Ohno-Shosaku, T., Tsubokawa, H., Ogata, H., Emoto, K., Maejima, T., Araishi, K., Shin, H.S. & Kano, M. (2005) Phospholipase Cbeta serves as a coincidence detector through its Ca2+ dependency for triggering retrograde endocannabinoid signal. *Neuron*, **45**, 257-268.

Herkenham, M., Lynn, A.B., Little, M.D., Johnson, M.R., Melvin, L.S., de Costa, B.R. & Rice, K.C. (1990) Cannabinoid receptor localization in brain. *Proc Natl Acad Sci U S A*, **87**, 1932-1936.

Herschman, H.R. (1996) Prostaglandin synthase 2. *Biochim Biophys acta*, **1299**, 125-140.

Hoffman, A.F. & Lupica, C.R. (2000) Mechanisms of cannabinoid inhibition of GABA(A) synaptic transmission in the hippocampus. *J Neurosci*, **20**, 2470-2479.

Hofmann, N.A., Barth, S., Waldeck-Weiermair, M., Klec, C., Strunk, D., Malli, R. & Graier, W.F. (2014) TRPV1 mediates cellular uptake of anandamide and thus promotes endothelial cell proliferation and network-formation. *Biol Open*, **3**, 1164-1172.

Hogestatt, E.D., Jonsson, B.A., Ermund, A., Andersson, D.A., Bjork, H., Alexander, J.P., Cravatt, B.F., Basbaum, A.I. & Zygmunt, P.M. (2005) Conversion of acetaminophen to the bioactive N-acylphenolamine AM404 via fatty acid amide hydrolase-dependent arachidonic acid conjugation in the nervous system. *J Biol Chem*, **280**, 31405-31412.

Holm, C. (2003) Molecular mechanisms regulating hormone-sensitive lipase and lipolysis. *Biochem Soc Trans*, **31**, 1120-1124.

Holm, C., Belfrage, P., Osterlund, T., Davis, R.C., Schotz, M.C. & Langin, D. (1994) Hormone-sensitive lipase: structure, function, evolution and overproduction in insect cells using the baculovirus expression system. *Protein Eng*, **7**, 537-541.

Holmquist, M. (2000) Alpha/Beta-hydrolase fold enzymes: structures, functions and mechanisms. *Curr Protein Pept Sci*, **1**, 209-235.

Hoover, H.S., Blankman, J.L., Niessen, S. & Cravatt, B.F. (2008) Selectivity of inhibitors of endocannabinoid biosynthesis evaluated by activity-based protein profiling. *ACS Med Chem Lett*, **18**, 5838-5841.

Horvath, P. & Barrangou, R. (2010) CRISPR/Cas, the immune system of bacteria and archaea. *Science*, **327**, 167-170.

Houslay, M.D. & Adams, D.R. (2010) Putting the lid on phosphodiesterase 4. *Nat Biotechnol*, **28**, 38-40.

Howlett, A.C. (2002) The cannabinoid receptors. *Prostaglandins Other Lipid Mediat*, **68-69**, 619-631.

Howlett, A.C., Barth, F., Bonner, T.I., Cabral, G., Casellas, P., Devane, W.A., Felder, C.C., Herkenham, M., Mackie, K., Martin, B.R., Mechoulam, R. & Pertwee, R.G. (2002) International Union of Pharmacology. XXVII. Classification of cannabinoid receptors. *Pharmacol Rev*, **54**, 161-202.

Howlett, A.C., Qualy, J.M. & Khachatrian, L.L. (1986) Involvement of Gi in the inhibition of adenylate cyclase by cannabimimetic drugs. *Mol Pharmacol*, **29**, 307-313.

Hsu, K.L., Tsuboi, K., Adibekian, A., Pugh, H., Masuda, K. & Cravatt, B.F. (2012) DAGLbeta inhibition perturbs a lipid network involved in macrophage inflammatory responses. *Nat Chem Biol*, **8**, 999-1007.

Hsu, P.D., Scott, D.A., Weinstein, J.A., Ran, F.A., Konermann, S., Agarwala, V., Li, Y., Fine, E.J., Wu, X., Shalem, O., Cradick, T.J., Marraffini, L.A., Bao, G. & Zhang, F. (2013) DNA targeting specificity of RNA-guided Cas9 nucleases. *Nat Biotechnol*, **31**, 827-832.

Hu, S.S., Bradshaw, H.B., Benton, V.M., Chen, J.S., Huang, S.M., Minassi, A., Bisogno, T., Masuda, K., Tan, B., Roskoski, R., Jr., Cravatt, B.F., Di Marzo, V. & Walker, J.M. (2009) The biosynthesis of N-arachidonoyl dopamine (NADA), a putative endocannabinoid and endovanilloid, via conjugation of arachidonic acid with dopamine. *Prostaglandins Leukot Essent Fatty Acids*, **81**, 291-301.

Huang, S.M., Bisogno, T., Trevisani, M., Al-Hayani, A., De Petrocellis, L., Fezza, F., Tognetto, M., Petros, T.J., Krey, J.F., Chu, C.J., Miller, J.D., Davies, S.N., Geppetti, P., Walker, J.M. & Di Marzo, V. (2002) An endogenous capsaicin-like substance with high potency at recombinant and native vanilloid VR1 receptors. *Proc Natl Acad Sci U S A*, **99**, 8400-8405.

Huizink, A.C. & Mulder, E.J. (2006) Maternal smoking, drinking or cannabis use during pregnancy and neurobehavioral and cognitive functioning in human offspring. *Neurosci Biobehav Rev*, **30**, 24-41.

Hwang, W.Y., Fu, Y., Reyon, D., Maeder, M.L., Tsai, S.Q., Sander, J.D., Peterson, R.T., Yeh, J.R. & Joung, J.K. (2013) Efficient genome editing in zebrafish using a CRISPR-Cas system. *Nat Biotechnol*, **31**, 227-229.

Iakoucheva, L.M., Radivojac, P., Brown, C.J., O'Connor, T.R., Sikes, J.G., Obradovic, Z. & Dunker, A.K. (2004) The importance of intrinsic disorder for protein phosphorylation. *Nucleic Acids Res*, **32**, 1037-1049.

Jain, T., Wager-Miller, J., Mackie, K. & Straiker, A. (2013) Diacylglycerol lipasealpha (DAGLalpha) and DAGLbeta cooperatively regulate the production of 2-arachidonoyl glycerol in autaptic hippocampal neurons. *Mol Pharmacol*, **84**, 296-302.

Jean-Gilles, L., Braitch, M., Latif, M., Aram, J., Fahey, A.J., Edwards, L.J., Adrian Robins, R., Tanasescu, R., Tighe, P.J., Gran, B., Showe, L.C., Alexander, S.P., Chapman, V., Kendall, D.A. & Constantinescu, C.S. (2015) Effects of pro-inflammatory cytokines on cannabinoid CB and CB receptors in immune cells. *Acta physiologica*, **214**, 63-74.

Jeong, W.I., Osei-Hyiaman, D., Park, O., Liu, J., Batkai, S., Mukhopadhyay, P., Horiguchi, N., Harvey-White, J., Marsicano, G., Lutz, B., Gao, B. & Kunos, G. (2008) Paracrine activation of hepatic CB1 receptors by stellate cell-derived endocannabinoids mediates alcoholic fatty liver. *Cell Metab*, **7**, 227-235.

Jesudason, D. & Wittert, G. (2008) Endocannabinoid system in food intake and metabolic regulation. *Curr Opin Lipidol*, **19**, 344-348.

Jhaveri, M.D., Richardson, D., Robinson, I., Garle, M.J., Patel, A., Sun, Y., Sagar, D.R., Bennett, A.J., Alexander, S.P., Kendall, D.A., Barrett, D.A. & Chapman, V. (2008) Inhibition of fatty acid amide hydrolase and cyclooxygenase-2 increases levels of endocannabinoid related molecules and produces analgesia via peroxisome proliferator-activated receptor-alpha in a model of inflammatory pain. *Neuropharmacology*, **55**, 85-93.

Jiang, W., Bikard, D., Cox, D., Zhang, F. & Marraffini, L.A. (2013) RNA-guided editing of bacterial genomes using CRISPR-Cas systems. *Nat Biotechnol*, **31**, 233-239.

Jiang, W., Zhang, Y., Xiao, L., Van Cleemput, J., Ji, S.P., Bai, G. & Zhang, X. (2005) Cannabinoids promote embryonic and adult hippocampus neurogenesis and produce anxiolytic- and antidepressant-like effects. *J Clin Invest*, **115**, 3104-3116.

Jin, K., Xie, L., Kim, S.H., Parmentier-Batteur, S., Sun, Y., Mao, X.O., Childs, J. & Greenberg, D.A. (2004) Defective adult neurogenesis in CB1 cannabinoid receptor knockout mice. *Mol Pharmacol*, **66**, 204-208.

Jinek, M., Chylinski, K., Fonfara, I., Hauer, M., Doudna, J.A. & Charpentier, E. (2012) A programmable dual-RNA-guided DNA endonuclease in adaptive bacterial immunity. *Science*, **337**, 816-821.

Jinek, M., East, A., Cheng, A., Lin, S., Ma, E. & Doudna, J. (2013) RNA-programmed genome editing in human cells. *Elife*, **2**, e00471.

Johnson, D.S., Ahn, K., Kesten, S., Lazerwith, S.E., Song, Y., Morris, M., Fay, L., Gregory, T., Stiff, C., Dunbar, J.B., Jr., Liimatta, M., Beidler, D., Smith, S., Nomanbhoy, T.K. & Cravatt, B.F. (2009) Benzothiophene piperazine and piperidine urea inhibitors of fatty acid amide hydrolase (FAAH). *ACS Med Chem Lett*, **19**, 2865-2869.

Johnson, L.N. & Lewis, R.J. (2001) Structural basis for control by phosphorylation. *Chem Rev*, **101**, 2209-2242.

Johnston, M., Bhatt, S.R., Sikka, S., Mercier, R.W., West, J.M., Makriyannis, A., Gatley, S.J. & Duclos, R.I., Jr. (2012) Assay and inhibition of diacylglycerol lipase activity. *Bioorg Med Chem Lett*, **22**, 4585-4592.

Jung, K.M., Astarita, G., Zhu, C., Wallace, M., Mackie, K. & Piomelli, D. (2007) A key role for diacylglycerol lipase-alpha in metabotropic glutamate receptor-dependent endocannabinoid mobilization. *Mol Pharmacol*, **72**, 612-621.

Jung, K.M., Sepers, M., Henstridge, C.M., Lassalle, O., Neuhofer, D., Martin, H., Ginger, M., Frick, A., DiPatrizio, N.V., Mackie, K., Katona, I., Piomelli, D. & Manzoni, O.J. (2012) Uncoupling of the endocannabinoid signalling complex in a mouse model of fragile X syndrome. *Nat Commun*, **3**, 1080.

Kaczocha, M., Glaser, S.T. & Deutsch, D.G. (2009) Identification of intracellular carriers for the endocannabinoid anandamide. *Proc Natl Acad Sci U S A*, **106**, 6375-6380.

Kang, R., Wan, J., Arstikaitis, P., Takahashi, H., Huang, K., Bailey, A.O., Thompson, J.X., Roth, A.F., Drisdel, R.C., Mastro, R., Green, W.N., Yates, J.R., 3rd, Davis, N.G. & El-Husseini, A. (2008) Neural palmitoyl-proteomics reveals dynamic synaptic palmitoylation. *Nature*, **456**, 904-909.

Kano, M., Ohno-Shosaku, T., Hashimotodani, Y., Uchigashima, M. & Watanabe, M. (2009) Endocannabinoid-mediated control of synaptic transmission. *Physiol Rev*, **89**, 309-380.

Kaplan, M.S. & Hinds, J.W. (1977) Neurogenesis in the adult rat: electron microscopic analysis of light radioautographs. *Science*, **197**, 1092-1094.

Karageorgos, I., Wales, T.E., Janero, D.R., Zvonok, N., Vemuri, V.K., Engen, J.R. & Makriyannis, A. (2013) Active-site inhibitors modulate the dynamic properties of human monoacylglycerol lipase: a hydrogen exchange mass spectrometry study. *Biochemistry*, **52**, 5016-5026.

Katona, I., Sperlagh, B., Magloczky, Z., Santha, E., Kofalvi, A., Czirjak, S., Mackie, K., Vizi, E.S. & Freund, T.F. (2000) GABAergic interneurons are the targets of cannabinoid actions in the human hippocampus. *Neuroscience*, **100**, 797-804.

Katona, I., Urban, G.M., Wallace, M., Ledent, C., Jung, K.M., Piomelli, D., Mackie, K. & Freund, T.F. (2006) Molecular composition of the endocannabinoid system at glutamatergic synapses. *J Neurosci*, **26**, 5628-5637.

Kawamura, Y., Fukaya, M., Maejima, T., Yoshida, T., Miura, E., Watanabe, M., Ohno-Shosaku, T. & Kano, M. (2006) The CB1 cannabinoid receptor is the major cannabinoid receptor at excitatory presynaptic sites in the hippocampus and cerebellum. *J Neurosci*, **26**, 2991-3001.

Keimpema, E., Alpar, A., Howell, F., Malenczyk, K., Hobbs, C., Hurd, Y.L., Watanabe, M., Sakimura, K., Kano, M., Doherty, P. & Harkany, T. (2013) Diacylglycerol lipase alpha manipulation reveals developmental roles for intercellular endocannabinoid signaling. *Sci Rep*, **3**, 2093.

Keimpema, E., Barabas, K., Morozov, Y.M., Tortoriello, G., Torii, M., Cameron, G., Yanagawa, Y., Watanabe, M., Mackie, K. & Harkany, T. (2010) Differential subcellular recruitment of monoacylglycerol lipase generates spatial specificity of 2-arachidonoyl glycerol signaling during axonal pathfinding. *J Neurosci*, **30**, 13992-14007.

Kim, J., Isokawa, M., Ledent, C. & Alger, B.E. (2002) Activation of muscarinic acetylcholine receptors enhances the release of endogenous cannabinoids in the hippocampus. *J Neurosci*, **22**, 10182-10191.

Kmietowicz, Z. (2010) Cannabis based drug is licensed for spasticity in patients with MS. *BMJ*, **340**, c3363.

Knoth, R., Singec, I., Ditter, M., Pantazis, G., Capetian, P., Meyer, R.P., Horvat, V., Volk, B. & Kempermann, G. (2010) Murine features of neurogenesis in the human hippocampus across the lifespan from 0 to 100 years. *PLoS One*, **5**, e8809.

Kohno, M., Hasegawa, H., Inoue, A., Muraoka, M., Miyazaki, T., Oka, K. & Yasukawa, M. (2006) Identification of N-arachidonylglycine as the endogenous ligand for orphan G-protein-coupled receptor GPR18. *Biochem Biophys Res Commun*, **347**, 827-832.

Kondo, S., Kondo, H., Nakane, S., Kodaka, T., Tokumura, A., Waku, K. & Sugiura, T. (1998) 2-Arachidonoylglycerol, an endogenous cannabinoid receptor agonist: identification as one of the major species of monoacylglycerols in various rat tissues, and evidence for its generation through CA2+-dependent and -independent mechanisms. *FEBS Lett*, **429**, 152-156.

Kovacic, P. & Somanathan, R. (2012) Redox processes in neurodegenerative disease involving reactive oxygen species. *Curr Neuropharmacol*, **10**, 289-302.

Kozak, K.R., Crews, B.C., Morrow, J.D., Wang, L.H., Ma, Y.H., Weinander, R., Jakobsson, P.J. & Marnett, L.J. (2002) Metabolism of the endocannabinoids, 2-arachidonylglycerol and anandamide, into prostaglandin, thromboxane, and prostacyclin glycerol esters and ethanolamides. *J Biol Chem*, **277**, 44877-44885.

Kozak, K.R., Prusakiewicz, J.J. & Marnett, L.J. (2004) Oxidative metabolism of endocannabinoids by COX-2. *Curr Pharm Des*, **10**, 659-667.

Kozak, K.R., Rowlinson, S.W. & Marnett, L.J. (2000) Oxygenation of the endocannabinoid, 2-arachidonylglycerol, to glyceryl prostaglandins by cyclooxygenase-2. *J Biol Chem*, **275**, 33744-33749.

Kreitzer, A.C. & Regehr, W.G. (2001) Retrograde inhibition of presynaptic calcium influx by endogenous cannabinoids at excitatory synapses onto Purkinje cells. *Neuron*, **29**, 717-727.

Krintel, C., Morgelin, M., Logan, D.T. & Holm, C. (2009) Phosphorylation of hormone-sensitive lipase by protein kinase A in vitro promotes an increase in its hydrophobic surface area. *FEBS J*, **276**, 4752-4762.

Kurat, C.F., Wolinski, H., Petschnigg, J., Kaluarachchi, S., Andrews, B., Natter, K. & Kohlwein, S.D. (2009) Cdk1/Cdc28-dependent activation of the major triacylglycerol lipase Tgl4 in yeast links lipolysis to cell-cycle progression. *Mol Cell*, **33**, 53-63.

Lampidonis, A.D., Rogdakis, E., Voutsinas, G.E. & Stravopodis, D.J. (2011) The resurgence of Hormone-Sensitive Lipase (HSL) in mammalian lipolysis. *Gene*, **477**, 1-11.

Lau, B.K. & Vaughan, C.W. (2014) Targeting the endogenous cannabinoid system to treat neuropathic pain. *Front Pharmacology*, **5**, 28.

Le Foll, B., Gorelick, D.A. & Goldberg, S.R. (2009) The future of endocannabinoid-oriented clinical research after CB1 antagonists. *Psychopharmacology*, **205**, 171-174.

Ledent, C., Valverde, O., Cossu, G., Petitet, F., Aubert, J.F., Beslot, F., Bohme, G.A., Imperato, A., Pedrazzini, T., Roques, B.P., Vassart, G., Fratta, W. & Parmentier, M. (1999) Unresponsiveness to cannabinoids and reduced addictive effects of opiates in CB1 receptor knockout mice. *Science*, **283**, 401-404.

Lee, J.S., Kallehauge, T.B., Pedersen, L.E. & Kildegaard, H.F. (2015) Site-specific integration in CHO cells mediated by CRISPR/Cas9 and homology-directed DNA repair pathway. *Sci Rep*, **5**, 8572.

Lee, S.J., Escobedo-Lozoya, Y., Szatmari, E.M. & Yasuda, R. (2009) Activation of CaMKII in single dendritic spines during long-term potentiation. *Nature*, **458**, 299-304.

Leung, D., Hardouin, C., Boger, D.L. & Cravatt, B.F. (2003) Discovering potent and selective reversible inhibitors of enzymes in complex proteomes. *Nat Biotechnol*, **21**, 687-691.

Leung, D., Saghatelian, A., Simon, G.M. & Cravatt, B.F. (2006) Inactivation of N-acyl phosphatidylethanolamine phospholipase D reveals multiple mechanisms for the biosynthesis of endocannabinoids. *Biochemistry*, **45**, 4720-4726.

Lichtman, A.H., Leung, D., Shelton, C.C., Saghatelian, A., Hardouin, C., Boger, D.L. & Cravatt, B.F. (2004a) Reversible inhibitors of fatty acid amide hydrolase that promote analgesia: evidence for an unprecedented combination of potency and selectivity. *J Pharmacol Exp Ther*, **311**, 441-448.

Lichtman, A.H., Shelton, C.C., Advani, T. & Cravatt, B.F. (2004b) Mice lacking fatty acid amide hydrolase exhibit a cannabinoid receptor-mediated phenotypic hypoalgesia. *Pain*, **109**, 319-327.

Ligresti, A., Cascio, M.G. & Di Marzo, V. (2005) Endocannabinoid metabolic pathways and enzymes. *Curr Drug Targets CNS Neurol Disord*, **4**, 615-623.

Liu, J., Wang, L., Harvey-White, J., Osei-Hyiaman, D., Razdan, R., Gong, Q., Chan, A.C., Zhou, Z., Huang, B.X., Kim, H.Y. & Kunos, G. (2006) A biosynthetic pathway for anandamide. *Proc Natl Acad Sci U S A*, **103**, 13345-13350.

Liu, Y., Patricelli, M.P. & Cravatt, B.F. (1999) Activity-based protein profiling: the serine hydrolases. *Proc Natl Acad Sci U S A*, **96**, 14694-14699.

Livak, K.J. & Schmittgen, T.D. (2001) Analysis of relative gene expression data using real-time quantitative PCR and the 2(-Delta Delta C(T)) Method. *Methods*, **25**, 402-408.

Llano, I., Leresche, N. & Marty, A. (1991) Calcium entry increases the sensitivity of cerebellar Purkinje cells to applied GABA and decreases inhibitory synaptic currents. *Neuron*, **6**, 565-574.

Lom, B., Hopker, V., McFarlane, S., Bixby, J.L. & Holt, C.E. (1998) Fibroblast growth factor receptor signaling in Xenopus retinal axon extension. *J Neurobiol*, **37**, 633-641.

Long, C., McAnally, J.R., Shelton, J.M., Mireault, A.A., Bassel-Duby, R. & Olson, E.N. (2014) Prevention of muscular dystrophy in mice by CRISPR/Cas9-mediated editing of germline DNA. *Science*, **345**, 1184-1188.

Long, J.Z., Li, W., Booker, L., Burston, J.J., Kinsey, S.G., Schlosburg, J.E., Pavon, F.J., Serrano, A.M., Selley, D.E., Parsons, L.H., Lichtman, A.H. & Cravatt, B.F. (2009a) Selective blockade of 2-arachidonoylglycerol hydrolysis produces cannabinoid behavioral effects. *Nat Chem Biol*, **5**, 37-44.

Long, J.Z., Nomura, D.K., Vann, R.E., Walentiny, D.M., Booker, L., Jin, X., Burston, J.J., Sim-Selley, L.J., Lichtman, A.H., Wiley, J.L. & Cravatt, B.F. (2009b) Dual blockade of FAAH and MAGL identifies behavioral processes regulated by endocannabinoid crosstalk in vivo. *Proc Natl Acad Sci U S A*, **106**, 20270-20275.

Machado Rocha, F.C., Stéfano, S.C., De Cássia Haiek, R., Rosa Oliveira, L.M. & Da Silveira, D.X. (2008) Therapeutic use of Cannabis sativa on chemotherapy-induced nausea and vomiting among cancer patients: systematic review and meta-analysis. *Eur J Cancer Care (Engl)*, **17**, 431-443.

Mackie, K. & Hille, B. (1992) Cannabinoids inhibit N-type calcium channels in neuroblastoma-glioma cells. *Proc Natl Acad Sci U S A*, **89**, 3825-3829.

Maeder, M.L., Linder, S.J., Cascio, V.M., Fu, Y., Ho, Q.H. & Joung, J.K. (2013) CRISPR RNA-guided activation of endogenous human genes. *Nat Methods*, **10**, 977-979.

Maejima, T., Hashimoto, K., Yoshida, T., Aiba, A. & Kano, M. (2001) Presynaptic inhibition caused by retrograde signal from metabotropic glutamate to cannabinoid receptors. *Neuron*, **31**, 463-475.

Maejima, T., Oka, S., Hashimotodani, Y., Ohno-Shosaku, T., Aiba, A., Wu, D., Waku, K., Sugiura, T. & Kano, M. (2005) Synaptically driven endocannabinoid release requires Ca2+-assisted metabotropic glutamate receptor subtype 1 to phospholipase Cbeta4 signaling cascade in the cerebellum. *J Neurosci*, **25**, 6826-6835.

Maison, P., Walker, D.J., Walsh, F.S., Williams, G. & Doherty, P. (2009) BDNF regulates neuronal sensitivity to endocannabinoids. *Neurosci Lett*, **467**, 90-94.

Majerus, P.W. & Prescott, S.M. (1982) Characterization and assay of diacylglycerol lipase from human platelets. *Methods Enzymol*, **86**, 11-17.

Makinen, P.I., Koponen, J.K., Karkkainen, A.M., Malm, T.M., Pulkkinen, K.H., Koistinaho, J., Turunen, M.P. & Yla-Herttuala, S. (2006) Stable RNA interference: comparison of U6 and H1 promoters in endothelial cells and in mouse brain. *J Gene Med*, **8**, 433-441.

Malcher-Lopes, R., Di, S., Marcheselli, V.S., Weng, F.J., Stuart, C.T., Bazan, N.G. & Tasker, J.G. (2006) Opposing crosstalk between leptin and glucocorticoids rapidly modulates synaptic excitation via endocannabinoid release. *J Neurosci*, **26**, 6643-6650.

Mali, P., Aach, J., Stranges, P.B., Esvelt, K.M., Moosburner, M., Kosuri, S., Yang, L. & Church, G.M. (2013a) CAS9 transcriptional activators for target specificity screening and paired nickases for cooperative genome engineering. *Nat Biotechnol*, **31**, 833-838.

Mali, P., Yang, L., Esvelt, K.M., Aach, J., Guell, M., DiCarlo, J.E., Norville, J.E. & Church, G.M. (2013b) RNA-guided human genome engineering via Cas9. *Science*, **339**, 823-826.

Marraffini, L.A. & Sontheimer, E.J. (2010) CRISPR interference: RNA-directed adaptive immunity in bacteria and archaea. *Nat Rev Genet*, **11**, 181-190.

Marrs, W.R., Blankman, J.L., Horne, E.A., Thomazeau, A., Lin, Y.H., Coy, J., Bodor, A.L., Muccioli, G.G., Hu, S.S., Woodruff, G., Fung, S., Lafourcade, M., Alexander, J.P., Long, J.Z., Li, W., Xu, C., Moller, T., Mackie, K., Manzoni, O.J., Cravatt, B.F. & Stella, N. (2010) The serine hydrolase ABHD6 controls the accumulation and efficacy of 2-AG at cannabinoid receptors. *Nat Neurosci*, **13**, 951-957.

Marsicano, G., Goodenough, S., Monory, K., Hermann, H., Eder, M., Cannich, A., Azad, S.C., Cascio, M.G., Gutierrez, S.O., van der Stelt, M., Lopez-Rodriguez, M.L., Casanova, E., Schutz, G., Zieglgansberger, W., Di Marzo, V., Behl, C. & Lutz, B. (2003) CB1 cannabinoid receptors and on-demand defense against excitotoxicity. *Science*, **302**, 84-88.

Martin-Sanchez, E., Furukawa, T.A., Taylor, J. & Martin, J.L. (2009) Systematic review and meta-analysis of cannabis treatment for chronic pain. *Pain Med*, **10**, 1353-1368.

Martin, B.R. & Cravatt, B.F. (2009) Large-scale profiling of protein palmitoylation in mammalian cells. *Nature Methods*, **6**, 135-138.

Masu, M., Tanabe, Y., Tsuchida, K., Shigemoto, R. & Nakanishi, S. (1991) Sequence and expression of a metabotropic glutamate receptor. *Nature*, **349**, 760-765.

Matsuda, L.A., Lolait, S.J., Brownstein, M.J., Young, A.C. & Bonner, T.I. (1990) Structure of a cannabinoid receptor and functional expression of the cloned cDNA. *Nature*, **346**, 561-564.

McCarron, R.M., Shohami, E., Panikashvili, D., Chen, Y., Golech, S., Strasser, A., Mechoulam, R. & Spatz, M. (2003) Antioxidant properties of the vasoactive endocannabinoid, 2-arachidonoyl glycerol (2-AG). *Acta Neurochir Suppl*, **86**, 271-275.

Mechoulam, R., Ben-Shabat, S., Hanus, L., Ligumsky, M., Kaminski, N.E., Schatz, A.R., Gopher, A., Almog, S., Martin, B.R., Compton, D.R. & et al. (1995) Identification of an endogenous 2-monoglyceride, present in canine gut, that binds to cannabinoid receptors. *Biochem Pharmacol*, **50**, 83-90.

Mechoulam, R. & Gaoni, Y. (1965) A Total Synthesis of Dl-Delta-1-Tetrahydrocannabinol, the Active Constituent of Hashish. *J Am Chem Soc*, **87**, 3273-3275.

Mechoulam, R., Lander, N., Breuer, A. & Zahalka, J. (1990) Synthesis of the Individual, Pharmacologically Distinct, Enantiomers of a Tetrahydrocannabinol Derivative. . *Tetrahedron: Asymmetry*, **1**, 315-318.

Mechoulam, R. & Lichtman, A.H. (2003) Neuroscience. Stout guards of the central nervous system. *Science*, **302**, 65-67.

Melis, M., Perra, S., Muntoni, A.L., Pillolla, G., Lutz, B., Marsicano, G., Di Marzo, V., Gessa, G.L. & Pistis, M. (2004) Prefrontal cortex stimulation induces 2-arachidonoyl-glycerol-mediated suppression of excitation in dopamine neurons. *J Neurosci*, **24**, 10707-10715.

Miled, N., Bussetta, C., De caro, A., Riviere, M., Berti, L. & Canaan, S. (2003) Importance of the lid and cap domains for the catalytic activity of gastric lipases. *Comp Biochem Physiol B Biochem Mol Biol*, **136**, 131-138.

Mimeault, M., Pommery, N., Wattez, N., Bailly, C. & Henichart, J.P. (2003) Anti-proliferative and apoptotic effects of anandamide in human prostatic cancer cell lines: implication of epidermal growth factor receptor down-regulation and ceramide production. *Prostate*, **56**, 1-12.

Mitchell, D.A., Vasudevan, A., Linder, M.E. & Deschenes, R.J. (2006) Protein palmitoylation by a family of DHHC protein S-acyltransferases. *J Lipid Res*, **47**, 1118-1127.

Molina-Holgado, F., Rubio-Araiz, A., Garcia-Ovejero, D., Williams, R.J., Moore, J.D., Arevalo-Martin, A., Gomez-Torres, O. & Molina-Holgado, E. (2007) CB2 cannabinoid receptors promote mouse neural stem cell proliferation. *Eur J Neurosci*, **25**, 629-634.

Moore, J.K. & Haber, J.E. (1996) Cell cycle and genetic requirements of two pathways of nonhomologous end-joining repair of double-strand breaks in Saccharomyces cerevisiae. *Mol Cell Biol*, **16**, 2164-2173.

Mor, M., Rivara, S., Lodola, A., Plazzi, P.V., Tarzia, G., Duranti, A., Tontini, A., Piersanti, G., Kathuria, S. & Piomelli, D. (2004) Cyclohexylcarbamic acid 3'- or 4'-substituted biphenyl-3-yl esters as fatty acid amide hydrolase inhibitors: synthesis, quantitative structure-activity relationships, and molecular modeling studies. *J Med Chem*, **47**, 4998-5008.

Morgese, M.G., Cassano, T., Cuomo, V. & Giuffrida, A. (2007) Anti-dyskinetic effects of cannabinoids in a rat model of Parkinson's disease: role of CB(1) and TRPV1 receptors. *Exp Neurol*, **208**, 110-119.

Muccioli, G.G., Xu, C., Odah, E., Cudaback, E., Cisneros, J.A., Lambert, D.M., Lopez Rodriguez, M.L., Bajjalieh, S. & Stella, N. (2007) Identification of a novel endocannabinoid-hydrolyzing enzyme expressed by microglial cells. *J neurosci*, **27**, 2883-2889.

Munro, S., Thomas, K.L. & Abu-Shaar, M. (1993) Molecular characterization of a peripheral receptor for cannabinoids. *Nature*, **365**, 61-65.

Nakane, S., Oka, S., Arai, S., Waku, K., Ishima, Y., Tokumura, A. & Sugiura, T. (2002) 2-Arachidonoyl-sn-glycero-3-phosphate, an arachidonic acid-containing lysophosphatidic acid: occurrence and rapid enzymatic conversion to 2-arachidonoyl-sn-glycerol, a cannabinoid receptor ligand, in rat brain. *Arch Biochem Biophys*, **402**, 51-58.

Nakazi, M., Bauer, U., Nickel, T., Kathmann, M. & Schlicker, E. (2000) Inhibition of serotonin release in the mouse brain via presynaptic cannabinoid CB1 receptors. *Naunyn Schmiedebergs Arch Pharmacol*, **361**, 19-24.

Nardini, M. & Dijkstra, B.W. (1999) Alpha/beta hydrolase fold enzymes: the family keeps growing. *Curr Opin Struct Biol*, **9**, 732-737.

Natarajan, V., Reddy, P.V., Schmid, P.C. & Schmid, H.H. (1982) N-Acylation of ethanolamine phospholipids in canine myocardium. *Biochim Biophys Acta*, **712**, 342-355.

Ng, S.C. & Chan, F.K. (2010) NSAID-induced gastrointestinal and cardiovascular injury. *Curr Opin Gastroenterol*, **26**, 611-617.

Nishimasu, H., Ran, F.A., Hsu, P.D., Konermann, S., Shehata, S.I., Dohmae, N., Ishitani, R., Zhang, F. & Nureki, O. (2014) Crystal structure of Cas9 in complex with guide RNA and target DNA. *Cell*, **156**, 935-949.

Nomura, D.K., Morrison, B.E., Blankman, J.L., Long, J.Z., Kinsey, S.G., Marcondes, M.C., Ward, A.M., Hahn, Y.K., Lichtman, A.H., Conti, B. & Cravatt, B.F. (2011) Endocannabinoid hydrolysis generates brain prostaglandins that promote neuroinflammation. *Science*, **334**, 809-813.

O'Shaughnessy, W. (1843) On the Preparations of the Indian Hemp, or Gunjah. *Prov Med J Retrosp Med Sci*, **5**, 363–369.

Oddi, S., Fezza, F., Pasquariello, N., D'Agostino, A., Catanzaro, G., De Simone, C., Rapino, C., Finazzi-Agro, A. & Maccarrone, M. (2009) Molecular identification of albumin and Hsp70 as cytosolic anandamide-binding proteins. *Chem Biol*, **16**, 624-632.

Ohno-Shosaku, T., Maejima, T. & Kano, M. (2001) Endogenous cannabinoids mediate retrograde signals from depolarized postsynaptic neurons to presynaptic terminals. *Neuron*, **29**, 729-738.

Ohno-Shosaku, T., Matsui, M., Fukudome, Y., Shosaku, J., Tsubokawa, H., Taketo, M.M., Manabe, T. & Kano, M. (2003) Postsynaptic M1 and M3 receptors are responsible for the muscarinic enhancement of retrograde endocannabinoid signalling in the hippocampus. *Eur J Neurosci*, **18**, 109-116.

Oka, S., Tsuchie, A., Tokumura, A., Muramatsu, M., Suhara, Y., Takayama, H., Waku, K. & Sugiura, T. (2003) Ether-linked analogue of 2-arachidonoylglycerol (noladin ether) was not detected in the brains of various mammalian species. *J Neurochem*, **85**, 1374-1381.

Okamoto, Y., Morishita, J., Tsuboi, K., Tonai, T. & Ueda, N. (2004) Molecular characterization of a phospholipase D generating anandamide and its congeners. *J Biol Chem*, **279**, 5298-5305.

Ortar, G., Bisogno, T., Ligresti, A., Morera, E., Nalli, M. & Di Marzo, V. (2008) Tetrahydrolipstatin analogues as modulators of endocannabinoid 2-arachidonoylglycerol metabolism. *J Med Chem*, **51**, 6970-6979.

Ortar, G., Ligresti, A., De Petrocellis, L., Morera, E. & Di Marzo, V. (2003) Novel selective and metabolically stable inhibitors of anandamide cellular uptake. *Biochem Pharmacol*, **65**, 1473-1481.

Oudin, M.J., Gajendra, S., Williams, G., Hobbs, C., Lalli, G. & Doherty, P. (2011a) Endocannabinoids regulate the migration of subventricular zone-derived neuroblasts in the postnatal brain. *J Neurosci*, **31**, 4000-4011.

Oudin, M.J., Hobbs, C. & Doherty, P. (2011b) DAGL-dependent endocannabinoid signalling: roles in axonal pathfinding, synaptic plasticity and adult neurogenesis. *Eur J Neurosci*, **34**, 1634-1646.

Overton, H.A., Babbs, A.J., Doel, S.M., Fyfe, M.C., Gardner, L.S., Griffin, G., Jackson, H.C., Procter, M.J., Rasamison, C.M., Tang-Christensen, M., Widdowson, P.S., Williams, G.M. & Reynet, C. (2006) Deorphanization of a G protein-coupled receptor for oleoylethanolamide and its use in the discovery of small-molecule hypophagic agents. *Cell Metab*, **3**, 167-175.

Panikashvili, D., Simeonidou, C., Ben-Shabat, S., Hanus, L., Breuer, A., Mechoulam, R. & Shohami, E. (2001) An endogenous cannabinoid (2-AG) is neuroprotective after brain injury. *Nature*, **413**, 527-531.

Parekh, A.B. & Putney, J.W., Jr. (2005) Store-operated calcium channels. *Physiol Rev*, **85**, 757-810.

Pattanayak, V., Lin, S., Guilinger, J.P., Ma, E., Doudna, J.A. & Liu, D.R. (2013) High-throughput profiling of off-target DNA cleavage reveals RNA-programmed Cas9 nuclease specificity. *Nat Biotechnol*, **31**, 839-843.

Pedicord, D.L., Flynn, M.J., Fanslau, C., Miranda, M., Hunihan, L., Robertson, B.J., Pearce, B.C., Yu, X.C., Westphal, R.S. & Blat, Y. (2011) Molecular characterization and identification of surrogate substrates for diacylglycerol lipase alpha. *Biochem Biophys Res Commun*, **411**, 809-814.

Perez-Pinera, P., Kocak, D.D., Vockley, C.M., Adler, A.F., Kabadi, A.M., Polstein, L.R., Thakore, P.I., Glass, K.A., Ousterout, D.G., Leong, K.W., Guilak, F., Crawford, G.E., Reddy, T.E. & Gersbach, C.A. (2013) RNA-guided gene activation by CRISPR-Cas9-based transcription factors. *Nat Methods*, **10**, 973-976.

Perez, E.E., Wang, J., Miller, J.C., Jouvenot, Y., Kim, K.A., Liu, O., Wang, N., Lee, G., Bartsevich, V.V., Lee, Y.L., Guschin, D.Y., Rupniewski, I., Waite, A.J., Carpenito, C., Carroll, R.G., Orange, J.S., Urnov, F.D., Rebar, E.J., Ando, D., Gregory, P.D., Riley, J.L., Holmes, M.C. & June, C.H. (2008) Establishment of HIV-1 resistance in CD4+ T cells by genome editing using zinc-finger nucleases. *Nat Biotechnol*, **26**, 808-816.

Perez Roque, M.E., Pasquare, S.J., Castagnet, P.I. & Giusto, N.M. (1998) Can phosphorylation and dephosphorylation of rod outer segment membranes affect phosphatidate phosphohydrolase and diacylglycerol lipase activities? *Comp Biochem Physiol B Biochem Mol Biol*, **119**, 85-93.

Pertwee, R.G. (2001) Cannabinoid receptors and pain. *Prog Neurobiol*, **63**, 569-611.

Pertwee, R.G. (2002) Cannabinoids and multiple sclerosis. *Pharmacol Ther*, **95**, 165-174.

Pertwee, R.G. (2005) The therapeutic potential of drugs that target cannabinoid receptors or modulate the tissue levels or actions of endocannabinoids. *AAPS*, **7**, E625-654.

Pertwee, R.G. (2006a) Cannabinoid pharmacology: the first 66 years. *Br J Pharmacol*, **147**, S163-171.

Pertwee, R.G. (2006b) The pharmacology of cannabinoid receptors and their ligands: an overview. *Int J Obes (Lond)*, **30**, S13-18.

Pertwee, R.G. (2009) Emerging strategies for exploiting cannabinoid receptor agonists as medicines. *Br J Pharmacol*, **156**, 397-411.

Pertwee, R.G., Howlett, A.C., Abood, M.E., Alexander, S.P., Di Marzo, V., Elphick, M.R., Greasley, P.J., Hansen, H.S., Kunos, G., Mackie, K., Mechoulam, R. & Ross, R.A. (2010) International Union of Basic and Clinical Pharmacology. LXXIX. Cannabinoid receptors and their ligands: beyond CB(1) and CB(2). *Pharmacol Rev*, **62**, 588-631.

Phillips, T.J., Cherry, C.L., Cox, S., Marshall, S.J. & Rice, A.S. (2010) Pharmacological treatment of painful HIV-associated sensory neuropathy: a systematic review and meta-analysis of randomised controlled trials. *PLoS One*, **5**, e14433.

Piomelli, D. (2003) The molecular logic of endocannabinoid signalling. *Nat Rev Neurosci*, **4**, 873-884.

Piomelli, D., Giuffrida, A., Calignano, A. & Rodriguez de Fonseca, F. (2000) The endocannabinoid system as a target for therapeutic drugs. *Trends Pharmacol Sci*, **21**, 218-224.

Piro, J.R., Benjamin, D.I., Duerr, J.M., Pi, Y., Gonzales, C., Wood, K.M., Schwartz, J.W., Nomura, D.K. & Samad, T.A. (2012) A dysregulated endocannabinoid-eicosanoid

network supports pathogenesis in a mouse model of Alzheimer's disease. *Cell Rep*, **1**, 617-623.

Pisani, V., Moschella, V., Bari, M., Fezza, F., Galati, S., Bernardi, G., Stanzione, P., Pisani, A. & Maccarrone, M. (2010) Dynamic changes of anandamide in the cerebrospinal fluid of Parkinson's disease patients. *Mov Disord*, **25**, 920-924.

Pitler, T.A. & Alger, B.E. (1992) Postsynaptic spike firing reduces synaptic GABAA responses in hippocampal pyramidal cells. *J Neurosci* **12**, 4122-4132.

Porter, A.C., Sauer, J.M., Knierman, M.D., Becker, G.W., Berna, M.J., Bao, J., Nomikos, G.G., Carter, P., Bymaster, F.P., Leese, A.B. & Felder, C.C. (2002) Characterization of a novel endocannabinoid, virodhamine, with antagonist activity at the CB1 receptor. *J Pharmacol Exp Ther*, **301**, 1020-1024.

Prescott, S.M. & Majerus, P.W. (1983) Characterization of 1,2-diacylglycerol hydrolysis in human platelets. Demonstration of an arachidonoyl-monoacylglycerol intermediate. *J Biol Chem*, **258**, 764-769.

Priestley, R.S., Nickolls, S.A., Alexander, S.P. & Kendall, D.A. (2014) A potential role for cannabinoid receptors in the therapeutic action of fenofibrate. *FASEB J*, **29**, 1446-1455.

Qiu, S., Adema, C.M. & Lane, T. (2005) A computational study of off-target effects of RNA interference. *Nucleic Acids Res*, **33**, 1834-1847.

Rajaraman, G., Simcocks, A., Hryciw, D.H., Hutchinson, D.S. & McAinch, A.J. (2015) G protein-coupled receptor 18: A potential role for endocannabinoid signalling in metabolic dysfunction. *Mol Nutr Food Res*.

Ramirez, B.G., Blazquez, C., Gomez del Pulgar, T., Guzman, M. & de Ceballos, M.L. (2005) Prevention of Alzheimer's disease pathology by cannabinoids: neuroprotection mediated by blockade of microglial activation. *J Neurosci*, **25**, 1904-1913.

Ran, F.A., Hsu, P.D., Lin, C.Y., Gootenberg, J.S., Konermann, S., Trevino, A.E., Scott, D.A., Inoue, A., Matoba, S., Zhang, Y. & Zhang, F. (2013a) Double nicking by RNA-guided CRISPR Cas9 for enhanced genome editing specificity. *Cell*, **154**, 1380-1389.

Ran, F.A., Hsu, P.D., Wright, J., Agarwala, V., Scott, D.A. & Zhang, F. (2013b) Genome engineering using the CRISPR-Cas9 system. *Nat Protoc*, **8**, 2281-2308.

Regehr, W.G., Carey, M.R. & Best, A.R. (2009) Activity-dependent regulation of synapses by retrograde messengers. *Neuron*, **63**, 154-170.

Reisenberg, M., Singh, P.K., Williams, G. & Doherty, P. (2012) The diacylglycerol lipases: structure, regulation and roles in and beyond endocannabinoid signalling. *Philos Trans R Soc Lond B Biol Sci*, **367**, 3264-3275.

Robbe, D., Kopf, M., Remaury, A., Bockaert, J. & Manzoni, O.J. (2002) Endogenous cannabinoids mediate long-term synaptic depression in the nucleus accumbens. *Proc Natl Acad Sci U S A*, **99**, 8384-8388.

Rockwell, C.E., Snider, N.T., Thompson, J.T., Vanden Heuvel, J.P. & Kaminski, N.E. (2006) Interleukin-2 suppression by 2-arachidonyl glycerol is mediated through peroxisome proliferator-activated receptor gamma independently of cannabinoid receptors 1 and 2. *Mol Pharmacol*, **70**, 101-111.

Rosenberger, T.A., Farooqui, A.A. & Horrocks, L.A. (2007) Bovine brain diacylglycerol lipase: substrate specificity and activation by cyclic AMP-dependent protein kinase. *Lipids*, **42**, 187-195.

Ross, R.A. (2003) Anandamide and vanilloid TRPV1 receptors. *Br J Pharmacol*, **140**, 790-801.

Ross, R.A., Gibson, T.M., Brockie, H.C., Leslie, M., Pashmi, G., Craib, S.J., Di Marzo, V. & Pertwee, R.G. (2001) Structure-activity relationship for the endogenous cannabinoid, anandamide, and certain of its analogues at vanilloid receptors in transfected cells and vas deferens. *Br J Pharmacol*, **132**, 631-640.

Rozengurt, E. (2007) Mitogenic signaling pathways induced by G protein-coupled receptors. *J Cell Physiol*, **213**, 589-602.

Rubin, B. & Denis, E.A. (1997) Lipases, Part B: Enzyme Characterization and Utilization. . *Methods in Enzymol.*, **286**, 3-563.

Russo, E.B., Jiang, H.E., Li, X., Sutton, A., Carboni, A., del Bianco, F., Mandolino, G., Potter, D.J., Zhao, Y.X., Bera, S., Zhang, Y.B., Lu, E.G., Ferguson, D.K., Hueber, F., Zhao, L.C., Liu, C.J., Wang, Y.F. & Li, C.S. (2008) Phytochemical and genetic analyses of ancient cannabis from Central Asia. *J Exp Bot*, **59**, 4171-4182.

Ryberg, E., Larsson, N., Sjogren, S., Hjorth, S., Hermansson, N.O., Leonova, J., Elebring, T., Nilsson, K., Drmota, T. & Greasley, P.J. (2007) The orphan receptor GPR55 is a novel cannabinoid receptor. *Br J Pharmacol*, **152**, 1092-1101.

Saffell, J.L., Williams, E.J., Mason, I.J., Walsh, F.S. & Doherty, P. (1997) Expression of a dominant negative FGF receptor inhibits axonal growth and FGF receptor phosphorylation stimulated by CAMs. *Neuron*, **18**, 231-242.

Safo, P.K. & Regehr, W.G. (2005) Endocannabinoids control the induction of cerebellar LTD. *Neuron*, **48**, 647-659.

Sagar, D.R., Gaw, A.G., Okine, B.N., Woodhams, S.G., Wong, A., Kendall, D.A. & Chapman, V. (2009) Dynamic regulation of the endocannabinoid system: implications for analgesia. *Mol Pain*, **5**, 59.

Salazar, C. & Hofer, T. (2009) Multisite protein phosphorylation--from molecular mechanisms to kinetic models. *FEBS J*, **276**, 3177-3198.

Sanchez-Fernandez, G., Cabezudo, S., Garcia-Hoz, C., Beninca, C., Aragay, A.M., Mayor, F., Jr. & Ribas, C. (2014) Galphaq signalling: the new and the old. *Cell Signal*, **26**, 833-848.

Sapranauskas, R., Gasiunas, G., Fremaux, C., Barrangou, R., Horvath, P. & Siksnys, V. (2011) The Streptococcus thermophilus CRISPR/Cas system provides immunity in Escherichia coli. *Nucleic Acids Res*, **39**, 9275-9282.

Savinainen, J.R., Saario, S.M. & Laitinen, J.T. (2012) The serine hydrolases MAGL, ABHD6 and ABHD12 as guardians of 2-arachidonoylglycerol signalling through cannabinoid receptors. *Acta Physiol*, **204**, 267-276.

Schaap, L.A., Pluijm, S.M., Deeg, D.J. & Visser, M. (2006) Inflammatory markers and loss of muscle mass (sarcopenia) and strength. *Am J Med*, **119**, 526 e529-517.

Schlicker, E. & Kathmann, M. (2001) Modulation of transmitter release via presynaptic cannabinoid receptors. *Trends Pharmacol Sci*, **22**, 565-572.

Schlosburg, J.E., Blankman, J.L., Long, J.Z., Nomura, D.K., Pan, B., Kinsey, S.G., Nguyen, P.T., Ramesh, D., Booker, L., Burston, J.J., Thomas, E.A., Selley, D.E., Sim-Selley, L.J., Liu, Q.S., Lichtman, A.H. & Cravatt, B.F. (2010) Chronic monoacylglycerol lipase blockade causes functional antagonism of the endocannabinoid system. *Nat Neurosci*, **13**, 1113-1119.

Schmid, H.H. (2000) Pathways and mechanisms of N-acylethanolamine biosynthesis: can anandamide be generated selectively? *Chem Phys Lipids*, **108**, 71-87.

Seamon, K.B. & Daly, J.W. (1986) Forskolin: its biological and chemical properties. *Advances in cyclic nucleotide and protein phosphorylation research*, **20**, 1-150.

Shen, B., Zhang, W., Zhang, J., Zhou, J., Wang, J., Chen, L., Wang, L., Hodgkins, A., Iyer, V., Huang, X. & Skarnes, W.C. (2014) Efficient genome modification by CRISPR-Cas9 nickase with minimal off-target effects. *Nat Methods*, **11**, 399-402.

Sheppard, D. (1994) Dominant negative mutants: tools for the study of protein function in vitro and in vivo. *Am J Respir Cell Mol Biol*, **11**, 1-6.

Shonesy, B.C., Wang, X., Rose, K.L., Ramikie, T.S., Cavener, V.S., Rentz, T., Baucum, A.J., 2nd, Jalan-Sakrikar, N., Mackie, K., Winder, D.G., Patel, S. & Colbran, R.J. (2013) CaMKII regulates diacylglycerol lipase-alpha and striatal endocannabinoid signaling. *Nat Neurosci*, **16**, 456-463.

Simmons, D.L., Botting, R.M. & Hla, T. (2004) Cyclooxygenase isozymes: the biology of prostaglandin synthesis and inhibition. *Pharmacol Rev*, **56**, 387-437.

Simon, G.M. & Cravatt, B.F. (2006) Endocannabinoid biosynthesis proceeding through glycerophospho-N-acyl ethanolamine and a role for alpha/beta-hydrolase 4 in this pathway. *J Biol Chem*, **281**, 26465-26472.

Simon, G.M. & Cravatt, B.F. (2008) Anandamide biosynthesis catalyzed by the phosphodiesterase GDE1 and detection of glycerophospho-N-acyl ethanolamine precursors in mouse brain. *J Biol Chem*, **283**, 9341-9349.

Simon, G.M. & Cravatt, B.F. (2010a) Activity-based proteomics of enzyme superfamilies: serine hydrolases as a case study. *J Biol Chem*, **285**, 11051-11055.

Simon, G.M. & Cravatt, B.F. (2010b) Characterization of mice lacking candidate N-acyl ethanolamine biosynthetic enzymes provides evidence for multiple pathways that contribute to endocannabinoid production in vivo. *Mol Biosyst*, **6**, 1411-1418.

Sinor, A.D., Irvin, S.M. & Greenberg, D.A. (2000) Endocannabinoids protect cerebral cortical neurons from in vitro ischemia in rats. *Neurosci Lett*, **278**, 157-160.

Smart, D., Gunthorpe, M.J., Jerman, J.C., Nasir, S., Gray, J., Muir, A.I., Chambers, J.K., Randall, A.D. & Davis, J.B. (2000) The endogenous lipid anandamide is a full agonist at the human vanilloid receptor (hVR1). *Br J Pharmacol*, **129**, 227-230.

Smith, P.B., Compton, D.R., Welch, S.P., Razdan, R.K., Mechoulam, R. & Martin, B.R. (1994) The pharmacological activity of anandamide, a putative endogenous cannabinoid, in mice. *J Pharmacol Exp Ther*, **270**, 219-227.

Smithies, O., Gregg, R.G., Boggs, S.S., Koralewski, M.A. & Kucherlapati, R.S. (1985) Insertion of DNA sequences into the human chromosomal beta-globin locus by homologous recombination. *Nature*, **317**, 230-234.

Srinivasan, B.D. & Kulkarni, P.S. (1989) Inhibitors of the arachidonic acid cascade in the management of ocular inflammation. *Prog Clin Biol Res*, **312**, 229-249.

Stella, N. & Piomelli, D. (2001) Receptor-dependent formation of endogenous cannabinoids in cortical neurons. *Eur J Pharmacol*, **425**, 189-196.

Stella, N., Schweitzer, P. & Piomelli, D. (1997) A second endogenous cannabinoid that modulates long-term potentiation. *Nature*, **388**, 773-778.

Sternberg, S.H. & Doudna, J.A. (2015) Expanding the Biologist's Toolkit with CRISPR-Cas9. *Mol Cell*, **58**, 568-574.

Stoving, R.K., Andries, A., Brixen, K., Flyvbjerg, A., Horder, K. & Frystyk, J. (2009) Leptin, ghrelin, and endocannabinoids: potential therapeutic targets in anorexia nervosa. *J Psychiatr Res*, **43**, 671-679.

Streit, W.J. (2002) Microglia as neuroprotective, immunocompetent cells of the CNS. *Glia*, **40**, 133-139.

Su, M.G., Huang, K.Y., Lu, C.T., Kao, H.J., Chang, Y.H. & Lee, T.Y. (2014) topPTM: a new module of dbPTM for identifying functional post-translational modifications in transmembrane proteins. *Nucleic Acids Res*, **42**, D537-545.

Sugiura, T., Kishimoto, S., Oka, S. & Gokoh, M. (2006) Biochemistry, pharmacology and physiology of 2-arachidonoylglycerol, an endogenous cannabinoid receptor ligand. *Prog Lipid Res*, **45**, 405-446.

Sugiura, T., Kobayashi, Y., Oka, S. & Waku, K. (2002) Biosynthesis and degradation of anandamide and 2-arachidonoylglycerol and their possible physiological significance. *Prostaglandins Leukot Essent Fatty Acids*, **66**, 173-192.

Sugiura, T., Kodaka, T., Nakane, S., Miyashita, T., Kondo, S., Suhara, Y., Takayama, H., Waku, K., Seki, C., Baba, N. & Ishima, Y. (1999) Evidence that the cannabinoid CB1 receptor is a 2-arachidonoylglycerol receptor. Structure-activity relationship of 2-arachidonoylglycerol, ether-linked analogues, and related compounds. *J Biol Chem*, **274**, 2794-2801.

Sugiura, T., Kondo, S., Sukagawa, A., Nakane, S., Shinoda, A., Itoh, K., Yamashita, A. & Waku, K. (1995) 2-Arachidonoylglycerol: a possible endogenous cannabinoid receptor ligand in brain. *Biochem Biophys Res Commun*, **215**, 89-97.

Sullivan, J.M. (1999) Mechanisms of cannabinoid-receptor-mediated inhibition of synaptic transmission in cultured hippocampal pyramidal neurons. *J Neurophysiol*, **82**, 1286-1294.

Sun, Y., Alexander, S.P., Garle, M.J., Gibson, C.L., Hewitt, K., Murphy, S.P., Kendall, D.A. & Bennett, A.J. (2007) Cannabinoid activation of PPAR alpha; a novel neuroprotective mechanism. *Br J Pharmacol*, **152**, 734-743.

Sun, Y.X., Tsuboi, K., Okamoto, Y., Tonai, T., Murakami, M., Kudo, I. & Ueda, N. (2004) Biosynthesis of anandamide and N-palmitoylethanolamine by sequential actions of phospholipase A2 and lysophospholipase D. *Biochem J*, **380**, 749-756.

Suplatov, D.A., Besenmatter, W., Svedas, V.K. & Svendsen, A. (2012) Bioinformatic analysis of alpha/beta-hydrolase fold enzymes reveals subfamily-specific positions responsible for discrimination of amidase and lipase activities. *Protein Eng Des Sel*, **25**, 689-697.

Sutherland, C.A. & Amin, D. (1982) Relative activities of rat and dog platelet phospholipase A2 and diglyceride lipase. Selective inhibition of diglyceride lipase by RHC 80267. *J Biol Chem*, **257**, 14006-14010.

Sylantyev, S., Jensen, T.P., Ross, R.A. & Rusakov, D.A. (2013) Cannabinoid- and lysophosphatidylinositol-sensitive receptor GPR55 boosts neurotransmitter release at central synapses. *Proc Natl Acad Sci U S A*, **110**, 5193-5198.

Szabo, B., Urbanski, M.J., Bisogno, T., Di Marzo, V., Mendiguren, A., Baer, W.U. & Freiman, I. (2006) Depolarization-induced retrograde synaptic inhibition in the mouse cerebellar cortex is mediated by 2-arachidonoylglycerol. *J Physiol*, **577**, 263-280.

Szabo, G.G., Lenkey, N., Holderith, N., Andrasi, T., Nusser, Z. & Hajos, N. (2014) Presynaptic Calcium Channel Inhibition Underlies CB1 Cannabinoid Receptor-Mediated Suppression of GABA Release. *J Neurosci*, **34**, 7958-7963.

Takahashi, K.A. & Linden, D.J. (2000) Cannabinoid receptor modulation of synapses received by cerebellar Purkinje cells. *J Neurophysiol*, **83**, 1167-1180.

Tanasescu, R. & Constantinescu, C.S. (2010) Cannabinoids and the immune system: an overview. *Immunobiology*, **215**, 588-597.

Tanimura, A., Yamazaki, M., Hashimotodani, Y., Uchigashima, M., Kawata, S., Abe, M., Kita, Y., Hashimoto, K., Shimizu, T., Watanabe, M., Sakimura, K. & Kano, M. (2010) The

endocannabinoid 2-arachidonoylglycerol produced by diacylglycerol lipase alpha mediates retrograde suppression of synaptic transmission. *Neuron*, **65**, 320-327.

Tessier-Lavigne, M. & Goodman, C.S. (1996) The molecular biology of axon guidance. *Science*, **274**, 1123-1133.

Thomas, K.R., Folger, K.R. & Capecchi, M.R. (1986) High frequency targeting of genes to specific sites in the mammalian genome. *Cell*, **44**, 419-428.

Tilley, S.L., Coffman, T.M. & Koller, B.H. (2001) Mixed messages: modulation of inflammation and immune responses by prostaglandins and thromboxanes. *J Clin Invest*, **108**, 15-23.

Torres, R., Martin, M.C., Garcia, A., Cigudosa, J.C., Ramirez, J.C. & Rodriguez-Perales, S. (2014) Engineering human tumour-associated chromosomal translocations with the RNA-guided CRISPR-Cas9 system. *Nat Commun*, **5**, 3964.

Tzavara, E.T., Davis, R.J., Perry, K.W., Li, X., Salhoff, C., Bymaster, F.P., Witkin, J.M. & Nomikos, G.G. (2003) The CB1 receptor antagonist SR141716A selectively increases monoaminergic neurotransmission in the medial prefrontal cortex: implications for therapeutic actions. *Br J Pharmacol*, **138**, 544-553.

Ueda, H., Kobayashi, T., Kishimoto, M., Tsutsumi, T. & Okuyama, H. (1993) A possible pathway of phosphoinositide metabolism through EDTA-insensitive phospholipase A1 followed by lysophosphoinositide-specific phospholipase C in rat brain. *J Neurochem*, **61**, 1874-1881.

Ueda, N., Liu, Q. & Yamanaka, K. (2001) Marked activation of the N-acylphosphatidylethanolamine-hydrolyzing phosphodiesterase by divalent cations. *Biochim Biophys Acta*, **1532**, 121-127.

Valerie, K. & Povirk, L.F. (2003) Regulation and mechanisms of mammalian double-strand break repair. *Oncogene*, **22**, 5792-5812.

van der Lee, M.M., Blomenrohr, M., van der Doelen, A.A., Wat, J.W., Smits, N., Hanson, B.J., van Koppen, C.J. & Zaman, G.J. (2009) Pharmacological characterization of receptor redistribution and beta-arrestin recruitment assays for the cannabinoid receptor 1. *J Biomol Screen*, **14**, 811-823.

van der Stelt, M., Mazzola, C., Esposito, G., Matias, I., Petrosino, S., De Filippis, D., Micale, V., Steardo, L., Drago, F., Iuvone, T. & Di Marzo, V. (2006) Endocannabinoids and beta-amyloid-induced neurotoxicity in vivo: effect of pharmacological elevation of endocannabinoid levels. *Cell Mol Life Sci*, **63**, 1410-1424.

van der Wel, T., Janssen, F.J., Baggelaar, M.P., Deng, H., den Dulk, H., Overkleeft, H.S. & van der Stelt, M. (2015) A natural substrate-based fluorescence assay for inhibitor screening on diacylglycerol lipase alpha. *J Lipid Res*, **56**, 927-935.

van Praag, H., Schinder, A.F., Christie, B.R., Toni, N., Palmer, T.D. & Gage, F.H. (2002) Functional neurogenesis in the adult hippocampus. *Nature*, **415**, 1030-1034.

Van Sickle, M.D., Duncan, M., Kingsley, P.J., Mouihate, A., Urbani, P., Mackie, K., Stella, N., Makriyannis, A., Piomelli, D., Davison, J.S., Marnett, L.J., Di Marzo, V., Pittman, Q.J., Patel, K.D. & Sharkey, K.A. (2005) Identification and functional characterization of brainstem cannabinoid CB2 receptors. *Science*, **310**, 329-332.

van Tilbeurgh, H., Sarda, L., Verger, R. & Cambillau, C. (1992) Structure of the pancreatic lipase-procolipase complex. *Nature*, **359**, 159-162.

Varma, N., Carlson, G.C., Ledent, C. & Alger, B.E. (2001) Metabotropic glutamate receptors drive the endocannabinoid system in hippocampus. *J Neurosci*, **21**, RC188.

Vellani, V., Petrosino, S., De Petrocellis, L., Valenti, M., Prandini, M., Magherini, P.C., McNaughton, P.A. & Di Marzo, V. (2008) Functional lipidomics. Calcium-independent activation of endocannabinoid/endovanilloid lipid signalling in sensory neurons by protein kinases C and A and thrombin. *Neuropharmacology*, **55**, 1274-1279.

Vincent, P. & Marty, A. (1993) Neighboring cerebellar Purkinje cells communicate via retrograde inhibition of common presynaptic interneurons. *Neuron*, **11**, 885-893.

Vyas, V.K., Barrasa, M.I. & Fink, G.R. (2015) A CRISPR system permits genetic engineering of essential genes and gene families. *Science advances*, **1**, e1500248.

Wahn, H., Wolf, J., Kram, F., Frantz, S. & Wagner, J.A. (2005) The endocannabinoid arachidonyl ethanolamide (anandamide) increases pulmonary arterial pressure via cyclooxygenase-2 products in isolated rabbit lungs. *Am J Physiol Heart Circ Physiol*, **289**, H2491-2496.

Walsh, F.S. & Doherty, P. (1997) Neural cell adhesion molecules of the immunoglobulin superfamily: role in axon growth and guidance. *Annu Rev Cell Dev Biol*, **13**, 425-456.

Walter, L., Dinh, T. & Stella, N. (2004) ATP induces a rapid and pronounced increase in 2-arachidonoylglycerol production by astrocytes, a response limited by monoacylglycerol lipase. *J Neurosci*, **24**, 8068-8074.

Walter, L. & Stella, N. (2003) Endothelin-1 increases 2-arachidonoyl glycerol (2-AG) production in astrocytes. *Glia*, **44**, 85-90.

Watson, S., Chambers, D., Hobbs, C., Doherty, P. & Graham, A. (2008) The endocannabinoid receptor, CB1, is required for normal axonal growth and fasciculation. *Mol Cell Neurosci*, **38**, 89-97.

Watson, S.J., Benson, J.A., Jr. & Joy, J.E. (2000) Marijuana and medicine: assessing the science base: a summary of the 1999 Institute of Medicine report. *Arch Gen Psychiatry*, **57**, 547-552.

Wiedenheft, B., Sternberg, S.H. & Doudna, J.A. (2012) RNA-guided genetic silencing systems in bacteria and archaea. *Nature*, **482**, 331-338.

Wiley, J.L. & Martin, B.R. (2003) Cannabinoid pharmacological properties common to other centrally acting drugs. *Eur J Pharmacol*, **471**, 185-193.

Willard, S.S. & Koochekpour, S. (2013) Glutamate, glutamate receptors, and downstream signaling pathways. *Int J Biol Sci*, **9**, 948-959.

Williams, E.J., Walsh, F.S. & Doherty, P. (2003) The FGF receptor uses the endocannabinoid signaling system to couple to an axonal growth response. *J Cell Biol*, **160**, 481-486.

Wilson, R.I. & Nicoll, R.A. (2001) Endogenous cannabinoids mediate retrograde signalling at hippocampal synapses. *Nature*, **410**, 588-592.

Winkler, F.K., D'Arcy, A. & Hunziker, W. (1990) Structure of human pancreatic lipase. *Nature*, **343**, 771-774.

Won, Y.J., Puhl, H.L., 3rd & Ikeda, S.R. (2009) Molecular reconstruction of mGluR5a-mediated endocannabinoid signaling cascade in single rat sympathetic neurons. *J Neurosci*, **29**, 13603-13612.

Wu, C.S., Zhu, J., Wager-Miller, J., Wang, S., O'Leary, D., Monory, K., Lutz, B., Mackie, K. & Lu, H.C. (2010) Requirement of cannabinoid CB(1) receptors in cortical pyramidal neurons for appropriate development of corticothalamic and thalamocortical projections. *Eur J Neurosci*, **32**, 693-706.

Xu, H., Lan, D., Yang, B. & Wang, Y. (2015) Biochemical Properties and Structure Analysis of a DAG-Like Lipase from Malassezia globosa. *Int J Mol Sci*, **16**, 4865-4879.

Yamada, K.M. & Hall, A. (2015) Reproducibility and cell biology. *J Cell Biol*, **209**, 191-193.

Yamaguchi, S., Mase, T. & Takeuchi, K. (1991) Cloning and structure of the mono- and diacylglycerol lipase-encoding gene from Penicillium camembertii U-150. *Gene*, **103**, 61-67.

Yan, Q., Zhang, Q., Yang, H., Zou, Q., Tang, C., Fan, N. & Lai, L. (2014) Generation of multi-gene knockout rabbits using the Cas9/gRNA system. *Cell regeneration*, **3**, 12.

Yanez-Mo, M., Barreiro, O., Gordon-Alonso, M., Sala-Valdes, M. & Sanchez-Madrid, F. (2009) Tetraspanin-enriched microdomains: a functional unit in cell plasma membranes. *Trends Cell Biol*, **19**, 434-446.

Yang, M., Zhang, L., Stevens, J. & Gibson, G. (2014) CRISPR/Cas9 mediated generation of stable chondrocyte cell lines with targeted gene knockouts; analysis of an aggrecan knockout cell line. *Bone*, **69**, 118-125.

Yang, R., Fredman, G., Krishnamoorthy, S., Agrawal, N., Irimia, D., Piomelli, D. & Serhan, C.N. (2011) Decoding functional metabolomics with docosahexaenoyl ethanolamide (DHEA) identifies novel bioactive signals. *J Biol Chem* **286**, 31532-31541.

Yang, W., Di Vizio, D., Kirchner, M., Steen, H. & Freeman, M.R. (2010) Proteome scale characterization of human S-acylated proteins in lipid raft-enriched and non-raft membranes. *Mol Cell Proteomics*, **9**, 54-70.

Yin, H., Xue, W., Chen, S., Bogorad, R.L., Benedetti, E., Grompe, M., Koteliansky, V., Sharp, P.A., Jacks, T. & Anderson, D.G. (2014) Genome editing with Cas9 in adult mice corrects a disease mutation and phenotype. *Nat Biotechnol*, **32**, 551-553.

Yoshida, T., Fukaya, M., Uchigashima, M., Miura, E., Kamiya, H., Kano, M. & Watanabe, M. (2006) Localization of diacylglycerol lipase-alpha around postsynaptic spine suggests close proximity between production site of an endocannabinoid, 2-arachidonoyl-glycerol, and presynaptic cannabinoid CB1 receptor. *J Neurosci*, **26**, 4740-4751.

Yoshida, T., Uchigashima, M., Yamasaki, M., Katona, I., Yamazaki, M., Sakimura, K., Kano, M., Yoshioka, M. & Watanabe, M. (2011) Unique inhibitory synapse with particularly rich endocannabinoid signaling machinery on pyramidal neurons in basal amygdaloid nucleus. *Proc Natl Acad Sci U S A*, **108**, 3059-3064.

Yoshino, H., Miyamae, T., Hansen, G., Zambrowicz, B., Flynn, M., Pedicord, D., Blat, Y., Westphal, R.S., Zaczek, R., Lewis, D.A. & Gonzalez-Burgos, G. (2011) Postsynaptic diacylglycerol lipase mediates retrograde endocannabinoid suppression of inhibition in mouse prefrontal cortex. *J Physiol*, **589**, 4857-4884.

Yu, M., Ives, D. & Ramesha, C.S. (1997) Synthesis of prostaglandin E2 ethanolamide from anandamide by cyclooxygenase-2. *J Biol Chem*, **272**, 21181-21186.

Yue, T.L. & Feuerstein, G.Z. (1994) Platelet-activating factor: a putative neuromodulator and mediator in the pathophysiology of brain injury. *Crit Rev Neurobiol*, **8**, 11-24.

Zajicek, J.P., Hobart, J.C., Slade, A., Barnes, D., Mattison, P.G. & Group, M.R. (2012) Multiple sclerosis and extract of cannabis: results of the MUSEC trial. *J Neurol Neurosurg Psychiatry*, **83**, 1125-1132.

Zhao, C., Deng, W. & Gage, F.H. (2008) Mechanisms and functional implications of adult neurogenesis. *Cell*, **132**, 645-660.

Zhong, P., Pan, B., Gao, X.P., Blankman, J.L., Cravatt, B.F. & Liu, Q.S. (2011) Genetic deletion of monoacylglycerol lipase alters endocannabinoid-mediated retrograde synaptic depression in the cerebellum. *J Physiol*, **589**, 4847-4855.

Zlokarnik, G., Negulescu, P.A., Knapp, T.E., Mere, L., Burres, N., Feng, L., Whitney, M., Roemer, K. & Tsien, R.Y. (1998) Quantitation of transcription and clonal selection of single living cells with beta-lactamase as reporter. *Science*, **279**, 84-88.

Zoerner, A.A., Batkai, S., Suchy, M.T., Gutzki, F.M., Engeli, S., Jordan, J. & Tsikas, D. (2012) Simultaneous UPLC-MS/MS quantification of the endocannabinoids 2-arachidonoyl glycerol (2AG), 1-arachidonoyl glycerol (1AG), and anandamide in human plasma: minimization of matrix-effects, 2AG/1AG isomerization and degradation by toluene solvent extraction. *J Chromatogr B Analyt Technol Biomed Life Sci*, **883-884**, 161-171.

Zygmunt, P.M., Petersson, J., Andersson, D.A., Chuang, H., Sorgard, M., Di Marzo, V., Julius, D. & Hogestatt, E.D. (1999) Vanilloid receptors on sensory nerves mediate the vasodilator action of anandamide. *Nature*, **400**, 452-457.